Premixed combustion of alternative fuels under varying conditions of temperature and pressure

Audrius Bagdanavicius

A Thesis submitted for the degree of Doctor of Philosophy

School of Engineering

Cardiff University

June 2010

ProQuest LLC
789 East Eisenhower Parkway
P.O. Box 1346
Ann Arbor, MI 48106-1346

Premixed combustion of alternative fuels under varying conditions of temperature and pressure

Audrius Baganavicius

June 2010

To my wife Dalia, our son Ignas and daughter Rusne

Summary

Growing environmental concerns and global warming issues stimulate the interest of using alternative fuels in power generation especially for gas turbine applications. This experimental and numerical study has been performed to investigate turbulent burning velocities of alternative gaseous fuels at atmospheric and elevated temperature and pressure conditions using Bunsen burner and generic swirl burner.

Five different gases: 100% methane, 85% methane - 15% carbon dioxide, 70% methane - 30% carbon dioxide, 85% methane - 15% hydrogen and 70% methane - 30% hydrogen mixtures have been tested at a range of equivalence ratios at atmospheric and 473 K, 573 K, 673 K temperature and 3 bar, 7 bar absolute pressure conditions.

Bunsen burner and generic swirl burner experiments at atmospheric conditions have been performed in Cardiff University's laboratory. Bunsen burner experiments at elevated conditions have been conducted using High Pressure Optical Combustor at the Gas Turbine Research Centre. Laser Doppler Anemometry has been utilised to determine the velocity profile and turbulence characteristics at the exit of the burner. Planar laser tomography has been used in order to measure the turbulent burning velocity for the different gas mixtures at a range of temperatures and pressures. Laser Induced Fluorescence of OH was used to obtain turbulent and laminar flame images. A generic swirl burner was used to test flashback and blowoff limits of alternative fuels at atmospheric conditions.

Temperature, pressure and CO_2 and H_2 addition to CH_4 effects on turbulent and laminar burning velocity have been found and discussed. Novel turbulent burning velocity determination methods are presented and uncertainties have been discussed. Turbulent burning velocity correlation with nondimensional numbers have been found and flames structures have been analysed.

Acknowledgements

First of all I would like to thank my supervisors Prof. Nick Syred and Prof. Phil Bowen, who encouraged and guided me through the whole process. Their ideas and advice were invaluable source of information, which helped me to study and learn.

I deeply appreciate the help and support of my colleagues Dr Peter Kay, Dr Andrew Crayford, Steven Morris, Terry Treherne and Paul Malpas. Discussions with them and their technical assitance in preparing and making the experiments were crucial in accomplishing this thesis.

I am thankful to my student colleagues Nasser Shelil, Mohammed Abdulsada and Piotr Plaza for fruitful discussions and cooperation.

Finally I would like to thank my wife and our children, for their understanding, patience and tremendous support during the last three years.

This research was financed by the Marie Curie programme Integrated Energy Conversion for Sustainable Environment (INECSE) (MEST-CT-2005-021018). High pressure and temperature research was financed by the European Commission programme Alternative Fuels for Industrial Gas Turbines (AFTUR) (ENK5-CT-2002-00662).

List of publications and conference papers

1. Bagdanavicius A., Bowen P., Syred N., Kay P., Crayford A., Wood J., 2009, "Burning Velocities of Alternative Gaseous Fuels at Elevated Temperature and Pressure", 47th AIAA Aerospace Sciences Meeting, Orlando, USA, ref. AIAA-2009-0229

2. Bagdanavicius A., Bowen P., Syred N., Kay P., Crayford A., Wood J., Sims G. 2010, "Burning Velocities of Alternative Gaseous Fuels at Elevated Temperature and Pressure", AIAA Journal 48(2), pp 317-329

3. Bagdanavicius A., Shelil N., Syred N., Griffiths A. J., Bowen P. J., 2010, "Premixed Swirl Combustion and Flashback Analysis with Hydrogen/Methane mixtures", 48th AIAA Aerospace Sciences Meeting, Orlando, USA, ref. AIAA-2009-1169 (submitted to Journal of Propulsion and Power)

4. Bagdanavicius A., Shelil N., Bowen P. J., Syred N., Crayford A., 2010, "Investigations Of Gaseous Alternative Fuels At Atmospheric And Elevated Temperature And Pressure Conditions", GT2010-23270, ASME Turbo Expo 2010, Glasgow, UK

5. Shelil N., Bagdanavicius A., Griffiths A.J., Roberts P. J., Syred N., 2009, "Flashback analysis of Hydrogen/Methane mixtures for premixed swirl combustion", 16th International IFRF members conference, Boston, USA

6. Shelil N., Bagdanavicius A., Griffiths A. J., Syred N., 2010, "Flashback Limits Of Premixed H2/CH4 Flames in Swirl-Stabilised Combustor", GT2010-23623, ASME Turbo Expo 2010, Glasgow, UK

Contents

List of Figures

List of Tables

Nomenclature

Latin symbols

A	Flame area, m^2
A_z	Zimont's model coefficient
A_T	Wrinkled flame area, m^2
A_L	Cross sectional area, m^2
a, b	Fraction ratio
B	Turbulent combustion model coefficient
c	Progress variable
c_p	Specific heat, $J/(kgK)$
C	Constant
C_D	Fluent coefficient
D	Turbulent combustion model coefficient
D_{eq}	Equivalent nozzle diameter
D_i	Gas diffusion coefficient, m^2/s
D_{ij}	Binary diffusion coefficient, m^2/s
G_x	Axial flux of axial momentum
G_θ	Axial flux of angular momentum
E_a	Activation energy, J/mol
f_c	Flame crossing frequency
f_D	Doppler frequency
f_i	Laser beam frequency
f_s	Scattered laser light frequency
g	Bray-Moss-Libby constant

h	Pixel height, mm
I_0	Stretch factor,
l	Length scale, m
l_0	Integral length scale, m
l_{11}	Longitudinal integral length scale, m
l_k	Kolmogorov length scale, m
l_λ	Taylor length scale, m
k	Number of pixel rows in the image
k_E	Turbulence kinetic energy, m^2/s^2
K^*	Flame stretch rate, $1/s$
K_c	Flame curvature, $1/s$
K_s	Flame strain rate, $1/s$
L_y	Wrinkling length scale
M	Molar mass, g/mol
$\dot{m}$	Mass flow rate, kg/s
N	Number of samples
n	Number of pixels
n_y	The number of flamelet crossings per unit length
$\vec{n}$	Vector normal to flame surface
Q	Heat of reaction, J
p	Pressure, Pa
q_i	Nondimensional heat release
q'	Averaged turbulence intensity, m/s
P	Presure, MPa
P_o	Atmospheric pressure, 0.1 MPa
R^0	Universal gas constant,$J/(molK)$
R_s	Specific gas constant,$J/(kgK)$
$R(\tau)$	Autocorrelation function
R_1, R_2	Flame radii of curvature
R_f	Flame cone radius, m
r	Burner radial position, mm
r_l	Distance between fixed and moving probes, mm

S	Swirl number
S_c	Reaction progress source term, $1/s$
S_L	Unstretched laminar burning velocity, m/s
S_T	Turbulent burning velocity, m/s
S_d	Flame displacement speed, m/s
S_g	Unburned gas velocity in combustion bomb, m/s
S_g^*	Geometric swirl number
S_s	Propagating flame speed in combustion bomb, m/s
t	Time, s
T	Temperature, K
T_0	Inner layer temperature, K
V	Diffusion velocity in conservation equation, m/s
u, v, w	Instantaneous axial, radial and tangential velocity, m/s
$\bar{u}, \bar{v}, \bar{w}$	Mean axial, radial and tangential velocity, m/s
u^*, v^*, w^*	Fluctuating axial, radial and tangentila velocity component, m/s
u', v', w'	Root mean square (RMS) axial, radial and tangential velocity, m/s
u'_k	Effective RMS turbulent velocity
$\vec{u}$	Velocity vector
$\dot{V}$	Volume flow rate, m^3/s
w^*	Pixel width, mm
$\dot{w}$	Chemical reaction rate in the conservation equation,
$\bar{\dot{w}}$	Mean reaction rate,
$\dot{w}_c$	Reaction rate per flamelet crossing,
X_i	Molar fraction
Y_i	Mass fraction

Greek symbols

α	Flame cone half angle
α	Thermal diffusivity, m^2/s
Φ	Equivalence ratio
ϕ_{ij}	Empirical coefficient for viscosity
δ_L	Laminar flame thickness, mm

δ_r	Reaction zone thickness, mm
δ_{ij}	Kronecker delta in the conservation equation,
ϵ	Energy dissipation rate
κ	Wave number
λ	Thermal conductivity, $W/(mK)$
λ_w	Laser light wavelength, nm
ν	Kinematic viscosity, m^2/s
μ	Dynamic viscosity, Pas
Θ	Angle between the incoming laser beams
ρ	Density, kg/m^3
$\rho(\tau)$	Temporal autocorrelation coefficient
ρ_l	Space autocorrelation coefficient
ρ_{11}	Longitudinal autocorrelation coefficient
ρ_{22}	Transverse autocorrelation coefficient
τ_0	Integral time scale, s
τ_c	Chemical time scale, s
τ_k	Kolmogorov time scale, s
τ	Lag time, s
τ_{ij}	Viscous tensor in the conservation equation,
σ	Standard deviation
σ^2	Variance
σ_y	Mean cosine angle
Σ	Flame surface density, $1/m$
ψ	Sample space variable

Non-dimensional numbers

Da	Damköhler number
K	Karlovitz stretch factor
Ka	Karlovitz number
$\mathcal{L}$	Markstein length
Le	Lewis number
Ma	Markstein number

Re	Reynolds number
Sc_t	Turbulent Schmidt number
Ze	Zeldovich number

Subscript

F	fuel
O	oxidiser
R	reactants
a	air
b	burnt
d	deficient reactant
e	efficient reactant
eff	effective
f	flame
g	gas
n	normal
rms	root mean square
st	stoichiometric
t	tangential
u	unburnt

Chapter 1

Introduction and literature review

1.1 Introduction

Industrial gas turbines and burners have been increasingly used for a wide range of applications in industry and for power generation. These processes rely mostly on conventional fuels, such as: oil, natural gas and coal. However existing conventional fuel resources are running short. Proven reserves of remaining conventional liquid fuels are 1342 billion barrels [1]. Therefore at a projected production of around 86.3 million barrels per day (2010) liquid fuel will run out after approximately 43 years [1]. Another conventional fuel, natural gas is also vital source of energy. The International Energy Outlook reported, that proved remaining reserves of natural gas are 177 trillion m^3 [1]. With the natural gas production of 3.15 trillion m^3 per year (2008) [2] natural gas resources should be able to sustain for another 56 years. The most abundant of all fossil fuels is coal. The estimated recoverable reserves of coal are 843 billion metric tones, which gives reserve-to-production ratio 137 years [1]. However fuel reserves are not the only issue. Pollution and global warming are also critical.

With growing concerns regarding global warming and energy security, a new range of alternative fuels are being considered for use in industrial gas turbines [3]. Existing gas turbines for power generation are mostly optimised to burn natural gas. This is well established and an energy efficient technology [4]. Therefore in order to partly replace conventional gaseous fuel, various blends of alternative fuels with natural gas need to be considered.

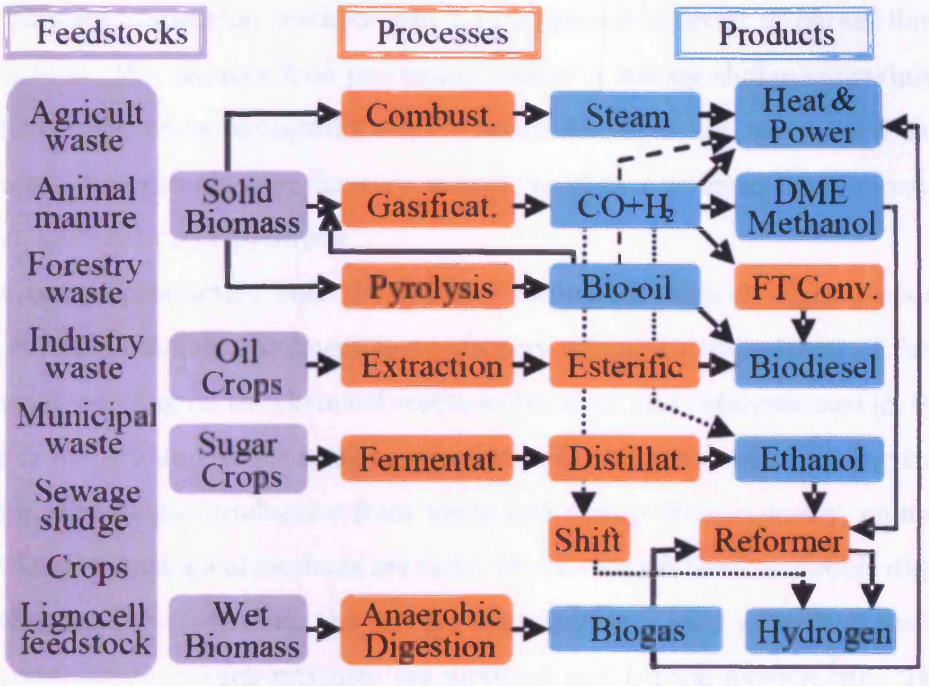

Figure 1.1: *Alternative fuel production methods from biomass [7]*

Gaseous alternative fuels can be divided broadly into two groups; those containing methane diluted with an inert gas, often carbon dioxide and those containing methane or natural gas enriched with hydrogen. Hydrogen is considered as one of the most promising alternative to existing fuels. However the high cost of production of pure hydrogen, safety issues and different combustion characteristics restrict its commercial usage. Instead of using pure hydrogen, hydrogen-methane blends receive more attention as an alternative fuel for power generation applications. The main reason of using hydrogen is related to the reduction of CO_2 emissions so decreasing global warming effects. The second reason is to enhance the utilization of gasified biomass and other by-product gases derived from some industrial processes in the form of producer gases containing mainly H_2 and CO which can also be mixed with methane [5, 6]. The third reason is to improve air quality by replacing petrol or diesel in transport.

Biomass and coal are considered as the most feasible sources for the production of alternative fuels. Biomass conversion methods are presented in Fig. 1.1 [7].

There are mainly three methods for biomass conversion: thermal (thermochemical), biological (biochemical) and extraction. Obviously for different biomass feed-

stock different conversion methods can be considered in order to obtain liquid or gaseous fuels. For instance food processing wastes or sewage sludge are mainly converted to biogas using biological method - anaerobic digestion, whilst solid biomass originating for example from forestry wastes could be converted using direct combustion, gasification or pyrolysis.

For biogas production only thermal and biological methods could be applied. Using thermal biomass treatment methods very different compositions of fuels are obtained depending on the chemical reactions involved and catalysts used [8, 9]. Hydrogen is being found as the main component in the biogas produced using thermal methods. For biogas production from waste and sewage from industry, municipalities and farms, biological methods are used. Due to complicated anaerobic digestion technology and the feedstock, the fuel gas composition is very variable as well. The main components in such mixtures are methane and carbon dioxide [10]. The gas mixture can consist of 30% to 70% of methane with the rest as carbon dioxide. Sometimes small amounts of other gases can be found [11, 12].

Alternative fuels produced from biomass will not be able to replace existing fossil fuels in coming decades. Fossil fuels amount for around 80% of total primary energy supply and will remain so at least until 2030 [13]. Coal is the most abundant fuel and it is recognised that it will retain its importance in the future. However exisiting coal combustion technologies are not acceptable due to large CO_2 emissions and other methods of coal conversion neet to be considered. Similarly as for biomass coal gasification, especially underground gasification, which allows the production of synthetic gas (syngas) directly at the source of the coal bed, are gaining more attention. Although the composition of syngases is variable one of the main components in these gases is hydrogen, which is perceived as clean fuel capable partly replace methane, such reducing the CO_2 emmisions.

1.2 Challenges

Combustion is the only realistic conversion technology allowing the generation of heat and power in gas turbines or large steam boilers, using hydrogen or carbon dioxide enriched fuels. Combustion is the chemical process in which substances mix

with oxygen in the air to produce heat and light [14], and these chemical processes vary depending on the gas composition. Increased hydrogen levels as well as addition of inert or other combustible gas in the methane or natural gas changes the combustion charactersitics. One of the most important fundamental characteristics of the combustion is the burning velocity or the flame speed, which obviously changes with the gas composition.

However not only gas composition influences burning velocity. In most industrial combustors and in gas turbines combustion occurs in turbulent flows. Turbulence by itself is complicated phenomenon, and turbulent combustion becomes even more complex as two interdependant events take place simultaneously. Flow characteristics and regimes have a significant impact on burning velocity and this effect must be evaluated.

In gas turbines combustion reactions take place under high pressure and temperature conditions, which in turn modifies combustion characteristics such as burning velocity. Therefore a greater understanding of the fuel behaviour at different conditions is required and investigation of alternative fuel combustion becomes of primary importance.

1.3 Aims and objectives

This study has been undertaken to evaluate carbon dioxide dilution or hydrogen enrichment effects on turbulent and laminar burning velocities of premixed methane flames at atmospheric and elevated temperature and pressure conditions, using the established Bunsen burner method and a generic swirl burner. The aim of this work is to add to the understanding of the turbulent and laminar burning velocities of alternative fuels over a range of equivalence ratios, temperatures and pressures.

Objectives:

- Develop and validate the new flame image processing method allowing to calculate burning velocity using Bunsen burners.
- Develop and validate the novel burning velocity calculation method using generic swirl burner.

- Analyse turbulence effects on burning velocity at atmospheric and elevated temperature and pressure conditions.
- Evaluate burning velocity variation due to temperature and pressure effects.
- Analyse temperature and pressure effects on turbulent flame structure.

In this work the investigation of turbulent and laminar burning velocities of methane - carbon dioxide and methane - hydrogen mixtures under atmopheric and elevated temperature and pressure conditions are discussed. Novel methods of calculation of turbulent burning velocity are presented and uncertainties emphasised.

1.4 Literature review

There have been many attempts to investigate laminar and turbulent methane flames [15–17], methane and carbon dioxide mixtures [18], methane and hydrogen mixtures [19–23] and even synthetic gas fuel mixtures [24] at atmospheric and non atmospheric conditions.

Laminar burning velocity of methane - air flames was investigated by Andrews and Bradley in early 1970s [15, 25] using a propagating flame method. They reviewed and critically assessed different burning velocity measurement methods [15]. Later they presented their results obtained using propagating flame methods and compared them with the data of other works [25]. Significant discrepancies between the laminar burning velocity results were found. The authors argued that these variations arose due to the quenching of the flame at tube wall or burner rims, i.e. the measurement method had affected the results.

Another review of different experimental burning velocity measurement methods was presented by Rallis and Garforth [26] in the 1980s. They assessed different methods and compared the experimental results and available numerical calculations. They concluded the uncertainty of measurements narrowed and suggested a benchmark value 0.37±0.2 m/s for stoichiometric methane - air mixture at 1 bar and 298 K.

Later the laminar methane flames were investigated by Egolfopoulus et al. [16] under both reduced and elevated pressures using counterflow flame methodologies.

Their study illustrated the influence of pressure on the laminar burning velocity, which decreases with increasing pressure.

In parallel to laminar burning research the investigations of the burning velocity of turbulent flames were undertaken. One of the first papers, where all known measurements of turbulent burning velocity values were reviewed, was that of Abdel-Gayed et al. [27]. The authors scrutinised all the experimental data and proposed the correlation of S_T/S_L vs u'_k/S_L depending on the straining rates and Le numbers. Later Bradley et al. [28] presented a more exact correlation based on known experimental data (Fig. 1.2), which involved a Karlovitz stretch factor K and Le number:

$$\frac{S_T}{u'_k} = 0.88(K \cdot Le)^{-0.3} \tag{1.1}$$

Later however Bradley et al. suggested a slightly modified correlation [29] and even proposed that Ma number should replace Karlovitz stretch factor K in these correlations [30].

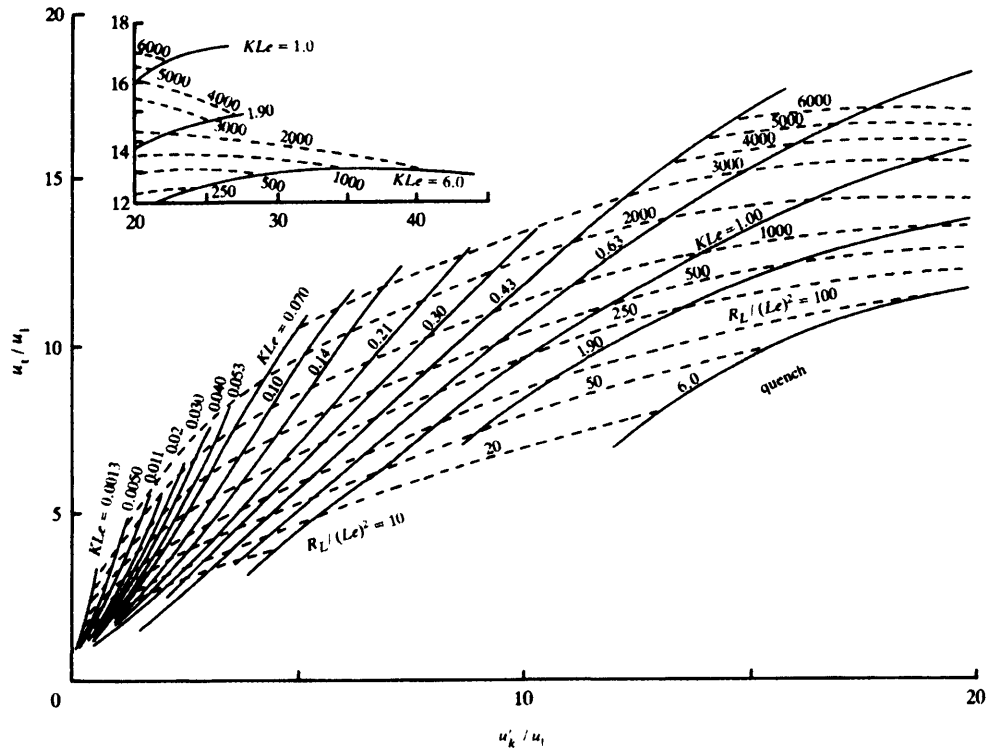

Figure 1.2: *Correlation of turbulent burning velocities proposed by Bradley et al. [28]*

Turbulent burning velocity modelling has always been a focus of combustion

researchers. Lipatnikov and Chomiak in their extensive review paper presented around 17 different models for predicting S_T [31]. It was noted by the authors that the well-established trends:

- an increase in S_T by u';

- an increase in S_T and dS_T/du' by S_L with the scaling component of around 0.5 - 0.8;

- an increase in S_T by pressure despite the decrease in S_L.

must be predicted by any model of turbulent combustion [31]. The authors concluded that only a restricted number of models can predict all qualitative trends. These included those of Zimont [32] and Peters [33]. Zimont's model is widely used in numerical computation and can be expressed using the equation:

$$S_T = Bu'Da^{0.25} \tag{1.2}$$

where B is the model constant.

Peters' model is more complex and is expressed using the equation:

$$S_T = S_L \left\{ 1 - \frac{0.39 l_0}{2\delta_L} + \left[\left(\frac{0.39 l_0}{2\delta_L} \right)^2 + 0.78 \frac{u' l_0}{S_L \delta_L} \right]^{0.5} \right\} \tag{1.3}$$

For comparison Zimont's and Peters' model are represented in Fig. 1.3. More detailed discussion about various models and review of experimental results of turbulent burning velocity measurements can be found in the Lipatnikov and Chomiak paper [31].

Pressure and temperature effect on turbulent methane flames were extensively studied by Kobayashi et al. [17, 34–36]. Kobayashi [17] investigated turbulent flames using a Bunsen burner technique and showed that turbulent and laminar flame ratio S_T/S_L is pressure dependent and rises with increasing pressure. The study also showed that flame shape becomes more wrinkled at higher pressures. In later investigations Kobayashi et al. proposed the correlation for S_T/S_L which encompassed the pressure effect [36]:

$$\frac{S_T}{S_L} = 5.04 \left(\frac{P}{P_o} \frac{u'}{S_L} \right)^{0.38} \tag{1.4}$$

where P is required pressure and P_o is atmosperic pressure 0.1 MPa.

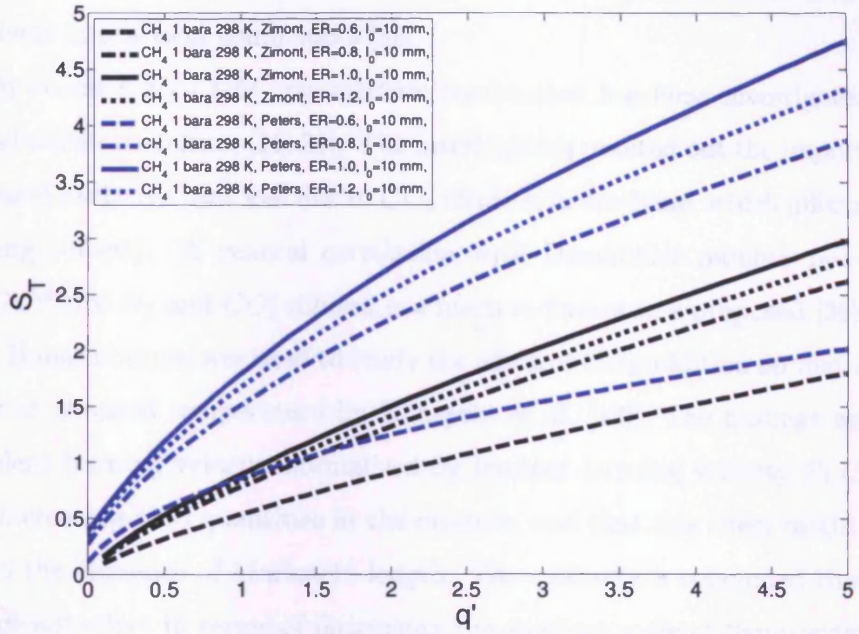

Figure 1.3: *Zimont's [32] and Peters' [33] turbulent burning velocity models*

Increasing demand for more sustainable fuels stimulated research into alternative fuels such as methane diluted with carbon dioxide or enriched with hydrogen. Carbon dioxide dilution reduces the burning velocity of the laminar flame, and this can be quantified through modelling tools such as Chemkin. However more detailed investigation is necessary for the turbulent flames, especially for pressure conditions greater than atmospheric. Different aspects of methane and carbon dioxide mixtures were investigated at different conditions [18, 21, 37–42].

Laminar flames of methane - carbon dioxide mixtures at 1 bar absolute and 298 K were tested in a combustion vessel at near-zero gravity conditions [37]. The results indicated that the laminar burning velocity of pure methane is around 37 cm/s. The CO_2 addition reduced burning velocity considerably. For instance the burning velocities of 80% CH_4 - 20% CO_2 mixture and 50% CH_4 - 50% CO_2 mixture were around 32 cm/s and 18 cm/s respectively. Based on these experiments the authors derived the coefficients for a quartic fitting equation, adapting it for a wide range of temperatures (295 K - 454 K) and pressures (0.5 bar - 10.4 bar).

Consideration of landfill gas, consisting mostly of CH_4 and CO_2, in the stagnation flow configuration revealed that laminar burning velocities and extinction

strain rates reduce in comparison with pure methane, which could create stability problems in practical combustors [38].

Turbulent CH_4 - CO_2 gas mixture combustion has been investigated in a fan-stirred cruciform burner [21, 39]. The investigators pointed out the importance of an increased radiative heat loss due to CO_2 dilution in methane, which affects turbulent burning velocity. A general correlation with Damköhler number $S_T - S_L/q' = 0.06Da^{0.58}$ for N_2 and CO_2 diluted gas mixture flames was proposed [39].

A Bunsen burner was used to study the effect of CO_2 addition on methane flames in air at elevated temperature by Kobayshi et al. [18]. The findings showed that turbulent burning velocity normalised by laminar burning velocity S_T/S_L reduces with increasing CO_2 quantities in the mixture, and that this effect might be caused due to the influence of Markstein length. The researchers concluded that CO_2 has "significant effect in terms of decreasing the smallest scale of flame wrinkles", and that this could possibly restrain oscillations in combustion systems with exhaust gas recirculation.

More recent work on laminar and turbulent flames conducted at elevated temperature and pressure of CH_4 - CO_2 gas mixtures was reported by Cohe et al. [42]. The comparison of laminar experimental results with Chemkin numerical calculations using the Premix code with the GRI-Mech v3.0 kinetic mechanism, showed modest discrepancies in estimating S_L at increased pressures. Turbulent flame image analysis showed that flame wrinkling parameters and flame surface density did not depend on CO_2 addition and that the pressure had more pronounced effect on flame structure. It was concluded that S_T/S_L increases with pressure and CO_2 addition rate.

Turbulent hydrogen and hydrogen enriched flames are of great interest for the combustion community. During the last decades significant progress has been achieved in understanding of methane as well as hydrogen flames. The hydrogen or hydrogen enriched premixed fuel combustion at atmospheric conditions and at elevated pressure conditions for laminar and turbulent flames were studied experimentally and numerically by many researchers [19–24, 43–56]. Most of these investigations were performed using propagating flames. All investigations of laminar and turbulent flames show an increase of the burning velocities as a result of hydrogen addition to

methane.

Kido et al. published their experiments performed with two components mixtures consisting of methane and hydrogen and propane and hydrogen [23]. They concluded that turbulent burning velocity was considerably increased for lean mixtures by hydrogen enrichment, however it was not always the case for rich mixtures. These findings were in good agreement with the observations of other investigations [22, 57].

Mandilas et al. [22] performed experiments with methane - hydrogen and iso-octane - hydrogen mixtures. Laminar and turbulent propagating flames at pressures up to 5 bar were investigated. They reported that hydrogen enriched methane mixture (30% by volume) approximately doubled turbulent burning velocity for lean mixtures, however no changes in turbulent burning velocity for rich mixtures were found. They concluded that hydrogen addition has a larger effect on burning velocity for lean flames and little effect for rich flames. Similiar findings at elevated temperature and pressure conditions were reported in [41].

Natarajan et al. [24] performed the experiments on $H_2/CO/CO_2$ gas mixtures at atmospheric conditions and at elevated temperature and pressure conditions. They used Bunsen flame and one-dimensional stagnation flame to calculate the laminar flame speed. Their research revealed that GRI-Mech v3.0 kinetic mechanism and experimental results were in good agreement for low hydrogen content mixture at ambient conditions. For the lean gas mixtures with higher hydrogen amount GRI-Mech uderpredicted burning velocity. The same findings were reported by di Sarli and di Benedetto [5], who investigated hydrogen effect on methane flames, and Ströhle and Myhrvold [58], who evaluated chemical kinetic mechanisms for hydrogen combustion at atmospheric and elevated pressure conditions.

Griebel et al. performed experiments at high temperature and pressure conditions [19]. They investigated lean blowout limits and NO_x emissions for lean premixed methane - hydrogen flames. The experiments showed that lean blowout limit was extended by adding hydrogen. They concluded, that because of the extension of lean blowout limit the lower NO_x emissions could be achieved due to lower combustion temperature.

Interesting results have also been obtained by Lafay et al. [52]. They used a V-shape laminar flame to investigate hydrogen addition effect on methane laminar

flame thickness using Rayleigh scattering thermometry. They compared experimental data with numerical calculations and concluded that hydrogen addition decreased flame thickness, which agreed with numerical calculations using GRI-Mech [59], San Diego [60] and Dagaut [61] chemical kinetic mechanisms.

The recent investigations of turbulent premixed methane - hydrogen flames by Halter et al. [20], Shy et al. [21] and Fairweather et al. [55] added to the understanding of hydrogen enrichment effect to turbulent combustion. Halter et al. performed the calculations of the flame structure quantities for hydrogen enriched methane flames at elevated pressure. An increase in S_T/S_L with hydrogen addition for elevated pressures of 3 and 5 bar was observed. They concluded that flame surface density increases with increase of hydrogen mole fraction in the mixture.

Shy et al. [21] presented $(S_T - S_L)/u'$ correlations with Da number for lean mixtures. The experimental results for different gas mixtures are presented in Fig. 1.4.

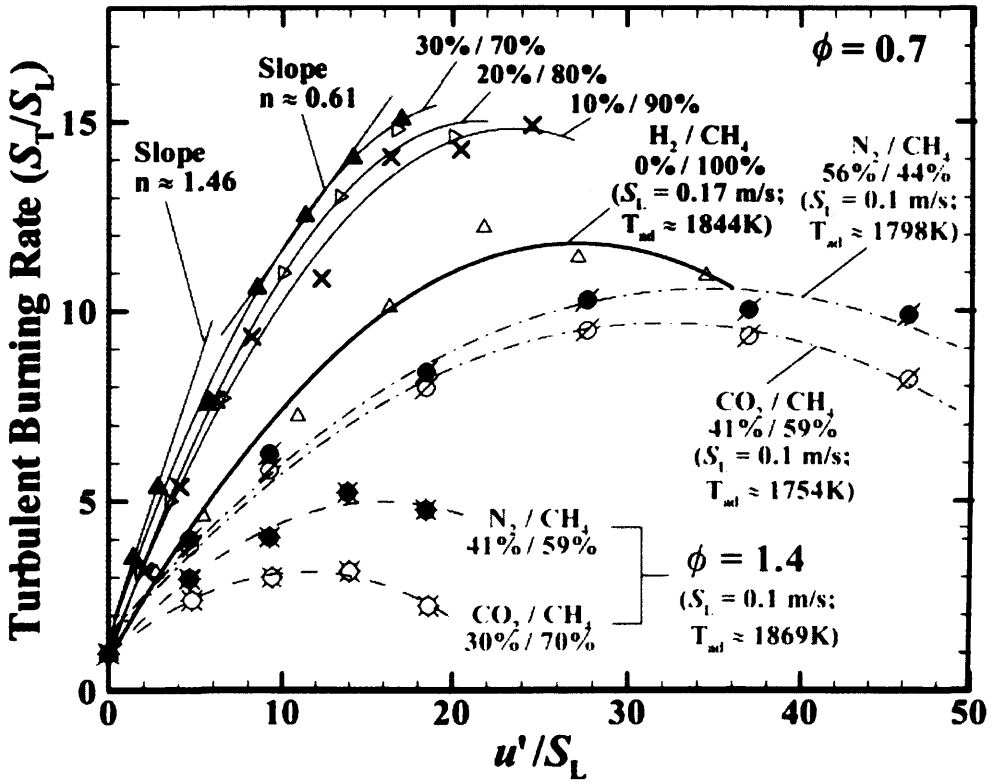

Figure 1.4: *Experimental results of Shy et al. [21]*

The latest experiments of Fairweather et al. [55] performed in a fan stirred bomb revealed a little influence of hydrogen addition to the burning velocity of rich methane - hydrogen mixtures. However a large impact on burning velocity was

observed for lean mixtures. They also presented S_T correlations with Ka number.

While hydrogen enriched fuel combustion technologies are under development, Lean Premixed (LP) combustion allowing the reduction of pollution emissions, particularly NO_x, is widely used in practical applications. LP combustion is mainly achieved by using swirl-stabilised combustion. It reduces the flame temperature so reducing thermal NO_x emissions. However LP combustion is often accompanied by stability problems. Premixed flames are naturally more susceptible to static and dynamic instability due to a lack of inherent damping mechanisms [62]. Therefore the understanding of swirl-stabilised combustion is an important prerequisite for the development of novel technologies.

Combustion in swirl burners has been studied for decades and the reviews can be found in the works of Syred [63, 64], Gupta et al. [65], Huang et al. [66, 67] and others. Vanoverberghe [68] and Coghe et al. [69] have demonstrated the reduction of emissions by increasing swirl, producing flames stabilized by the surrounding structures, such as inner and outer recirculation zones, formed as a consequence of the dynamics of the swirling mechanism. Huang et al. [66], and Huang and Yang [67] studied combustion dynamics and instability in lean premixed swirl-stabilized combustors. They concluded that in combustion systems the dominant mechanism responsible for driving unsteady flow oscillations arise from either heat release or gasdynamic fluctuations, or both [67].

Valera-Medina [70, 71] investigated coherent structures in swirl flows. He performed flashback analysis [70] for a swirl burner using different exit geometries and concluded that there are two types of flashback. Type 1 flashback occurred due to the backwards propagation of Central Recirculation Zone (CRZ), and type 2 flashback occurred due to radial propagation into the outer swirl chamber from the exhaust sleeve. He argued that type 2 flashback occurred as a consequence of S_T, boundary layer flame propagation and Combustion Induced Vortex Breakdown (CIVB).

CIVB and its effect on flame flashback has been discussed by Kröner et al. [72]. They stated that there are four causes initiating flame flashback in swirl burners:

- Flame propagation in the boundary layer;
- Turbulent flame propagation in the boundary core flow;
- Combustion instabilities;

- Combustion induced vortex breakdown.

They derived the flame quench factor as the ratio of flame chemical time and mixing time, and emphasised that using this factor, flashback behaviour of the burner can be characterised.

Several studies of the fuel dilution effect, oscillations, and combustion instability in swirl burners have been recently conducted [73–75].

The gas turbine combustor operability issues: blowout, flashback, combustion instability, and autoignition were discussed by Lieuwen et al. [73]. The researchers reviewed the fuels and their properties emphasising the differences in combustion properties of individual gases compared to combustions properties of mixtures of the same gases. They have used the Damköhler number, which can be expressed as the inverse of the quench factor, to relate the blowout limits, and showed that blowout occurs at $Da = 0.6$ for a number of permutations of $CO/H_2/CH_4$ blends. Turbulent burning velocity behaves in a nonlinear manner as the fuel mixture changes, and a possible reason for that are the changes in chemical kinetic rates and radiative heat transfer [73].

The oscillation mechanism in the industrial swirl combustor were investigated by Dhanuka et al. [74]. PIV and PLIF techniques were used to obtain velocity profiles and images. The authors concluded that the lean premixed prevaporised combustor, used in the experiments, at off-design conditions exhibits unsteady behavior if the ratio of the main fuel flow rate to the pilot fuel flow rate exceed a critical value. Two major recirculation zones Primary Recirculation Zone (PRZ) and Lip Recirculation Zone (LRZ) were identified, both having a stabilising effect. The low frequency unsteadiness found during the experiments was driven by periodic flashback oscillations through the premixed reactants that fill the Corner or External Recirculation Zone (ERZ).

The premixed turbulent combustion burning rate determination has a great practical importance, however experimental investigation is not always feasible. Therefore premixed turbulent models become more important. The closures of chemical source term in different models are of great importance and these models rely ultimately on experimental research [76]. The necessity to validate modelling results with experimental findings arises. In some models the flame surface density Σ,

which relates turbulent and combustion interactions is used. It can be related with turbulent burning velocity S_T [76, 77]:

$$\frac{S_T}{S_L} = I_0 \int_{-\infty}^{\infty} \Sigma d\eta \tag{1.5}$$

where I_0 is the flame stretch factor, η is coordinate normal to $c = 0.5$.

Flame surface density, turbulent flame thickness and other flame structure quantities are important parameters in the numerical investigation and modeling. It has been recommended to create and record the database of these values for each flame category [77]. Many researchers performed experiments to investigate these quantities [44, 76, 78–90].

Deschamps et al. [78] investigated Bunsen flames and propagating flames in a spark-ignition engine. They calculated two dimensional flame surface densities and flame front orientation angles, which were used to obtain three dimensional flame surface density values. The Bray-Moss-Libby coefficient $g/\sigma_y L_y$ was calculated using a fractal model. In their conclusions they pointed out that the cosine of flame front orientation angle was about 0.7, and that flame surface density did not vary much for the range of u'/S_L from 0.25 to 2.0.

Shepherd [79] investigated flame surface density and burning rates of the V-shape flame. He proposed that burning rate, $W = S_T/S_L$, can be estimated from the equation $W = \delta_T \Sigma_{max}$. Later Shepherd et al. [80] calculated burning rates using the conditional mass flux method. The scalar and conditional mass flux methods were adopted by Shepherd and Cheng to investigate methane-air flames in a low swirl burner [76]. They concluded that scalar measurements of the flame surface density and conditional mass flux method gave very different results in many investigations, and displacement and consumption speed must be distinguished. They proposed that flame surface measurements should be used to appraise theoretical models.

In recent investigations Gülder and Smallwood [86] investigated Bunsen flames at medium and high turbulence intensities. They found that flame surface density profile as a function of progress variable did not show any dependence on turbulence intensity, and the integrated flame surface density was insensitive to turbulence intensity as well. They concluded that increases in the flame surface density by turbulence may not be the dominant mechanism for flame velocity enhancement in

the flamelet combustion regime.

In their latest research Halter et al. [87] analysed flame surface density in turbulent premixed combustion. They investigated lean methane Bunsen flames at elevated pressure. They tested two formulations linking two dimensional and three dimensional flame surface densities. They concluded that the assumption of cosine of the flame front orientation angle of 0.6 led to underestimation of burning rate for atmospheric pressure flames and overestimation for high pressure flames.

An extensive reserch of the flame stuctures of methane and hydrogen flames was conducted by Chen and Bilger [44, 88–90]. They argued that flame brush thickness may not be correlated with the turbulence integral length scale if the eddy/flame-front interaction time, which is considered as the residence time of large-scale eddies in the local turbulent flame brush, is smaller than the eddy turnover time [88]. They also proposed a slightly modified Borghi-Peters diagram for Bunsen burner flames [89].

Although many investigations were conducted and good progress was achieved in turbulent flame research "only partially do we have answers to the fundamental questions" [91] and "the real challenges actually lie ahead" [92].

Chapter 2

Theoretical background

2.1 Laminar flame characteristics

The research of the premixed laminar flames is the basis for the investigation of the premixed turbulent flames. The investigation of the turbulent flames in flamelet and thin reaction zone regimes is based on theories developed for laminar flames. In this section the important quantities of laminar flames with respect to premixed turbulent flames are discussed.

First premixed laminar flame experiments were performed in the XIX century [93]. A Bunsen burner was used for this purpose, but later many more different techniques were developed [26]. Through experiments and the study of chemical and physical processes classical laminar flame theories were developed. One of the most important was the thermal theory of Mallard and Le Chatelier. According to this theory the flame could be divided into two zones: preheat zone and reaction zone. In the preheat zone the gases are heated to ignition temperature and in the reaction zone the chemical reactions of combustion take place. According to this theory laminar burning velocity S_L is proportional to chemical reaction rate, and based on the Arrhenius law it can be expressed [93]:

$$S_L \propto e^{-\frac{E_a}{2R_u T}} \tag{2.1}$$

Based on Mallard and La Chatellier theory Zeldovich, Frank-Kamenetsky and Semenov developed a comprehensive theory of premixed laminar flames, which was based on adoption of two flame zones. They used energy equation and species

conservation equation to relate S_L with chemical reaction rate. In this theory the basic relationship 2.1 remains the same, however temperature T is replaced with flame temperature T_f. This theory is valid for high activation energy reactions and it does not predict very accurate results, but shows the trend of the flame propagation speed [93].

In later research Tanford and Pease [94] proposed a hypothesis that the diffusion of radicals may play an important role for laminar flame speed. It was assumed that the diffusion of active radicals into the unburned gas, but not the temperature gradient, is of major importance in determining the burning velocity. Later Hirschfelder encompassed thermal and diffusion theories.

With the development of high speed computers the traditional theories and analytical methods have been replaced with numerical models, which can be programmed to solve complicated continuity equations. For the constant pressure and low Mach number flames the conservation equations can be derived [95]:

- Mass conservation

$$\frac{\partial \rho}{\partial t} + \frac{\partial(\rho u_i)}{\partial x_i} = 0 \tag{2.2}$$

- Species conservation, for $k = 1$ to $N - 1$, where N is number of species

$$\frac{\partial \rho Y_k}{\partial t} + \frac{\partial}{\partial x_i}(\rho(u_i + V_{k,i})Y_k) = \dot{w}_k \tag{2.3}$$

- Momentum

$$\frac{\partial}{\partial t}\rho u_j + \frac{\partial}{\partial x_i}\rho u_i u_j = -\frac{\partial p}{\partial x_j} + \frac{\partial \tau_{ij}}{\partial x_i} \tag{2.4}$$

here

$$\tau_{ij} = -\frac{2}{3}\mu\frac{\partial u_k}{\partial x_k}\delta_{ij} + \mu\left(\frac{\partial u_i}{\partial x_j} + \frac{\partial u_j}{\partial x_i}\right) \tag{2.5}$$

- Energy

$$\rho c_p \frac{DT}{Dt} = -\sum_{k=1}^{N} h_k \dot{w}_k + \frac{\partial}{\partial x_i}\left(\lambda\frac{\partial T}{\partial x_i}\right) - \rho\frac{\partial T}{\partial x_i}\left(\sum_{k=1}^{N} c_{p,k} Y_k V_{k,i}\right) \tag{2.6}$$

The laminar flame is assumed to be a steady one dimensional combustion problem, therefore these equations can be further modified and the set of equations obtained. The momentum equation is not necessary anymore.

$$(\rho u_n)_b = (\rho S_L)_u \tag{2.7}$$

$$\frac{\partial}{\partial x}(\rho(u + V_k)Y_k) = \dot{w}_k \tag{2.8}$$

$$\rho c_p u \frac{\partial T}{\partial x} = -\sum_{k=1}^{N} h_k \dot{w}_k + \frac{\partial}{\partial x}\left(\lambda \frac{\partial T}{\partial x}\right) - \frac{\partial T}{\partial x}\left(\rho \sum_{k=1}^{N} c_{p,k} Y_k V_k\right) \tag{2.9}$$

These equations can be solved if the model for the reaction rate $\dot{w}_k$ and for the diffusion velocities V_k is provided and proper boundary conditions are known. Solving these equations yields S_L [95–97].

2.1.1 Laminar burning velocity

One of the most important laminar flame characteristics is laminar flame speed or laminar burning velocity S_L, which is the property of the mixture, "indicating its reactivity and exothermicity in a given diffusive medium" [98]. Many different experimental methods can be applied to measure S_L [26], however measurement results differ depending on the measurement techniques [15, 25, 99]. However S_L varies depending on temperature and pressure [16], therefore numerical calculation tools are often used to calculate laminar flame burning velocity, saving time on experiments.

The main objective of the laminar flame theory is to define the laminar burning velocity S_L. The classical device to research laminar burning flames is the Bunsen burner (Fig. 2.1) [100].

The unburned gas velocity v_u can be split into two components tangential velocity $v_{t,u}$ and normal velocity $v_{n,u}$ (Fig. 2.1). Due to mass conservation the mass flow ρv must remain the same for burnt and unburnt gases, although ρ changes due to the gas expansion, therefore $(\rho v_n)_u = (\rho v_n)_b$. Hence the normal component of unburnt gas mixture can be expressed $v_{n,b} = v_{n,u}\rho_u/\rho_b$. Tangential velocity components of burnt and unburnt gases are equal $v_{t,u} = v_{t,b}$ since they are not affected by gas

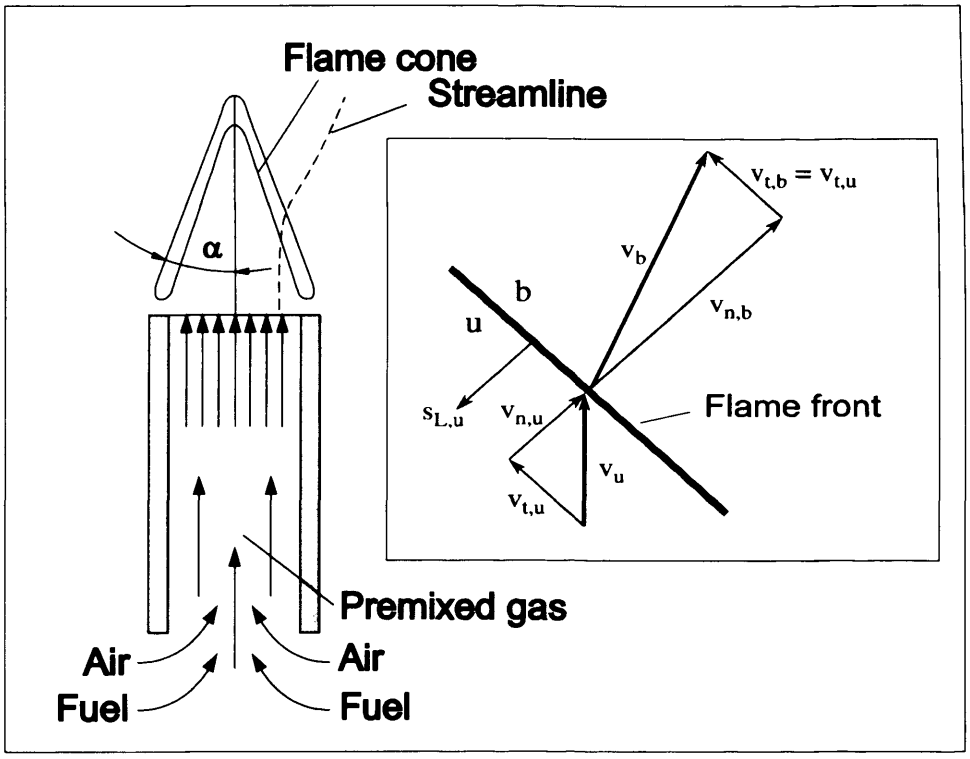

Figure 2.1: *Bunsen burner and kinematic balance scheme taken from [100].*

expansion. The flame front is stationary, therefore the burning velocity S_L must be equal to normal component of the unburnt gas mixture $S_L = v_{n,u}$. If the angle α is known, then $v_{n,u} = v_u sin\alpha$, and the laminar burning velocity can be calculated $S_L = v_u sin\alpha$.

With the development of digital imaging and image processing methods new opportunities arose. A new method of flame image processing was proposed for Bunsen type burners [1]. The method consists of several steps. At first digital images of the flame are taken. As laminar flames are stable it is sufficient to take one or few images. The raw flame images are then converted to the binary images, where each pixel obtains a value of 1 in the flame region or value 0 in the outer region. The flame front is then rotated around its axis and the area of the flame A is found. When the mass flow rate and the density of the air/gas mixture are known then S_L can be easily calculated using the equation. Full description or this method and application is discussed in chapter 4.

Another stationary flame method used to investigate laminar flame velocity is

[1]Private communication with Dr P. Kay from Cardiff University, November 2007

the flat flame burner method. The flat flame burner consists of a vertically placed pipe and a porous metal plate mounted on the top of the pipe. The gas mixture is delivered through the pipe and ignited just above the plate. The oxidiser and fuel mixture flow rate is adjusted in order to obtain a flat flame just above the porous plate. The flame is stabilised above the burner and it is normal to the gas mixture flow direction. In order to avoid atmospheric effects an inert gas can be supplied around the main burner, thus isolating flame from the environment. As the flame area is well defined the S_L can be calculated by dividing volumetric flow rate by the flame area. However this method has disadvantages, which arise due to heat transfer from the flame to the burner. The flame is inherently nonadiabtic [98], therefore corrections must be made in order to obtain a theoretical S_L. The heat loss reduction by increasing the flow rate can distort the flame surface [98]. The flame can be stabilised by changing the heat loss rate by cooling. Varying the gas flow rate and recording the cooling rate needed to obtain a stable flame the S_L dependence on heat loss can be calculated. As it is not possible to achieve the stable flame at zero heat loss, theoretical S_L value must be found by extrapolating. Further development of the flat flame burner, the heat flux burner method developed by de Goey et al. [101], allowed the circumvention of this problem.

The heat flux burner method is based on the compensation of the heat loss by a heat gain of the unburnt gases when they pass through the burner plate [101]. This compensation stabilises the flame above the burner. At these conditions, when there are no heat gain and loss the flame becomes adiabatic, and laminar burning velocity equals the inlet velocity of the gas mixture. However as it is difficult to adjust the gas mixture velocity accurately in practice, the S_L is calculated by interpolating values towards zero heat flux [51, 102].

One of several propagating flame methods to calculate the S_L is the spherical combustion bomb method, which has been widely used by many researchers. The main distinction of this method is that the flame front propagates in space. Using this method the gaseous mixture of air or oxidiser and the combustible gas is prepared in the spherical or cylindrical vessel. The vessel must be equipped with the windows to observe the flame propagation. The mixture is ignited with the spark in the centre of the vessel and the flame front propagation speed $S_s = dr_f/dt$

is recorded. As the flame propagates towards the vessel wall it creates pressure rise and temperature changes, which must be taken into account [103]. There are several expressions to calculate S_L with respect to unburned gases. In equation $S_L = \rho_b/\rho_u S_s$ the expansion coefficient (density ratio) must be properly determined. The determination of ρ_b is the difficult task and accurate experimental or numerical methods must be used. Another equation $S_L = S_s - S_g$ involves unburnt gas velocity S_g. This velocity can be measured directly [25] or indirectly. The combustion bomb method has also been used to investigate turbulent flames. For this purpose additional fans are installed to create turbulence. The applications of using combustion bombs for turbulent flame research are described elsewhere [22, 53, 104, 105].

Another propagating flame method, used for laminar flame research, is the cylindrical tube method. Using this method the tube is placed vertically in order to avoid buoyancy effect. The gas mixture is ignited at an open pipe end on the top. The flame front travels downwards, towards the gas mixture supply pipe. The flame front travel speed is equal to S_L. The main drawback of this methods is that the flame front and wall interaction effect must be carefully determined. However it is doubtful if this estimation can be accurately obtained [26, 106]. Despite the disadvantages this method has been used not only in laminar flame investigations, but also in turbulent flame research [21, 39, 107–109].

Numerical computation is often used in flame research as a replacement for analytical calculations and experiments. Numerical computation models and various chemical kinetic mechanisms have been validated extensively. Premix [110] is one of the widely used numerical codes. Fig. 2.2 shows the results of computation, obtained using Chemkin-Pro software and Premix code. Temperature, unburnt fuel fraction, OH and CH radicals mole fraction variation along the flame at one particular equivalence ratio are shown.

Typical results of laminar flame burning velocity S_L calculations at atmospheric conditions, obtained using Chemkin-Pro are presented in Fig. 2.3.

In this work Chemkin-Pro [111] software and Premix code [110] have been used to define laminar burning velocities at atmospheric conditions and at elevated pressure and temperature conditions.

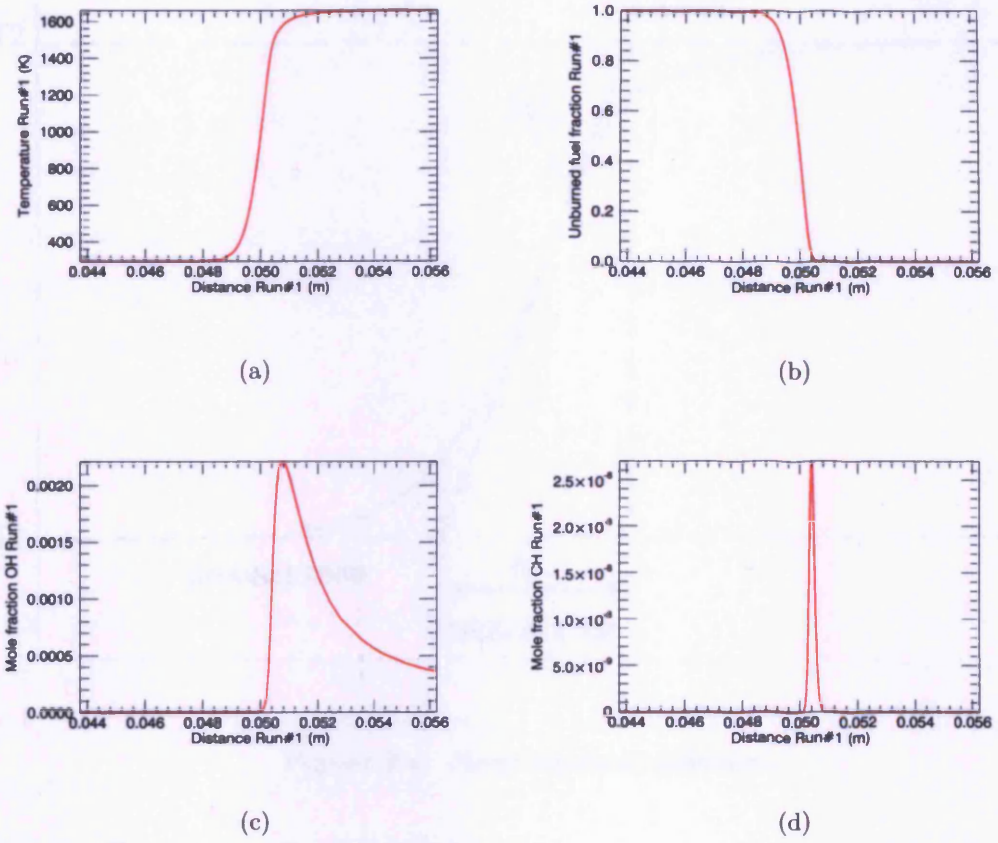

Figure 2.2: *Numerical computation results of CH_4 using Chemkin-Pro. a) temperature profile; b) fuel fraction c) OH concentration; d) CH concentration.*

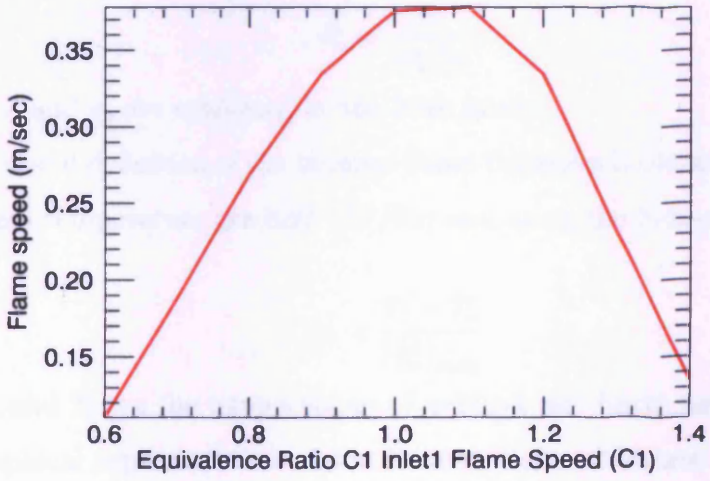

Figure 2.3: *Flame speed results of CH_4 computed using Chemkin-Pro.*

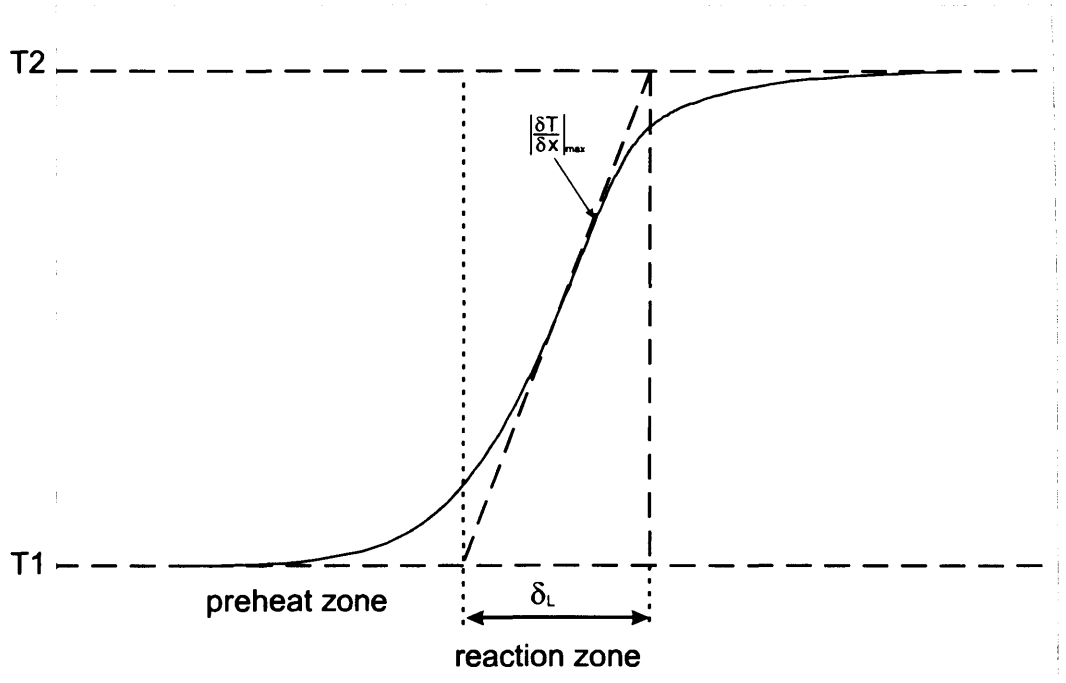

Figure 2.4: *Flame thickness definition.*

2.1.2 Laminar flame thickness

Laminar flame thickness is an important characteristic. It can be computed using different methods. The fast approximation of the laminar flame thickness δ_L can be done using the equation:

$$\delta_L = \frac{\lambda}{\rho c_p S_L} \tag{2.10}$$

Here ρ, λ and c_p are evaluated in the fresh gases.

A more useful definition of the laminar flame thickness is obtained by calculating the maximum temperature gradient $|\partial T/\partial x|$ and using the formula:

$$\delta_L = \frac{T_b - T_u}{\left|\frac{\partial T}{\partial x}\right|_{max}} \tag{2.11}$$

Here T_u and T_b are the temperatures of unburnt and burnt gases.

The graphical representation of the laminar flame thickness definition is presented in Fig. 2.4.

The most important task defining the laminar flame thickness using temperature

gradient method is to find the maximum of the temperature gradient. Incorrectly estimated temperature gradient gives too large δ_L values.

There are other methods to estimate laminar flame thickness. One of the simplest methods is to define the distance over which the temperature starts to change from initial unburnt gas temperature to burnt gas temperature, and drawing the tangential line to calculate its gradient. However this method produces global flame thicknesses [95], which are much larger than estimated using the temperature gradient method.

2.2 Turbulent flame characteristics

The theory of turbulent flames is based on the application of the methods used to investigate laminar flames. For laminar flames the chemistry plays the important role, while for turbulent flames the interaction of chemistry and turbulence is of the greatest importance. The turbulence distorts the flow, therefore the normally smooth flame front becomes wrinkled. The wrinkling of the flame front changes the flame behaviour. To solve the turbulent flame problems using analytical solutions is very difficult as the turbulence itself is very complicated. Many attempts to predict the behaviour of turbulent flames have been made by many researchers [32, 112], who tried to find the solution for the different turbulent flames. However the practice shows that particular models predict turbulent flames well only in certain conditions.

2.2.1 Statistical description of turbulence

A turbulent flow velocity field is random [113], which means that it may be best described using statistical methods. For laminar flows the velocity component u can be calculated using Navier-Stokes equations. However since velocity component u is randomly variable in turbulent flows its value is inherently unpredictable [113]. Therefore the theory can only predict the probability of u value. This is often presented as the mean value $\bar{u}$ of random events together with fluctuating component u^*. Some typical turbulent flow velocity component fluctuations as a function of time are presented in Fig. 2.5.

The mean velocity $\bar{u}$ is the averaged instantaneous velocity u over time t. This

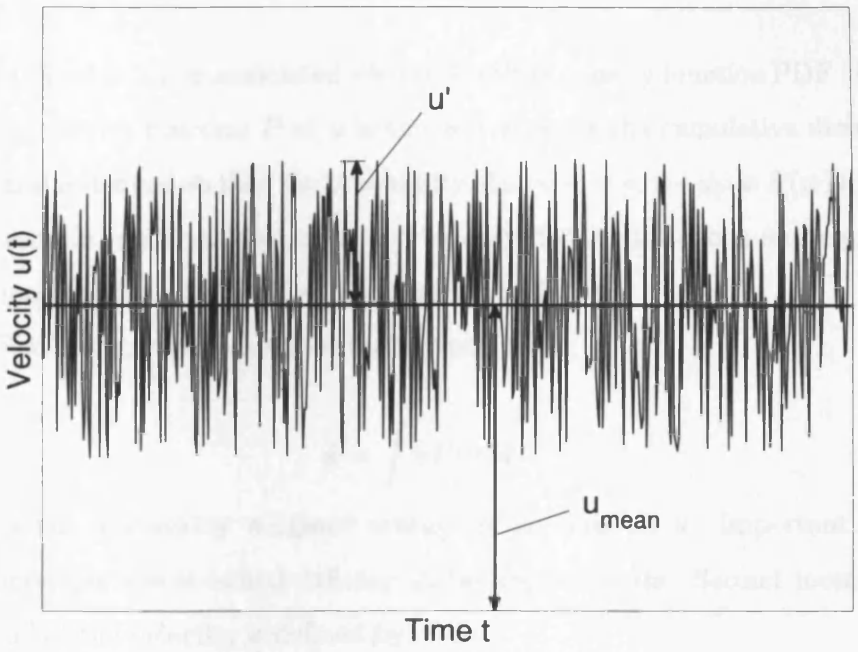

Figure 2.5: *Turbulent velocity fluctuation.*

is called Reynolds averaging. Another often used method of averaging variables is mass weighted averaging (Favre averaging). The conventional time averaging is defined:

$$\bar{u} = \lim_{t\to\infty} \frac{1}{t} \int_0^t u(t)dt \tag{2.12}$$

The upper limit t should be long enough finite time for the integral to converge. This is valid if $\bar{u}$ is independent of time. In practice an ensemble average compiled from different realisations is often used, especially when large velocity oscillations exist. In this case for N realisations of u the ensemble average can be defined:

$$\bar{u} = \frac{1}{N} \sum_{j=1}^{N} u_j \tag{2.13}$$

The axial velocity component u can be decomposed into two parts: mean velocity $\bar{u}$ and fluctuating velocity component u^* (equation 2.14).

$$u(x,t) = \overline{u\,(x)} + u^*(x,t) \tag{2.14}$$

The same applies for radial velocity v and pressure, density and other scalar variables.

The variable u can be associated with probability density function PDF (P). The probability density function P of u is the derivative of the cumulative distribution function and is defined so that the probability that $\psi < u < \psi + d\psi$ is $P(\psi)d\psi$, where ψ is the sample space variable of u. Probability density functions and cumulative distribution function characterises the random variable u.

The PDF can be used as an averaging tool, then:

$$\bar{u} = \int uP(u)du \tag{2.15}$$

This is the probability weighted average of all possible u. Important velocity field components are obtained defining statistical moments. Second moment, the variance σ^2 of the velocity, is defined by:

$$\sigma^2 = \int (u - \bar{u})P(u)du = \overline{u^2} - \bar{u}^2 \tag{2.16}$$

The variance is the measure of the width of the PDF. More often for turbulent flows the standard deviation of the velocity field is defined. Standard deviation also refered as root mean square (rms) is the square root of the variance, which express the turbulent intensity of the velocity:

$$\sqrt{\sigma^2} = \sigma = u' \tag{2.17}$$

In this work the standard deviation of the axial and radial velocity will be expressed as rms velocity u' and v'.

2.2.2 Turbulent scales

In turbulence research the turbulent time and length scales are of great importance. The turbulent length scale l_0 can not be directly measured, but is calculated from autocorrelation. Autocorrelation describes the correlation between velocity values at different point in time $\overline{u^*(t)u^*(t+\tau)}$. One point temporal autocorrelation function is normally used for practical calculations. It is defined by the equation:

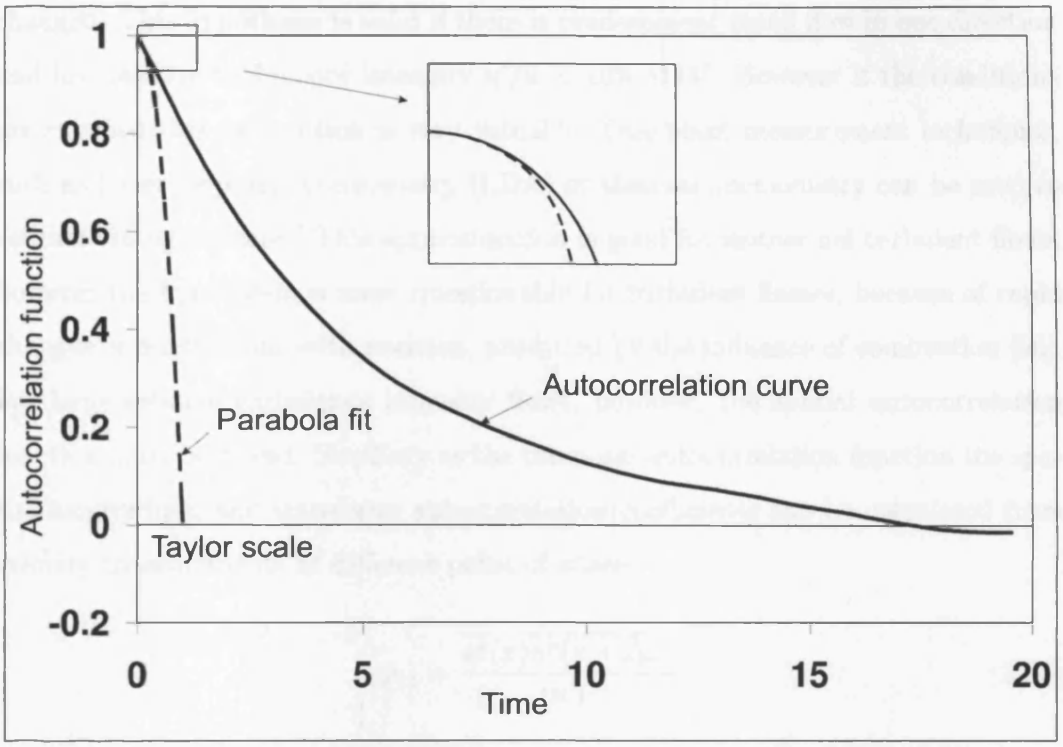

Figure 2.6: *Autocorrelation function and Taylor scale definition*

$$\rho(\tau) = \frac{R(\tau)}{R(0)} = \frac{\overline{u^*(t)\, u^*(t+\tau)}}{u^*(t)^2} \tag{2.18}$$

where τ is the time lag, $R(0)$ is the correlation estimated at lag time zero, $R(\tau)$ is the estimated correlation. One point autocorrelation means that measurements are performed at a point of space over time and the velocity values, obtained during measurements which are then processed, in order to calculate autocorrelation coefficients. The typical autocorrelation function is presented in Fig. 2.6.

The integral time scale τ_0 can be found by integrating autocorrelation function:

$$\tau_0 = \int_0^\infty \rho(\tau)\, d\tau \tag{2.19}$$

Then assuming that the field has uniform mean velocity and accepting Taylor's hypothesis the integral length scale can be computed from the formula:

$$l_0 = \bar{u} \cdot \tau_0 \tag{2.20}$$

Taylor's hypothesis states that turbulence might be considered to be "frozen" as it advects past the sensor, i.e. the fundamental properties of the eddies remain un-

changed. This hypothesis is valid if there is predominant mean flow in one direction and low relative turbulence intensity $u'/\bar{u} < 10\%$ [114]. However if the conditions are satisfied this assumption is very valuable. One point measurement techniques, such as Laser Doppler Anemometry (LDA) or thermal anemometry can be used to estimate integral scales. This approximation is good for isothermal turbulent flows, however the hypothesis is more questionable for turbulent flames, because of rapid changes of fluctuations with position, produced by the influence of combustion [96]. For large relative turbulence intensity flows, however, the spatial autocorrelation function must be found. Similiary as the temporal autocorrelation function the spatial longitudinal and transverse autocorrelation coefficients can be calculated from velocity measurements at different point of space:

$$\rho_{11} = \frac{\overline{u^*(x)u^*(x+\Delta x)}}{(u')^2} \tag{2.21}$$

$$\rho_{22} = \frac{\overline{v^*(x)v^*(x+\Delta x)}}{(v')^2} \tag{2.22}$$

Finally the integral length scales l_0 can be computed by integrating longitudinal or transverse autocorrelation coefficient:

$$l_0 = \int_0^\infty \rho_{11} dx \tag{2.23}$$

From the turbulent scales and velocity field variables other important characteristics, such as: turbulence kinetic energy, energy dissipation rate, Kolmogorov and Taylor scales can be calculated. Turbulence kinetic energy k_E is the mean kinetic energy of eddies per unit mass. It can be estimated from general equation:

$$k_E = \frac{1}{2}((u')^2 + (v')^2 + (w')^2) \tag{2.24}$$

The dissipation of kinetic energy per unit mass ϵ is the rate at which kinetic energy dissipates in transition from large eddies to small eddies. This process is governed mostly by large eddies. The energy dissipation rate can be estimated from equation:

$$\epsilon \approx \frac{u^3}{l_0} \tag{2.25}$$

Besides turbulence kinetic energy k_E and dissipation rate ϵ, obtained from numerical calculations ($k-\epsilon$ model), can be used to estimate integral length scale l_0 and time scale τ_0.

$$l_0 = \frac{k^{3/2}}{\epsilon} \tag{2.26}$$

$$\tau_0 = \frac{k}{\epsilon} \tag{2.27}$$

The equation 2.25 is very important in turbulence. It shows that ϵ does not depend on viscosity and Reynolds number, however the smallest scales, where energy dissipation occurs, depends on viscosity. Kolmogorov scales are the smallest scales that are responsible for dissipating energy. Kolmogorov's first similarity hypothesis states that in every turbulent flow at high Re number the statistics of the small scale motions have a universal form that is determined by viscosity ν and dissipation ϵ [113]. Applying dimensional analysis the Kolmogorov length and time scales can be formed:

$$l_k = \left(\frac{\nu^3}{\epsilon}\right)^{1/4} \tag{2.28}$$

$$\tau_k = \left(\frac{\nu}{\epsilon}\right)^{1/4} \tag{2.29}$$

From equations 2.26, 2.27 it is seen that the largest length and time scales does not depend on viscosity, however the smallest Kolmogorov scales do. According to Kolmogorov's second similarity hypothesis for high Reynolds numbers, the statistic motions of scale l in the range $l_0 >> l >> l_k$ have a universal form that is determined by ϵ and is independent of ν. Kolmogorov's energy dissipation energy theory is based on the assumption that at sufficiently high Re number the small scale ($l << l_0$) turbulent motions are statistically isotropic. This implies that even for anisotropic flows, at small length scales, the flow is locally isotropic. In general Kolmogorov theory implies that the energy contained in large scale eddies is transfered to smaller and smaller eddies and finally dissipates within the smallest eddies due to viscosity. This energy cascade is presented in picture 2.7 [113].

From Kolmogorov's hypothesis applying dimension analysis the energy spectrum $E_{\epsilon,\kappa}$ can be derived:

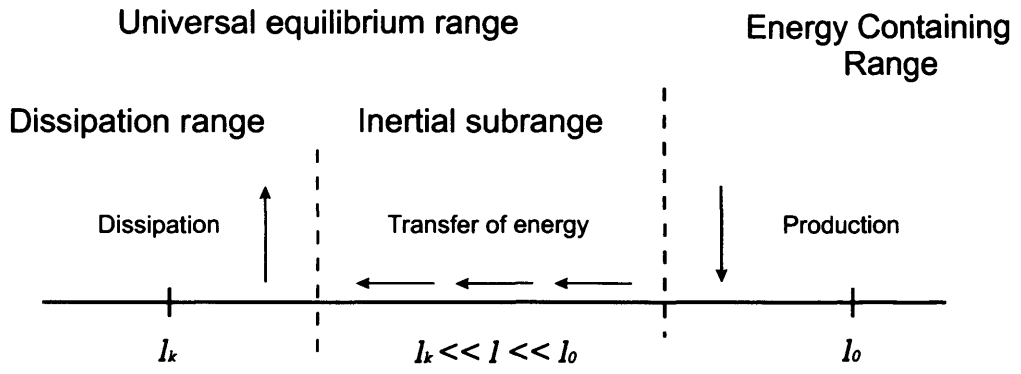

Figure 2.7: *Schematic of energy cascade, taken from [113].*

$$E_{\epsilon,\kappa} = C\epsilon^{2/3}\kappa^{-5/3} \tag{2.30}$$

Here κ is the wavenumber $\kappa = 2\pi/l$. From the equation 2.30 it follows that Kolmogorov $-5/3$ spectrum applies only to inertial range. The bulk of the energy is in the largest scales, and the bulk of the dissipation is in small scales.

The length scale, which is located within the inertial subrange is called the Taylor microscale l_λ. The Taylor microscale l_λ is defined by:

$$l_\lambda^2 = -\frac{2}{\rho''(0)} \tag{2.31}$$

After some modifications the autocorrelation coefficient near the origin can be expressed as:

$$\rho(\tau) \approx 1 - \frac{\tau^2}{l_\lambda^2} \tag{2.32}$$

From the equation 2.32 follows that the intersection of osculating parabola with time τ axis is the Taylor scale l_λ. The Taylor scale definition graph is presented in Fig. 2.6. The measurement and calculation of l_λ is complicated by experimental and data processing errors [115]. Calculating l_λ it is important to correctly select maximum and minimum τ values in order to fit parabola. The practical method to calculate l_λ is to plot autocorrelation coefficient versus lag time squared τ^2. On such plot the parabolic behaviour for small lag time becomes a linear decay. The

linear fitting curve is plotted for the data points. The slope of the fitting line gives the Taylor scale l_λ [115].

The Taylor scale l_λ is related to the dissipation rate:

$$\epsilon = 15\frac{\nu u'^2}{l_\lambda^2} \tag{2.33}$$

Therefore l_λ can be computed using numerical calculations or experiments, having dissipation rate ϵ estimated from equation 2.25. In this text l_λ has been calculated using the equation 2.33.

2.2.3 Turbulent flame stretch

According to Damköhler theory the increase in burning velocity is proportional to the increase in flame area $S_T/S_L = A_T/A_L$. Following this theory the changes in flame area are one of the most important factors affecting S_T. Flame stretch K^* is a flame characteristic, which is defined as the relative change of flame area of an infinitesimal element on the surface with the boundary of this surface element moving tangentially along the surface [98]:

$$K^* = \frac{1}{A}\frac{dA}{dt} \tag{2.34}$$

The flame stretch is responsible for the variation in S_T for turbulent flames and S_L for laminar flames. It consists of two different terms: flame curvature K_c and flame strain rate K_s. Flame stretch effect due to curvature (with no strain) and strain (with no curvature) is graphically represented in Fig. 2.8.

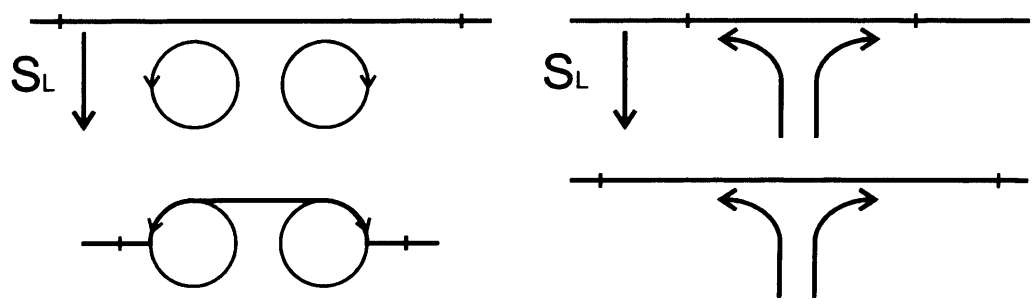

Figure 2.8: *Flame stretch effect due to curvature and strain*

In vector form the flame stretch K^* can be defined [95]:

$$K^* = K_s + S_d K_c = \nabla_t \cdot \vec{u} + S_d \nabla_t \cdot \vec{u} \tag{2.35}$$

Here the term $K_s = \nabla_t \cdot \vec{u}$ is the divergence of the velocity vector, which represents the influence of flow nonuniformity along the flame surface. Therefore the script t for operator ∇ refers to tangential component. Another term $K_c = \nabla_t \cdot \vec{n}$ is the divergence of unit vector normal to the flame surface, which is simply flame curvature. The expression $S_d \nabla_t \cdot \vec{u}$ represents the flame stretch effect due to flame curvature. The flame curvature in three dimensional Cartesian coordinates space can be expressed as:

$$K_c = -\left(\frac{1}{R_1} + \frac{1}{R_2}\right) \tag{2.36}$$

Here R_1 and R_2 are the radii of curvature. For Bunsen laminar flames the flame stretch can be calculated using the equation [98]:

$$K^* = -\frac{u \cdot sin(2\alpha)}{2R_f} \tag{2.37}$$

This equation is valid assuming that the flame surface is a circular cone with the sharp apex. From the equation it follows that for a Bunsen burner flame the flame stretch varies with the flame radius R_f. As its stretch rate is negative the flame suffers compression which increases with decreasing the flame radius R_f. This compression tends to decrease S_L and S_T.

2.2.4 Progress variable

When performing numerical turbulent flame computations and modeling different models are used. Most of these models are based on the variable which is expressed as reduced temperature:

$$c = \frac{T - T_u}{T_b - T_u} \tag{2.38}$$

This reduced temperature is called progress variable c. For fresh unburnt gas $c = 0$, and for burnt gas $c = 1$. Experimentally the progress variable can be found by measuring temperatures in the flame and plotting the temperature isolines. Another

method is take flame images then superimpose them so obtaining the averaged flame. The progress variables then can be calculated by processing averaged flame images. Progress variable can also be expressed as the reduced density.

2.2.5 Flame brush thickness

Turbulent flame brush thickness δ_T is another important flame characteristic used in modeling. δ_T can be simply defined as the distance between progress variable value $c = 0.1$ and $c = 0.9$ [116] or the distance between $c = 0.05$ and $c = 0.95$ [78]. There has also been another similar definition of δ_T related with the density of burnt and unburnt gases [31], however as there are no unique definition the the measure of the distance between $c = 0.05$ and $c = 0.95$ is considered to be sufficient.

2.2.6 Flame surface density

In wrinkled and corrugated flame regimes (generally called flamelets), the flame structure becomes distorted due to turbulent eddies' interaction with the laminar flame front. Therefore it can be assumed that for the flamelets the laminar flame structure remains, although the flame front becomes more wrinkled. One of the proposed solutions to quantify the mean reaction rate was to define crossing frequency of the flame front at a given location. This approach suggests that the mean reaction rate, $\bar{\dot{w}}$, could be calculated from the equation:

$$\bar{\dot{w}} = \dot{w}_c f_c \tag{2.39}$$

here, $\dot{w}_c$ is reaction rate per flamelet crossing, and f_c the crossing frequency. The idea of the theory is represented in Fig. 2.9. The fluctuating flame front crosses the marked point and the mean reaction rate is high. If the temperature were measured at a given point, the temperature fluctuation would be recorded. Having temperature signals the crossing frequency can be calculated. However moving to the right or to the left from the presented point the mean reaction rate $\bar{\dot{w}}$ decreases. This simple observation leads to equation 2.39.

Another similar approach, which is also valid for the flamelets, is based on the flame surface density Σ. Flame surface density is the available flame surface area per

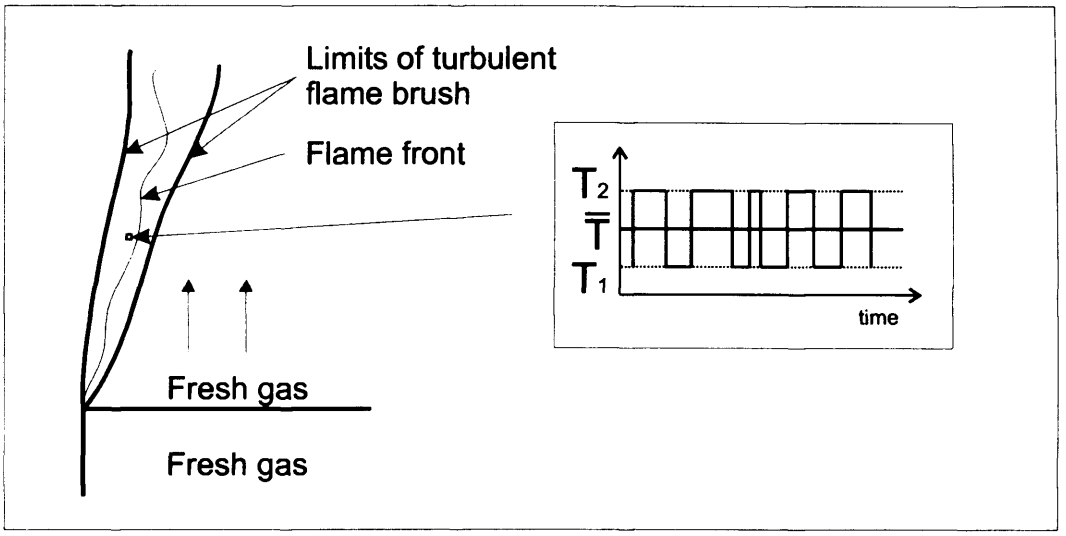

Figure 2.9: *Temperature signal measurement in turbulent flame*

unit volume. The mean reaction rate therefore can be calculated from the equation:

$$\bar{\dot{w}} = \rho_u S_L I_0 \Sigma \tag{2.40}$$

here I_0 is the stretch factor, which describes the stretch effect on the laminar flame speed S_L. The advantage of the flame surface density approach is that chemistry features, incorporated into S_L, are separated from turbulent and combustion interaction $I_0\Sigma$.

Flame surface density can be determined using several different methods [83]. In the Bray-Moss-Libby model an algebraic expression for Σ is used:

$$\Sigma = n_y / \langle \sigma_y \rangle = \frac{g}{\sigma_y} \frac{\bar{c}(1-\bar{c})}{L_y} \tag{2.41}$$

Here $\langle \sigma_y \rangle$ is the mean cosine angle of the instantaneous flame front with the $\bar{c}$ iso-surface, $\sigma_y = \overline{cos\alpha}$, and n_y is the measure of the numbers of flamelet crossing per unit length along a constant $\bar{c}$ direction. L_y is the wrinkling length scale of the flame front, and g is a model constant. The explanation is presented in Fig. 2.10

Another statistical flame surface density definition is given by Pope [117]:

$$\Sigma = \overline{|\nabla c| \, \delta(c - c*)} = (\overline{|\nabla c| \, | c = c*}) p(c*) \tag{2.42}$$

Here $\delta(c)$ is the Dirac δ function, $(\overline{|\nabla c| \, | c = c*})$ is the conditional average of $|\nabla c|$

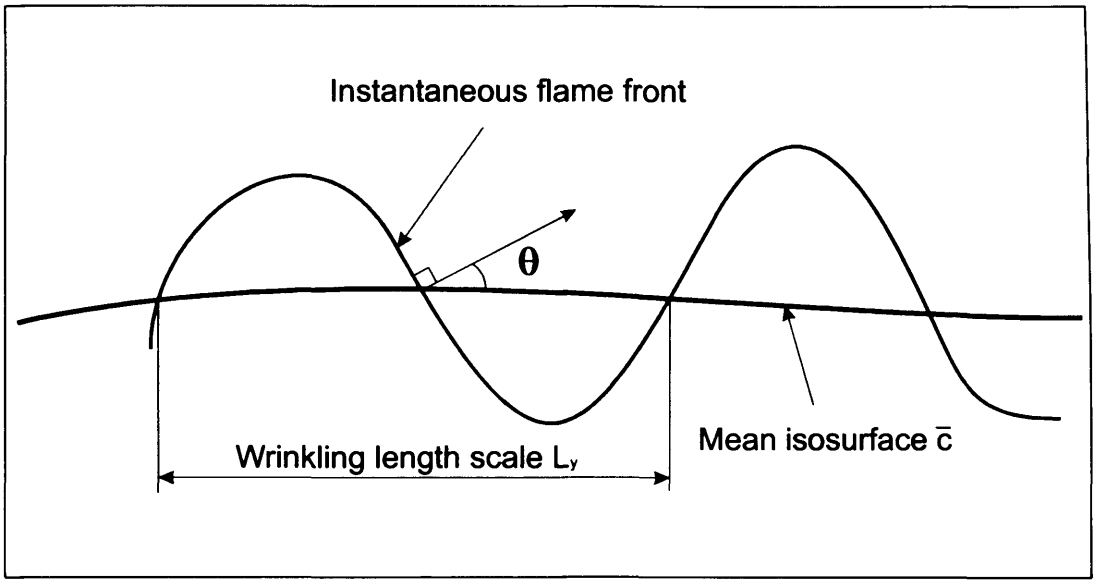

Figure 2.10: *BML model flame surface density definition, taken from [95].*

for $c = c*$ and $p(c*)$ is the probability to find $c = c*$ at the given location.

2.2.7 Turbulent flame burning velocity

Turbulent flame burning velocity is probably one of the most important premixed turbulent flame characteristics. It has been investigated by many research groups for different fuels and different operating conditions [21, 23, 27–29, 39, 55, 108, 109, 118–121]. A comprehensive review of turbulent burning velocity experiments and various models was presented by Lipatnikov and Chomiak [31]. Driscoll in his review paper [77] specifies several turbulent burning velocity definitions: global consumption speed, local consumption speed and local displacement speed. Consumption speed merely indicates the mass per second of reactants consumed, while the displacement speed is the measure of how rapidly the leading edge of the brush moves a certain distance [77]. In this work only consumption speed is investigated, because it is a typical quantity measured in Bunsen burners. This global consumption speed - turbulent burning velocity S_T - is defined as:

$$S_T = \frac{\dot{m}_R}{\rho_R \cdot A} = \frac{\dot{V}}{A} \tag{2.43}$$

When performing the experiments practically the only undefined variable in the equation 2.43 is the flame front area, A. Therefore, in order to solve this equation,

the main task is to find A.

Following the Damköhler theory laminar and turbulent burning velocities can be related:

$$\frac{S_T}{S_L} = \frac{A_T}{A_L} \tag{2.44}$$

here A_T is the surface area of wrinkled flame and A_L is the cross sectional area (Fig. 2.11).

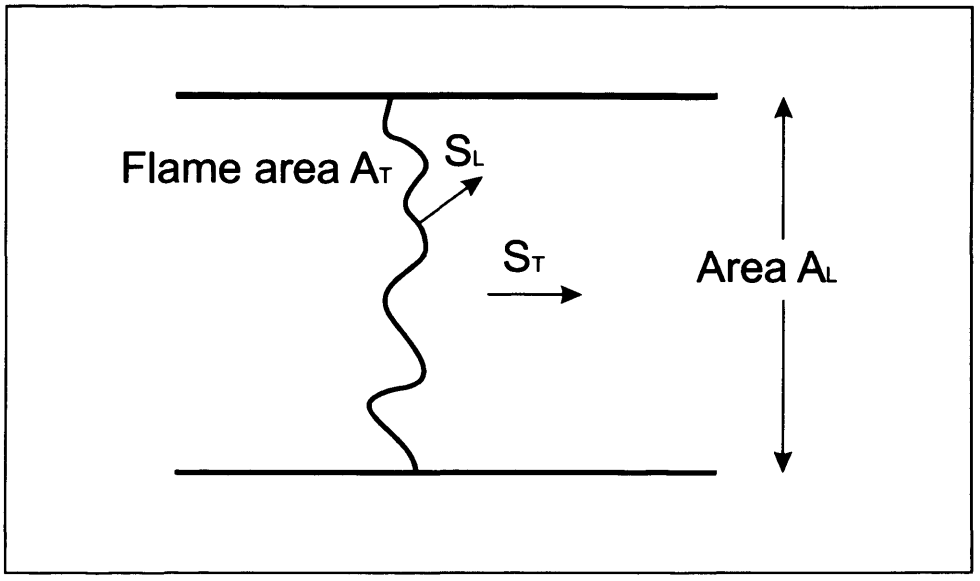

Figure 2.11: *Turbulent burning velocity by Damhöhler.*

Therefore if A_T could be found and S_L calculated the S_T would be easily defined. This simplification is often used in experimental research. The turbulent combustion must be treated as a random process due to the turbulence, which is by itself a random process [96] effect on the flame. However for many practical turbulent flames in wrinkled and corrugated flamelet regimes a correlation between S_L and S_T is assumed and various turbulent burning models are developed based on this assumption.

2.3 Fluid properties and non-dimensional numbers

In combustion research many results may be obtained using dimensional analysis. The relevant parameters can be used to construct non-dimensional numbers. Fluid properties, which are used in fluid mechanics, such as: density, viscosity, specific heat, thermal conductivity, thermal diffusivity, mass diffusivity, are important parameters in combustion research as well. Combining these properties and turbulence parameters, such as: turbulence intensity, integral length scale, turbulence time scale etc., the very important non-dimensional numbers are obtained. The non-dimensional numbers have an important role, as these are often used to predict burning velocities and other combustion characteristics.

Correct definition of fluid properties and turbulence parameters allows the construction of nondimensional numbers, which may be used for comparison of different flame regimes. The importance of quantifying molecular transport properties accurately has been demonstrated elsewhere [31, 122]. Many of these fluid properties can be found in the reference books or calculated using available approximation equations. However there are still many uncertainties in defining some properties, especially for multi-component gases at higher temperatures and pressures.

In the next sections the short review of thermodynamical and transport fluid properties and nondimensional numbers, used in combustion research, will be provided.

2.3.1 Fluid properties

Density and specific heat are fundamental fluid properties. These properties for different pressure and temperature conditions can be calculated using ideal gas law or found in the reference tables or in combustion textbooks [106, 123].

Fuel mixture density has been calculated using the statement of the ideal gas law:

$$\rho = \frac{p}{R_s T \sum_1^n \left(\frac{Y_i}{M_i}\right)} \tag{2.45}$$

Specific heat of the mixture has been calculated using equation:

$$c_{p,mix} = \sum_{1}^{n} c_{p,i} Y_i \tag{2.46}$$

Viscosity and thermal conductivity data for the single gases may be found in the reference tables or computed. The calculation of these properties for the mixture is more complicated [123]. The mixture dynamic viscosity is calculated using formula:

$$\mu_{mix} = \sum_{i=1}^{n} \frac{\mu_i}{1 + \sum_{j \neq 1} \frac{X_j}{X_i} \phi_{ij}} \tag{2.47}$$

Thermal conductivity can be calculated using the equation:

$$\lambda_{mix} = \sum_{i=1}^{n} \frac{\lambda_i}{1 + \sum_{j \neq 1} X_j \cdot 1.065 \phi_{ij}} \tag{2.48}$$

Here ϕ_{ij} is empirical coefficient for the viscosity and thermal conductivity calculated by the formula:

$$\phi_{ij} = \frac{1}{2\sqrt{2}} \left(1 + \frac{M_i}{M_j}\right)^{-0.5} \cdot \left[1 + \left(\frac{\mu_i}{\mu_j}\right)^{0.5} \left(\frac{M_j}{M_i}\right)^{0.25}\right]^2 \tag{2.49}$$

Viscosity and thermal conductivity do not depend on pressure. However these properties are temperature dependent.

Mass diffusivity is an important gas characteristic, which is used to define Lewis number. Binary diffusion coefficients, which are used to calculate mixture diffusivity, can be found in the reference tables or computed using equations from kinetic gas theory. Finally the diffusion of the gas into the mixture of other components can be calculated using the Stefan equation:

$$D_i = \frac{1 - Y_i}{\sum_{j \neq i} \frac{X_j}{D_{ij}}} \tag{2.50}$$

According to the equation 2.50 only the diffusion coefficient of one gas into the mixture can be calculated, therefore it is important to choose the right gas. For lean mixtures the fuel gas is deficient, thus the diffusion coefficient into the air can be calculated. For rich mixtures the diffusion of oxygen into the mixture must be calculated, as the oxygen is the deficient gas. Sometimes, for simplification, gas or air diffusion coefficients into the nitrogen are taken, because nitrogen is the prevailing gas in the fuel air mixture.

The equations for dynamic viscosity, thermal conductivity and diffusivity presented above are reasonably accurate, however if the accuracy higher than 10% is required the Chapman-Enskog theory must be referenced [123].

The final very important property, thermal diffusivity α, is calculated by the formula:

$$\alpha = \frac{\lambda}{\rho c_p} \tag{2.51}$$

This property depends on pressure and temperature and is used to define the Lewis and Karlovitz numbers.

Although the properties can be obtained from reference tables or computed, the main question remains. What temperature should be used? For instance estimation of Re number, based on kinematic viscosity ν could produce different outputs, as ν depends on dynamic viscosity μ and on density, which varies with temperature. Figure 2.12 represents the dependence of Re number on temperature at atmospheric pressure.

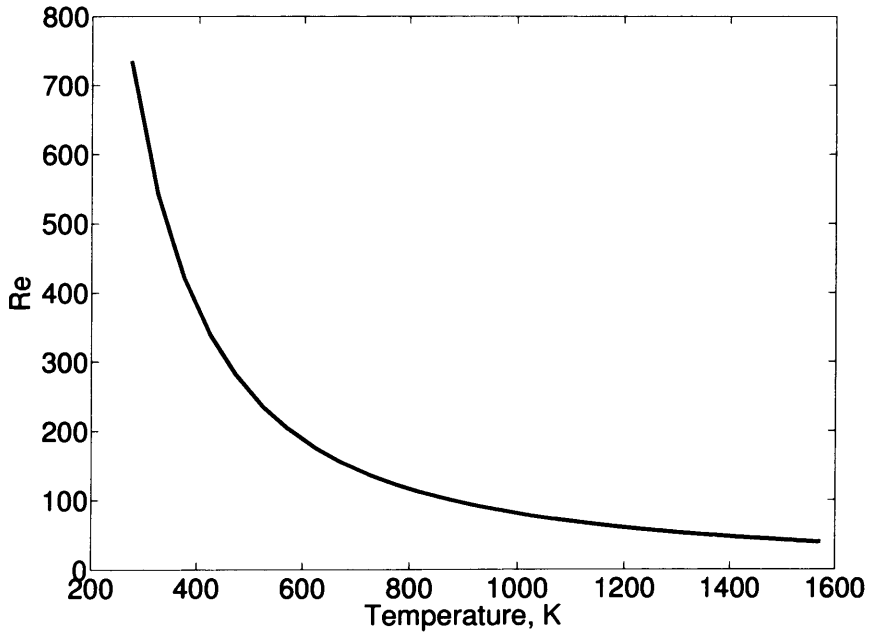

Figure 2.12: *Reynolds number dependence on temperature*

As it is seen from Fig. 2.12 Re numbers varies considerably with presure.

Peters has proposed [97] to use an alternative way of calculating Re number,

$Re = q'l_0/\delta_L S_L$. According to that $\nu = \delta_L S_L$. Veynante and Vervich [124] reported that the relation between thermal flame thickness δ_L, the laminar unstretched flame speed S_L and the kinematic viscosity of reactants ν is $Re_f = \delta_L S_L/\nu \approx 4$, which means that the Reynolds number would differ by the factor of 4.

Peters claims [97] that such properties as specific heat capacity, c_p and thermal conductivity λ should be calculated at the inner layer temperature T_0. The inner layer temperature does not depend on the preheating temperature and equivalence ratio, but it increases with increasing pressure [97, 125]. It has been reported that this temperature depends on the hydrogen content in the methane [51, 126] for $CH_4 - H_2$ mixtures. The hydrogen decreases the inner layer temperature T_0, because of the increase of the oxidation layer thickness due to increasing amount of H_2 and CO to be oxidised in the oxidation layer [126]. In this work inner layer thickness temperature calculations at elevated pressures have been performed using the maximum temperature gradient method with the GRI-Mech v3.0 kinetic mechanism. The temperature varied between 1400-1600 K.

2.3.2 Reynolds number

Reynolds number is defined as the ratio of inertial forces and viscous forces. Mathematically this statement is expressed as:

$$Re = \frac{\rho v l}{\mu} = \frac{v l}{\nu} \tag{2.52}$$

The characteristic length, l is sometimes defined as the diameter of the pipe in fluid mechanics. However in turbulent combustion research this characteristic length could be the integral length scale l_0, Taylor length scale l_λ or Kolmogorov length scale l_k. Thus several different Re numbers can be defined using these length scales.

$$Re_l = \frac{u' l_0}{\nu} \tag{2.53}$$

$$Re_\lambda = \frac{u' l_\lambda}{\nu} \tag{2.54}$$

$$Re_k = \frac{u' l_k}{\nu} \tag{2.55}$$

The average velocity u in the equations above is replaced by root mean square velocity u', which is one of the key parameters in turbulent flows. Reynolds number based on integral length scale Re_l is an important characteristic, which indicates the flow regime. The Re_l above unity shows that the flow is turbulent, while the laminar flow exists at $Re_l < 1$.

Peters proposed to calculate Re for the turbulent flames using the equation:

$$Re_\eta = \frac{u'}{l_0}\frac{S_L}{\delta_L} \tag{2.56}$$

Reynolds numbers calculated using this equation are 5-7 times less compared with the equation 2.53.

2.3.3 Damköhler number

Damköhler number indicates the ratio of turbulent time scale τ_t and chemical time scale τ_c. This relationship of chemical reaction and turbulence gives information about the flame regime.

$$Da = \frac{\tau_t}{\tau_c} = \frac{S_L}{u'}\frac{l_0}{\delta_L} \tag{2.57}$$

For the flame of $Da > 1$ the chemical reaction time is faster than turbulence, which means that turbulence cannot disturb the reaction zone. Almost all industrial flames are in this region. For the flames $Da < 1$ turbulence is faster than chemical reaction, therefore the products and reactants are rapidly mixing and the reaction zone breaks up.

2.3.4 Karlovitz number and stretch factor

Another important parameter, nondimensional Karlovitz number, is linked with Damköhler number. Karlovitz number is the ratio of chemical time τ_c and the smallest Kolmogorov time scale, τ_k. It has many different definitions. Peters suggested to define Ka number in the same manner as Da number using integral length scale l_0, laminar flame thickness δ_L, turbulence intensity u' and laminar flame speed S_L:

$$Ka = \frac{\tau_c}{\tau_k} = \left(\frac{u'}{S_L}\right)^{1.5} \left(\frac{l_0}{\delta_L}\right)^{-0.5} \tag{2.58}$$

Driscoll proposed to use this Peters' definition in order to avoid the ambiguities that now exist [77]. In this work the Karlovitz number equation proposed by Driscoll [77] is mostly used. In his equation nitrogen thermal diffusivity $\alpha = 0.15\ cm^2/s$ at 300 K is used. To simplify the equation thermal diffusivity α of nitrogen can been replaced with the thermal diffusivity of gas mixture at the inner layer temperature, which is approximately equal to the average temperature of the products and reactants:

$$Ka = \left(\frac{u'}{S_L}\right)^{1.5} \left(\frac{S_L l_0}{\alpha}\right)^{-0.5} \left(\frac{(T_P + T_R)/2}{300}\right)^{0.5} = \left(\frac{u'}{S_L}\right)^{1.5} \left(\frac{S_L l_0}{\alpha}\right)^{-0.5} \tag{2.59}$$

If inner layer temperature is unknown thermal diffusivity α can be calculated at 1300-1500 K degrees. The variation of Ka due to temperature effect on α is not significant. Care must be taken using this simplification, when calculating Ka for the conditions other then atmospheric.

Another Karlovitz number definition Ka_δ, which is based on reaction zone thickness δ_r is often used in analysis of thin reaction zones and broken reaction zones flame regimes. In those regimes the flame inner structure is strongly distorted by turbulence motion. The reaction zone thickness, where the heat is released is much lower than laminar flame thickness $\delta_r \approx 0.1\delta_L$ [124]. Therefore Ka_δ is defined as:

$$Ka_\delta = \frac{1}{100}\left(\frac{\delta_L}{l_k}\right)^2 = \frac{Ka}{100} \tag{2.60}$$

This definition of Ka_δ will be used in discussions about flame regimes.

Another representation of stretch effect is used by Bradley and co-workers [28, 29]. The so called nondimensional Karlovitz stretch factor K is often used in their work. Although these variables are closely related, the main difference concerns the length scale used to calculate these quantities. The Kolmogorov length scale, accounting the change of thermal diffusivity due to temperature effect, is used to define Ka number [77], and Taylor's length scale is used for the determination of Karlovitz stretch factor K [28, 127]. Karlovitz stretch factor is found from the equation:

$$K = \frac{q'}{l_\lambda}\frac{\delta_L}{S_l} = \frac{Ka}{100} \tag{2.61}$$

In this paper both Karlovitz number Ka and Karlovitz stretch factor K are used.

2.3.5 Zeldovich number

Zeldovich number measures the effects of the temperature sensitivity of the reaction [98]. It is defined as:

$$Ze = \frac{E_a(T_b - T_u)}{R^0(T_b^2)} \approx \frac{4(T_b - T_u)}{T_b - T_0} \tag{2.62}$$

Here E_a is activation energy, which represents the minimum energy the colliding molecules must possess for the reaction to be possible [98]. For $T_u << T_0$ right hand side formula can be used. Zeldovich number is not constant and varies with the mixture composition and pressure as T_b is composition dependent and T_0 is pressure dependent [97]. Zeldovich number can be perceived as fuel property which depends on pressure.

2.3.6 Lewis number

Lewis number is defined as the ratio of thermal diffusivity and mass diffusivity. This number expresses the property of the fluid and it is of great importance in combustion research.

$$Le = \frac{\alpha}{D_{ij}} = \frac{\lambda}{\rho c_p D_{ij}} \tag{2.63}$$

Lewis number of a substance can be calculated by formula 2.63, however defining Le number for a mixture is not straightforward, as mass diffusion coefficients to multi-component mixtures should be evaluated. For single combustible gas and air mixture, Le number obtains different values for lean and rich mixtures. For rich mixtures oxygen is deficient reactant, therefore oxygen diffusion coefficient to the mixture, consisting of combustible gas and nitrogen is calculated. For lean mixtures the combustible gas is deficient reactant, thus gas diffusion coefficient to the multi-component mixture consisting of nitrogen and oxygen is calculated. Calculations are more complicated for the multi-component combustible gas mixtures, which consist of more than one gas. In this case effective Lewis number, Le_{eff}, must be calculated.

There have been several methods proposed to calculate Le_{eff}. Law et al. [46] has proposed to use the formula:

$$Le_{eff} = 1 + \frac{q_1 (Le_1 - 1) q_2 (Le_2 - 1)}{q_1 + q_2} \tag{2.64}$$

Here q_1 and q_2 are non dimensional heat release of gas, defined as $q_i = (QY_{i,u}) / (c_p T_u)$. When $q_1 = q_2$ the fuels Le numbers are weighted equally and Le_{eff} becomes equal to the average of two.

A similar representation of Le_{eff} has been proposed by Bechtold and Matalon [128]:

$$Le_{eff} = 1 + \frac{(Le_e - 1) + (Le_d - 1)[1 + Ze(\Phi - 1)]}{2 + Ze(\Phi - 1)} \tag{2.65}$$

Later Matalon [129] has modified the equation by introducing separate equations of Le_{eff} for lean conditions:

$$Le_{eff} = \frac{Le_O + (1 - \bar{\Phi}) Le_F}{2 - \bar{\Phi}} \tag{2.66}$$

and for rich mixtures:

$$Le_{eff} = \frac{Le_F + (1 + \bar{\Phi}) Le_O}{2 + \bar{\Phi}} \tag{2.67}$$

Here $\bar{\Phi} = Ze(\Phi - 1)$.

The simplest equation for Le_{eff} has been proposed by Dinkelacker [130]. He argues that the effective Lewis number of the fuel, consisting of more than one gas, can be calculated using the formula:

$$\frac{1}{Le_{eff}} = \frac{X_1 D_1}{\alpha} + \frac{X_2 D_2}{\alpha} = \frac{X_1}{Le_1} + \frac{X_2}{Le_2}; \tag{2.68}$$

Here X_1 and X_2 are the mole fraction of the gases, D_1 and D_2 are diffusion coefficient of corresponding gas to the multi-component mixture, α is the thermal diffusivity. In this work the effective Lewis number representation has been used.

2.3.7 Markstein number

One of the most complicated nondimensional numbers is Markstein number. For the case of laminar flames Markstein number characterises thermodiffusive effects [77].

The classical Markstein number is the physicochemical parameter that expresses the response of the local burning rate in laminar flamelets to perturbations induced by stretching [28]. A similar definition was propsed by Matalon, which defines Markstein length as the measurement of the sensitivity of the flame speed to stretch [129]. The turbulent Ma number characterises variations in S_T under the influence of the global stretching of the whole turbulent flame by the mean flow [131]. As it has slightly different definitions for laminar and for turbulent flames, the Markstein number, obtained from laminar flames, cannot be directly used for turbulent flame research. There have been many investigations performed to quantify Markstein number for laminar flames [125, 128, 132–134]. However Markstein number calculation for turbulent flames is not as simple as for laminar flame, because "of difficulties in determining the instantaneous propagation speed and stretch rate of a three-dimensional interface" [77], although several attempts to apply laminar Markstein numbers for the investigation of turbulent flames have been made [105, 135]. There are different Ma number definitions for unburnt gases and for burnt gases. Further only Ma numbers with respect to unburnt gases will be discussed. Markstein number can be defined as $Ma = \mathcal{L}/\delta_L$. Markstein length $\mathcal{L}$ can be calculated performing laminar propagating flame experiments. There can be found several Ma number definitions in the literature. Law [98] proposed to use a simple definition of Markstein number:

$$Ma = \frac{Ze}{2}\left(\frac{1}{Le} - 1\right) \tag{2.69}$$

Clavin and William [136] presented equation to calculate Ma number for a two reactant mixture:

$$Ma = \frac{\mathcal{L}}{\delta_L} = \frac{1}{\gamma} ln \frac{1}{1-\gamma} + \frac{Ze(Le-1)}{2}\frac{(1-\gamma)}{\gamma}\int_0^{\gamma/(1-\gamma)} \frac{ln(1+x)}{x} dx \tag{2.70}$$

Here $\gamma = (\rho_u - \rho_b)/\rho_u$ is, x is dummy variable.

A more complicated equation for calculating Ma number has been proposed by Matalon [129]:

$$Ma = \frac{\mathcal{L}}{\delta_L} = \frac{\sigma}{\sigma - 1}\int_1^{\sigma} \frac{\lambda(t)}{t} dt + \frac{Ze(Le_{eff} - 1)}{2(\sigma - 1)}\int_1^{\sigma} \frac{\lambda(t)}{t} ln\left(\frac{\sigma - 1}{t - 1}\right) dt \tag{2.71}$$

Here $\sigma = \rho_u/\rho_b$ is thermal expansion parameter, λ is dimensionless thermal conductivity of the mixture, depending on temperature, so that $\lambda = \lambda(t)$ with $t = T/T_u$.

2.4 Borghi-Peters diagram

In order to analyse premixed turbulent combustion flames, combustion diagrams are used to identify flame regimes. Several diagrams have been proposed to define regimes of turbulent combustion flames [97]. The Borghi-Peters diagram is often used for that purpose (Fig. 2.13). It should be mentioned though that this diagram is a "sketch map" of the combsution process without firm and fixed boundaries.

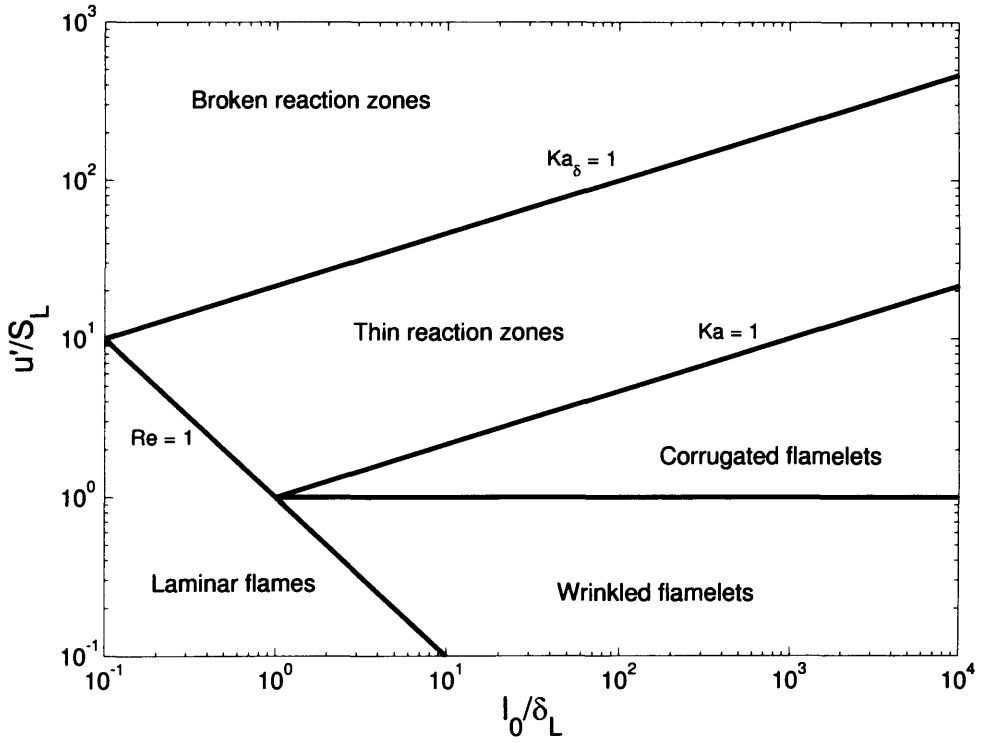

Figure 2.13: *Borghi-Peters diagram*

Five different flame regions can be distinguished: laminar flames, flamelets regime, thin reaction zones and broken reaction zones.

In laminar flames regime fluctuations of turbulence intensity u' are small compared with S_L, and the lengthscales of the flame structures l_0 are smaller than laminar flame thickness δ_L. In this regime Re based on l_0 is below unity.

The flamelet regime comprises wrinkled flamelet and corrugated flamelet regions. In wrinkled flamelet zone $Re > 1$, $Ka < 1$ and $u'/S_L < 1$, therefore the flame retains the laminar flame structure. The u' is small, thus the flame front is only slightly wrinkled as it passes turbulent flow eddies. In corrugated flamelet zone $Re > 1$, $Ka < 1$ and $u'/S_L > 1$. The u' values are higher than in wrinkled flame zone and than S_L. Due to higher turbulence intensity the flame front becomes distorted, therefore pockets of burnt and unburnt mixtures start to form. The unburned areas burn out by themselves, separately from the main flame front.

Thin reaction zones, which is sometimes called reaction sheet regime, is of great importance in industrial application. In this regime $Re > 1$, $Ka > 1$, $Ka_\delta < 1$ and $u'/S_L > 1$. $Ka_\delta < 1$ is Karlovitz number based on reaction zone thickness. In this regime the small eddies penetrate into the preheat zone and enhance the heat and the mass transfer, although for the large eddies the flame may behave as a flamelet.

In the broken reaction zones, which is sometimes called well stirred reactor regime $Re > 1$, $Ka_\delta > 1$ and $u'/S_L > 1$. Here Kolmogorov length scales are smaller than the reaction zone δr, therefore the eddies can penetrate into the reaction zone and reduce flame temperature or even extinguish the flame. The reactions take place not in the flame front, but is separate space regions, i.e. the flow behaves like a well stirred reactor. This work discusses mainly the flames in the flamelet regime, i. e. wrinkled flamelet zone and corrugated flamlet zone.

Chapter 3

Experimental facilities

In this research programme different experimental conditions, methods, fuels and experimental rigs were used. Experiments at atmospheric conditions were performed in the Cardiff University combustion laboratory. Tests at elevated temperature and pressure were conducted in the Gas Turbine Research Centre (GTRC) of Cardiff University in Port Talbot. Three different rigs were used: atmospheric Bunsen burner, swirl burner and High Pressure Optical Combustor (HPOC). Four different research diagnostics were applied: Laser Doppler Anemometry (LDA), Planar Laser Tomography (PLT), Planar Laser Induced Fluorescence (PLIF) and flame imaging. The list of all testing conditions and methods used is presented in Table 3.1.

Table 3.1: *Research programme experimental methods and conditions*

	Bunsen burner	Swirl burner	HPOC
Gas mixture	100% CH_4	100% CH_4	100% CH_4
	70% CH_4 - 30% H_2	85% CH_4 - 15% CO_2	85% CH_4 - 15% CO_2
		70% CH_4 - 30% CO_2	70% CH_4 - 30% CO_2
		85% CH_4 - 15% H_2	85% CH_4 - 15% H_2
		70% CH_4 - 30% H_2	70% CH_4 - 30% H_2
Pressure, bar	1	1	3, 7
Temperature, K	293	293	473, 573, 673
Method	LDA, PLIF	Imaging	LDA, PLT

In this chapter the description of experimental equipment is provided. Discussions about the different research methods is presented in the next chapter.

3.1 Elevated temperature and pressure experiments in GTRC

All elevated temperature and pressure experiments were conducted in the Gas Turbine Research Centre of Cardiff University. This facility is located at ECM^2 in Port Talbot. It consists of two major combustion rigs each designed for detailed investigation of combustion and emissions in gas turbines. The GTRC is equipped with a 2.2 MW air compressor, which supplies air to the testing rigs, a large scale 5 MW heat exchanger, which is used to preheat air, delivered to the testing rigs, to the required temperature. Compressor capacity is 5 kg/s, 16 bar. The GTRC consists of two test rigs: Sector Combustor Rig (SCR) and High Pressure Combustor Rig (HPCR).

The SCR is used for the internal pollutant mapping of gas turbine combustors. This rig provides a unique opportunity to perform online gas analysis of NOx, SOx, CO etc., traversing inside combustors - i.e. within the combustion zone, allowing the development of combustion phenomena understanding and providing data for the development and verification of mathematical models. The gas sampling probe can reach any point within the combustor across the full operating range. Various bespoke traversing probes can be used. Various fuels, such as: kerosene, diesel, biodiesel, natural gas etc. can be tested. Maximum operating pressure of the rig is 10 bar, maximum operating temperature is 900 K, maximum supplied air inlet flow is 5 kg/s.

The HPCR rig is a multi-purpose combustion facility for fundamental research and development work for various fuels including kerosene, diesel, bio-diesels, natural gas, methane and a range of simulated synthesis gases. Maximum operating pressure of the HPCR is 16 bar, maximum operating temperature is 900 K, maximum supplied air inlet flow is 5 kg/s. An extensive range of state-of-the-art measurement sections are available, some unique, each with different capabilities, all of which are predominately non-intrusive. The Combustion Instability Measurement Section (CIMS) can be used to measure flame dynamics using a unique in-line siren. The Auto-Ignition Measurement Section (AIMS) measures auto-ignition delay time for gaseous and liquid fuels. The Wall Cooling Measurement Section (WCMS) can be

used for fundamental research on heat transfer. The Hot End Simulator (HES) is a facility that sits behind a combustor, mimicking the behaviour of a turbine section in a gas turbine. This component reduces the pressure and temperature of the exhaust gases by removing heat rather than work from the exit gases. Intermediate sampling points between the sub-stages can take gas samples for subsequent analysis. The High Pressure Optical Chamber section (HPOC) can be used for the measurement of burning velocity, flame flashback, using different non-intrusive laser techniques, such as: Laser Doppler Anemometry, Planar Laser Tomography Particle Image Velocimetry, Planar Laser Induced Fluorescence, Laser Induced Incandescence.

All tests at elevated temperature and pressure were performed in the High Pressure Optical Chamber (HPOC) (Fig. 3.1). The HPOC consists of a horizontally mounted burner firing into an inner combustion chamber, enclosed within an optical pressure casing. The HPOC can operate with working pressures of up to 16 bar and inlet temperatures of up to 900 K. The pressure casing is a cylindrical geometry with four opposed quartz windows, affording excellent optical access (Fig. 3.1).

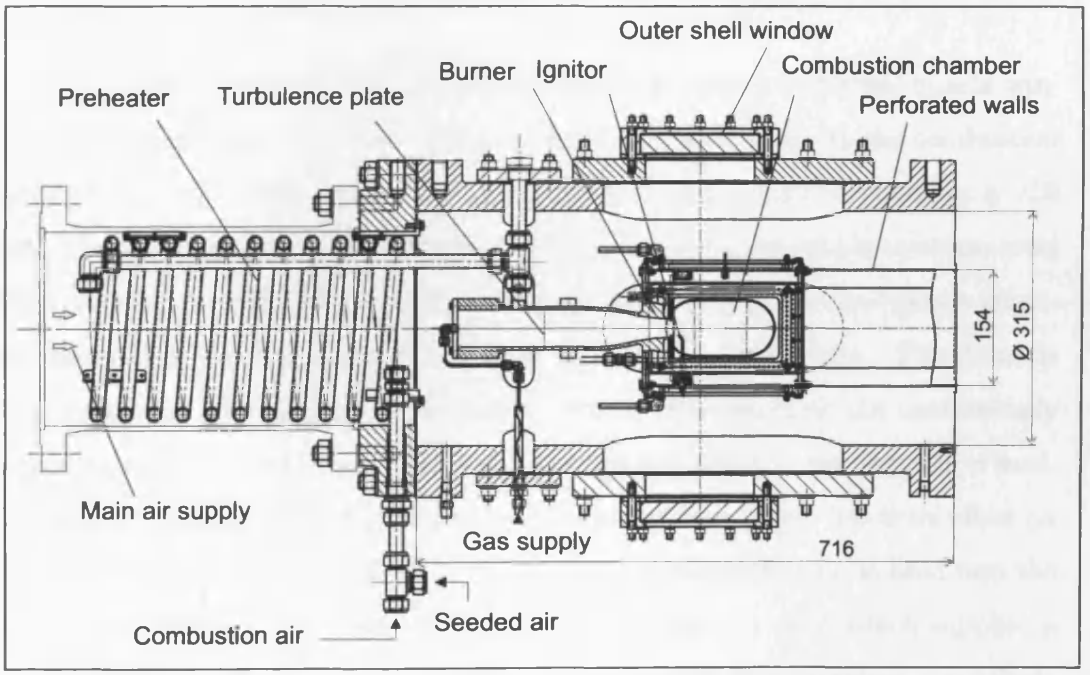

Figure 3.1: *Cross section of the High Pressure Optical Chamber*

The optical combustion section is connected to a compressor and heat exchanger, allowing combustion air to be preheated to required operating temperatures. The

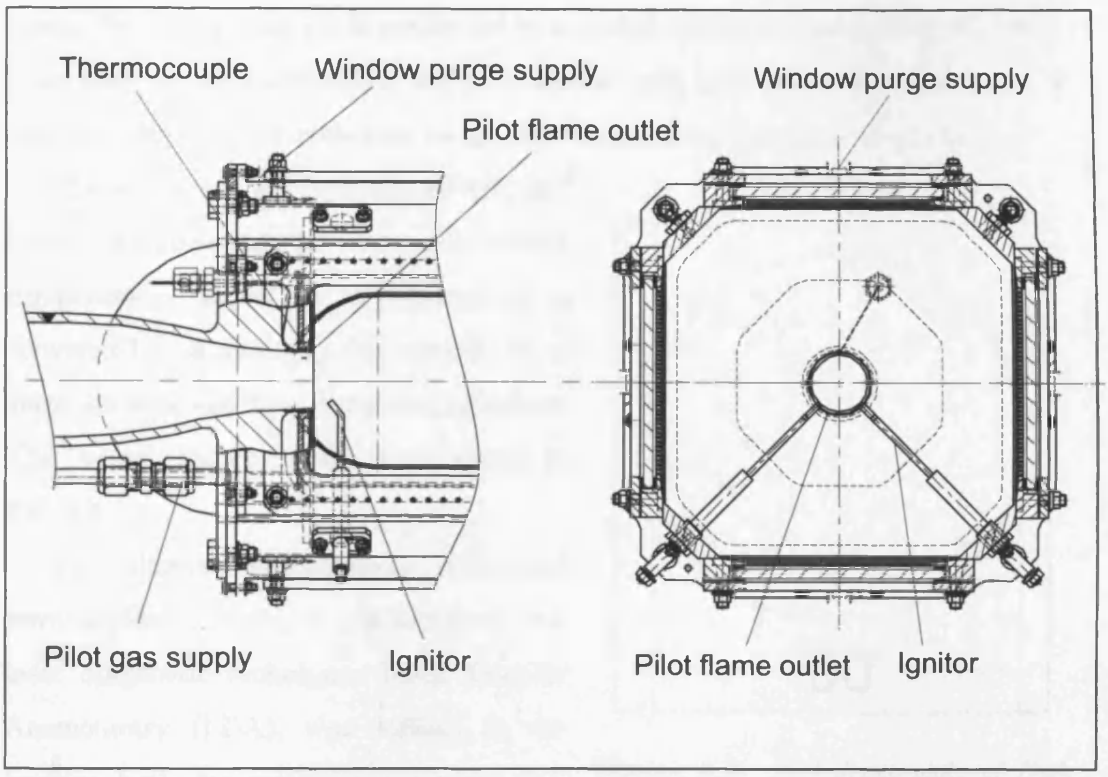

Figure 3.2: *Detailed combustor geometry*

inner combustion chamber is of rectangular form and has four internal quartz windows which align with the outer casing, giving full optical access to the combustion chamber Fig. 3.2). The width and the height of the combustion chamber is 150 mm. The inner combustion chamber is constructed from aero-grade stainless steel sheet allowing (if required) external cooling air to pass into the combustion chamber, mimicking the behaviour of practical gas turbine combustors. The flame is thus confined to the combustion chamber. The internal windows are continuously purged with air during the tests to ensure they are kept clear of any deposits of seed. Extensive experience with the rig shows that the windows purge has little effect on measured values. A simple Bunsen type burner, diameter 25 mm, is fired into the combustion chamber. The burner is fitted with an annular pilot which supplies a methane diffusion flame to aid stability while adjusting the operating conditions. This pilot is switched off prior to making measurements.

The main burner is fed premixed fuel and air via a turbulence mixing plate, 50 mm diameter, with 53 holes each of 1.5 mm diameter and blockage ratio 95% (Fig. 3.3). This creates uniform turbulence and aids in the mixing of the reac-

tants. The fuel gas supply is connected to a mixing chamber upstream of this plate. Preheated air for combustion, which is seeded with aluminium oxide particles, is delivered through the preheater to the top of the mixing chamber of the burner.

The air supply for both the HPOC and burner is pressurised by the main facility compressor. Seeded air for combustion is delivered by an auxiliary compressor. Fuel gases are supplied from premixed cylinders. The overall scheme for the rig is shown in Fig. 3.4.

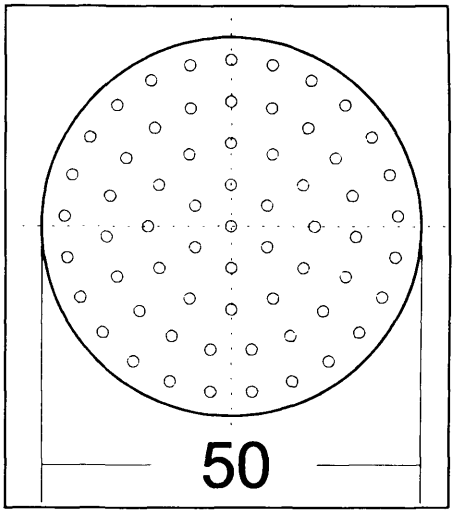

Figure 3.3: *Turbulence plate of High Pressure Optical Combustor rig.*

Two different measurement techniques were applied. First, a non-intrusive 2-D laser diagnostic technique, Laser Doppler Anemometry (LDA), was utilised to determine both the velocity profile and turbulence characteristics at the exit of the burner at elevated pressures and temperatures (Fig. 3.5). A Dantec laser system was used for this purpose. Secondly, planar laser tomography was applied in order to measure the turbulent burning velocity for the different gas mixtures at a range of temperatures and pressures. Images of the flame front were recorded using a Photron APX-rs high speed camera mounted perpendicularly and synchronised with a pulsed (Nd:YAG) sheet laser. To ensure reliability for each test 1000 images were recorded at 10 Hz.

Aluminium oxide particles were used as seeding for Laser Doppler Anemometry and Planar Laser Tomography. The size of aluminium oxide particles was below 1 μm.

The experiments were run and monitored from a remote control room. LDA and laser planar tomography systems were controlled from their own dedicated computers, and the facility was controlled from its own PLC system.

Experiments were conducted under elevated temperature and pressure conditions. The pressure in the rig was created by the compressor. It was important to keep the pressure difference between inside and outside the combustion chamber as

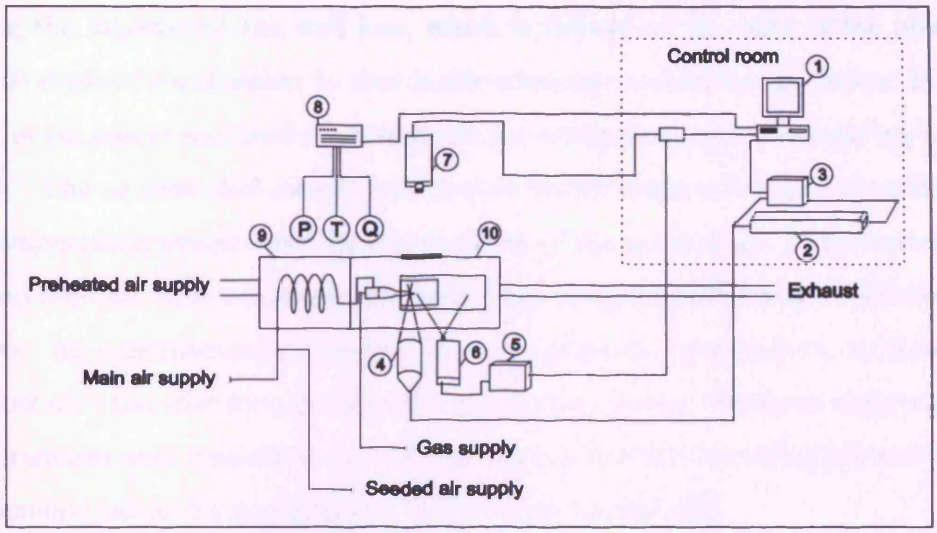

Figure 3.4: *Experimental setup. 1 - Data acquisition and laser control system, 2 - LDA laser, 3 - LDA laser processor, 4 - LDA laser probe, 5 - Sheet laser controller, 6 - Sheet laser, 7 - High-speed digital camera, 8 - Data logger, 9 - Combustion air preheater, 10 - High pressure optical combustor.*

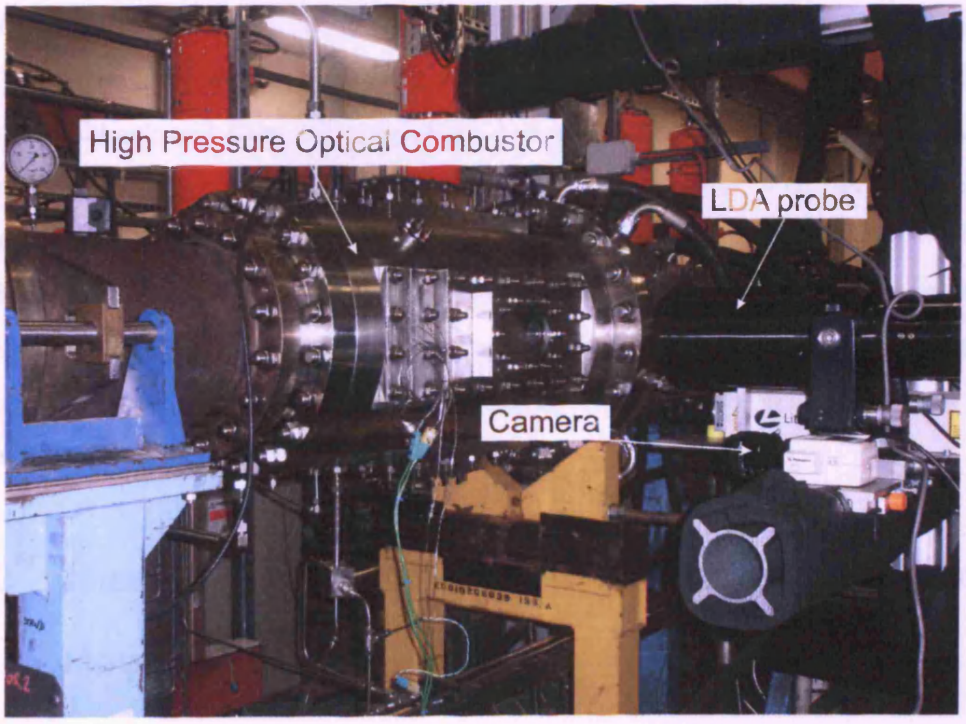

Figure 3.5: *Laser system set up in GTRC.*

low as possible. This was achieved by adjusting the air flow by a valve. In all cases during the experiment the wall loss, which is defined as the ratio of the pressure outside combustion chamber to that inside combustion chamber was below ±1%.

The gas heater was used to preheat air for combustion prior to supplying to the HPOC. The air mass flow rate for combustion varied between 2-24 g/s depending on the temperature, pressure and equivalence ratio of the gas mixture. Fuel, combustion air and seed air were measured simultaneously using suitably ranged Coriolis flow meters. All experimental conditions, such as: pressure, temperature, air flow and gas flow were recorded by a facility data acquisition system. Measured temperatures and pressures were reasonably steady with fluctuations not exceeding 5% and 3% of the nominal values for pressure and temperature respectively.

It was decided to perform tests at 3 bar and 7 bar (absolute) pressure, 473 K, 573 K and 673 K temperature for the gas mixtures with equivalence ratio of around $\phi \approx 0.6, 0.8, 1, 1.2, 1.4, 1.6$. Therefore it was estimated to perform approximately 180 tests for all gas mixtures: 100% methane, 85% methane - 15% carbon dioxide, 70% methane - 30% carbon dioxide, 85% methane - 15% hydrogen, 70% methane - 30% hydrogen.

During the tests, however, it was difficult to obtain stable flames at exactly the same equivalence ratio, therefore the equivalence ratio varied from test to test. Flame flashback and blow off frequently occurred, therefore a pilot flame was used as stabiliser, while adjusting necessary air and gas flow rates. The pilot flame was normally switched off during the imaging.

Laser Doppler Anemometry was conducted with air seeded with aluminium oxide particles at elevated temperature and pressure conditions. As LDA was conducted before the flame imaging, the real gas velocities at the Bunsen burner exit was not known.

3.2 Bunsen burner tests at atmospheric conditions

Turbulent burning velocity measurements using the Bunsen burner at atmospheric conditions were conducted in Cardiff University combustion laboratory. Laser Doppler

Anemometry (LDA) and Planar Laser Induced Fluorescence (PLIF) were used.

LDA tests were undertaken to find out the velocity and turbulence intensity characteristics at isothermal conditions. Three different burner nozzles were used in LDA experiments. Nozzle drawings are presented in Fig. 3.6.

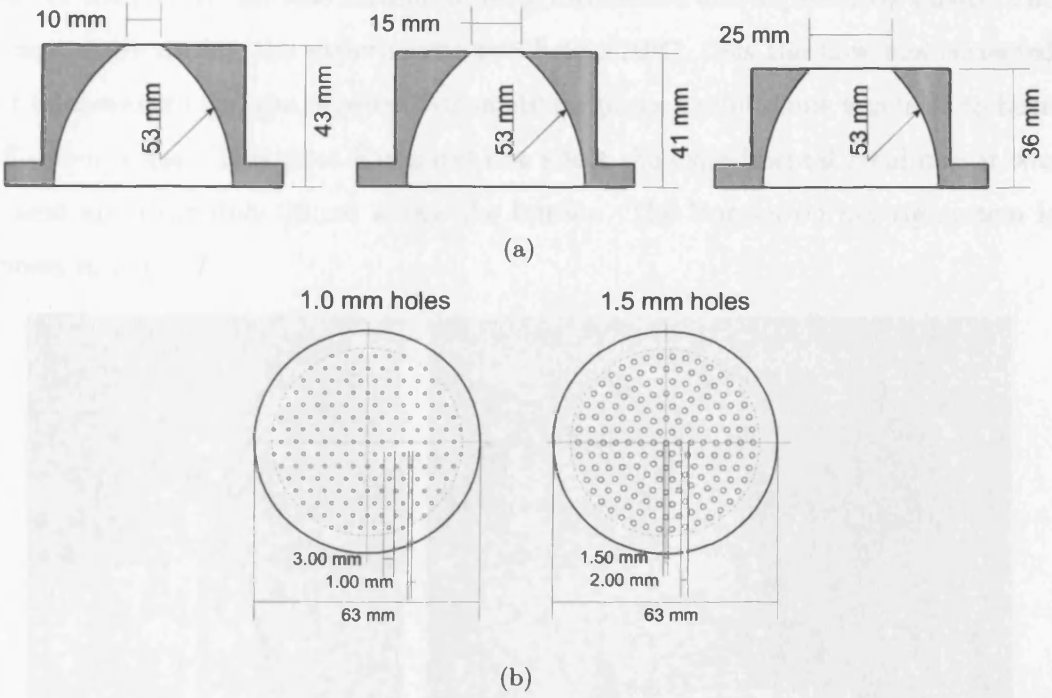

Figure 3.6: *Bunsen burner nozzles and turbulence plates. a) nozzles; b) turbulence plates used for LDA experiments*

To create turbulence two different types of the turbulence plates were used with 1.5 mm holes and with 1 mm holes (Fig. 3.6). Turbulence plates were placed at the burner exit between the burner and the nozzle. Nozzles were fixed to the burner using four bolts, which facilitated good access to the burner plates and fast burner nozzle replacement. Burner nozzles were designed to produce flat axial velocity profile. Comprehensive investigation of these nozzles can be found in [137].

Air for experiments was delivered from University pressurised air system. A pressure regulator was used to avoid pressure fluctuations in compressed air system. For LDA experiments aluminium oxide was used for seeding. Seeds were delivered to the burner by the air stream from the pressurised tank. For further investigation using PLIF, 25 mm diamter burner nozzles and a turbulence plate with 1.5 mm diamter holes were chosen. More details about the LDA results are provided in the

next chapter.

During combustion experiments using PLIF the premixed gas cylinders: 100% methane, 85% methane - 15% hydrogen and 70% methane - 30% hydrogen delivered by BOC were used. Air was delivered from the compressed air network. The flow rate of the gas and air was measured using rotameters and adjusted by valves. The temperature during the experiments was below 20°C, thus the flow was corrected for temperature and gas density. For safety purposes a pilot flame was used to burn off unburnt gas. This pilot flame did not affect the experimental results as it was placed approximately 20 cm above the burner. The Bunsen burner rig system is shown in Fig. 3.7.

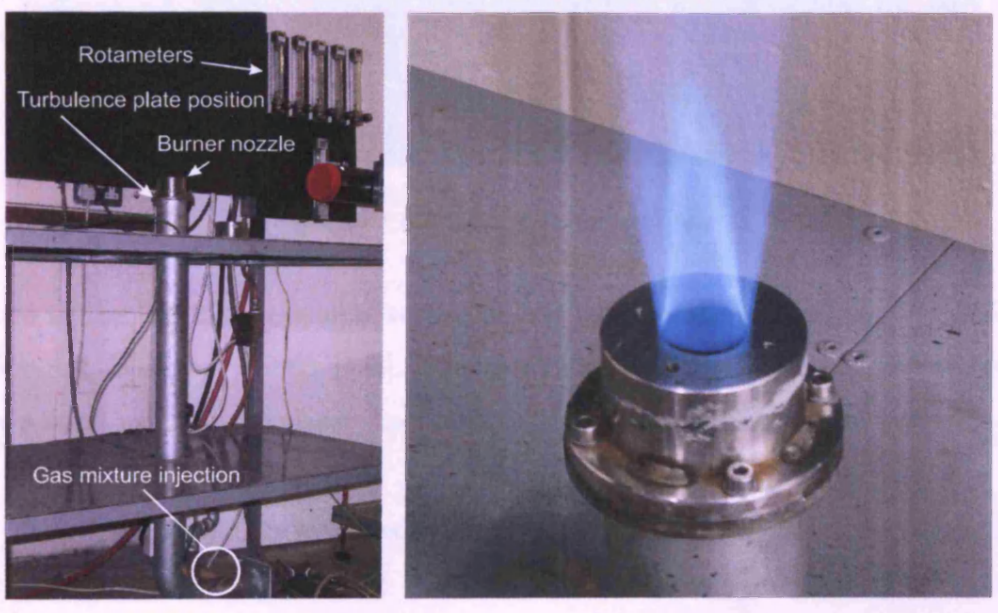

(a) (b)

Figure 3.7: *Bunsen burner rig: a) Bunsen burner setup; b) 25 mm diameter burner nozzle.*

For PLIF experiments the laser system consisting of dye tunable laser Quantel TDL 90 pumped by a pulsed Spectra-Physics Nd:YAG laser at 10 Hz was used. The second harmonic radiation (532 nm wavelength) from Nd:YAG laser was used for pumping the dye laser. The required wavelength was achieved via doubling of the fundamental frequency of the dye laser and using Rhodamine 590 dissolved in ethanol. The measured energy of the pumping laser was about 300 mJ. Typically around 12-15 mJ per pulse was obtained at around 283 nm. The wavelength was

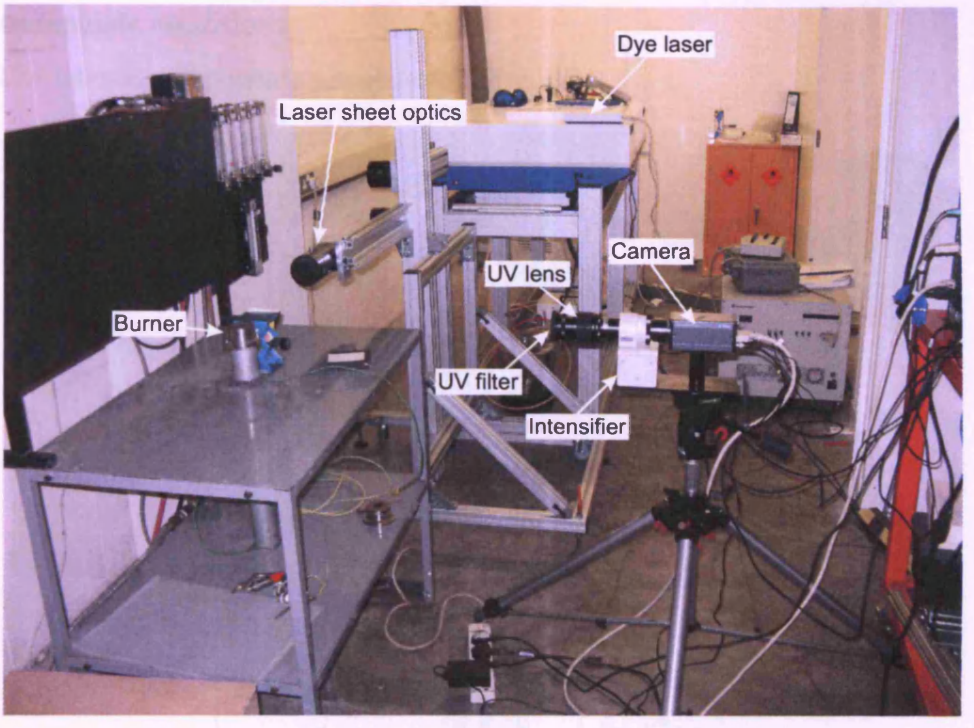

Figure 3.8: *PLIF system set up.*

tuned to the 283.22 nm, which was estimated beforehand by using freely accesible software Lifbase ver. 2.0.63 [138]. The laser beam from the dye laser was converted into a sheet using Dantec laser sheet optics. The width of the laser sheet was around 30 mm.

The receiving system consisted of the Dantec Hi Sense MkII camera, intensifier with UV lense and Melles Griot UV filter with a center wavelength at 308.4 nm. Camera and intensifier were synchronised with laser pulses. The system was controlled using Dantec DynamicStudio v2.30 software. To ensure reliability for each test 450 images were recorded at 10 Hz. The system setup is presented in Fig. 3.8.

3.3 Generic swirl burner experiments

Flame stability and flashback experiments were conducted using the generic swirl burner designed and commissioned at Cardiff University. The burner was designed to produce premixed, non premixed and partially premixed flames. Only premixed combustion was considered in this programme. Air and fuel flows were measured simultaneously using suitably ranged Coriolis flow meters. The tests were conducted

at atmospheric conditions.

The burner components are shown in Fig. 3.9.

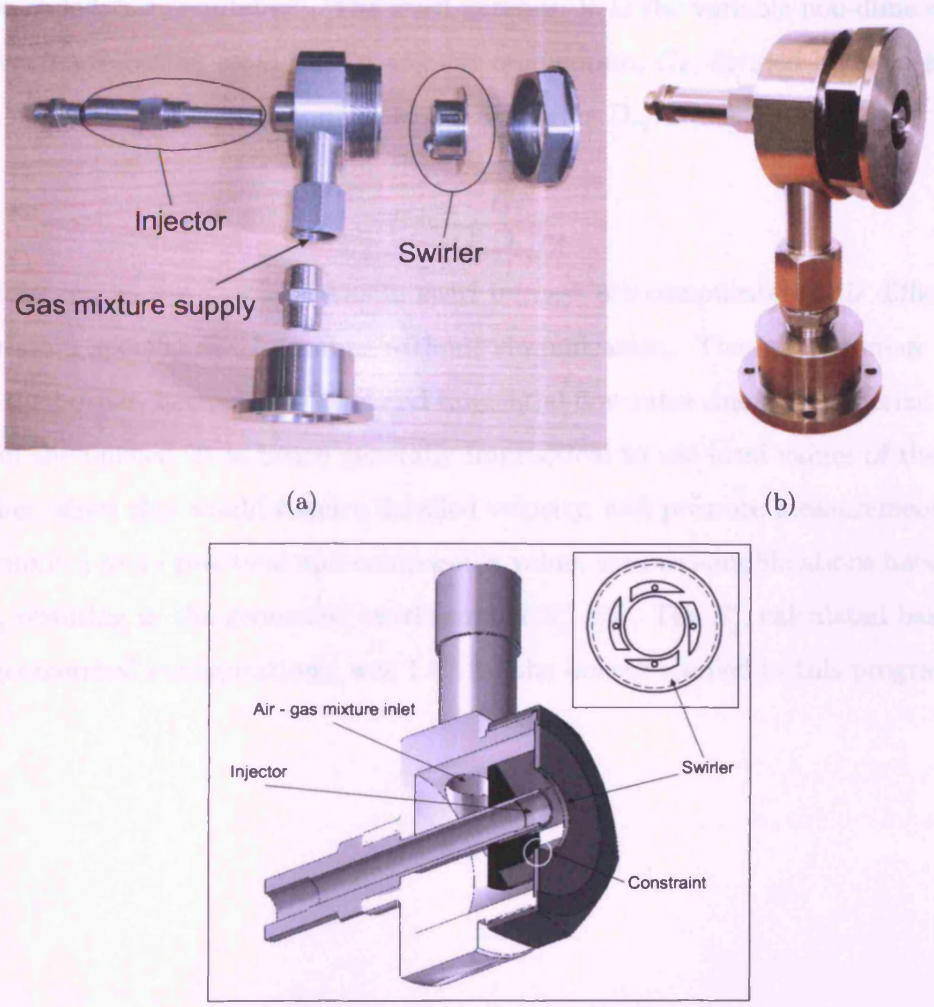

Figure 3.9: *Generic swirl burner*

Air/fuel gas mixture is supplied through a tangential inlet pipe into a plenum chamber, then via 4 tangential inlets into the swirl chamber forming the main part of the burner. The fuel injector, which is normally used for the non premixed and partially premixed flames, is not used in our experiments, but is left in place as being representative of industrial practice, where it might for instance be used for liquid fuel injection. Such a burner design normally produces a Central Recirculation Zone (CRZ), which plays an important role in flame stabilisation. The effect of CRZ is reduced by fitting a constraint in the nozzle (Fig. 3.9c), which also helps to reduce

flashback.

Swirl burners and combustors are usually characterised by the degree of swirl or the so-called "swirl number". The swirl number, S, is the variable non-dimensional number representing axial flux of angular momentum, G_θ, divided by axial flux of axial momentum, G_x, and equivalent nozzle radius $D_{eq}/2$ [64]:

$$S = \frac{G_\theta}{G_x D_{eq}/2} \tag{3.1}$$

However, as the flow patterns in swirl burners are complicated, it is difficult to calculate a specific swirl number without simplification. The swirl number varies with the burner, because the axial and tangential flow rates change at different levels within the burner. It is hence generally impractical to use local values of the swirl number, since this would require detailed velocity, and pressure measurements. To determine a more practical and comparable value, various simplifications have been used, resulting in the geometric swirl number S_g^* [65]. The S_g^*, calculated based on the geometrical configurations, was 1.47 for the burner studied in this programme.

Chapter 4

Research methods and techniques

Three different laser techniques: Laser Doppler Anemometry (LDA), Planar Laser Tomography (PLT) and Planar Laser Induced Fluorescence (PLIF) were used in this research programme to analyse Bunsen burner flames at atmospheric and elevated temperature and pressure conditions. The flame imaging method was applied to perform flashback analysis in the swirl burner. LDA data were used to investigate Bunsen burner turbulence characteristics and velocities. Images obtained from PLT and PLIF were used to find burning velocities. In this chapter these methods are described and the advantages and uncertainties of using it in combustion research are emphasised.

4.1 Laser Doppler Anemometry

LDA is relatively simple method permiting the researcher to quickly obtain necessary flow velocity data at various conditions. In this section a short introduction to LDA method and description of how this method have been utilised is presented.

4.1.1 Introduction to LDA

Laser Doppler Anemometry (LDA) is a single point optical measuring technique used to measure the velocity and turbulence distribution of the particles conveyed by air. The basic of LDA technique is the frequency shift of the light reflected from a moving body and received by a stationary detector. This phenomenon is known as Doppler effect. The first application of LDA was described in 1964 [139]. Progress

has been made on many aspects of LDA since then, especially in signal processing systems. Therefore LDA became accessible and widely used tool in fluid mechanics for the research of laminar and turbulent flows.

An LDA probe emits the laser light, which has velocity c and frequency f_i, but due to the particle movement, the seeding particle "sees" a different frequency f_s, which is scattered towards the probe. From the receiver's point of view, the seeding particle acts as a moving transmitter, and the movement introduces an additional Doppler shift in the frequency of the light reaching the receiver. In practice this frequency change can only be measured directly for very high particle velocities, therefore often two laser beams are used. Then the light scattered from two intersecting laser beams is mixed and scattered towards the receiver. In this case slightly different frequencies of the beams are obtained. When two wave beams of slightly different frequency are superimposed, interference occurs, producing the beat frequency, also called Doppler frequency f_D, which corresponds to the difference of two frequencies [140]. This Doppler frequency is directly proportional to the x component of the particle velocity:

$$u_x = \frac{\lambda_w}{2sin(\Theta/2)} f_D \tag{4.1}$$

where λ_w is known wave length, Θ is the angle between the incoming laser beams and f_D is Doppler frequency.

The fringe model is commonly used in LDA to explain the principle of velocity measurement. Two laser beams are directed through optical fibers to the probe. The focal length of the probe determines the size and position of the crossing point of the two beams. Lenses are used to guide the two laser beams into the measurement point where the beams cross. Thus the measurement volume formed by the laser beams is an ellipsoid. The crossing beams form interference fringes, so that there are high intensity planes of light and between them low intensity planes which are perpendicular to the laser beam plane. The spacing between the planes is determined by optical parameters of the setup, namely the laser light wavelength, and the angle between the beams. The flow is seeded with small particles, which can follow the turbulent motion of the fluid. When these particles pass by the measurement volume they scatter light. The intensity fluctuation of the scattered light depends on the

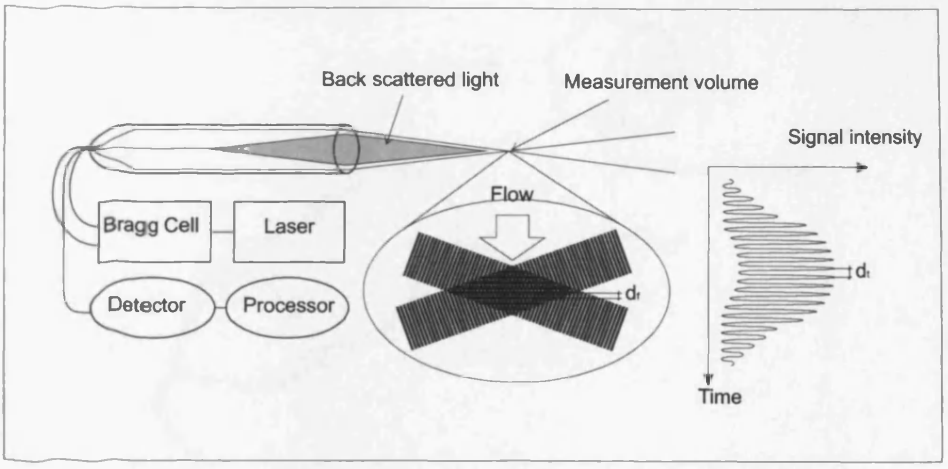

Figure 4.1: *LDA fringe model.*

velocity of the particle (Fig. 4.1). The time d_t can be easily measured and then the velocity of the particle can be calculated by dividing the traveled distance d_f by the time d_t.

The important part of LDA technique is signal processing. The electronic signal sent out by the photodetector contains periods when there are no particles in the measurement volume, randomly interspersed with bursts of signal. The overall shape of the burst is a consequence of the fact that the laser beams producing the measurement volume will inevitably be stronger at their center than at their edges. As the particle passes through the edge of the measurement volume where the fringes are weakly illuminated the signal fluctuations are also weak. As the particle passes through the measurement volume centre the signal fluctuations become larger and then decay again. As a consequence the signal can be split into two parts - a low frequency part and a high frequency part that actually contains the Doppler signal. Modern signal processors use digital technology to analyze each burst and extract the frequency and thus velocity at that instant. The hardware has to be quite sophisticated because the frequencies are so high. Typically such processors have "burst-detection" circuits to tell them when there is a signal. They then digitize that signal and determine its frequency.

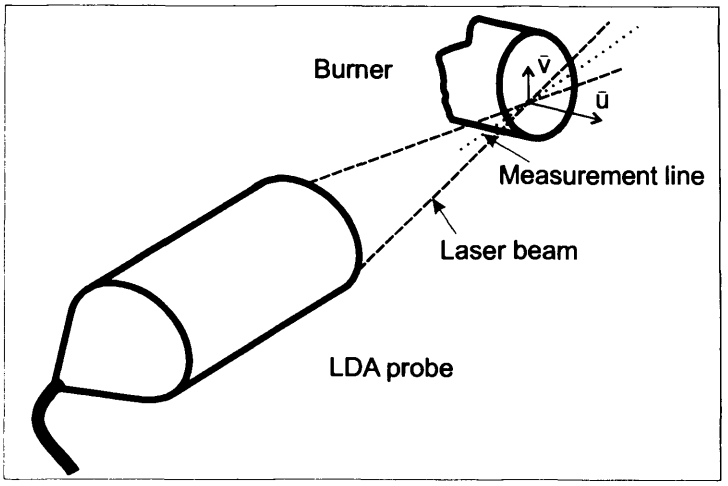

Figure 4.2: *LDA measurement setup.*

4.1.2 LDA measurements at elevated temperature and pressure conditions

In our experiments at elevated pressure and temperature four beams two velocity components backscattered LDA method was used. A Dantec laser system was used for this purpose. Two velocity and turbulence components: axial velocity u and radial velocity v were measured. The backscattering method had been chosen due to simpler system setup and data collection.

Dantec Dynamics BSA Flow version 4.11 software was used as a main tool to collect and process the data. The probe was attached to the traverse system, which was controlled by the main data acquisition computer. The axial and radial velocities were recorded for a range of exit velocities at ambient absolute pressures of 3 and 7 bar and temperatures of 473 K to 673 K. The velocity of air flow preheated to the required temperature at elevated pressure seeded with aluminium oxide particles was measured 10 mm downstream of the burner exit across the burner axis on the centreline plane. The measurement position was moved across the burner by every 1 mm starting from one burner edge to another. Up to 5000 samples were collected at each position across the burner centre, radial position $r = -9...9$ mm, at each condition. Due to the flow stream shape the seeding rate was lower at the edges of the burner, radial position $r = 9...13$ mm. A schematic drawing of LDA measurement setup is presented in Fig. 4.2.

The data validation rate during the experiments was above 90% during all tests.

The relative error was calculated for axial (u) and radial (v) velocity components using the equation:

$$\epsilon = \frac{u'}{\bar{u}\sqrt{N}} 100\% \tag{4.2}$$

where ϵ is relative error, u' axial (or radial v') RMS velocity and $\bar{u}$ is axial (or radial $\bar{v}$) mean velocity.

Calculated relative error did not reach 0.5% for the measurements in the centre of the burner and did not exceed 3% for the measurements at the edges of the burner.

Mean velocity and RMS velocity data were obtained directly using the BSA Flow software. Using these data the typical velocity profile across the burner can be plotted (Fig. 4.3). The axial and radial RMS velocity data were used to calculate turbulence intensity q'.

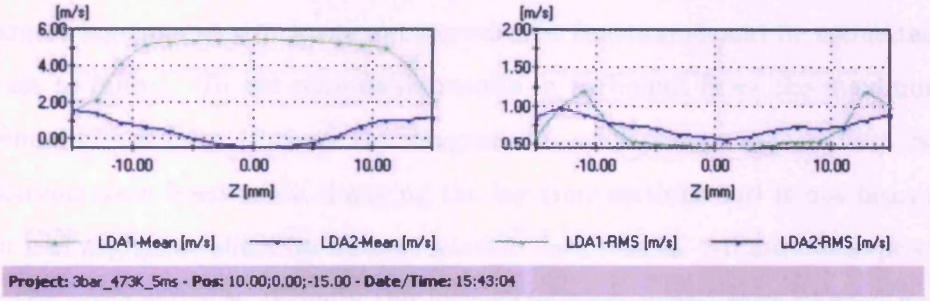

Figure 4.3: *Axial and RMS velocity data presentation using BSA Flow software.*

Integral length scale is an important flow characteristic, however it can not be measured directly using LDA. One of the methods to find the integral length scale is to use two-point LDA [115]. The integral length scale can then be calculated:

$$l_0 = \int \rho_l dr_l \tag{4.3}$$

where ρ_l is space autocorrelation coefficient and r_l is the distance between fixed and moving probe volumes.

Applying this method one LDA probe is fixed stationary in the required measurement position and another probe is moved across or along the flow stream. This method allows to collect data simultaneously from two probes at two different locations for the full range of distances between these locations. Therefore the data collected at different space positions can be correlated and the integral length scale

calculated using the equation 4.3 without major difficulties [141]. This was however an ambitious task and it was not possible to accomplish in our experiments.

For this reason one point LDA method was used in our experiments. To obtain integral time scale the "Correlation" option has been selected in BSA Flow package. The option allows to estimate autocorrelation function on the basis of the measured data. The autocorrelation coefficient $\rho(\tau)$ is calculated using the equation:

$$\rho(\tau) = \frac{R(\tau)}{R(0)} = \frac{\overline{u^*(t)\,u^*(t+\tau)}}{(u')^2} \tag{4.4}$$

where τ is the time lag, $R(0)$ is the correlation estimated at lag time zero, $R(\tau)$ is the estimated correlation.

The property "Correlation samples", which determines the number of discrete lag times at which the autocorrelation function should be estimated, has been chosen to be 1024 samples. The value of property "Maximum lag-time", which determines the largest lag-time at which the autocorrelation function should be estimated, has been set to 50 ms. To get reasonable results in turbulent flows the maximum lag time should be at least 10 times the integral time scale or even higher [140]. Several calculations have been made changing the lag time settings and it has been found that it had negligible effect for autocorrelation data results. All data were processed using the same settings. Finally the autocorrelation curves were plotted and the integral time scale τ_0 calculated using the equation:

$$\tau_0 = \int_0^\infty \rho(\tau)\,d\tau \tag{4.5}$$

In Fig. 4.4 typical autocorrelation curves are presented, taken in the same spatial position at different pressure and temperature conditions.

In order to calculate the integral length scale l_0, some simplifications must be made. It has been assumed that turbulence is convected with negligible change past the fixed measurement position at the constant average velocity. This assumption is called Taylor hypothesis, which assumes that because the turbulence has high power at large length scales, the advection contributed by the turbulent fluctuations themselves must be small, compared with the advection produced by the larger integral scales, therefore the advection of a field of turbulence at a fixed point can be taken as being due to larger, energy containing scales [142]. Although this "frozen

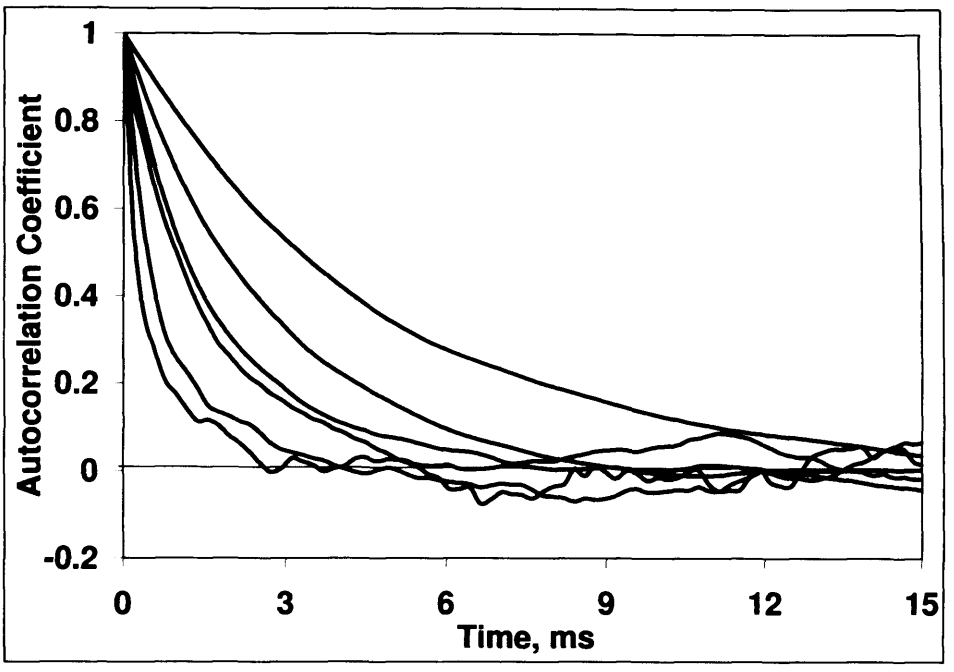

Figure 4.4: *Typical autocorrelation coefficient curves.*

turbulence" hypothesis can be applied only for low relative turbulence intensity ($u'/\bar{u} << 1$) flows [143], and according to some authors its validity for turbulent flows is questionable anyway [96], it has been used in many combustion investigations [17, 88, 144]. If the "frozen turbulence" hypothesis is assumed the integral length scale l_0 is calculated from the integral time scale τ_0 using the equation:

$$l_0 = \bar{u} \cdot \tau_0 \tag{4.6}$$

It was assumed that the flow is statistically axi-symmetric, therefore radial and circumferential root mean square velocities are equal, thus the total turbulence intensity q' can be calculated:

$$q' = \sqrt{\frac{(u')^2 + 2 \cdot (v')^2}{3}} \tag{4.7}$$

Measured velocities and turbulence characteristics data of isothermal air flow at different conditions later have been used to define velocities and turbulence parameters for every particular gas mixture.

4.1.3 LDA measurements at atmospheric conditions

LDA was used to measure velocity and turbulence characteristics at atmospheric conditions for the Bunsen burner. This was the first stage for the preparation for PLIF experiments.

Turbulence and velocity characteristics have to be investigated in order to obtain necessary data for further turbulent flame research. Three different Bunsen burner nozzles: 25 mm, 15 mm and 10 mm diameter, have been choosen for tests. In order to create turbulence several different turbulence plates were designed and tested. The turbulence plate with 1.5 mm holes, which created the most uniform turbulence intensity at the centre of the burner with 25 mm nozzle was later taken and used in the PLIF experiments (Fig. 3.6).

Due to the prevailing axial velocity component u one dimensional Dantec LDA system "Flow Lite" has been chosen. "FlowLite" is a low weight small size turnkey non-intrusive flow measurement system, which does not require adjustment. Due to its simplicity and reliability it was the best choice for performing experiments. The Dantec BSA Flow package was used for data processing.

Velocity characteristics were measured 5 mm downstream across the burner exit at the initial development region. Aluminium oxide particle were used for seeding the air flow. The tests were conducted for isothermal air flow. Typical "FlowLite" system settings were as follows: laser light wavelength - 532 nm, probe focal length - 160 mm, beam spacing - 38 mm, beam diameter - 1 mm, laser control volume - 0.210×0.210×3.432 mm. 3000 data samples were collected at each point measuring across the burner. The data samples rate was lower at the edges of the burner.

It was important to obtain uniform axial velocity profiles, i. e. to obtain the flows in the potential core. This was ensured by using a contracting shape burner nozzle. The axial measured velocity normalised by axial velocity at the centre of the burner u/u_c versus nondimensional radial burner measuring position r/d is plotted in Fig. 4.5. The colors represent different nozzles: red - 10 mm nozzle, blue - 15 mm nozzle, green - 25 mm nozzle. The numbers in the legend key represent approximate flow exit velocity.

It is seen from the graph that an unusual shape of the velocity profile is observed. The velocity profile convexes towards the nozzle exit at the centre of the burner.

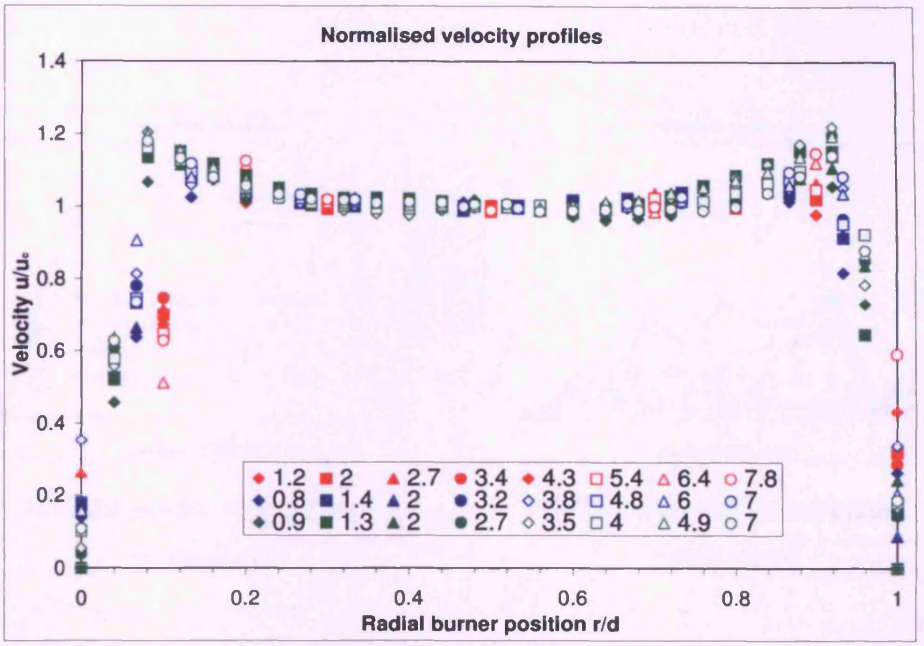

Figure 4.5: *Normalised velocity profiles with 1.5 mm turbulence plate for 10 mm, 15 mm and 25 mm nozzles. Colour coding: red - 10 mm nozzle, blue - 15 mm nozzle, green - 25 mm nozzle. Numbers in the legend represent gas exit velocity in m/s.*

One of the explanations of this phenomena is the spherical contracting shape of the burner, and the wall effect upon the axial velocity profile. Measurements conducted for the same nozzles further downstream did not show this effect [137] and fully developed flows were observed as expected.

Further investigation of the nozzles revealed that almost uniform axial flow velocity across the burner is obtained for exit velocities of up to 4.3 m/s for 10 mm nozzle, 3.8 m/s for 15 mm nozzle and 2 m/s for 25 mm nozzle (Fig. 4.6). This convex shape develops faster, i. e. at lower velocities, for larger nozzles, which implies that larger burners are more susceptible to wall effects on the velocity profile.

The RMS velocity profiles presented in Fig. 4.6 show large data scattering. For the 10 mm nozzle with 1.5 mm turbulence plate higher RMS velocities are observed at the centre of the burner, while for 25 mm higher magnitudes of u' are at the edges of the burner. RMS velocity is more uniform at the centre of the burner for larger nozzles, which implies that the nozzle diameter is an important factor for RMS velocity distribution across the burner.

To obtain more uniform profile of RMS velocities another turbulent plate with

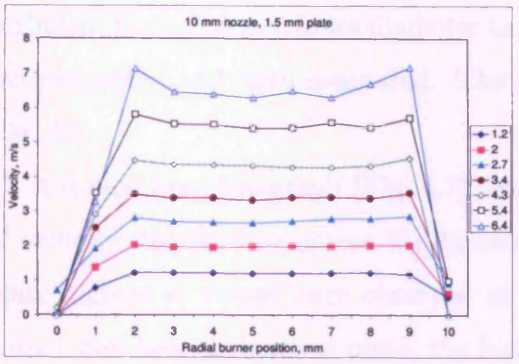

(a) axial velocity 10 mm nozzle

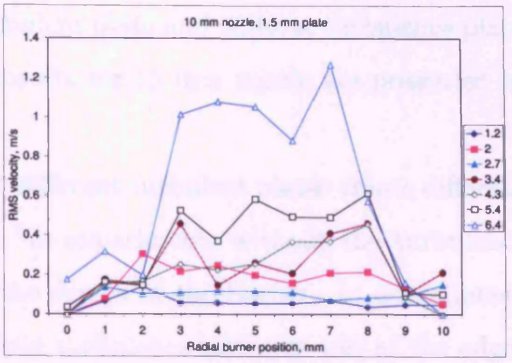

(b) RMS velocity 10 mm nozzle

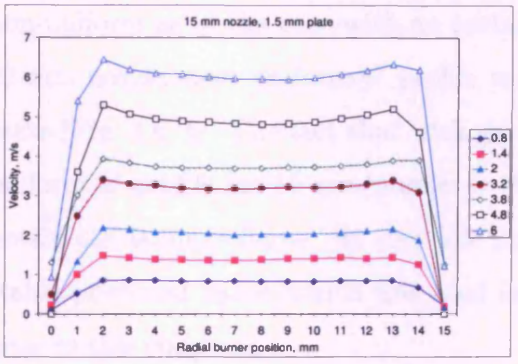

(c) axial velocity 15 mm nozzle

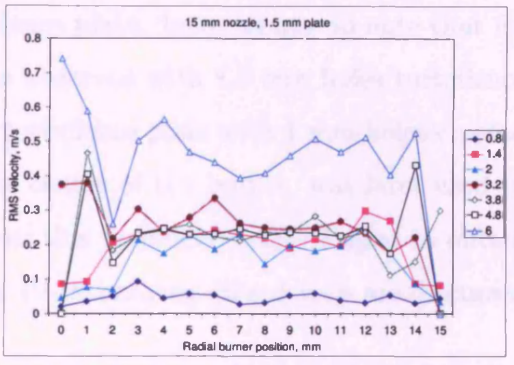

(d) RMS velocity 15 mm nozzle

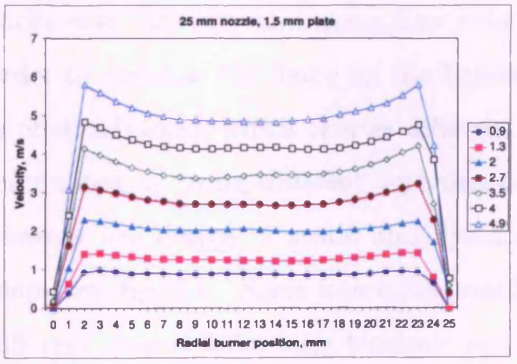

(e) axial velocity 25 mm nozzle

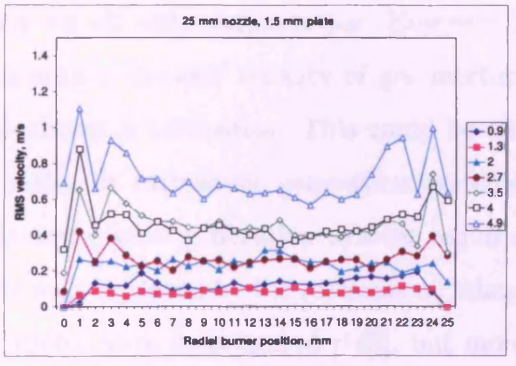

(f) RMS velocity 25 mm nozzle

Figure 4.6: *Bunsen burner velocity profiles with 1.5 mm turbulence plate: a) axial velocity 10 mm nozzle; b) RMS velocity 10 mm nozzle; c) axial velocity 15 mm nozzle; d) RMS velocity 15 mm nozzle ; e) axial velocity 25 mm nozzle; f) RMS velocity 25 mm nozzle. Numbers in legends represent gas exit velocity in m/s.*

smaller holes diameter was designed. When designing this plate the purpose was to obtain equal distance between the holes. The tests with 1 mm holes diameter turbulent plate, 1.5 mm holes diameter turbulent plate and without turbulence plate were repeated and data compared. The results for 15 mm nozzle are presented in Fig. 4.7.

It is seen from the graph (Fig. 4.7) that different turbulent plates create different u' velocity distribution across the burner. In experiments without the turbulence plate highest u' values were observed at the centre of the burner. In experiments with 1 mm hole turbulence plate, the highest turbulence intensity was at the edges of the burner. With the larger turbulence plate (1.5 mm holes) the u' profile became non-uniform as in the case with no turbulence plate. Interestingly to note that for 25 mm nozzle most uniform u' profile was observed with 1.5 mm holes turbulence plate (Fig. 4.6, f). The fact that with the turbulence plate with 1 mm holes created uniform u' profile for 15 mm nozzle at the centre of the burner, was later used to obtain the laminar flame. At very low flows this turbulence plate helped to obtain stable premixed flame, which was used for PLIF imaging (the details are discussed later in this chapter).

Using the Bunsen burner for investigation of S_T it is important to create similiar turbulence intensity and mean flow velocity for all equivalence ratios. However in order to stabilise the flame on the Bunsen burner the exit velocity of gas mixture is often adjusted, which creates different turbulence intensities. This could be circumvented by using different turbulence plates or turbulence generation systems, however the design of static and dynamic turbulence generation system requires more investigation. Some interesting results were reported by the researchers, where different shaped holes high blockage ratio plates were investigated [145], but more effort is needed.

Other turbulent characteristics at atmospheric conditions were calculated using the same technique as at elevated temperature and pressure conditions. The data processing was carried out using Dantec BSA Flow v4.11 software. The autocorrelation coefficient $\rho(\tau)$ was calculated using the equation 4.4 and the integral time scale τ_0 was found using 4.5.

The integral length scale l_0 was computing using the equation 4.6, assuming that

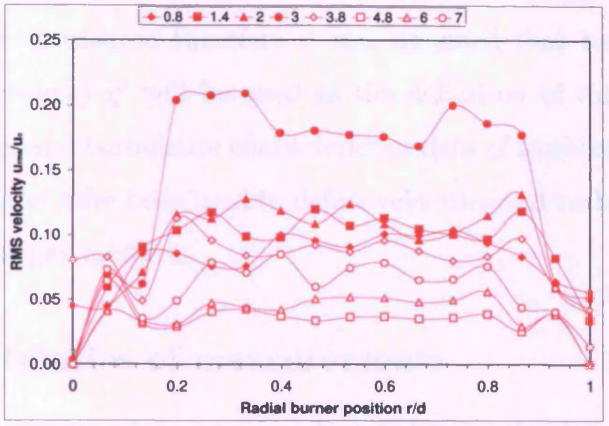

(a) without turbulent plate

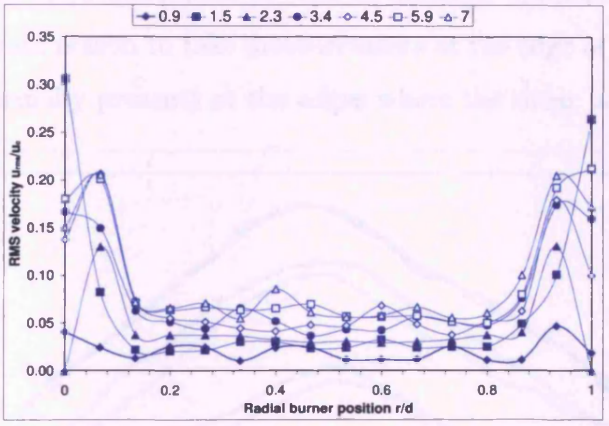

(b) turbulence plate with 1 mm holes diameter

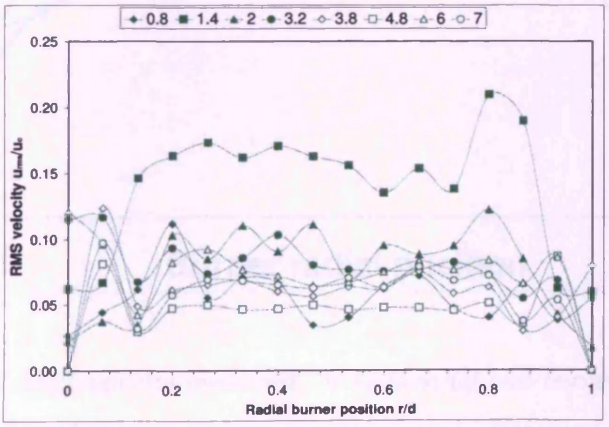

(c) turbulence plate with 1.5 mm holes diameter

Figure 4.7: *RMS velocity profiles for 15 mm nozzle with different turbulence plates. Colour coding: red - without turbulence plate, blue - 1 mm turbulence plate, green - 1.5 mm turbulence plate. Numbers in legends represent gas exit velocity in m/s.*

the field has uniform mean velocity and accepting Taylor's hypothesis. Only axial velocity profile was measured therefore it was assumed that turbulence intensity $q' = u'$. For consistency q' will be used as the definition of turbulence intensity. Measured velocities and turbulence characteristics data of isothermal air flow at different conditions later have been used to define velocities and turbulence parameters for every particular gas mixture.

4.1.4 Uncertainties of measurements

The turbulence intensity, q', has been calculated from the data measured at the edges of the burner at atmospheric as well as elevated temperature and pressure conditions. The main reason to take measurements at the edge of the burner is that the flame front normally presents at the edges where the shear layer forms.

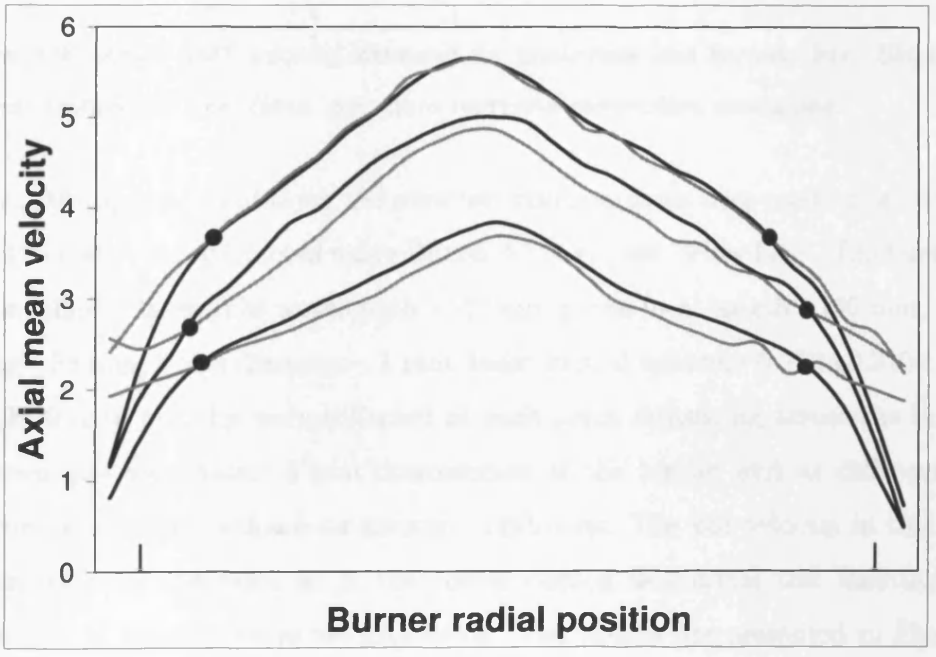

Figure 4.8: *Axial mean velocity measured for isothermal and burning jets. Black lines represent isothermal conditions, grey lines represent combustion conditions.*

However high temperature affects the velocity field via its influence on turbulence characteristics [95]. Flame and turbulence interaction change the turbulence characteristics. In order to test the influence of the flame on velocity fields, several experiments were performed using the Bunsen burner with fully developed turbu-

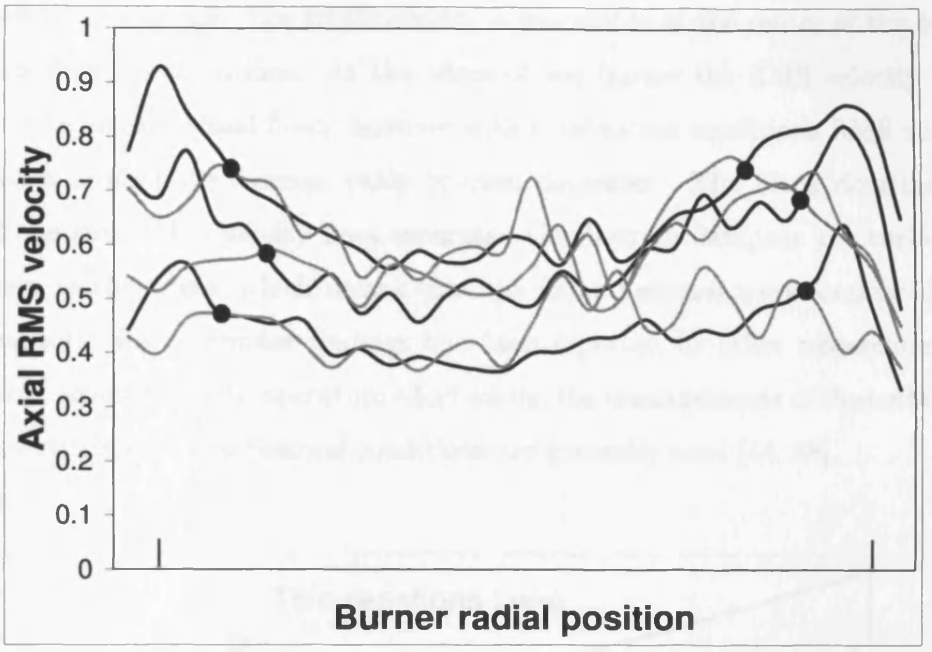

Figure 4.9: *Axial RMS velocity measured for isothermal and burning jets. Black lines represent isothermal conditions, grey lines represent combustion conditions.*

lence at atmospheric conditions. Aluminium oxide particles were used for seeding air flow. The tests were conducted using Dantec LDA system "Flow Lite". LDA settings were as follows: laser light wavelength - 532 nm, probe focal length - 160 mm, beam spacing - 38 mm, beam diameter - 1 mm, laser control volume - 0.210×0.210×3.432 mm. 3000 data samples were collected at each point measuring across the burner. Measurements were taken 5 mm downstream of the burner exit at different exit velocities under rich methane-air mixture conditions. The exit velocity in this combustion test was the same as in the corresponding isothermal test facilitating a comparison of the respective velocity fields. The results are presented in Figs. 4.8 and 4.9. Black lines represent isothermal conditions and gray lines represent combustion conditions. In order to better visualize the difference in velocity fields, black dots have been used to indicate the position where the velocity lines separate.

From the Fig. 4.8 it is observed that axial mean velocity is almost identical at isothermal and combustion conditions in the centre of the burner. At the edges, where the flame front normally exists, the axial velocity at combustion conditions is higher. This is due to the temperature effect on the velocity field. The opposite effect

is observed in Fig. 4.9. The RMS velocity is less stable at the centre of the burner with combustion conditions. At the edges of the burner the RMS velocity tends to increase at isothermal flows, however with combustion conditions RMS velocity fluctuates around the average value or even decreases. The black dots indicate where the two RMS velocity lines separate. Combustion dampens the turbulence intensity at the edges, which means that the flame becomes more laminar due to temperature effect. Similar findings has been reported by other researchers [88]. However, although the temperature effect exists, the measurements of the turbulence characteristics under isothermal conditions are generally used [44, 88].

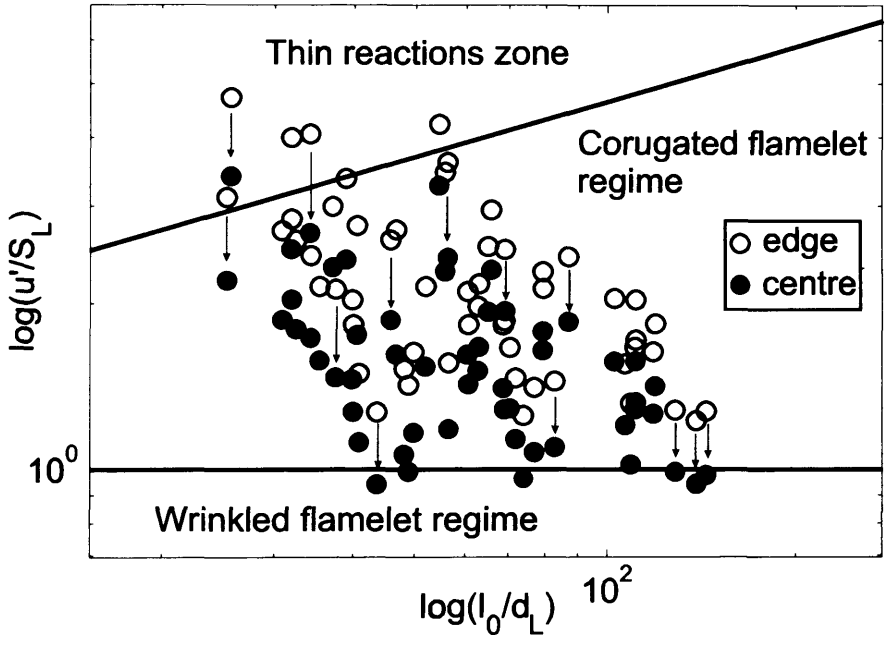

Figure 4.10: *Experiment results plotted in Borghi-Peters diagram*

As turbulence intensity fluctuates across the burner the question arises of where the turbulence characteristics should be measured. The turbulence intensity measured at the edge of the burner differs from the measurements at the centre of the burner (Fig. 4.9). However, it is shown here that this difference has very little effect on the turbulent flame regime. The magnified Borghi-Peters diagram is plotted in Fig. 4.10. An empty mark represents data collected from the edge of the burner, and for each empty mark there is a corresponding black mark representing the data

from the centre of the burner. Arrows represent the shift of data points due to the measuring position. Hence, data presented in Fig. 4.10 exist in pairs corresponding to the same experimental conditions. It can be seen that the vast majority of experiments have been conducted in the corrugated flamelet regime. The reduced turbulence intensity has not changed the position of the data points - represented by the separation distance between data pairs - in the diagram considerably. Therefore it can be concluded that the measurement position of the turbulence intensity is not a decisive factor in determining the turbulent combustion regime. This, however, is not a case for integral length scales. We have not obtained integral length scale measurements at the edge of the burner in our experiments [41]. Therefore it is not possible to estimate the changes of the integral length scale due to the measurement position, and its corresponding effect on the turbulent combustion regime.

4.2 Planar Laser Tomography

With the development of laser diagnostic techniques many different methods, such as: coherent anti-Stokes Raman scattering (CARS), cavity ringdown spectroscopy (CRDS), laser induced breakdown spectroscopy (LIBS), laser induced fluorescence (LIF), laser induced incandescence (LII), laser Doppler anemometry (LDA), particle image velocimetry (PIV) and others have been developed and are constantly improving [146]. These methods are used for determination of different combustion parameters, such as: concentration, temperature, velocity, emissions etc., however the flame visualisation remains one of the important part of combustion research. One of the often used methods for flame visualisation is Planar Laser Tomography (PLT), which gives an opportunity to observe the cross section of laminar and turbulent flames. This technique has been widely used for the investigations of laminar and turbulent flames using different combustion rigs [80, 104, 107, 144].

Several different methods have been utilised previously to identify the flame front of Bunsen type burner premixed turbulent flames. A popular approach to identify the average flame front is to superimpose raw flame images [17, 147] and calculate the threshold based on the ensemble average of the mean and maximum signal intensities [148].

Another common technique is to binarize raw images using bimodal intensity histograms [149] or to define the image conversion threshold value using manual or automatic methods. These binary images are subsequently averaged. The burning velocity can then be calculated using the flame cone angle method [36] or by rotating the averaged image around its central axis [147]. Most of the methods found in the literature rely on flame averaging.

In this section the PLT method used in experiments is discussed and the image processing techniques are presented. The flame front calculation methods are discussed and compared.

4.2.1 Flame Imaging

The planar laser tomography technique used in this study is based on the observation that the density of the products is lower than that of the reactants. Consequently when the uniformly seeded reactants are converted to products the seed density reduces and the scattered light intensity falls. As the flame thickness is small, a clear demarcation is generated between products and reactants which can be identified as the flame front.

First, all raw flame images are averaged (Fig. 4.11, a) using a bespoke Matlab script. Then a set of the background images (taken at the end of the test when the flame is no longer present) are averaged using the same image processing technique (Fig. 4.11, b). The average background image is then subtracted from the average flame front image (Fig. 4.11, c). The average flame front image is converted to the binary image using a defined threshold value (Fig. 4.11, d).

However, the "Averaged Flame Shape" method based on raw images is reliant on user interpretation of the results before defining the threshold value, which could introduce systematic errors. Also, it was observed that the flame front was very irregular in shape for all experiments independent of pressure and temperature. Hence this technique is considered unrepresentative for calculating the average flame front area from the average flame shape based on raw flame images.

As is seen from the image (Fig. 4.11, c), due to the different levels of light, the conversion from a grey scale image to the binary image could be misinterpreted. Although the threshold value can be selected manually or automatically, using an

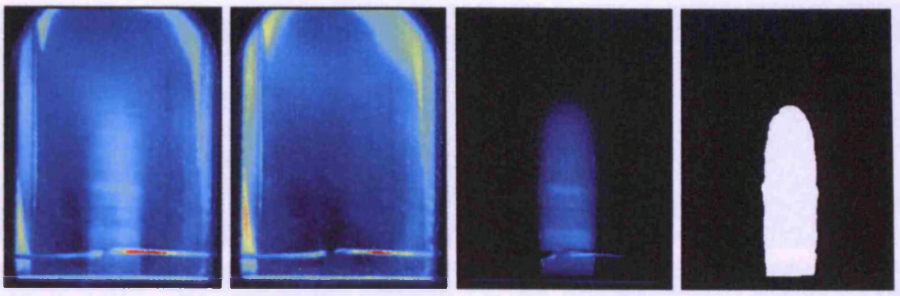

(a) (b) (c) (d)

Figure 4.11: *"Averaged Flame Shape" method based on raw images. a) - averaged flame image, b) - averaged background image, c) - averaged flame image background subtracted, d) - converted binary image.*

image processing technique, subjectivity cannot be eliminated. Hence a more robust method for calculating the area of the flame front was developed, the so called "Averaged Flame Area" method.

In this method, the area of each single flame image was calculated using Matlab. First, each individual image was filtered, using morphological image processing techniques and median filters, and the background subtracted. Subsequently the greyscale image is converted into a binary image using manually selected threshold values. Different threshold values are required for each test case, due to the variance of background noise and seed rates. After conversion of the grey scale images to the binary images (Fig. 4.12) the pixels of the flame area of every single image are counted and flame area calculated.

Flame area of each individual flame image is calculated using:

$$A = \sum_{1}^{k} (\pi \cdot n_k \cdot h \cdot w) \tag{4.8}$$

Here n - number of pixels; h - pixel height 0.353 mm; w^* - pixel width 0.353 mm, the pixel height and width were found by imaging a scale within the test section. To calculate the flame area each row of pixels within the image were then "rotated" around it own centreline axis. The side area of every cylinder made of pixels was calculated and summed. It was found by applying this method that there was substantial frame to frame variation in the surface area of the flames at a single operating point. In order to calculate the average turbulent burning velocity for

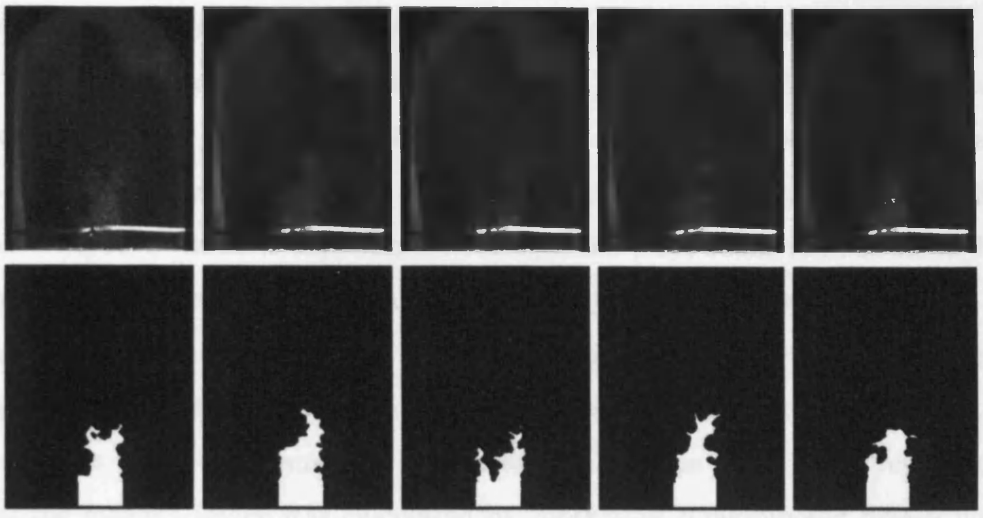

Figure 4.12: *Raw (top row) and processed binary (bottom row) methane - hydrogen mixture flame images*

each condition the statistical software Minitab was applied. Using this approach it was possible to identify and reject all results which were outside the limit of two standard deviations. A new mean flame area could then be found and finally the turbulent burning velocity calculated.

The image processing of the images obtained using the Bunsen burner was carried out in order to calculate the turbulent burning velocity. Several different methods are utilised to identify the flame front of premixed turbulent flames [17, 147–149]. Most of these techniques rely on the averaging of the flame images. One of the biggest issues in image processing is the conversion of gray scale images into the binary images as the image intensity is variable. Some researchers suggest converting images applying a dynamic threshold technique, which selects variable threshold values depending on image intensity at different image areas [150].

In our investigation we used two different methods. The first image processing method was based on statistical data treatment of the set of images. Using this method every single gray scale image was converted to the binary image. At first all images were reviewed and unreadable images were deleted. The background images were subtracted from every single image, in order to avoid background noise. Then, using morphological image processing functions, which are as standard included in Matlab Image Processing Toolbox, the gray scale images were filtered. The threshold value was calculated and the gray scale images were converted to binary images. The

binary images then were used to calculate the flame front area [41].

The second image processing method is a well established and widely used image averaging method. Using this method every single image was treated using the same image processing technique. Then all binary images were superimposed and the final image obtained. In such superimposed images the pixel count reached its highest value (which was equal to the number of binary images) in the areas where the flame was present in all images. In the areas where the flame is present in fewer images, obviously the pixel value was lower than the maximum possible value. In the patches where the flame was not present at all, the pixel values remained 0. Thus the average image was calculated by converting superimposed binary image to binary image, using the threshold value which was equal to half the number of all processed images. This technique allowed the production of the averaged image which represents the progress variable 0.5.

It was noted that using the binary image averaging technique, image conversion problems could be recognised easier than using a "statistical" method. When the final average binary images were processed, it was found that in some cases pixel values outside the flame region were equal to 1, although in reality it should have been zero, as the region was not in the flame zone. This can occur because of the large background noise due to large quantities of seeding passing into the combustion chamber (especially during methane tests). Aluminium oxide particles collected in the combustion chamber and created a background noise. Even after the subtraction of the background images the noise remained in the gray scale images and then created unwanted spots in the final average binary image. The averaging technique was more reliable in comparison with the "statistical" method, as it helped to identify the areas which were "polluted" with seed.

The flame front area of every single image was calculated using the "statistical" method. Therefore in order to calculate the average flame front area for each condition the statistical data processing was carried out. Using this approach it was possible to identify and reject all results which were outside the limit of two standard deviations. A new mean flame area then was found and accepted as the representative value.

Only one flame front area value was obtained using "averaging" method. For

both methods the same equation 4.8 was used to calculate the flame front area.

Each row of pixels within the image were "rotated" around it own centreline axis. The side area of every cylinder made of pixels was calculated and summed.

Finally having the flame front areas calculated, the burning velocity is computed by the equation 2.43. The mass flow rate $\dot{m}$ is measured during experiments, and the density of the reactants ρ_R is calculated from the experiment conditions. Flame front area A is calculated using either "statistical" or "averaging" methods.

The comparison of two flame front area calculation methods for methane-carbon dioxide mixtures and methane - hydrogen mixtures are presented in Fig. 4.13 and Fig. 4.14 respectively.

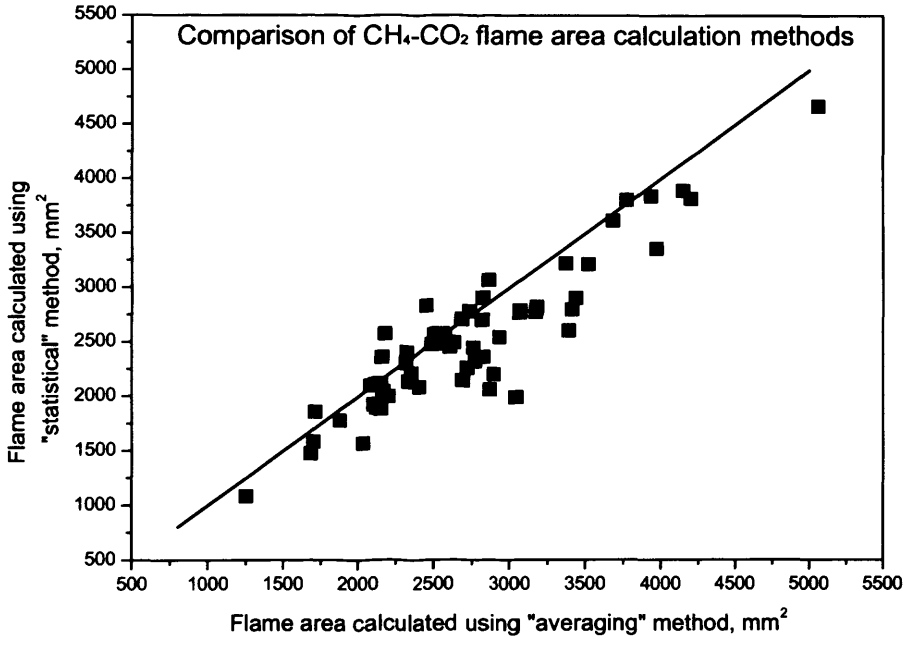

Figure 4.13: *Comparison of methane and methane-carbon dioxide flame area calculation results obtained using different image processing methods.*

The results show reasonably good agreement, though some degree of data scatter can be observed. The flame front area computed using the average binary image processing method, based on binary images is in most cases lower than obtained using "statistical" method, which means that the burning velocity calculated from equation 2.43 gives the higher results. The variation in calculated flame area between two methods is approximately 5%. Statistical non-parametric hypothesis test shows that there is no significant difference in these data sets. The single image processing

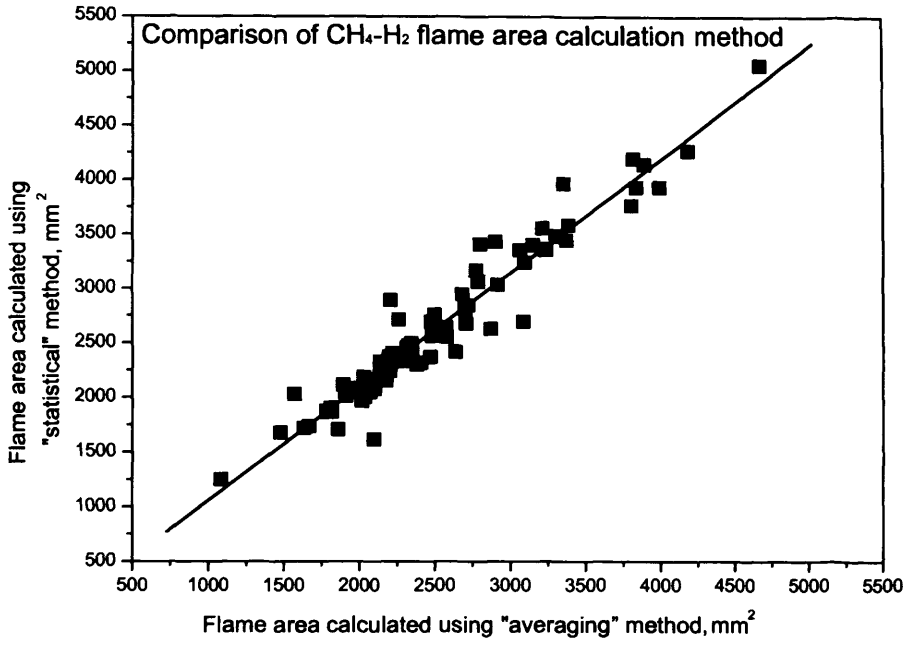

Figure 4.14: *Comparison of methane and methane-hydrogen flame area calculation results obtained using different image processing methods.*

technique is supposed to be more reliable due to the fact that every single image is processed and statistical methods can be applied for the set of data. However this approach requires some assumptions to be made. One of the assumptions is that the flame area is evenly distributed around the axis. Processing images using different technique produces very similar results and both techniques could be used to calculate the flame front area for the flames in the flamelet regime. However the statistical method is not suitable to investigate such flame structure quantities as turbulent flame thickness and flame surface density. Therefore the data obtained using average binary image technique has been used for turbulent flame structure analysis and discussions (chapter 9).

4.2.2 Image Analysis

In previous section the sequence of the PLT process has been described. One of the most important part of the whole method is image analysis. In this section the image processing techniques using Matlab are discussed.

To process the images, Matlab Image Processing Toolbox (IPT) was used. IPT provides a comprehensive set of functions for digital image manipulation, analysis

and processing. Matlab code has been written using functions included in IPT. During the image processing it was important to define the types of images in order to use appropriate treatment method and gain the necessary information from every type of images. Two types of images were used: intensity and binary images. An intensity image is a data matrix containing the information of image pixel intensity, which is represented as integer value in the range of [0, 255]. These images are also called grey scale images. Image processing was conducted mostly with these grey scale images, because they contained useful information. However these images were not suitable for final data processing therefore they were converted to binary images. Binary images are data matrices containing only value 0 or 1. In order to define which image region must be converted to pixel values 1 and which must obtain value 0 was the most important task. Improper image treatment could lead to large error. It was decided that in the binary image the area where the flame exists the pixels would have value 1 and others would be 0. The image size was 416 $\times$ 512, which means that image consisted of 456 pixel rows and 512 pixel columns.

The main disadvantage of using PLT technique is that seeding is required. Obviously seeding is necessary to distinguish the unburnt mixture zone from burnt gases, however it also creates additional problems, such as background noise. Background noise must be avoided as it could influence the results. One of the best methods to delete background noise is to use filters or to perform fundamental morphological operation, such us: dilation and erosion [151].

During every test 1000 images were collected. Some images were not suitable for image processing therefore they were deleted beforehand. Every single image of the experiment was treated using the same algorithm. After each test the background images of the combustion chamber were taken. These images were used during the image processing.

The progress of flame image processing is presented in Fig. 4.15. A single image of a methane flame is used. The raw image (Fig 4.15 a) contains a lot of useless information, which must be erased. Therefore the background image (Fig 4.15 b) is subtracted from the raw image and modified raw image is obtained (Fig 4.15 c). The erosion function is applied on the subtracted raw image. Erosion shrinks the object. To control the erosion function a special structuring element was used, which

defined how erosion function should act. The eroded image was then reconstructed and eroded again (Fig 4.15 d). This procedure improved the image quality by filtering the noise and filling the holes which appeared due to the ignitors. However morphological image processing was not sufficient for some very "noisy" images. For that reason additional median type filter was used. The filtered image did not loose useful information (Fig 4.15 e), and a smoother image was obtained.

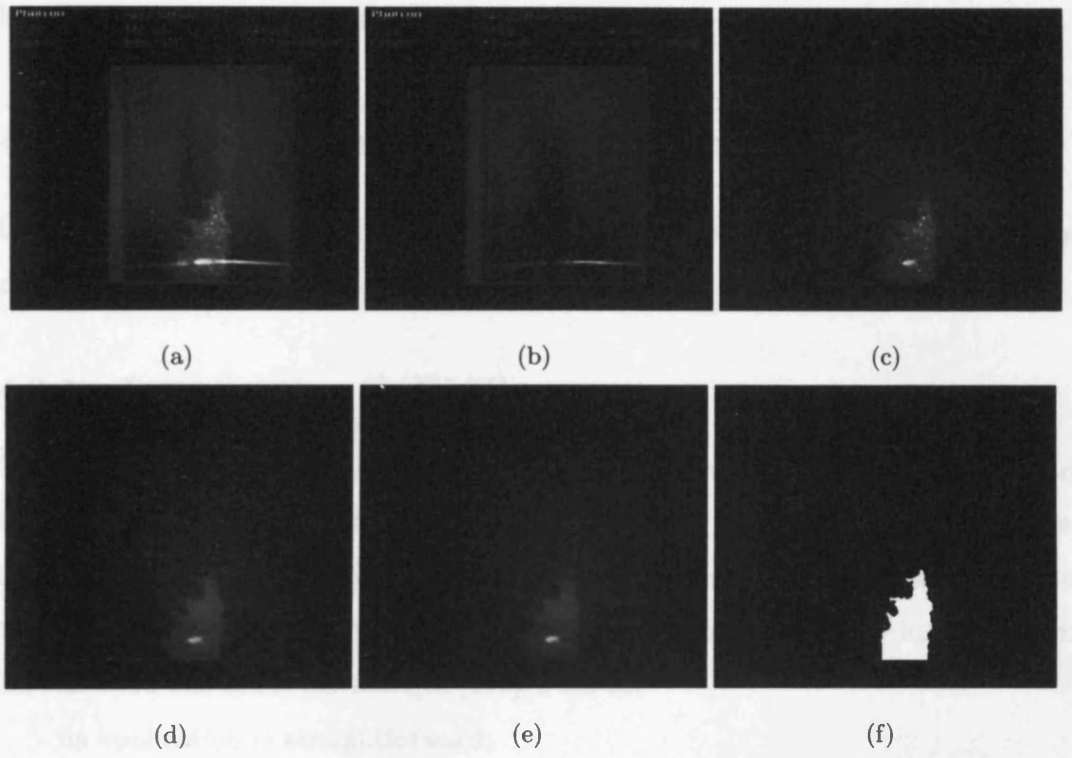

Figure 4.15: *Flame image processing progress: a) raw image; b) background image; c) subtracted raw image; d) reconstructed image; e) filtered image, f) binary image.*

All processed grey scale images then had to be converted to binary image. Several problems may arise during the conversion. The main problem is the image intensity and selection of the threshold value. Grey scale images are normally converted to binary images by defining the threshold value, which defines which pixels must turn into 1 or 0. Threshold value must be selected or calculated carefully, as the results due to incorrectly chosen value can produce errors. For this purpose an automated threshold finding technique is often used [151]. However, in this work the manual threshold determination method was used, as the automated method produced unacceptable results. This happens due to uneven laser light and uneven

seed distribution for different images. The manual method was more reliable as the exact demarcation line was visually recognised and verified. However for some images it produced the dark areas in the flame region where the laser sheet light intensity was lower. To circumvent that issue the mask for every set of images obtained during different tests was used. The purpose of this was to cover the areas where the flame definitely existed. Adding the mask and binary image the final binary image was obtained (Fig 4.15 f).

4.3 Planar Laser Induced Fluorescence

In this section a more detail description of PLIF method is provided and the image processing techniques using this method are discussed.

4.3.1 Introduction to PLIF

Laser Induced Fluorescence (LIF) is a process when molecules or atoms are excited to higher electronic energy states via laser absorption and subsequently fluoresce. This laser spectroscopic method is widely used in combustion research for the qualitative and quantitative analysis of combustion species or for flame front identification. This method has many advanatges [152], such as:

- its application is straightforward;
- it produces 2D images which have much of useful information;
- short exposure times give sharp images;
- it can be used for many species which are importnt in combution research.

However as every method, PLIF has several drawbacks [152], such as:

- difficult to choose the exitation and detection wavelengths;
- tunable dye lasers are complex in construction and difficult to operate;
- more interesting species have a very low concentration and are not easily detected.

Despite all these disadvantages PLIF is still a very important tool used for flame front detection. For that reason PLIF is normally adjusted to excite OH radicals, which are good markers of the flame front. The OH radicals appear when the temperature increases to a certain value (Fig. 2.2). It occurs inside the reaction

zone, therefore it is assumed that appearance of OH radical indicates the flame front. When reaction zone ends OH radicals concentration falls, although they spread all over the products zone which can be seen from the images.

Another possible flame front marker might be CH radicals, which have a very short lifetime, but which is found only in the region of the flame front and does not spread with the products. Experimental research of simultaneous OH and CH PLIF revealed that both these techniques produced very similiar results [150]. However CH detection is more complicated due to CH sensitivity to local equivalence ratio [150].

Detection of molecules or atoms in PLIF is dependent on excitation and detection wavelengths. These wavelengths must be carefully selected in order to conduct successful experiments. The laser sheet of particular wavelength illuminates the molecules or atoms (OH radicals in this case). Absorption of the laser light produces OH radicals in the excited state, i.e. with a lot of internal energy. OH radicals loose energy, but there are different mechanisms by which this decay in energy occurs. The main pathways of energy decay are represented in Fig. 4.16. Incident laser light is resonant with the transition between levels 1 and 2. Absorption of the photon excites molecule and transfers it energy from level 1 to 2. Excited molecule may loose energy by radiation (A in figure), nonradiative collision-induced decay (quenching Q in figure), dissociation (D) and chemical reaction (C) [153]. Only one lower state level 3 is indicated in Fig. 4.16.

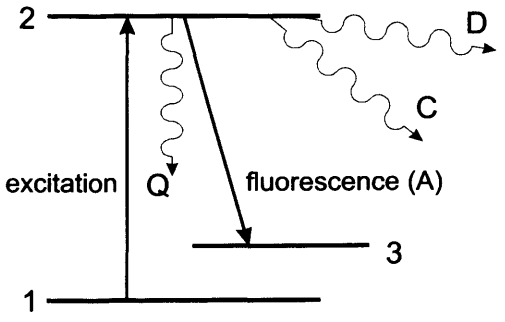

Figure 4.16: *Schematic energy level scheme in PLIF experiments. Reprinted from [153].*

Strong light absorption leads to a strong fluorescence, therefore correct laser wavelength selection and suitable image capture system settings are crucial. There are several wavelength bands, which could be used for excitation of OH radicals. The

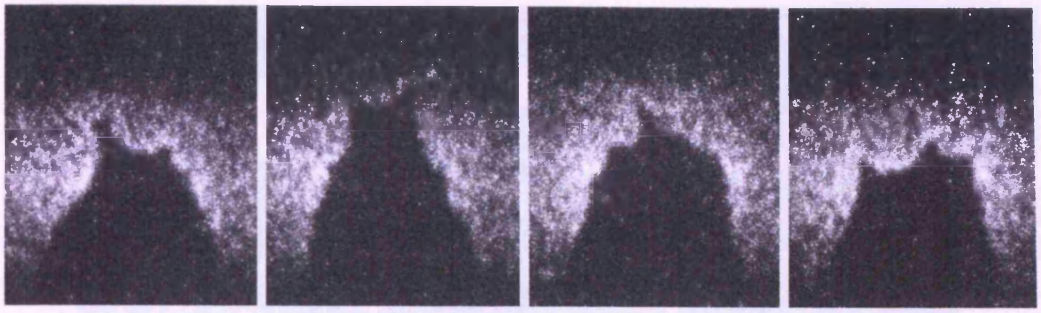

Figure 4.17: *PLIF OH raw images*

excitation of around 283 nm wavelength and detection at around 310 nm wavelength scheme is often used as it provides good results [150, 152, 154].

4.3.2 Flame imaging and image processing

PLIF used in this study is based on the observation of OH radicals. OH radicals, which are produced by combustion are located outside the flame envelope. Laser light sheet tuned specifically to excite OH radicals is used. Some of these radicals absorbs the incident light and are promoted to higher electronic energy state and emit light (fluorescence). The light is caught by camera. In the region where are no OH radicals the light intensity is low, and in the area where are many OH radicals the light intensity is high. The reactants have no OH radicals, which start to appear in products, therefore a clear demarcation, generated between products and reactants, can be identified as the flame front, assuming that the flame thickness is very small. This technique has been widely used by researchers to investigate turbulent and laminar flames [44, 88–90, 120, 155–160].

It has been shown in previous sections that the flame area calculated from the averaged binary images and using statistical data treatment of single binary images has no significant difference [161], therefore the flame area calculated from averaged binary flames and the S_T derived from it are used in further discussions.

Raw images taken using PLIF are presented in Fig. 4.17. It is seen that these images differs from the PLT images (Fig. 4.12), therefore a slightly different approach was used to process these images. The images obtained using PLT were more "noisy" and the background needed to be subtracted in order to alleviate unnecessary data appearing in the image. PLIF images did not contain unwanted details (such as

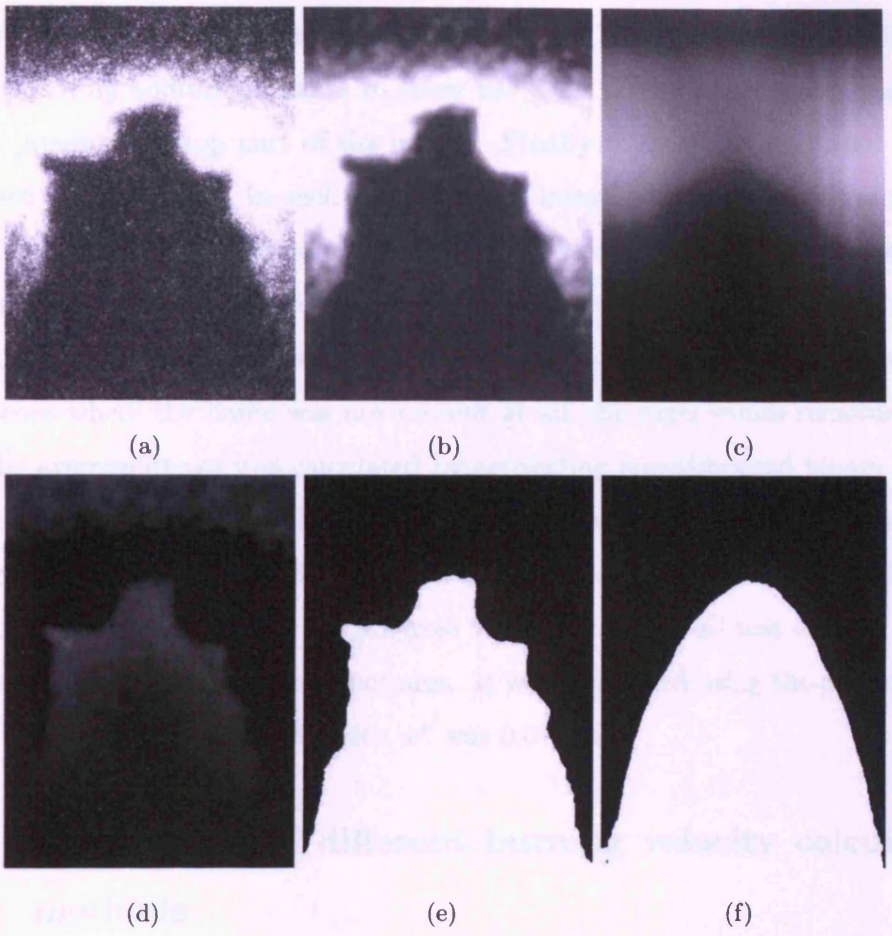

Figure 4.18: *PLIF flame image processing progress: a) raw image; b) filtered image; c) created background image; d) subtracted image; e) binary image, f) averaged image.*

ignitors in HPOC) and the images were less "noisy" although some graininess was observed. 450 images were taken for every test conditions for all fuels. The Matlab Image Processing Toolbox (IPT) was used to treat the images. The evolution of single image processing is presented in Fig. 4.18.

At first every single image was cropped in order to reduce the processing time. Then raw flame image (Fig. 4.18a) was filtered using the median filter in order to reduce the graininess (Fig. 4.18b). Then the averaging filter using a large mask size was applied, which created the background image (Fig. 4.18c). This background image accounted for the non-uniformity of the light intensity. Averaging filter function parameters were selected manually for every data set. These parameters were almost the same for all tests. Subtracting original filtered image (Fig. 4.18b) from the created background image the new subtracted image was obtained (Fig. 4.18d).

The conversion of the subtracted image into the binary image (Fig. 4.18e) was conducted using additional masks to cover the areas of the image which the flame did not present (the top part of the image). Finally filtered and converted images were used for averaging. In such superimposed images the pixel count reached its highest value (which was equal to the number of binary image) in the areas where the flame was present in all images. In the areas where the flame is present in fewer images, obviously the pixel value was lower than the maximum possible value. In the patches where the flame was not present at all, the pixel values remained zero. Thus the average image was calculated by converting superimposed binary images to a binary image, using the threshold value which was equal to half the number of all processed images. This technique allowed the production of the averaged image (Fig. 4.18f), which represents the progress variable 0.5. For all test average images were used to calculate the flame front area. It was caluclated using the equation 4.8. In this case pixel height h and width w^* was 0.079 mm.

4.3.3 Comparison of different burning velocity calculation methods

Processed binary images are used to calculate burning velocity. It has been shown in previous section that to calculate turbulent flame front area A the equation 4.8 needs to be used. It must be emphasised that laminar flames can be calculated using the same equation as well. The validity of this equation was tested against the well known flame cone angle method, which is widely used to calculate S_T and S_L [26, 36, 106].

For that reason the laminar flame at stoichiometric conditions was obtained using the 15 mm nozzle. The main reason to choose the 15 mm nozzle was that the laminar flame stabilisation was much easier and the flame length was not high, i. e. the flame was in the region covered by the PLIF laser sheet. 150 raw flame images were recorded. Using the flame cone method the flame cone half angle α can be estimated (Fig. 4.19). For laminar flames the estimation of α is not difficult as a sharp flame apex is usually observed. However for turbulent flames this procedure is much more dubious, as the flame cone has no sharp apex (Fig. 4.19, b). Every single image was treated using the same procedure as for turbulent flames described

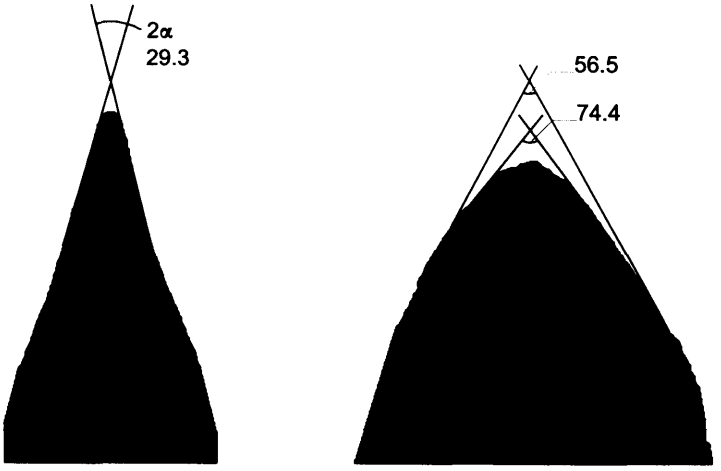

Figure 4.19: *Burning velocity calculation using the flame cone method. a) averaged laminar flame, 15 mm burner nozzle; b) averaged turbulent flame, 25 mm burner nozzle.*

above. Flame images were binarised and the average image obtained. Flame cone angle was measured and S_L calculated from the equation:

$$S_L = u \cdot sin\alpha \tag{4.9}$$

where u is axial mean velocity of gas air mixture and α is the flame cone half angle.

Average axial velocity during the test was $u \approx 1.42$ m/s and $\alpha = 29.3/2$. Therefore the estimated $S_L = 0.359$ m/s.

Using the equation 4.8 for the same binary flame image, the flame front area A and S_L (based on equation 2.43) were calculated. The computed value $S_L = 0.363$ m/s was very close to the flame cone angle method result, therefore it implies that equation 4.8 provides a very good estimation of S_L and could be used for calculations. Based on these findings and taking into account that the flame cone method is ambiguous for turbulent flames it can be concluded that equations 4.8 and 2.43 are more accurate for calculation of S_T.

4.4 Summary

Different research methods were presented in this chapter. Several different image processing techniques are derived: single image processing using statistical approach and averaged flame image data treatment. The comparison of two flame image processing methods presented has shown that both methods have produced very similar results with an error of approximately 5%. Although statistical image processing method have been shown to be acceptable it can not be used for the determination of flame structure characteristics, such as: flame surface density and flame brush thickness.

Uncertainties in LDA measurements for isothermal and non-isothermal flows were discussed. Comparison of experiments of isothermal and non-isothermal velocity and turbulence intensity measurements was presented and combustion effects on the velocity field and turbulence intensity at the edges of the burner, where normally the flame front is located, was emphasised. The local axial velocity increases and the turbulence intensity is reduced due to the flame effect. Therefore for the Bunsen burner, velocity measurements under combustion conditions produce more reliable results at the edges of the burner than for isothermal measurements. This should be considered in future studies.

The importance of measuring position of the turbulence intensity and turbulent length scale was shown. Turbulence intensity measured at different burner radial positions across the burner at elevated temperature and pressure conditions was found to be variable, however its effect on the general flame regime, defined in Borghi diagram, was shown to be small. In the vast majority of test cases, the flames was found to lie in the corrugated flamelet regime for both the centre and edge of the burner in the tests conducted in HPOC.

Chapter 5

Numerical calculation of laminar flames

The investigation of premixed laminar flames forms an important part of turbulent flame research. Many models developed for premixed turbulent flames rely on the data of laminar flames. Laminar flame speed S_L can be calculated using analytical or semi-analytical methods, when chemistry and transport are suitably simplified [95], however numerical solutions are most often used for more complicated chemical schemes. S_L of laminar premixed flame is defined as the propagation velocity of a plane, undisturbed flame without heat loss and buoyancy effect [162]. It is difficult to produce such flames experimentally, however this definition is suitable for numerical calculations using detailed kinetic reaction schemes. As S_L is constant under specific pressure and temperature it can be assumed as a gas property similar to density or viscosity.

In this chapter the results of the calculation of unstretched laminar burning velocity S_L and laminar flame thickness δ_L for methane, methane - hydrogen and methane - carbon dioxide flames using the Chemkin-Pro software package is presented. Different chemical kinetic mechanisms are used in combustion research, therefore a short review of these mechanisms and their limitations is provided. The emphasis is made on methane and methane - hydrogen gas mixtures, because kinetic mechanisms produce different results with hydrogen addition. Carbon dioxide addition is not so critical as CO_2 is incombustible gas and is assumed to act as a ballast gas.

5.1 Chemkin-Pro numerical tool

Unstretched laminar burning velocity of gas mixtures have been modelled using the Chemkin-Pro [111] software package. It consists of a set of different application models, which are used to solve various chemical kinetic problems. "Flame Speed Calculator" reactor model has been used to determine the laminar speed of one-dimensional freely propagating flame. The Premix [110] code, developed by Sandia National Laboratories, has been used to run this model.

"Flame Speed Calculator" model with "Parameter Study Facility" option has been utilised to perform the numerical burning velocity calculations. The model simulates a freely propagating flame in which the point of reference is a fixed position on the flame, thus the flame speed is defined as the velocity of unburned gas moving towards the flame. This model uses mixture averaged transport properties formulation. Equivalence ratio has been chosen as the variable parameter. A number of runs have been performed for different temperature and pressure conditions. The domain length of 10 cm has been specified and the grid of 200 points has been selected, which has facilitated faster convergence. Adaptive grid control parameter based on gradient GRAD = 0.1 and adaptive grid control parameter based on curvature CURV = 0.1 have been selected. The initial grid based on temperature profile estimate has been specified. Mixture averaged transport correction velocity formalism, with automatic estimation of temperature profile options, has been used.

"Flame Speed Calculator" reactor model requires the set of gas phase kinetic data, species thermal properties data and species transport properties data to be chosen before calculation. There are many chemical kinetic mechanisms developed for combustion research. Different kinetic models should be used for different gas mixtures as no one mechanism can be considered as a universal model for all possible gas mixtures.

5.2 Chemical kinetic mechanisms

There are many chemical kinetic mechanisms developed for numerical calculations. GRI-Mech [59] mechanism is often used in the combustion research of hydrocarbons. It considers 53 species and 325 elementary reactions. This mechanism has been

developed to investigate methane and natural gas flames and has been validated at various pressure and temperature conditions. Various researchers have reported that this mechanism could also be suitable to some extent for biomass gasification-derived producer gas [54], methane hydrogen mixtures [47, 56] and for hydrogen air mixtures [43, 58] at atmospheric conditions. However there have been significant discrepancies observed between experimental data and numerical calculations using GRI-Mech kinetic mechanism for pure and diluted hydrogen at higher pressures [58, 163].

Another well known kinetic mechanism, which has been developed by University of California in San Diego, is often used in combustion research. This kinetic mechanism considers 46 species and 235 elementary reactions. Lafay et al. [52] has utilised GRI-Mech and San Diego mechanisms to calculate flame thickness. They have proved that these mechanisms are in good agreement with the experimental data at the atmospheric conditions at equivalence ratio above 0.55.

The comparison of GRI-Mech v3.0 and San Diego kinetic mechanisms at elevated temperature and pressure conditions is presented in Fig. 5.1. GRI-Mech v3.0 and San Diego results are almost identical for the 70% methane and 30% hydrogen mixture. Significant discrepancies between these two models can be observed in the region of equivalence ratio below 1 and above 1.4, although in the region from 1 to 1.4 GRI-Mech produces higher flame speed results. At higher hydrogen concentrations in the mixture GRI-Mech underpredicts flame speed. This supports similar findings of other researchers [58].

For pure hydrogen combustion several kinetic mechanisms have been recently developed. Konnov reviewed these models and presented updated chemical kinetic mechanisms [164]. Ströhle and Myhrvold reported [58] that Li et al. [165] and O'Conaire et al. [163] chemical kinetics mechanisms for hydrogen provide more accurate results in comparison with experimental data at elevated pressures, whilst GRI-Mech underpredicts laminar flame speed considerably. They also showed that the San Diego [60] mechanism yields reasonable results for helium diluted high pressure hydrogen flames. Sarli and Benedetto [5] found that the GRI-Mech kinetic mechanism, used in their simulation, underpredicted laminar burning velocity at high hydrogen content in the methane - hydrogen mixture.

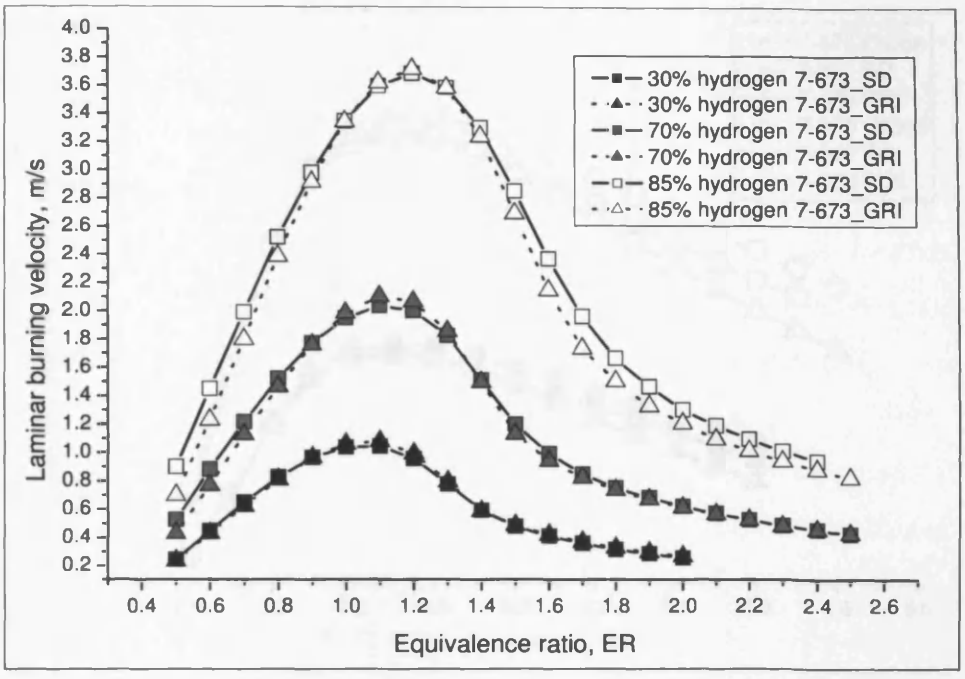

Figure 5.1: *Laminar flame speed calculated using Chemkin-Pro at 7 bar and 673 K. Numbers in the legend key represent hydrogen amount in the mixture.*

The results of calculations using O'Conaire et al. [163], San Diego and GRI-Mech v3.0 chemical kinetic mechanisms are presented in Fig. 5.2. The calculation have been performed at 7 bar 473 K and 673 K. The O'Conaire et al. mechanism has been developed to simulate the combustion of hydrogen and oxygen in a variety of combustion environments and over a wide range of temperatures, pressures and equivalence ratios. The O'Conaire kinetic mechanism comprises of 8 species and 19 elementary reactions. The temperature ranges from 298 to 2700 K, the pressure from 0.05 to 87 atmospheres, and the equivalence ratios from 0.2 to 6.

It is seen from Fig. 5.2 that GRI-Mech v3.0 mechanism underpredicts hydrogen flame speed in the region of equivalence ratio of up to 1 and above 1.5 in comparison with O'Conaire mechanism. The San Diego mechanism predictions are more accurate in comparison with GRI-Mech. The O'Conaire mechanism predicts the highest flame speed.

Taking into account the above research it has been concluded that different mechanisms for different methane - hydrogen fuel mixtures should be used. The GRI-Mech mechanism has been used for methane - hydrogen with hydrogen content up to 50%, because it is believed that methane combustion kinetics prevail in the

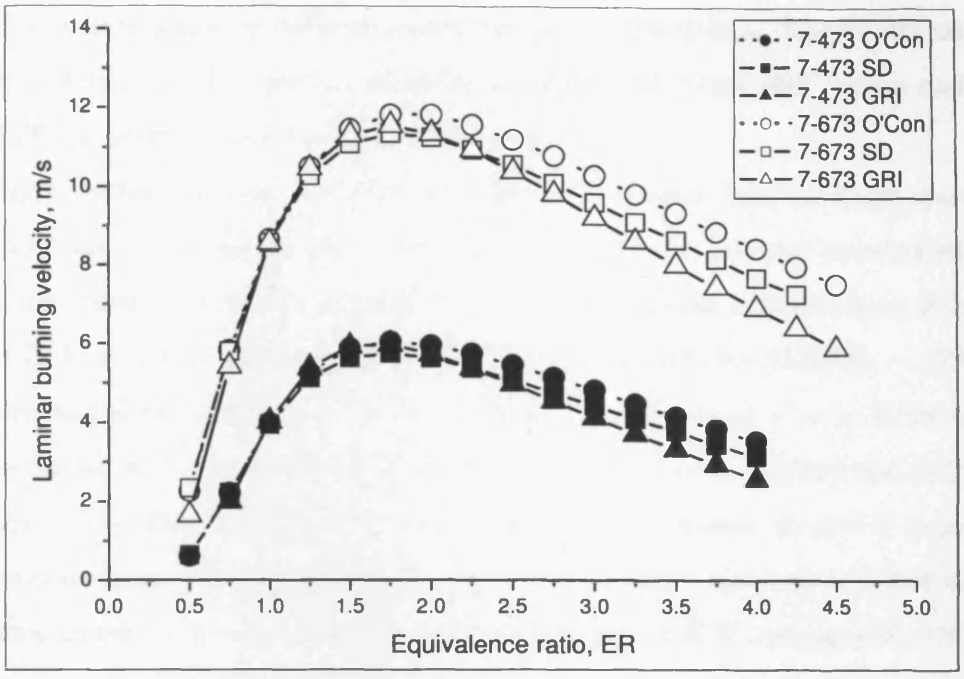

Figure 5.2: *Hydrogen laminar flame speed computed using GRI-Mech, San Diego and O'Conaire mechanisms at at 7 bar and 473 K and 7 bar and 673 K.*

combustion process. The San Diego mechanism could be suitable for the investigation of methane - hydrogen mixtures with the hydrogen content above 50% at elevated pressures, because it has been shown [58], that this mechanism predicts hydrogen laminar flame speed more accurately at elevated pressures. The O'Conaire at el. mechanism can be utilised for laminar flame speed calculation for pure hydrogen, as its accuracy has been supported by other reseachers [58, 163].

As the hydrogen content in the mixture is not high (up to 30% by volume) it is believed that methane combustion kinetics prevail in the combustion process. Therefore taking into account other work it has been decided to use GRI-Mech v3.0 mechanism for all our methane - hydrogen mixtures at atmospheric and elevated temperature and pressure conditions.

5.3 Laminar burning velocity modelling results

5.3.1 Chemkin results

Laminar burning velocities S_L of lean and rich methane - carbon dioxide mixtures and methane - hydrogen mixtures have been calculated using GRI-Mech v3.0 chem-

ical kinetic mechanism at different pressures and temperatures. The results are presented in Figs. 5.3, 5.4 and 5.5. Marking in legend key "15_1-300" means methane and 15% gas mixture at 1 bar and 300 K conditions.

Higher carbon dioxide quantities in methane decreases laminar flame speed for all conditions. Temperature has an enhancing effect on S_L, however pressure reduces the flame speed. In general it is observed that temperature augmentation from 300 K to 673 K at 1 bar pressure increases S_L by about 440% for $85\%CH_4 - 15\%CO_2$ mixture and about 460% for $70\%CH_4 - 30\%CO_2$ mixture at $\phi = 1$. Even higher augmentation of S_L by about 490% for $85\%CH_4 - 15\%CO_2$ mixture and 510% for for $70\%CH_4 - 30\%CO_2$ mixture is observed at 3 bar pressure at $\phi = 1$ increasing temperature from 473 K to 673 K. Further increase of pressure up to 7 bar reveals the same trends. The augmentation of S_L measured at 300 K compared to 673 K at $\phi = 1$ aproaches 530-570% although the absolute values of S_L decreases compared to 3 bar. It implies that pressure affects S_L differently at ambient and elevated temperatures.

Higher hydrogen content in methane - hydrogen mixture increases S_L. The results observed for methane - hydrogen mixtures resembles the results obtained from calculations of methane - carbon dioxide mixtures. Temperature increases S_L and pressure reduces it. However for methane - hydrogen mixtures the effect of temperature increase from 300 K to 673 K was less pronounced at higher pressures. At 1 bar pressure the increase of S_L due to the temperature augmentation was about 425-435% at $\phi = 1$ for both mixtures. At 3 bar pressure the increase of S_L due to the temperature rise was about 480%, and at 7 bar pressure the increase of S_L due to the temperature rise was about 510-520% for both mixtures at $\phi = 1$. Although at higher pressure the temperature effect is more significant in terms of increase of S_L for both: methane - carbon dioxide and methane - hydrogen mixtures, aparently methane - hydrogen mixture is less susceptable to pressure effects.

The addition of noncombustible gas CO_2 and highly flammable H_2 to CH_4 has different effects on S_L. Similar trends of the change of S_L due to the temperature and pressure effect was observed. The interesting behaviour of methane - carbon dioxide mixtures was observed. With increasing carbon dioxide content in the methane, a larger difference of S_L measured at 1 bar and 3 bar pressure due to temperature

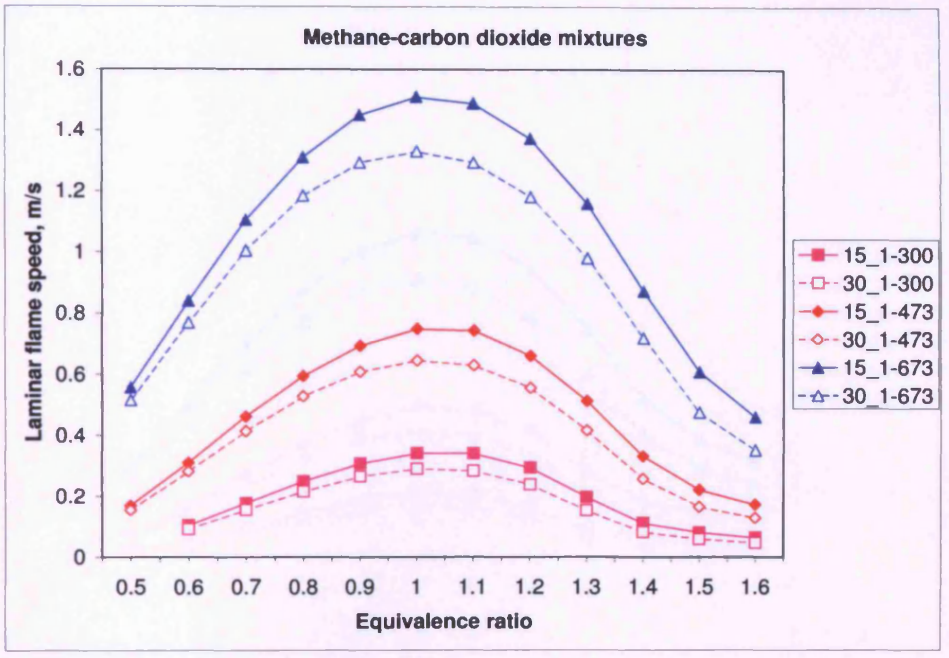

(a) methane - carbon dioxide mixtures

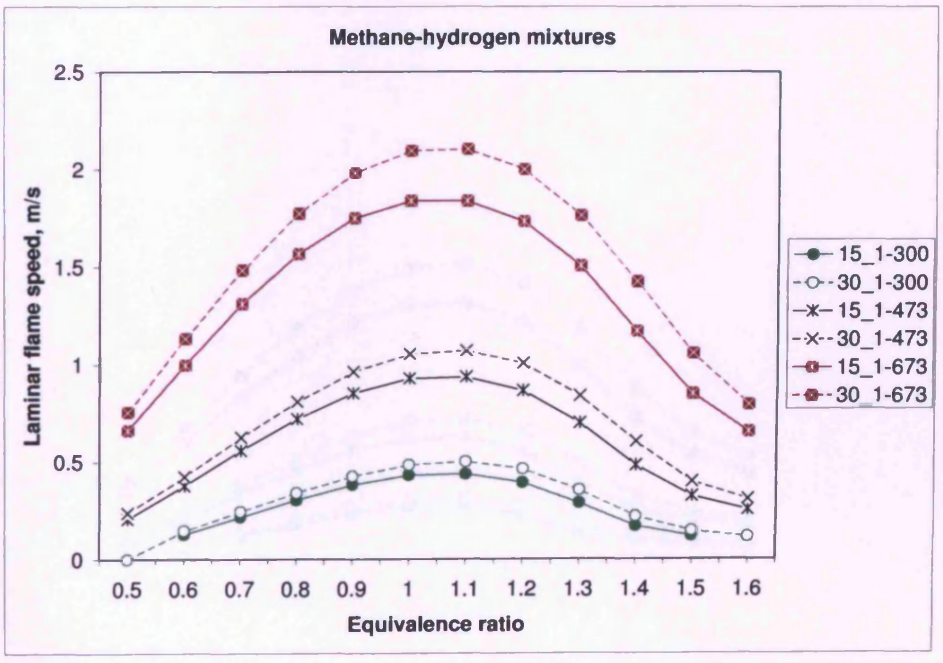

(b) methane - hydrogen mixtures

Figure 5.3: *Laminar flame speed calculated using GRI-Mech kinetic mechanism at 1 bar.*

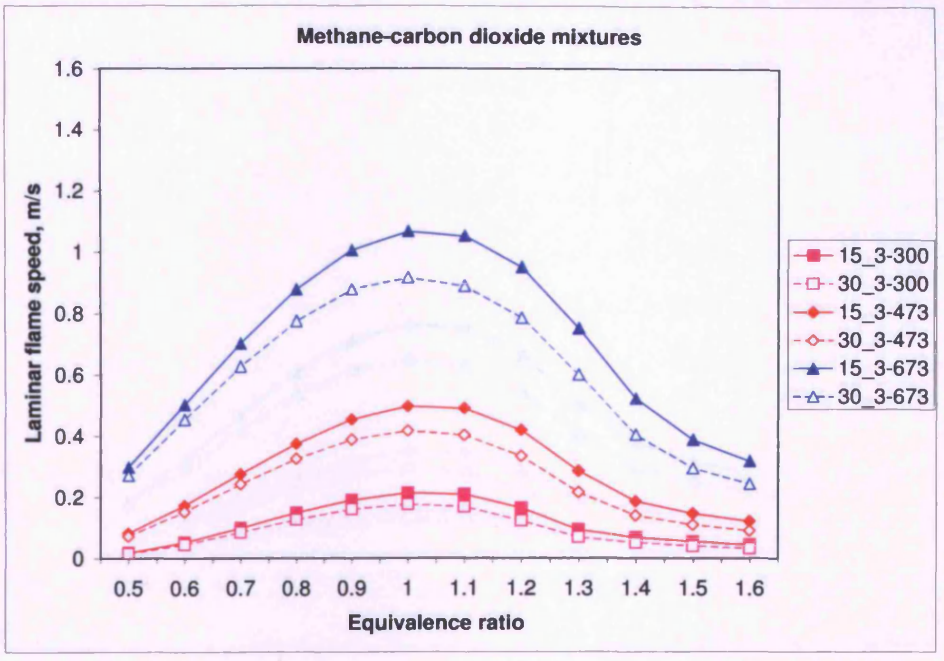

(a) methane - carbon dioxide mixtures

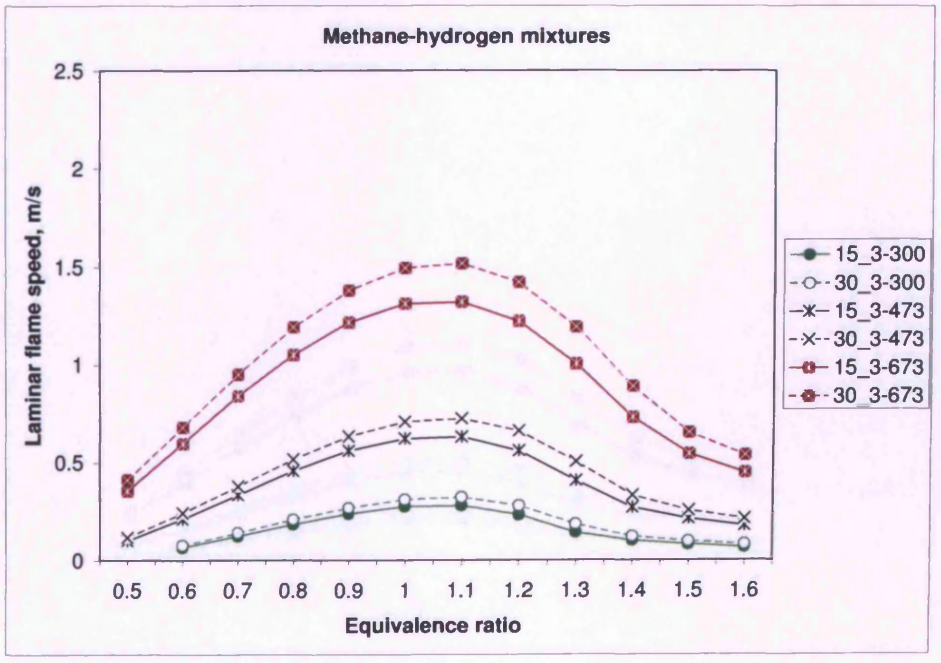

(b) methane - hydrogen mixtures

Figure 5.4: *Laminar flame speed calculated using GRI-Mech kinetic mechanism at 3 bar.*

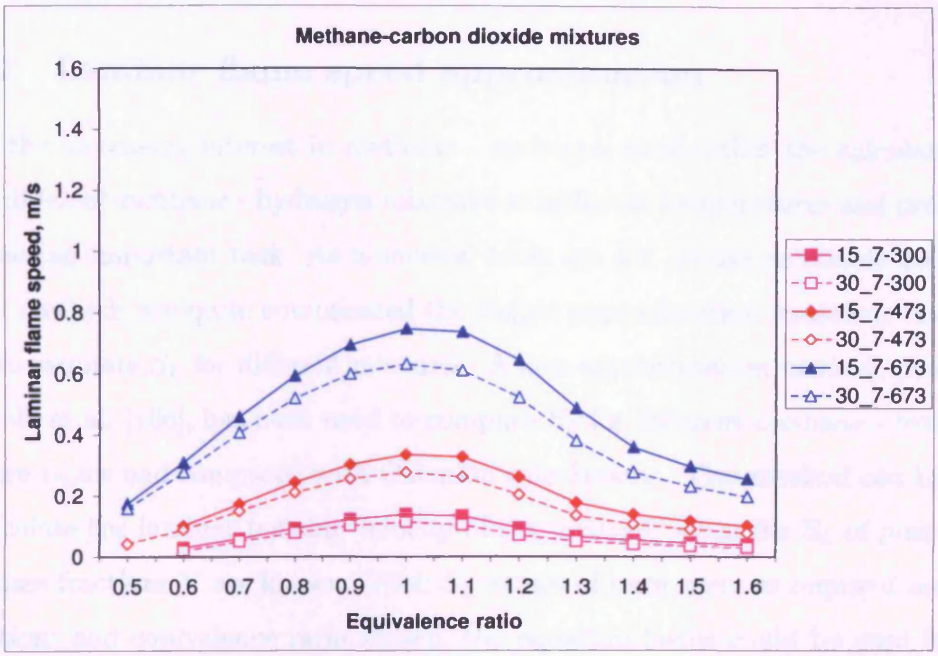

(a) methane - carbon dioxide mixtures

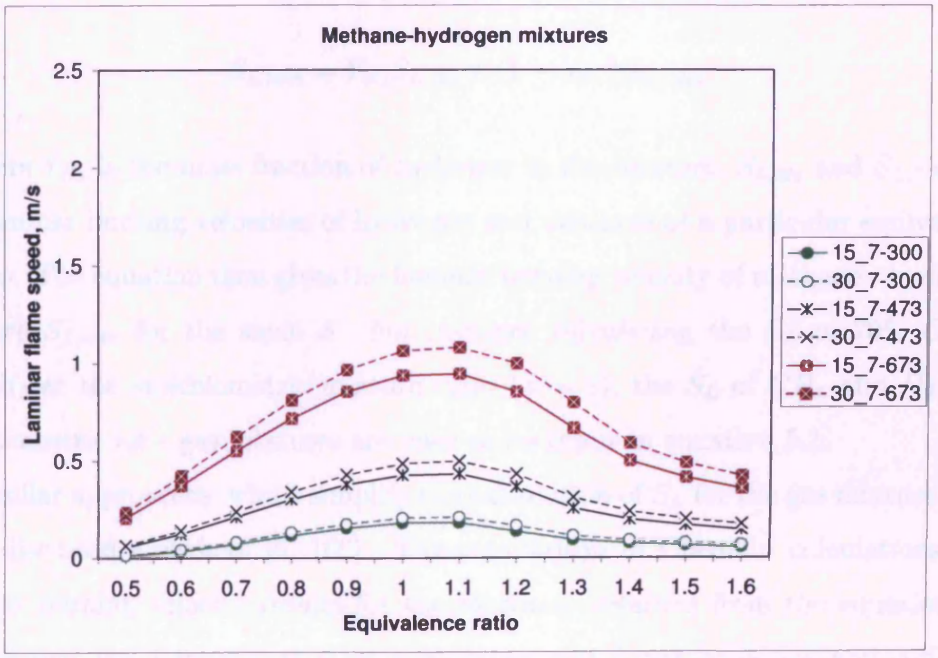

(b) methane - hydrogen mixtures

Figure 5.5: *Laminar flame speed calculated using GRI-Mech kinetic mechanism at 7 bar.*

augmentation from 300 K to 673 K was computed. Similar behaviour was observed for premixed turbulent methane - carbon dioxide flames [41].

5.3.2 Laminar flame speed approximation

With the increasing interest in methane - hydrogen combustion the calculation of S_L of different methane - hydrogen mixtures at different temperatures and pressures becomes an important task. As numerical tools are not always accessible and analytical methods are quite complicated the simple approximation equations could be used to estimate S_L for different mixtures. A new approximation method, proposed by Shelil et al. [166], has been used to compute S_L for different methane - hydrogen mixture ratios and compared with Chemkin calculations. This method can be used to calculate the laminar burning velocity of the mixture, when the S_L of pure gases and mass fractions Y are known. With S_L values of pure gases at required ambient conditions and equivalence ratio known, the equation below could be used for the stoichiometric and close to the stoichiometric mixtures:

$$S_{L,mix} = Y_{H_2} S_{L,H_2} + (1 - Y_{H_2}) S_{L,CH_4} \tag{5.1}$$

Here Y_{H_2} is the mass fraction of hydrogen in the mixture, S_{L,H_2} and S_{L,CH_4} are the laminar burning velocities of hydrogen and methane of a particular equivalence ratio ϕ. The equation then gives the laminar burning velocity of methane - hydrogen mixture $S_{L,mix}$ for the same ϕ. For instance calculating the S_L of 70% CH_4 - 30% H_2 at the stoichiometric mixture ratio ($\phi = 1$), the S_L of CH_4 and H_2 with stoichiometric air - gas mixtures are used as an input in equation 5.1.

Similar approaches, which simplify the calculation of S_L for the gas mixture have been discussed elsewhere [5, 166]. The comparison of Chemkin calculations and laminar burning velocity results for the mixtures obtained from the equation 5.1 for different gas mixtures at $\phi = 1$ at 1 bar and 3 bar pressures and different temperatures is presented in Fig. 5.6.

It is seen from the graphs that the equation 5.1 predicts the S_L values fairly well especially for the mixtures with lower hydrogen quantities in the mixture (mole fraction $X < 0.5$) and lower pressure. For higher hydrogen quantities the difference

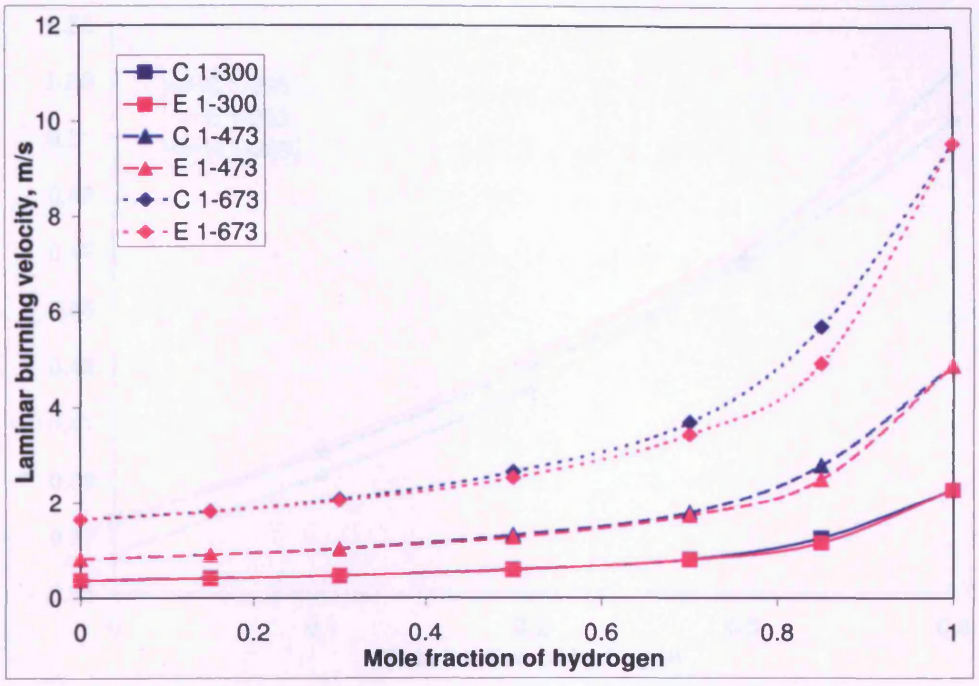

(a) at 1 bar pressure

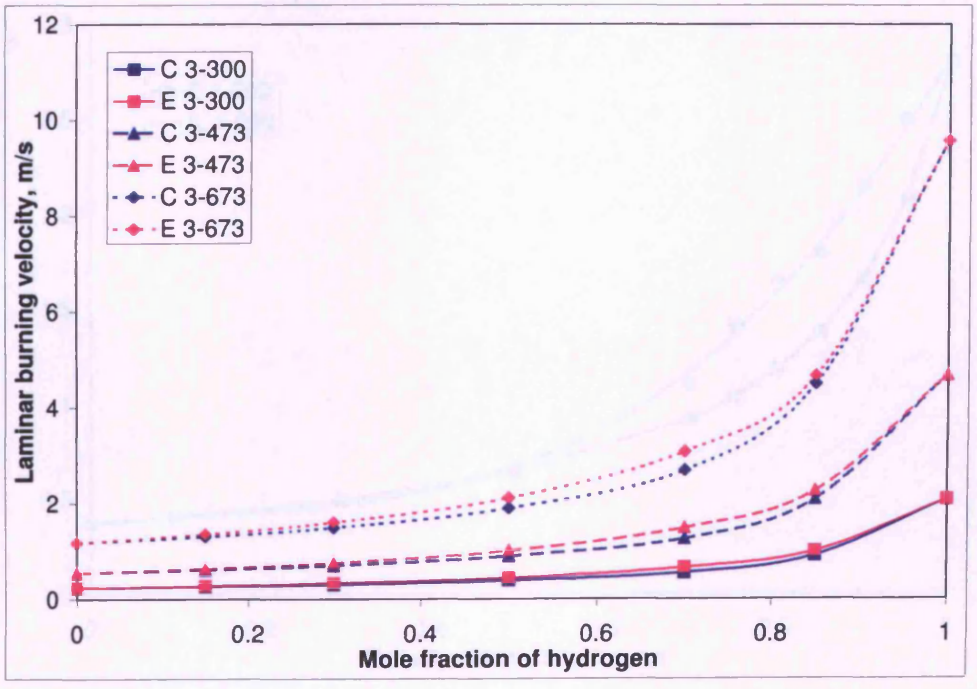

(b) at 3 bar pressure

Figure 5.6: *Laminar burning velocity of stoichiometric mixtures obtained from Chemkin computations (C) and using equation 5.1 (E). 1-300 represents 1 bar 300 K conditions and 3-300 represents 3 bar 300 K conditions.*

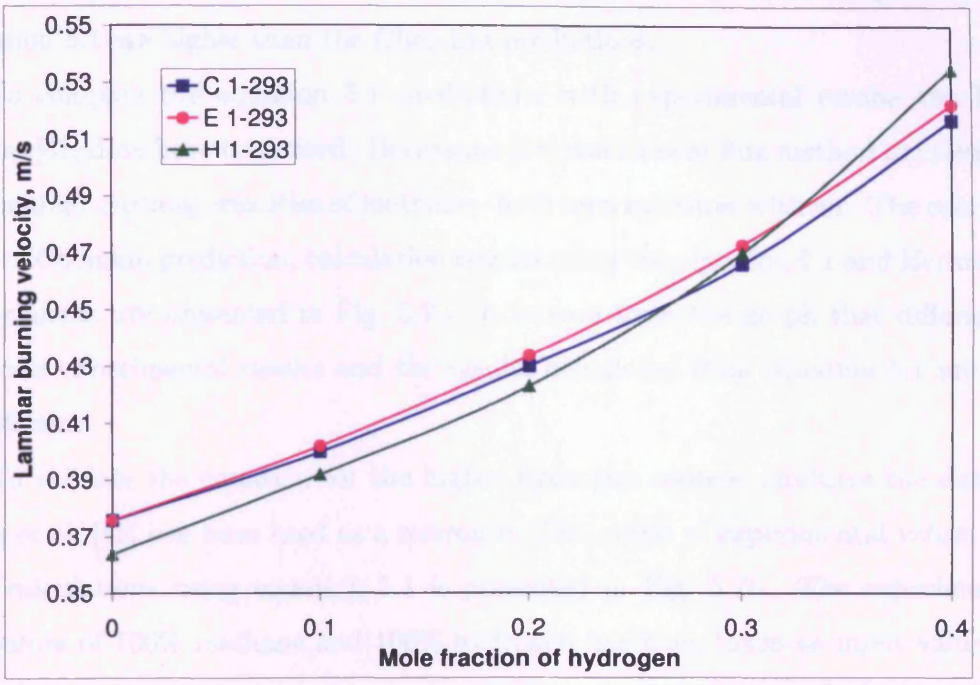

(a) Hermanns experimental results

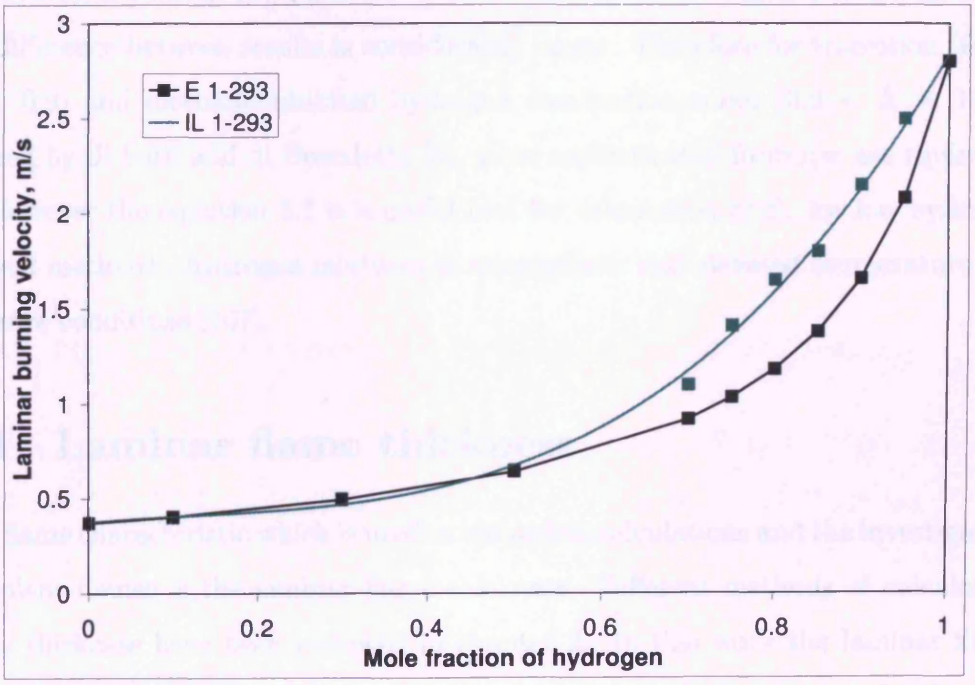

(b) Ilbas et al. experimental results

Figure 5.7: *Comparison of S_L results obtained from Chemkin (C) and calculated from the equation 5.1 (E) with experimental results of Hermanns [51] (H) and Ilbas et al. [48] (IL) at atmospheric conditions, $\phi = 1$.*

is larger. At higher pressure (Fig. 5.6b) the calculated S_L values computed using equation 5.1 are higher than the Chemkin predictions.

To compare the equation 5.1 predictions with experimental results the Hermanns [51] data have been used. Hermanns [51] used a heat flux method to calculate the laminar burning velocities of methane - hydrogen mixtures with air. The comparison of Chemkin prediction, calculation results using the equation 5.1 and Hermanns experiments are presented in Fig. 5.7a. It is seen from the graph that differences between experimental results and the results calculated from equation 5.1 are not significant.

To validate the equation for the higher hydrogen content mixtures the data of Ilbas et al. [48] has been used as a reference. The graph of experimental values [48] and calculations using equation 5.1 is presented in Fig. 5.7b. The experimental S_L values of 100% methane and 100% hydrogen has been taken as input values in equation 5.1. It is seen from the graph that the equation predicts S_L fairly well for low hydrogen content mixtures ($X < 0.5$). For higher hydrogen content mixtures the difference between results is considerably larger. Therefore for transition ($0.5 < X < 0.9$) and methane-inhibited hydrogen combustion zones ($0.9 < X < 1$), as defined by di Sarli and di Benedetto [5], more sophisticated formulae are rquired.

However the equation 5.1 is a useful tool for calculation of S_L for low hydrogen content methane - hydrogen mixtures at atmospheric and elevated temperature and pressure conditions [167].

5.4 Laminar flame thickness

One flame characteristic which is used in numerical calculations and the investigation turbulent flames is the laminar flame thickness. Different methods of calculating flame thickness have been reviewed in chapter 2. In this work the laminar flame thickness, also called thermal flame thickness, has been calculated using the classical approach of defining temperature gradient using equation 2.11. This thermal flame thickness is larger than the diffusive flame thickness, but it is normally accepted as the best definition [95].

To calculate flame thickness the temperature evolution over distance calculated

using Chemkin-Pro was taken for every gas mixture at all conditions and equivalence ratios. Then the temperature gradient was calculated. From this the laminar flame thickness δ_L was defined. The numerically calculated flame thickness values for different gas mixtures at different conditions are plotted in Fig. 5.8.

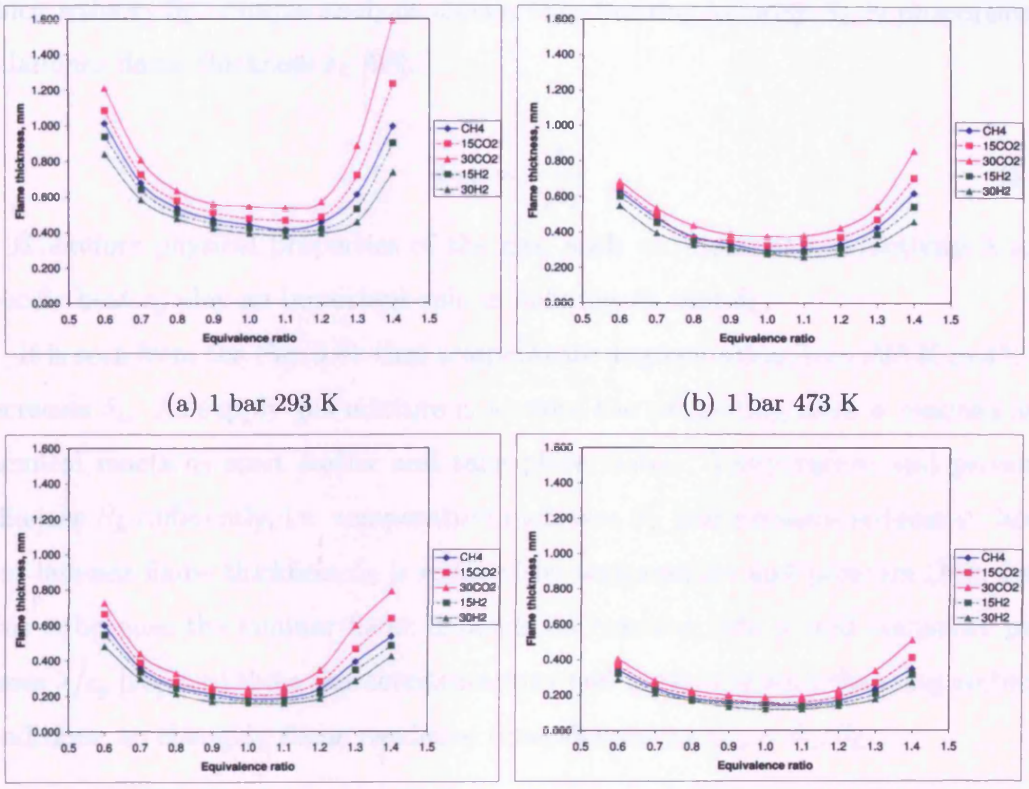

(a) 1 bar 293 K

(b) 1 bar 473 K

(c) 3 bar 293 K

(d) 3 bar 473 K

Figure 5.8: *Laminar flame thickness ate different ambient conditions.*

It is seen in the graph that flame thickness depends on gaseous fuel mixture. These results match the experimental findings of Lafay et al. [52] for lean mixtures very well. The GRI-Mech v3.0 chemical kinetic mechanism used for calculations accurately predicted temperature evolution curve, from which the δ_L was derived. It was observed in experiments [52] that hydrogen reduced δ_L, and good agreement between experimental values and numerical calculations was found for flames $\phi > 0.55$. Lafay et al. [52] in their investigation concluded that hydrogen enrichment leads to an increase of the maximum heat release rate, which enhances the rate of reaction whilst the heat release rate increases faster in the flame front at low temperature.

For methane - carbon dioxide flames the opposite effect is observed. Carbon dioxide additions increases laminar flame thickness and reduces S_L. One of the explanations of such behaviour is the different thermal conductivity and heat capacity of CO_2 compared with CH_4, and consequently lower combustion temperature, which reduces S_L. Simple analysis shows, that burning velocity S_L is proportional to laminar flame thickness δ_L [98]:

$$S_L \rho = \frac{\lambda}{c_p \delta_L} \tag{5.2}$$

Therefore physical properties of the gas, such as: thermal conductivity λ and specific heat c_p play an important role in defining S_L and δ_L.

It is seen from the Fig. 5.8b that temperature augmentation from 293 K to 473 K decreases δ_L. As supply gas mixture is warmer the preheating zone is reduced and chemical reactions start earlier and take place faster. Temperature and pressure influence S_L differently, i.e. temperature increases S_L and pressure reduces it, however laminar flame thickness δ_L is reduced by temperature and pressure (Fig. 5.8). This is because the laminar flame depends on reaction rate $\dot{w}$ and transport processes λ/c_p [98], and these characteristics vary non-uniformly with changing ambient conditions, so changing flame residence time, defined as $t_{res} = \delta_L/S_L$.

5.5 Summary

Numerical tools and methods of calculation of laminar flame speed and laminar flame thickness have been presented in this chapter. Investigation of chemical kinetic mechanism used in numerical calculations has revealed uncertainties and limitations. Presssure and temperature effect on S_L have been discussed and results presented. With increasing carbon dioxide content in the methane a larger difference of S_L measured at 1 bar, 3 bar and 7 bar absolute pressure due to temperature increase from 300 K to 673 K has been observed in comparison with methane - hydrogen mixtures.

A laminar burning velocity calculation equation, based on the mass fraction of the gas which compose the mixture, for methane - hydrogen mixtures proposed by Shelil [166] has been investigated and compared with the experimental results

and numerical calculations. The equation is reasonably accurate for low hydrogen content mixtures and could be used as a tool for practical calculations when S_L of pure methane and hydrogen is known. For mixtures containing large hydrogen quantities ($> 50\%$) more accurate equations should be developed.

Chapter 6

Bunsen burner experiments at elevated temperature and pressure

Due to the growing concerns regarding global warming an increased interest in using alternative fuels for gas turbines is observed [3]. Combustion conditions in gas turbine are considerably different in comparison with industrial burners. Higher than atmospheric temperatures and pressures are important factors influencing combustion characteristics.

In this experimental programme, five different gaseous fuels were tested over a range of pressures and temperatures. Approximately 20 data sets were generated for each gas mixture (by volume): 100% methane, 85% methane - 15 % carbon dioxide, 70% methane - 30 % carbon dioxide, 85% methane - 15% hydrogen and 70% methane - 30% hydrogen were carried out for lean and rich mixtures from 0.65 to 1.45 equivalence ratio at different pressures and temperatures (Table 6.1). The

Table 6.1: *Investigated gas mixtures at elevated temperature and pressure conditions.*

Gas mixture	CH_4, %	CO_2, %	H_2, %	Pressure, bar	Temperature, K
100%CH_4	100	0	0	3, 7	473, 673
85%CH_4-15%CO_2	85	15	0	3, 7	473, 673
70%CH_4-30%CO_2	70	30	0	3, 7	473, 673
85%CH_4-15%H_2	85	0	15	3, 7	473, 673
70%CH_4-30%H_2	70	0	30	3, 7	473, 673

tests were performed in the High Pressure Optical Chamber, integrated within the High Pressure Combustion Rig, which is located at the Gas Turbine Research Centre (GTRC).

Two different measurement techniques were applied. A non-intrusive 2-D laser diagnostic technique, Laser Doppler Anemometry (LDA), was utilised to determine both the velocity profile and turbulence characteristics at the exit of the burner at elevated pressures and temperatures. PLT was applied in order to measure the turbulent burning velocity for the different gas mixtures at a range of temperatures and pressures. More detail description of experimental facility is provided in chapter 3.

6.1 Calculation method

General stoichiometric combustion reactions for methane, methane - carbon dioxide and methane - hydrogen gas mixtures, based on methane gas, can be written as follows:

$$CH_4 + 2 \cdot (O_2 + 3.76 \cdot N_2) = CO_2 + 2 \cdot H_2O + 2 \cdot 3.76 \cdot N_2 \tag{6.1}$$

$$CH_4 + a \cdot CO_2 + 2 \cdot (O_2 + 3.76 \cdot N_2) = (a+1) \cdot CO_2 + 2 \cdot H_2O + 2 \cdot 3.76 \cdot N_2 \tag{6.2}$$

$$CH_4 + b \cdot H_2 + \left(\frac{b+4}{2}\right) \cdot (O_2 + 3.76 \cdot N_2) = CO_2 + (b+2) \cdot H_2O + \left(\frac{b+4}{2}\right) \cdot 3.76 \cdot N_2 \tag{6.3}$$

Here a and b are the molar fraction ratios of additional gas in methane: $a = X_{CO_2}/X_{CH_4}$ and $b = X_{H_2}/X_{CH_4}$.

Stoichiometric air fuel ratios (AFR) of methane, methane - carbon dioxide and methane - hydrogen mixtures are calculated:

$$AFR_{st}^{CH_4} = \frac{2 \cdot (M_{O_2} + 3.76 \cdot M_{N_2})}{M_{CH_4}} \tag{6.4}$$

$$AFR_{st}^{CH_4-CO_2} = \frac{2 \cdot (M_{O_2} + 3.76 \cdot M_{N_2})}{M_{CH_4} + a \cdot M_{CO_2}} \tag{6.5}$$

$$AFR_{st}^{CH_4-H_2} = \frac{\left(\frac{b+4}{2}\right) \cdot (M_{O_2} + 3.76 \cdot M_{N_2})}{M_{CH_4} + b \cdot M_{H_2}} \tag{6.6}$$

The mass flow rate of gas mixture and air is measured and the equivalence ratio is calculated thus:

$$\phi = \frac{AFR_{st}}{\dot{m}_{air}/\dot{m}_{fuel}} \tag{6.7}$$

The tests were performed using a Bunsen type burner, thus, the tested flames were "envelope" category flames. This means that the flame forms an envelope around the reactants and all reactants must pass through the flame [91]. Thus the burning velocity is related to global consumption speed [85] and is calculated using equation 2.43.

It has been proposed that the consumption speed should be used to define the turbulent burning velocity [168] and that only flames within a particular category should be compared because the flame wrinkling process can be different for different flame types [77]. However in our study we compared "envelope" category flames as well as "spherical" type flames, due to the lack of research performed at elevated pressures and temperatures for the studied gas mixtures.

The exit velocity from the burner of the gas-air mixture is derived from the mass flow of combustion air, seed air and fuel flows, and displayed and logged simultaneously by the data acquisition system. Density, viscosity, diffusion coefficients and other gas properties of the combustible mixture at the required temperature and pressure were calculated using polynomial fit coefficients available within the Chemkin database or taken from reference tables. Lewis number, defined as the ratio of thermal diffusivity of the mixture and mass diffusivity of deficient species, was calculated for all mixtures considered.

The Chemkin-Pro software and GRI-Mech v3.0 reaction mechanism were used to calculate laminar burning velocities and flame thicknesses for the various gas mixtures at different pressures, temperatures and equivalence ratios. The laminar flame thickness calculation method was based on a classical approach of defining temperature gradient and agreed well with findings of Lafay et al. [52], who made hydrogen enriched methane-air flame thickness measurements. These results support the computational results obtained using the GRI-Mech v3.0 reaction mechanism for equivalence ratios above 0.55.

The LDA results were utilised to ensure that turbulence intensity and burner exit velocity profiles are uniform and to find integral time scales of turbulence. The description of LDA method is presented in chapter 4.

The PLT technique was used in this study to find S_T. Detailed description of this method is presented in chapter 4.

6.2 Isothermal LDA Results

Figures 6.1, 6.2 shows the variation of mean axial velocity and velocity fluctuations respectively with radial position for a range of exit velocities. The two vertical lines at radial position r = 12.5 mm and r = -12.5 mm represent the burner edges. Overall the results show that the axial velocity profiles are uniform, confirming the suitability of the burner for this study. Pressure has little effect on axial velocity and axial velocity fluctuations.

LDA measurements of the isothermal flow showed that, in agreement with others [84], turbulence intensity is almost insensitive to variation in pressure and temperature. Fig. 6.3 shows that the turbulence intensity q' measured at the burner radial position r = 12 mm shows a dependence on bulk flow velocity. During the experiments bulk exit velocity varied between 4 to 16 m/s and thus turbulence intensity values at different bulk flow velocities were interpolated from this correlation.

The evolution of relative turbulence intensity as a function of bulk flow velocity is represented in Fig. 6.4. The increase in relative turbulence intensity, $q'/\bar{u}$, at low bulk flow velocities is clearly seen from the graph.

Data obtained by LDA were used to derive one point temporal velocity correlation and calculate the integral time scale and integral length scale of the turbulent isothermal flow at different pressures, temperatures and bulk flow velocities. 1024 correlation samples and a lag time τ = 100 ms were chosen to find autocorrelation coefficients. The integral time scale was found by integrating the autocorrelation function over time. The integral length scale was calculated using formula 4.6, based on Taylor's hypothesis of isotropic turbulence. As this frozen-turbulence hypothesis is a good approximation only if $q'/\bar{u} << 1$, the calculation of integral time scale should only be performed where the velocity fluctuation is relatively low [143]. Two point spatial velocity correlation should be carried out in order to calculate integral time scale where stronger turbulence prevails. Spatial and temporal correlation agree well for low turbulence flows, whilst strong streamline development of turbulence invalidates the frozen-turbulence assumption of Taylor's hypothesis [88].

Typical autocorrelation function curves are represented in Fig. 6.5. It was found that at 10 m/s bulk exit velocity at 7 bar, 473 K and 673 K conditions, few data points around the centre of burner exit correlated, while others oscillated and did not

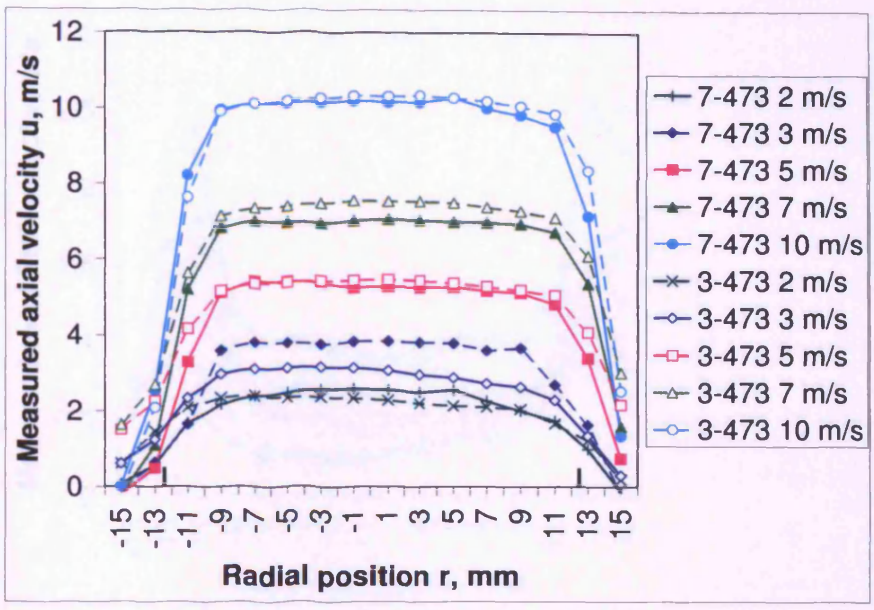

(a) axial mean velocity at 473 K

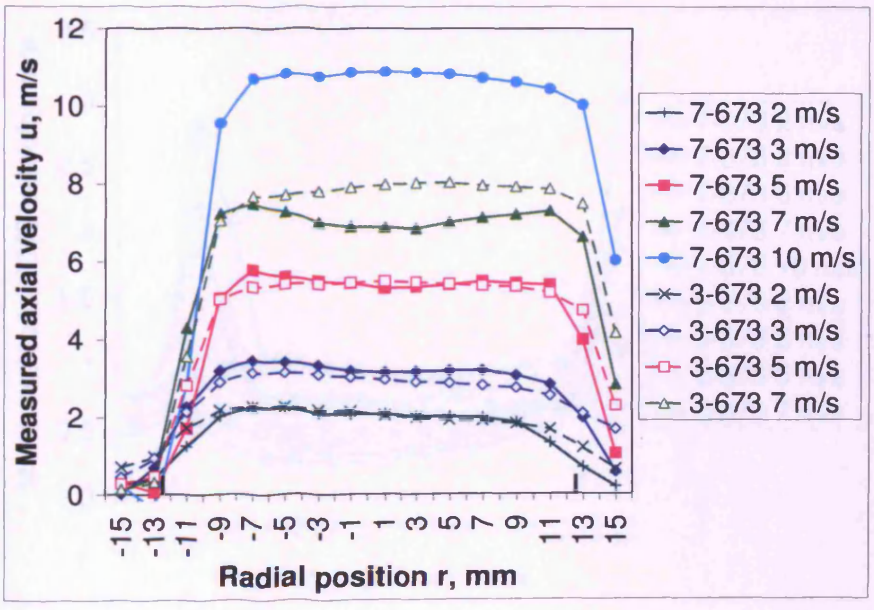

(b) axial mean velocity at 673 K

Figure 6.1: *Axial mean velocity $\bar{u}$ measured 10 mm downstream burner exit at different bulk gas flow velocities. Velocities indicated in the legend represents bulk exit velocity at 3 bar 473 K (3-473), 7 bar 473 K (7-473), 7 bar 473 K (7-473) and 7 bar 673 K (7-673).*

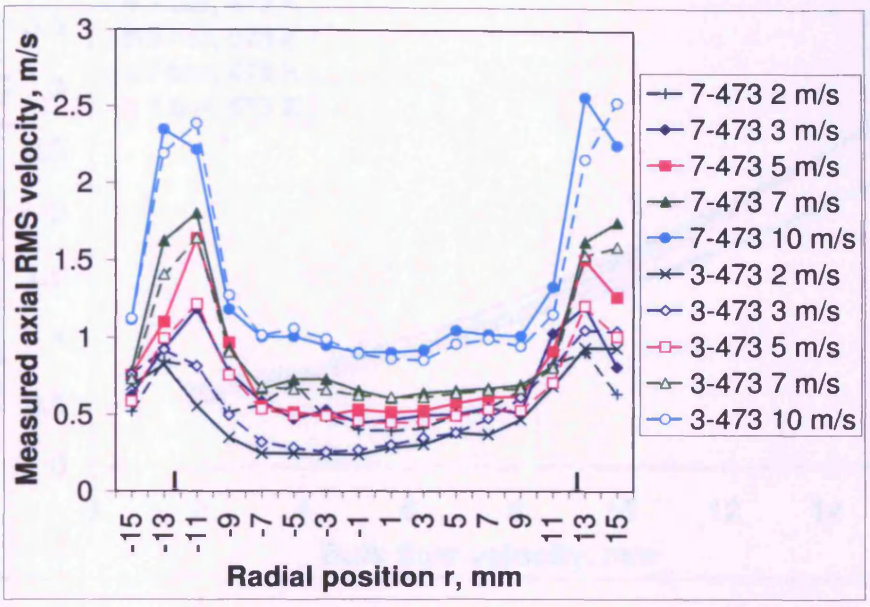

(a) axial RMS velocity at 473 K

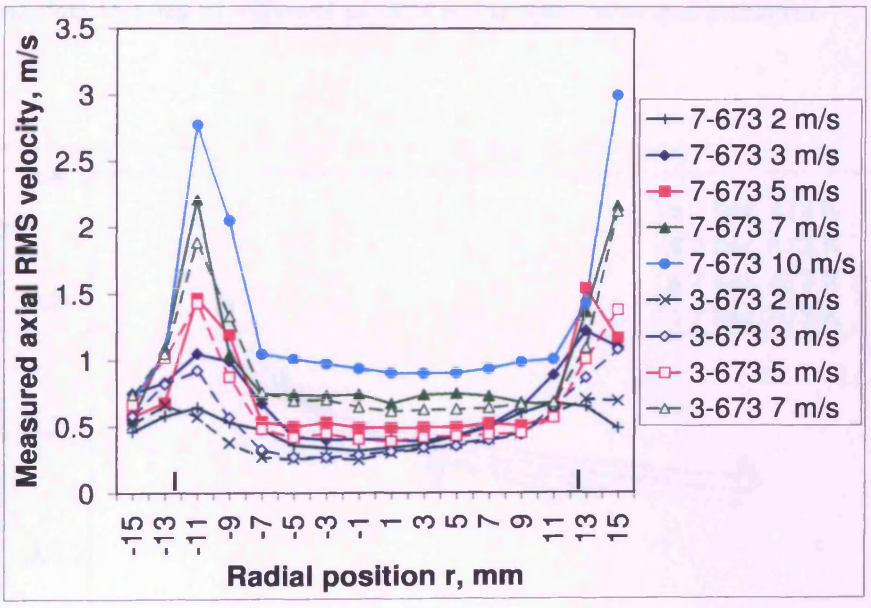

(b) axial RMS velocity at 673 K

Figure 6.2: *Axial RMS velocity u' measured 10 mm downstream burner exit at different bulk gas flow velocities. Velocities indicated in the legend represents bulk exit velocity at 3 bar 473 K (3-473), 7 bar 473 K (7-473), 7 bar 473 K (7-473) and 7 bar 673 K (7-673).*

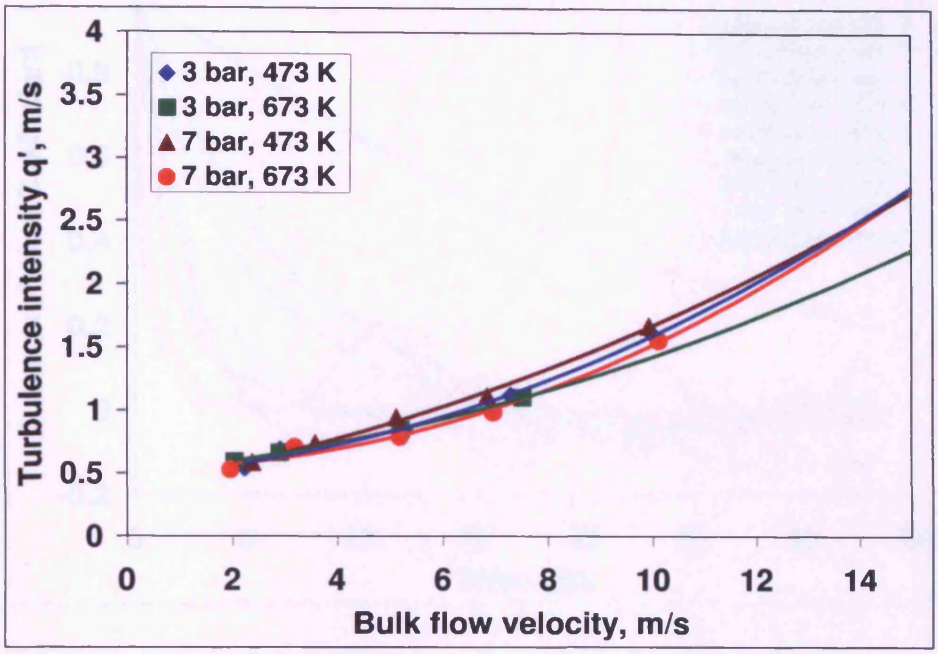

Figure 6.3: *Turbulence intensity, q', measured at radial position $r = 12$ mm, depending on bulk gas flow velocity at different at different temperatures and pressures.*

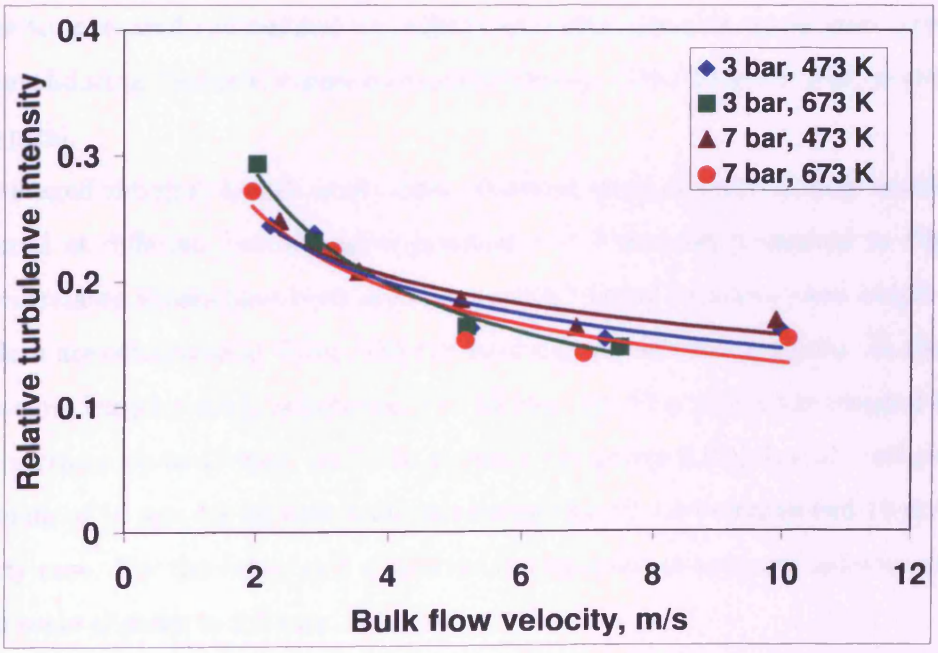

Figure 6.4: *The evolution of relative turbulence intensity, $q'/\bar{u}$, depending on bulk gas flow velocity at different temperatures and pressures.*

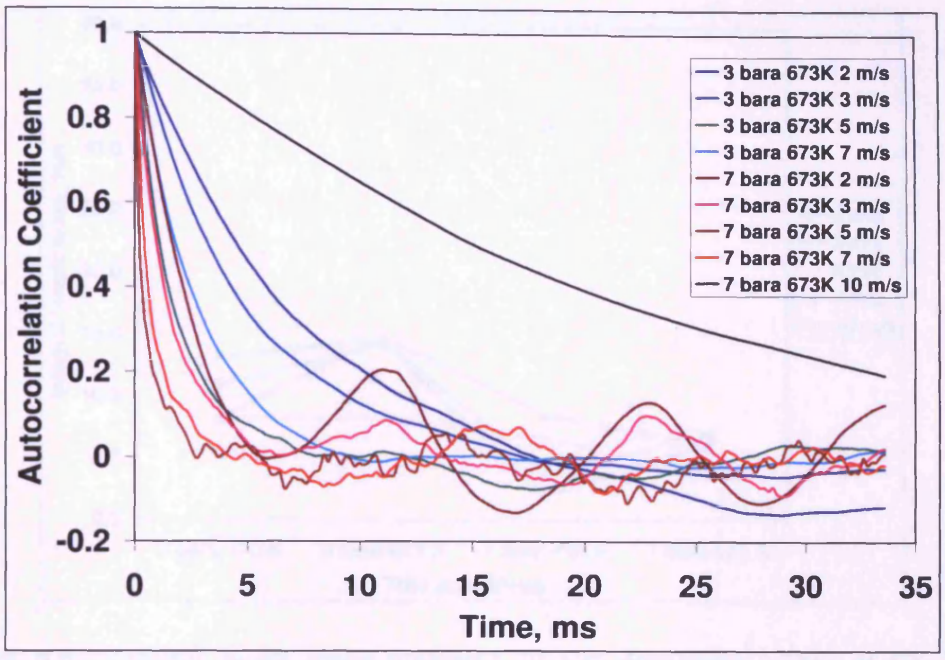

Figure 6.5: *Autocorrelation coefficient curves at burner radial position r = 3 mm for different gas flow velocities at 3 bar and 7 bar, 673 K.*

cross zero or weakly correlated. The same behaviour was observed processing LDA data taken from the data points close to the burner rim ($r \approx 12$ mm). This could be due to increased normalized turbulence intensity (relative turbulence intensity) $q'/\bar{u}$ invalidating Taylor's frozen-turbulence theory. This data for this condition is not typical.

Averaged integral length scale data obtained from autocorrelation coefficients measured at different burner radial position $r < 5$ mm are presented in Fig. 6.6. Only correlated values have been used to process integral time scale and length scale. The data are consistent at 3 bar, 473 K conditions for all exit velocities. In this case the integral length scale l_0 is between 5 to 13 mm. At 3 bar 673 K the integral length scale increases up to 15 mm. At 7 bar pressure the integral length scale reduces to a maximum of 10 mm for all exit velocities except for the aforementioned 10 m/s exit velocity case. For the other exit velocities the increase in pressure reduces integral length scale slightly to 2.5 mm - 10 mm.

The differences in the integral length scale results appears to arise from a number of interacting factors. Although the mean axial velocity profiles follow well known similarity trends, this is not so with the turbulence (Fig. 6.4), which clearly shows

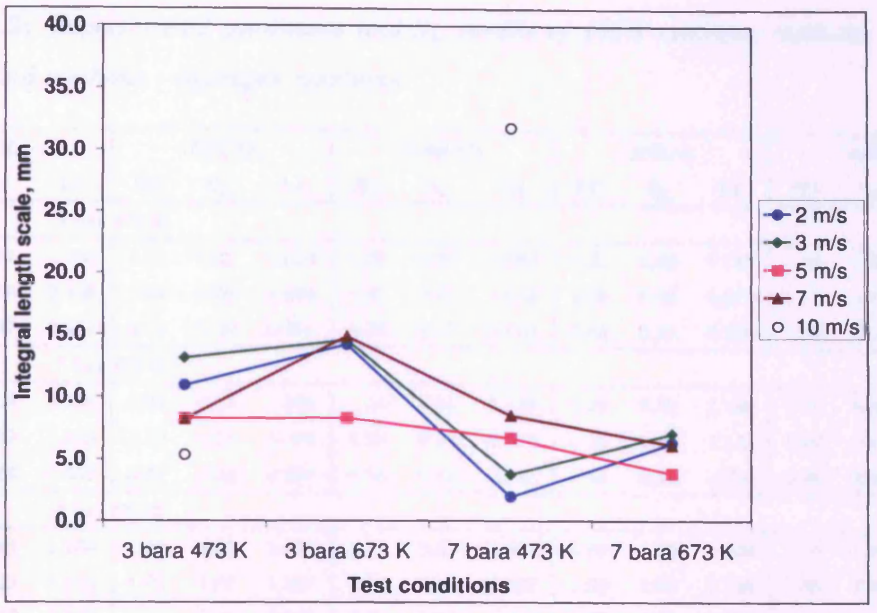

Figure 6.6: *Integral length scales measured 10 mm dowstream burner at the burner centerline exit.*

much higher levels of relative turbulence intensity at low bulk flow velocities with a somewhat weaker effect due to pressure and temperature. These results translate into the shown variation of integral length scale and seem to arise from variations in the jet potential core and the generated shear flow on its boundary. Reynolds number effects are clearly important, the lowest value being around 2400 (2 m/s, 3 bar, 673 K), up to 58000 (10 m/s, 7 bar, 473 K), and do affect such jets in the lower Reynolds numbers ranges. Unfortunately for such measurements it is impossible to obtain higher Reynolds numbers without the use of very much larger throughput rigs allowing larger diameter jets to be used.

6.3 Turbulent burning velocity

This study has investigated a range of flames at elevated temperatures and pressures. Laminar burning velocities, calculated using CHEMKIN, and Lewis numbers for different gas mixtures at different temperatures and pressures are presented in Table 6.2.

Only values close to the stoichiometric conditions are listed in order to show the variation trends of S_L and Lewis number.

Table 6.2: *Experimental conditions and S_L results of 100% methane, methane - carbon dioxide and methane - hydrogen mixtures*

CH_4			$15\%CO_2$			$30\%CO_2$			$15\%H_2$			$30\%H_2$		
ER	S_L	Le	ER	S_L	Le	ER	S_L	Le	ER	S_L	Le	ER	S_L	Le
3 bar 473 K														
1.18	0.52	1.106	1.21	0.41	1.096	1.20	0.33	1.083	1.22	0.54	1.145	1.24	0.61	1.194
0.96	0.56	0.948	1.04	0.50	1.096	1.02	0.41	1.084	1.00	0.62	0.725	1.01	0.71	1.178
0.75	0.37	0.954	0.71	0.29	0.951	0.74	0.27	0.944	0.82	0.48	0.724	0.90	0.63	0.593
7 bar 473 K														
1.20	0.32	1.106	1.39	0.14	1.096	1.18	0.21	1.083	1.23	0.32	1.145	1.23	0.40	1.193
1.01	0.39	1.105	1.20	0.26	1.096	0.99	0.27	0.935	1.06	0.42	1.139	0.99	0.48	0.596
0.78	0.24	0.953	0.81	0.25	0.948	0.76	0.18	0.944	0.86	0.34	0.724	0.85	0.39	0.592
3 bar 673 K														
1.14	1.16	1.104	1.25	0.86	1.094	1.17	0.82	1.081	1.19	1.23	1.139	1.25	1.30	1.187
1.04	1.20	1.103	1.03	1.07	1.094	1.03	0.91	1.082	1.02	1.31	1.134	0.99	1.46	0.595
0.73	0.82	0.948	0.79	0.86	0.942	0.74	0.68	0.937	0.82	1.08	0.722	0.82	1.21	0.591
7 bar 673 K														
-	-	-	1.19	0.67	1.094	1.20	0.52	1.081	1.22	0.81	1.140	1.22	0.93	1.186
-	-	-	1.04	0.76	1.094	1.01	0.63	1.082	1.03	0.94	1.134	1.01	1.03	1.172
-	-	-	0.77	0.56	0.942	0.78	0.50	0.936	0.79	0.69	0.722	-	-	-

For pure methane gas, the methane diffusion coefficient to the multi-component mixture consisting of nitrogen and oxygen was calculated for lean mixtures. For rich mixtures oxygen diffusion to the mixture was calculated. For methane carbon dioxide mixtures methane was taken as the deficient component for lean mixtures and oxygen for the rich ones. However for methane carbon dioxide mixture the methane diffusion to the three component mixture (nitrogen, oxygen, carbon dioxide) was assumed. For methane and hydrogen gases methane and hydrogen were deficient species for lean mixtures and oxygen was the deficient gas for the rich mixtures.

Lewis number of methane for all equivalence ratios was close to unity for the conditions considered. Lewis number decreased slightly with CO_2 addition compared with 100% methane. The most significant change in Lewis number are observed for methane hydrogen mixtures. Temperature and pressure had negligible effect on Lewis number.

To identify combustion regime, the flames studied under stoichiometric combustion are plotted on the Borghi diagram (Fig. 6.7). Turbulence intensity q', turbulent length scale l_0, obtained from our experiments (Figs. 6.3 and 6.6), and laminar flame

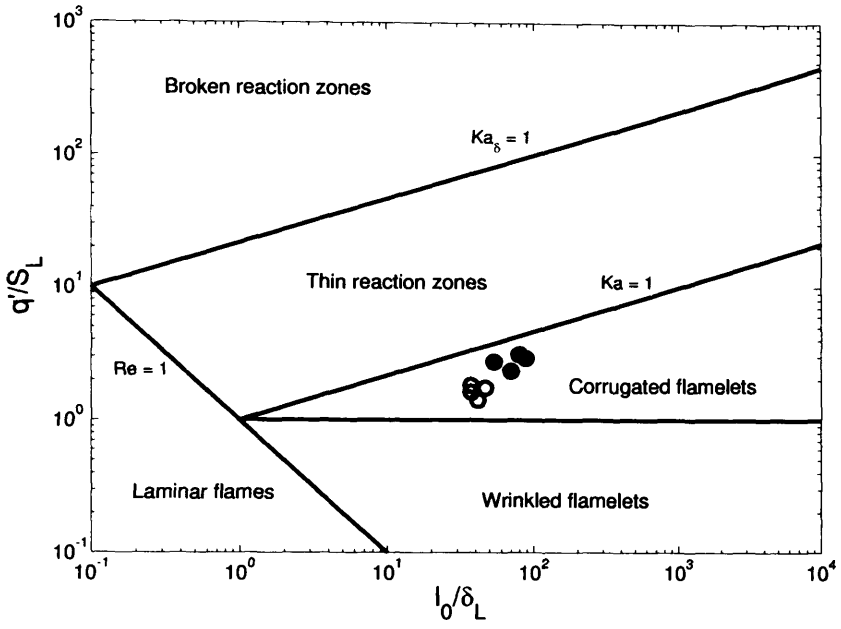

Figure 6.7: *Borghi - Peters diagram plotted on the logarithmic scale. Empty circles represent 3 bar 473 K, full circles - 7 bar 473 K conditions; CH_4 gas, and $CH_4 - CO_2$ and $CH_4 - H_2$ mixtures.*

thickness δ_L, laminar burning velocity S_L, obtained from Chemkin, have been used to calculate the data points. The graph shows that all the flames are within the 'corrugated flamelet regime'. This is consistent with the aims of the project as it was undesirable to produce flames located in different regions of the Borghi diagram, for instance higher temperatures may well have moved the operating regime to that of 'wrinkled flamelets'.

A pilot flame was required to stabilize the main flame for some cases of lean methane - carbon dioxide mixtures and with lean methane for all pressures and temperatures. This pilot was switched off before taking images. Methane - hydrogen mixtures stabilised easily for all conditions, and the pilot flame was not required. The methane - hydrogen flames were found to be much more stable. No significant change in flame shape was noticed when comparing methane, methane - carbon dioxide and methane - hydrogen mixtures, although increased wrinkledness of the methane - hydrogen flames was observed, as anticipated [22].

6.3.1 Turbulent burning velocity measurements

Turbulent burning velocity dependence on the equivalence ratio of different gas mixtures are presented in Figs. 6.8, 6.9, 6.10 and 6.11. Methane data are presented in all graphs as a benchmark indicator. The turbulent burning velocity, S_T, has been normalised by the methane turbulent burning velocity at $\phi = 0.96$, 3 bar and 473 K, obtained in experiments. Trendlines are plotted through each data set. Only one test for each condition was conducted. The relative errors of the burning velocities, computed from the flame images, were below 1%, therefore the error bars were not determined. The graphs are grouped so that the dependence of S_T on pressure (Figs. 6.8 and 6.10) and temperature (Figs. 6.9 and 6.11) can be shown. Normalised S_T of methane and methane - carbon dioxide mixtures are presented in Figs. 6.8 and 6.9, and methane and methane - hydrogen mixtures in Figs. 6.10 and 6.11.

Turbulence intensity q' varied during the tests depending on the conditions and gas mixture. Average values of q' are presented in the table 6.3.

Table 6.3: *Variation of turbulence intensity q' depending on the test conditions and gas mixture.*

Conditions	q', m/s CH_4	q', m/s 15%CO_2	q', m/s 30%CO_2	q', m/s 15%H_2	q', m/s 30%H_2
3 bar 473 K	0.8	0.8	0.7-0.8	0.7-0.9	1-1.1
3 bar 673 K	1.5	1.3-1.5	1.2-1.4	1.3-1.6	1.7-1.9
7 bar 473 K	0.8-0.9	0.8-0.9	0.7-0.9	1-1.2	1.1-1.3
7 bar 673 K	1.6-1.7	1.4-1.5	0.9-1.2	1.6-1.7	2.4-2.6

The relative turbulence intensity $q'/\bar{u}$ was almost constant for all tests at approximately 15-18%, independently of equivalence ratio. The variations of relative turbulence intensity are presented in Fig. 6.12 and discussed in the next section.

The peak of S_T of methane is observed at $\phi = 1$ - 1.1 at all conditions. When the methane air mixture at 3 bar is preheated to 673 K the burning velocity rises by approximately 55-60% in comparison with the methane burning velocity at 473 K at $\phi = 1$ (Fig. 6.8, a). For $\phi = 1.2$ the increase in S_T is around 50%. At $\phi = 0.8$, 70% increase in S_T is observed at 3 bar pressure. The data consistently show that

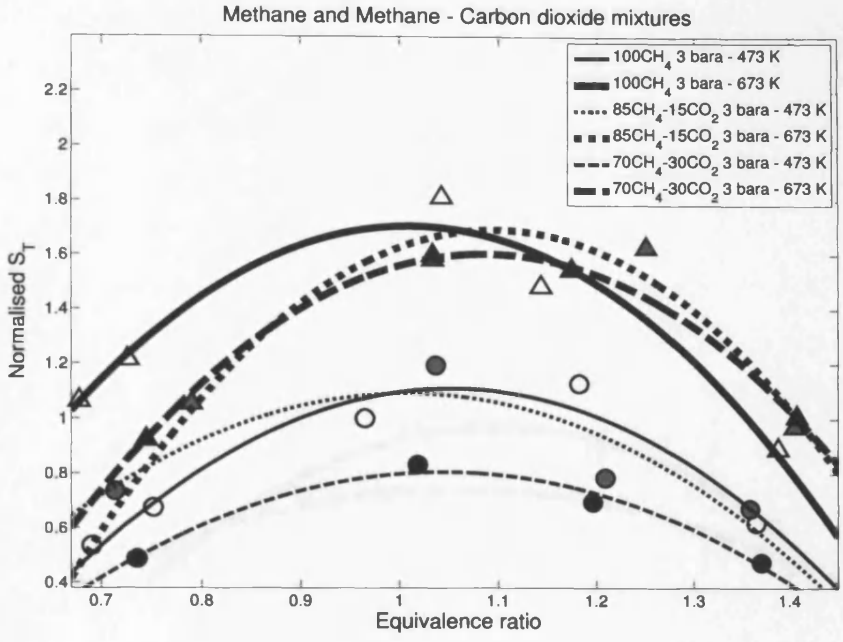

(a) 3 bar pressure

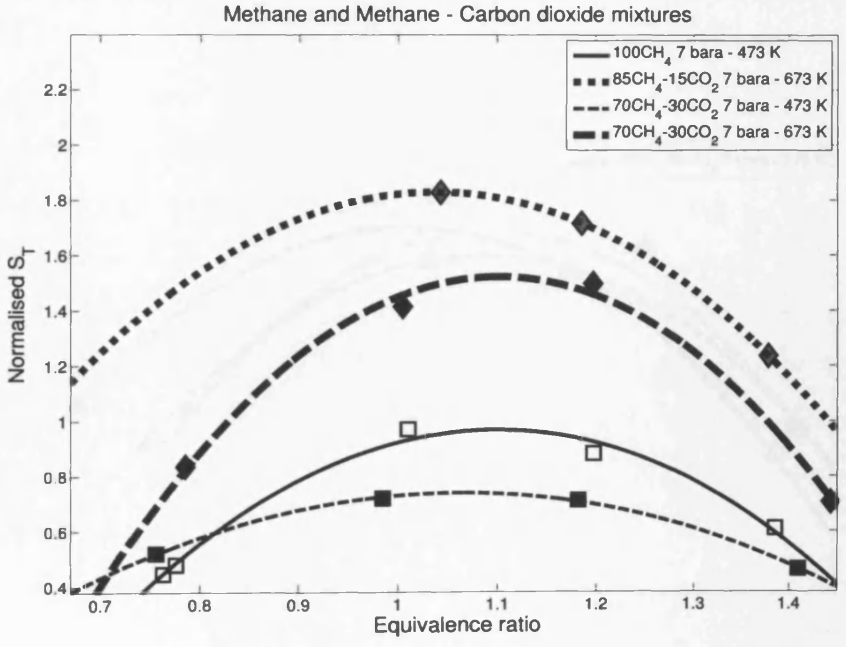

(b) 7 bar pressure

Figure 6.8: *Normalised burning velocity of methane and methane - carbon dioxide mixtures at different pressures. Symbols:* ◯ *- 3 bar 473 K,* △ *- 3 bar 673 K,* □ *- 7 bar 473 K,* ◊ *- 7 bar 673 K, blank -* CH_4*, grey -* $85\%CH_4 - 15\%CO_2$*, black -* $70\%CH_4 - 30\%CO_2$*. Relative turbulent intensity values vary from 15% to 18%.*

temperature has a stronger effect on S_T for lean mixtures than for rich.

Increasing ambient pressure from 3 bar to 7 bar at 473 K reduces methane turbulent burning velocity by approximately 15-20% at $\phi = 1$ (Fig. 6.9, a). For the same temperature at $\phi = 1.2$ the increase in S_T is about 10%. Increased pressure has more influence for lean methane - air mixtures than is observed for rich ones.

The peaks of S_T of methane - carbon dioxide mixtures are observed at $\phi = 1$ - 1.1 at all conditions. For the higher temperatures, the peak of S_T is slightly shifted to richer mixtures. Small amounts of carbon dioxide added to methane did not change the mixture burning velocity significantly at 3 bar 473 K across all equivalence ratios (Fig. 6.8, a). The turbulent burning velocity of $85\%CH_4 - 15\%CO_2$ mixture remained virtually unchanged at this condition. However a decrease in S_T by approximately 20% is measured at 3 bar 673 K for $\phi = 0.8$ (Fig. 6.8, a) in comparision with pure methane. S_T of $85\%CH_4 - 15\%CO_2$ for rich mixtures ($\phi > 1.1$) at 3 bar 673 K are slightly higher than S_T of pure methane. This implies that the temperature effect on CO_2 enriched methane is stronger than for pure methane for rich mixtures ($\phi > 1.1$), whereas the converse holds for $\phi < 0.8$.

30% carbon dioxide content in methane reduced turbulent burning velocity. The burning velocity recorded for $70\%CH_4 - 30\%CO_2$ was approximately 20-25% lower than that measured for pure methane at 3 bar 473 K at $\phi = 1$ (Fig. 6.8, a). Temperature increase had a larger influence for $70\%CH_4 - 30\%CO_2$, where burning velocity increased by 100-110% at 3 bar pressure at $\phi = 1$. At 3 bar 473 K the difference of S_T between methane and $70\%CH_4 - 30\%CO_2$ was higher than at 3 bar 673 K (Fig. 6.8, a), which supports the conclusion that the temperature effect on S_T is stronger for $70\%CH_4 - 30\%CO_2$, and the temperature effect rises with the increase of CO_2 content in methane.

The temperature increase raised the S_T of $85\%CH_4 - 15\%CO_2$ by 60-70% at 3 bar pressure at $\phi = 1$ (Fig. 6.8, a). However an even larger increase of S_T by 70-80% was observed at 3 bar at $\phi = 1.2$. At 7 bar 673 K, the burning velocity of $85\%CH_4 - 15\%CO_2$ is slightly higher than at 3 bar 673 K.

The S_T of $70\%CH_4 - 30\%CO_2$ at 7 bar 673 K is lower than at 3 bar 673 K (Fig. 6.9, b). However the difference does not exceed 5% at $\phi = 1.1$. Thus, it can be concluded that there is a consistent trend for the effect of pressure on turbu-

lent burning velocity of methane and methane carbon dioxide mixtures. This is supported by the findings of other researchers who have reported that increased pressure has little effect on the turbulent burning velocity of methane [147], and methane carbon dioxide mixtures [21].

Hydrogen addition to methane increased the turbulent burning rate considerably (Fig. 6.10). Hydrogen addition also improved flame stability. It was noted that significantly leaner mixtures could be stabilised on the burner than was possible during the methane and methane - carbon dioxide experiments. Temperature increase also improved flame stability. These trends are expected, and similar to those reported by other researchers [19].

The peaks of S_T of methane - hydrogen mixtures are observed at ϕ = 1 - 1.1 at 473 K temperature, however the peaks are shifted to leaner mixtures at 673 K. 15% hydrogen addition increased burning velocity by approximately 20% for 3 bar 473 K at ϕ = 1 in comparison with pure methane (Fig. 6.10). The increase of S_T at 3 bar 673 K at ϕ = 1 was about 40-45% in comparison with pure methane (Fig. 6.10, a). 30% hydrogen addition increased turbulent burning velocity by up to 45-50% at 3 bar 473 K at ϕ = 1 (Fig. 6.10) in comparison with pure methane. A larger increase by 80-90% of S_T was realised at 7 bar 473 K conditions at ϕ = 1. The difference of S_T between $85\%CH_4 - 15\%H_2$ and $70\%CH_4 - 30\%H_2$ at 3 bar and 7 bar 473 K was about 15-20% (Fig. 6.11, a), and about 25-30% at 3 bar and 7 bar 673 K for stoichiometric mixtures (Fig. 6.11, b). Therefore it implies that the augmentation of S_T of methane - hydrogen mixtures is more susceptible to temperature increase, than for pure methane at stoichiometric conditions. The largest difference between burning velocity rates of methane and different methane hydrogen mixtures was found to be around stoichiometric combustion conditions. On the fuel-rich side the difference becomes smaller. These trends are generally consistent with those reported by Mandilas et al. [22].

The effect of pressure increase from 3 bar to 7 bar was very small on S_T for $85\%CH_4 - 15\%H_2$ at 473 K and 673 K at ϕ = 1 (Fig. 6.11). For rich mixtures the pressure effect at the same temperatures was negligible, however the effect was more significant for lean mixtures. The burning velocity of $85\%CH_4 - 15\%H_2$ at ϕ = 0.8 increased by approximately 65% at 473 K, and by 40% at 673 K in comparison

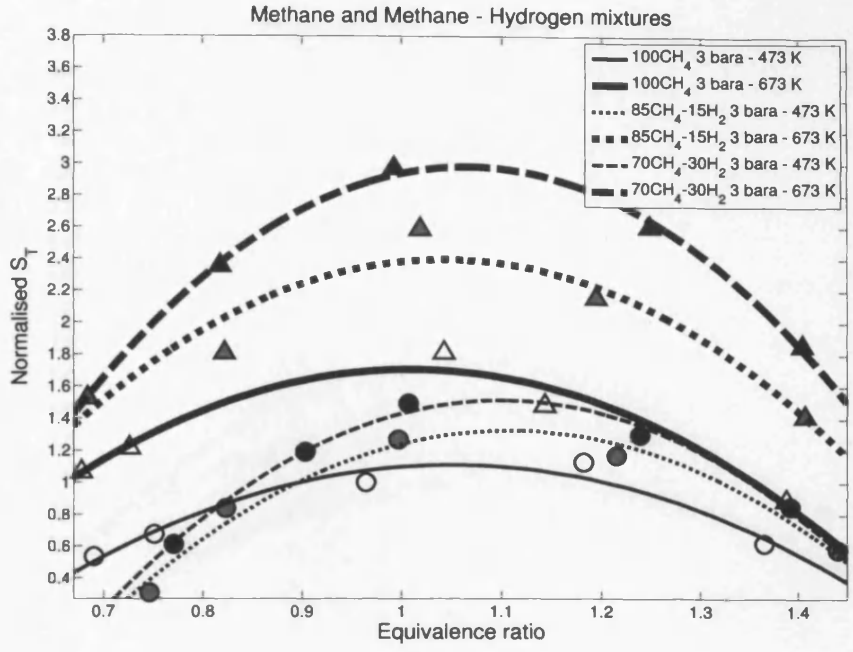

(a) 3 bar pressure

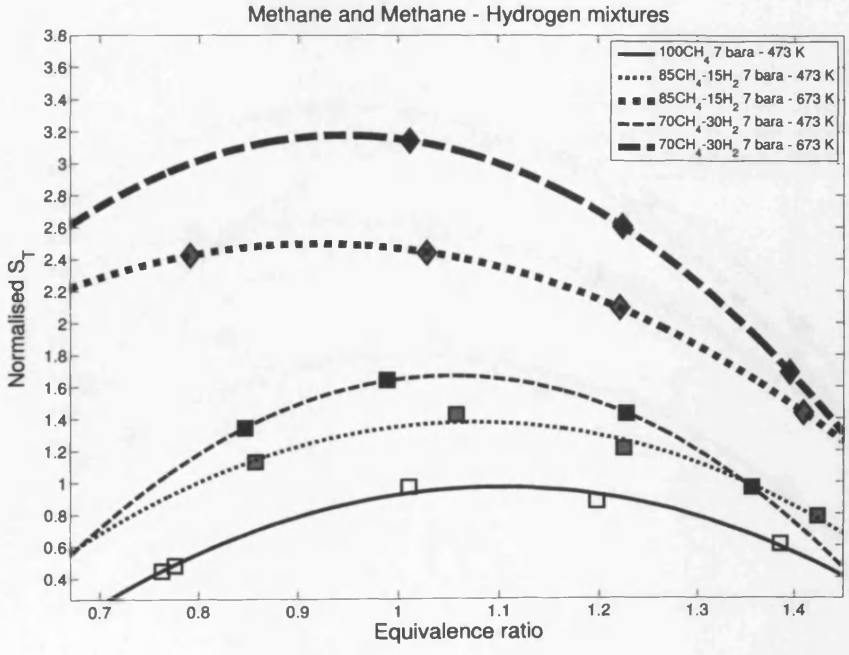

(b) 7 bar pressure

Figure 6.10: *Normalised burning velocity of methane and methane - hydrogen mixtures at different pressures. Symbols:* ◯ *- 3 bar 473 K,* △ *- 3 bar 673 K,* □ *- 7 bar 473 K,* ◇ *- 7 bar 673 K, blank - CH_4, grey - $85\%CH_4 - 15\%H_2$, black - $70\%CH_4 - 30\%H_2$. Relative turbulent intensity values vary from 15% to 18%.*

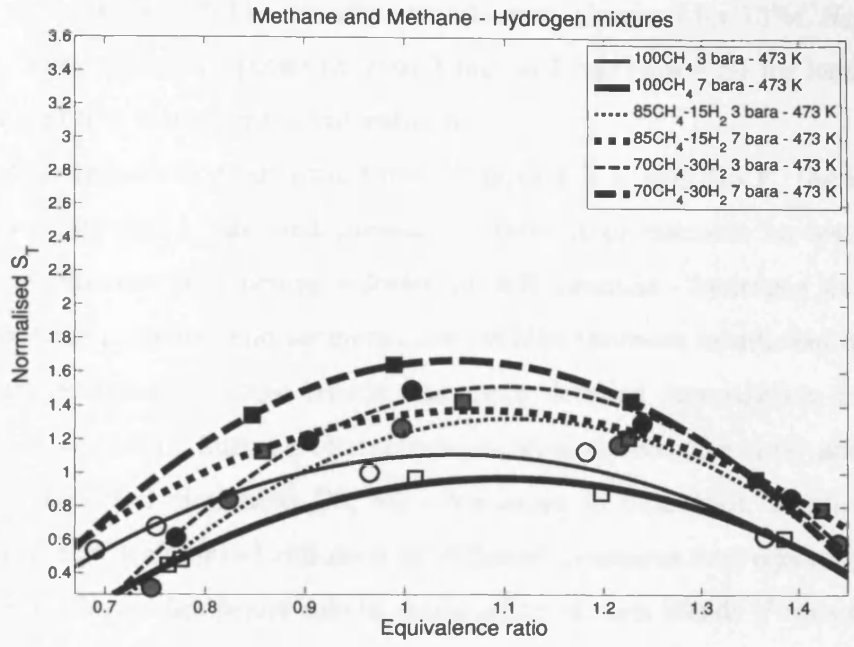

(a) 473 K temperature

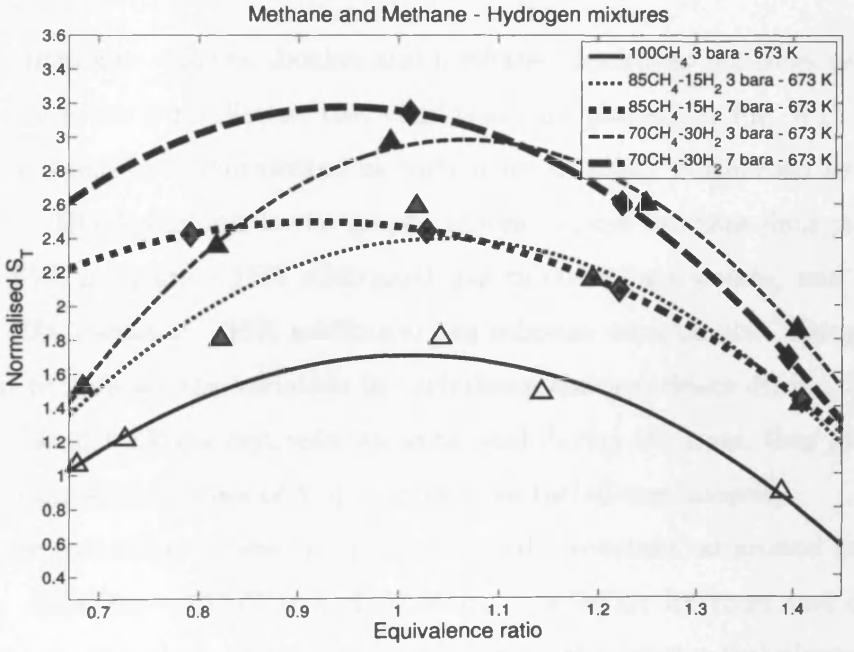

(b) 673 K temperature

Figure 6.11: *Normalised burning velocity of methane and methane - hydrogen mixtures at different temperatures. Symbols:* ◯ *- 3 bar 473 K,* △ *- 3 bar 673 K,* □ *- 7 bar 473 K,* ◇ *- 7 bar 673 K, blank - CH_4, grey - $85\%CH_4 - 15\%H_2$, black - $70\%CH_4 - 30\%H_2$. Relative turbulent intensity values vary from 15% to 18%.*

with S_T at 3 bar (Fig. 6.11). Similiar trends were observed for $70\%CH_4 - 30\%H_2$ mixture. The increase in pressure from 3 bar to 7 bar raised S_T for lean mixtures at 473 K and 673 K ambient temperatures.

For all methane - hydrogen mixtures, at both 473 K and 673 K, the increase in burning velocity due to ambient pressure increase is appreciable for lean mixtures (Fig. 6.11), whereas the burning velocity of rich methane - hydrogen mixtures are similar for both pressures and temperatures. Whilst there are insufficient data points to be fully confident of these trends and more detailed investigation is required, variation in turbulent burning characteristics with equivalence ratio and pressure have been reported elsewhere [23, 53]. Variation in Markstein number and the influence of the preferential diffusion at different pressures and equivalence ratios are likely to play a significant role in explanation of such trends if consolidated by other experiments.

6.3.2 Relative turbulence intensity

Methane, methane - carbon dioxide and methane - hydrogen mixtures relative turbulence intensities for different test conditions are plotted in Fig. 6.12. Relative turbulence intensity is represented as turbulence intensity normalised by mean velocity, $q'/\bar{u}$. Blank symbols in the graphs represent pure methane data points, grey symbols 85% methane - 15% additional gas mixture data points, and full black symbols 70% methane - 30% additional gas mixture data points. The graphs are presented to indicate the variation in turbulence characteristics during the experiment. Different bulk gas exit velocity were used during the tests, thus giving some variation in absolute values of $\bar{u}$, q' and relative turbulence intensity.

Relative turbulence intensity remained broadly constant, at around 14-18%, for methane, $85\%CH_4 - 15\%CO_2$ and $70\%CH_4 - 30\%CO_2$ for most test conditions (Fig. 6.12, a). For pure methane at 7 bar 473 K, the relative turbulence intensity is slightly higher, at around 19%. Variable $q'/\bar{u}$ is observed for $70\%CH_4 - 30\%CO_2$ also at 7 bar 473 K. Here $q'/\bar{u}$ drops from 20% for lean mixtures to 18% for rich mixtures. This is due to the higher bulk exit velocity of the gas mixture required to stabilise rich mixtures during the experiments. For $70\%CH_4 - 30\%CO_2$ at 7 bar 473 K at $\phi = 0.76$, very low bulk exit velocity at $\bar{u} = 3.5$ m/s has been maintained

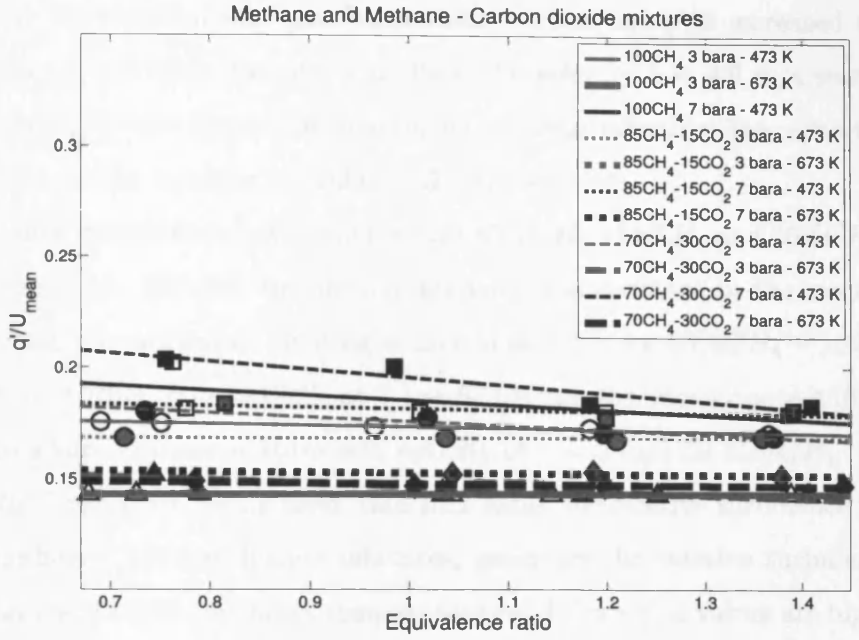

(a) CH_4 and $CH_4 - CO_2$ mixtures

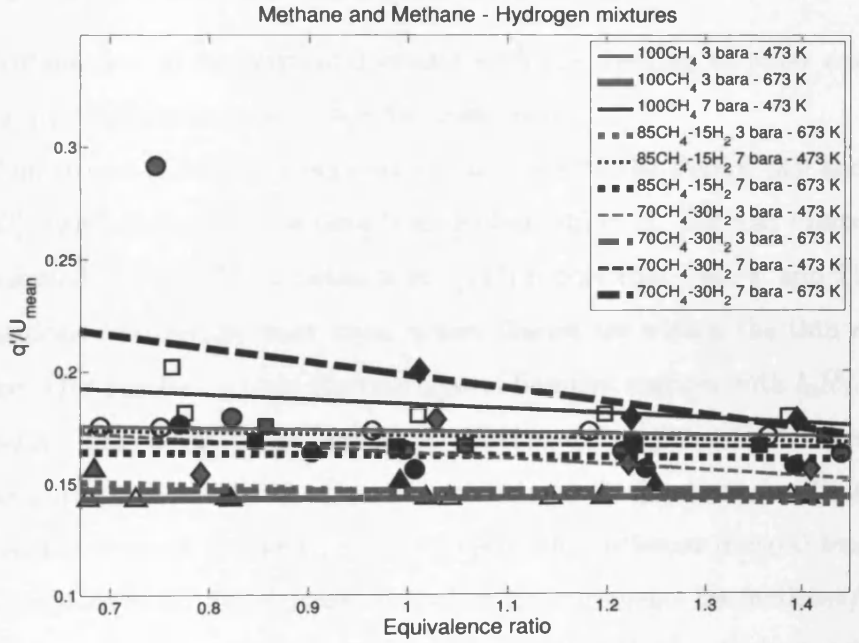

(b) CH_4 and $CH_4 - H_2$ mixtures

Figure 6.12: *Relative turbulence intensity of methane, methane - carbon dioxide and methane - hydrogen mixtures. Symbols:* ○ *- 3 bar 473 K,* △ *- 3 bar 673 K,* □ *- 7 bar 473 K,* ◇ *- 7 bar 673 K, blank - CH_4, grey - $85\%CH_4 - 15\%CO_2(H_2)$, black - $70\%CH_4 - 30\%CO_2(H_2)$.*

to keep the slow burning gas flame stable. Thus the $q'/\bar{u}$ increased to 20%. For methane $\phi = 0.78$ at the same condition the velocity $\bar{u} = 4.9$ m/s was maintained, therefore $q'/\bar{u}$ was lower. In general for all lean mixtures the velocity had to be slightly reduced in order to stabilise the flame.

Similar trends have been observed for $85\%CH_4-15\%H_2$ and $70\%CH_4-30\%CO_2$ (Fig. 6.12, b). Relative turbulence intensity was constant in the majority of tests undertaken for methane - hydrogen mixtures. Only for $85\%CH_4 - 15\%H_2$ at 3 bar 473 K and $70\%CH_4 - 30\%H_2$ at 7 bar 673 K are the variations significant. This is due to a very low gas mixture exit velocity of $\bar{u} = 2$ m/s for $85\%CH_4 - 15\%H_2$ at $\phi = 0.75$, 3 bar 473 K being used, thus increasing the relative turbulence intensity. As for methane - carbon dioxide mixtures, generally the relative turbulence intensity was around 14-18%. At lower temperature conditions $q'/\bar{u}$ values are higher, because the exit velocity required for flame stabilisation was lower.

6.3.3 Data comparison and correlation

The comparison of experimental results with the findings of other researchers and turbulent combustion models are discussed here.

Comparison of methane experiment results with the Peters' [33] and Zimont's et al. [32] correlations, and the data from Kobayashi et al. [36] and Filatyev et al. [85] is presented in Fig. 6.13. Griebel et al. [147] report that Peters' and Zimont's at al. correlations overpredict their data, where flames are within the thin reaction zone regime. Our results - within the corrugated flamelet regime, with l_0/δ_L in the range of 60-100 - are closer to the Peters' correlation although, as for Griebel et al., they are also overpredicted by the Peters' predictions. Correlations for Zimont et al. are plotted for elevated temperature and pressure for different integral length scales l_0.

Kobayashi et al. [36] performed similar measurements for methane/air flames at elevated temperature and pressures. Consistent with the work reported here, the flames studied fell into the corrugated regime on the Borghi diagram making the results of Kobayashi et al. a useful comparison. As observed from Fig. 6.13, the turbulent and laminar burning velocity ratio recorded by Kobayashi et al. is higher than the current results. Their data is also significantly under predicted by Peters' correlation despite the fact it was seen to over predict the measurements reported

here, as well as those by Griebel et al. [147] and Filatyev et al. [85].

One possible explanation for these discrepancies could be the different interpretation methods of processed flame images. Kobayashi et al. has calculated flame areas from contours obtained at progress variable value 0.1. This means that smaller flame areas have been derived and therefore higher burning velocities obtained, compared to those obtained from progress variable value 0.5, which the author contends represents the averaged flame contour more accurately. The difference in image processing techniques employed may also account for some of the difference - here the single image processing technique is utilised, whereas Kobayashi et al. used the average image processing technique.

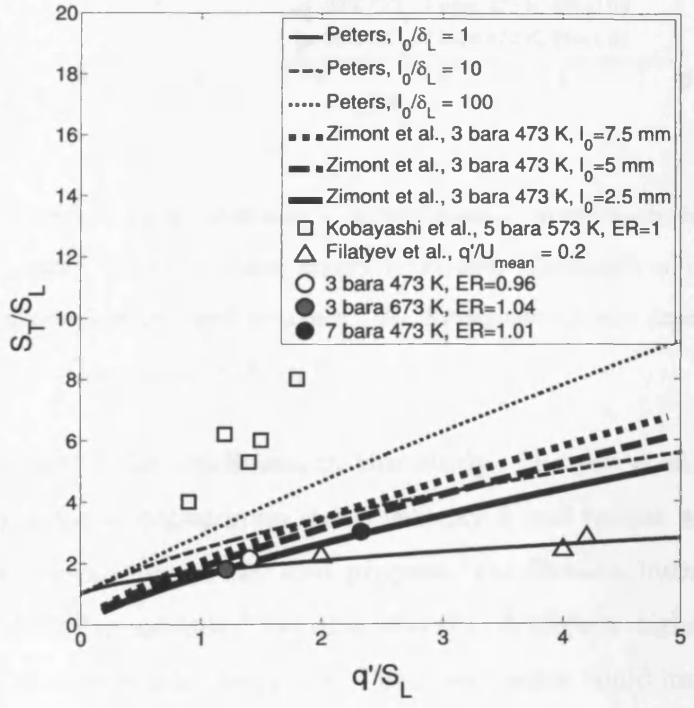

Figure 6.13: *Comparison of methane turbulent and laminar burning velocities ratio S_T/S_L of these experiments with Peters [33] and Zimont et al. [32] correlations at different lengthscale ratios l_0/δ_L and different integral length scales l_0, and Kobayashi et al. [36] and Filatyev et al. [85] experiments data.*

Another comparison with Filatyev et al. experiments [85] is presented in Fig. 6.13. Filatyev et al. have performed experiments in a slot type burner at 1 bar 296 K ambient conditions. The relative turbulence intensity in their experiment is 20%,

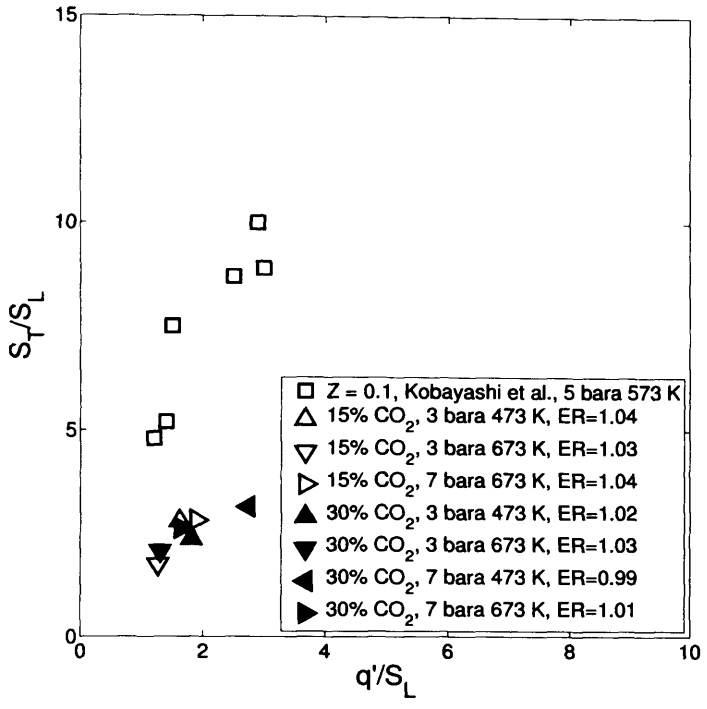

Figure 6.14: *Comparison of methane - carbon dioxide mixtures turbulent and laminar burning velocity ratio S_T/S_L of these experiments with Kobayashi et al. [18] experiment data at elevated temperature and pressure. In Kobayashi et al. experiments CO_2 was diluted in air, $Z = X_{CO_2}/(X_{air} + X_{CO_2})$.*

which is very close to the conditions in this study. Filatyev et al. argue that turbulent burning velocity depends on mean velocity $\bar{u}$ and burner width, or in other words on burner geometry. They also propose that Bunsen burner flames should display a nonlinear dependence ("bending effect"). A slightly higher value of S_T/S_L at 7 bar 473 K is observed in the graph. This observation could imply that pressure affects turbulent and laminar burning velocity ratio as indeed has been reported by other researchers [17, 36].

In Fig. 6.14 a comparison of the turbulent and laminar burning velocity ratio from this test programme and the Kobayashi et al. [18] findings are presented. The data of Kobayashi et al. for methane and methane carbon dioxide mixtures are consistently higher that the current experiments, with contributory reasons for these findings discussed earlier. The effects of carbon dioxide addition have been reported by Kobayashi et al. [18]. They found that the ratio of turbulent to laminar burning

rate and mean fuel consumption rate decreased with increasing CO_2 dilution ratio. A possible explanation is offered by the effect of increased Markstein length [18], which means that local burning velocity in the turbulent flame region decreases with local stretch due to turbulence. Another possible influence considered concerns variation of the smallest wrinkling scale of a CH_4/air/CO_2 flame, which was smaller than that of the flame with no CO_2 dilution.

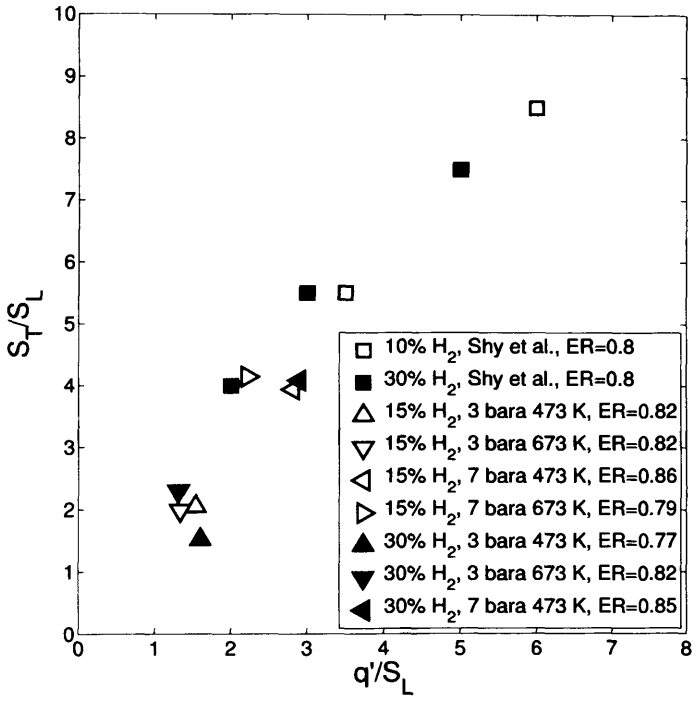

Figure 6.15: *Methane - hydrogen mixtures turbulent burning velocity comparison of these experiments with Shy et al. [21] results. Turbulent burning velocity data normalised by laminar burning velocity.*

The comparison of the methane - hydrogen results from this programme with those of Shy et al. [21] and Kido et al. [23] are presented in Figs. 6.15 and 6.16. Shy et al. performed their experiments at atmospheric conditions and show that the trends for S_T/S_L as a function of q'/S_L are in reasonable agreement with ours (Fig. 6.15). The same trends are reported for pure hydrogen in the paper of Kitagawa et al. [53]. Figure 6.16 presents the turbulent burning velocity reported by Kido et al. (after normalizing the data by the methane burning velocity at 3 bar 473 K at $\phi = 0.96$). Kido's et al. experiments were undertaken utilising propagating flames.

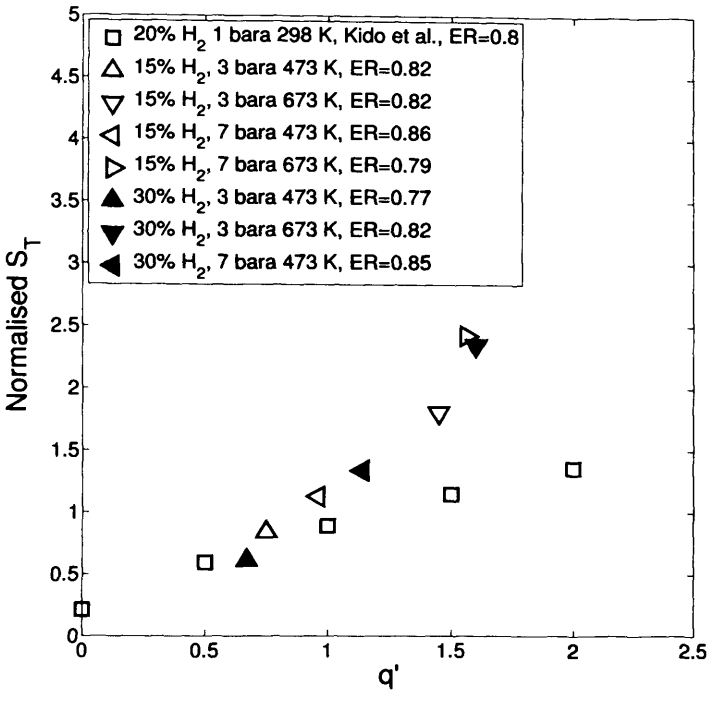

Figure 6.16: *Methane - hydrogen mixtures turbulent burning velocity comparison of these experiments with Kido et al. [23]. Kido et al. results of turbulent burning velocity are normalised by methane burning velocity at 3 bar 473 K at ϕ = 0.96 obtained in our experiments.*

The current data correlates well with their findings for q' less than 1. For higher q' the differences are noticeable. This implies that both temperature and pressure have a strong effect on S_T, and this effect arises from differences both in the type of flames and especially the turbulence characteristics of a propagating as opposed to that of a conical shape flame.

6.4 Conclusion

1. Investigations of turbulent burning velocity of gaseous alternative fuels at elevated pressure and temperature have been undertaken in a new large-scale High Pressure Optical Combustor facility. Methane, methane - carbon dioxide and methane - hydrogen mixtures have been tested across a broad range of equivalence ratio with pressures up to 7 bar and inlet temperature up to 673

K. All flames considered chosen have been in the corrugated flamelet regime, through appropriate choice of operating conditions.

2. An alternative analysis method for turbulent flame image processing and hence turbulent burning velocity calculation has been proposed and applied. The results have been assessed against other commonly used methodologies, and although the method proved to be reliable in this programme, further investigation and refinement is ongoing.

3. Methane and methane - carbon dioxide mixtures turbulent burning velocity results have been compared with Peters' and Zimont's et al. correlations and recent data of Kobayashi et al. and Filatyev at al. The results show reasonable agreement with Peters' predictions. However, the results show differences with the findings of Kobayashi et al., most likely due to data analysis differences, such as the selected value of progress variable.

4. Methane - hydrogen mixture results correlate well with recent data from Shy et al., who utilised the alternative propagating flame method for quantifying turbulent burning velocity, notwithstanding differences in pressure and temperature between datasets.

5. These data quantify the reduction in turbulent burning rate induced by carbon dioxide addition to methane for a variety of equivalence ratios. Increase in initial ambient gas temperature significantly increases turbulent burning velocity, while increase in ambient pressure induces a reduction. Methane and methane - carbon dioxide mixtures demonstrate similar trends with respect to the influence of ambient conditions.

6. Hydrogen addition to methane has been found to considerably increase turbulent burning velocity even for small volumes of hydrogen addition. For lean hydrogen-methane mixtures, an increase in temperature or pressure augments turbulent burning velocity, whereas the influence of ambient pressure is minimal for rich mixtures.

Chapter 7

Bunsen burner experiments at atmospheric conditions

Despite the huge interest in gas turbine combustion at elevated temperature and pressure, fundamental knowledge of fuel combustion at atmospheric conditions is still essential. In most industrial processes combustion occurs at atmospheric conditions, therefore the research into alternative fuels at these conditions is of primary importance, and serves as a basis of comparison for higher temperature and pressure results.

In this experimental programme, three different gaseous fuels: 100% methane, 85% methane - 15% hydrogen and 70% methane - 30% hydrogen were tested at atmospheric conditions. Approximately 6 data sets were generated for each gas mixture for $0.7 < \phi < 1.1$.

The tests were performed using a Bunsen burner. Two different measurement techniques were applied. LDA was used to determine the velocity profile and turbulence characteristics at the exit of the burner for isothermal flows. PLIF was applied in order to measure the turbulent burning velocity S_T. Images of the flame front were recorded using a camera with intensifier synchronised with a pulsed dye laser. Detail description of the experiment setup is presented in chapter 3.

Fuel and combustion air were measured simultaneously using rotameters. The flow measured with rotameter was corrected depending on gas density variation. The measuring accuracy of rotameters was 3%. Air flow and gas flow were kept constant by using pressure regulators during the tests.

Calculations for equivalence ratios were performed using equations 6.4, 6.6, 6.7 presented in chapter 6. The turbulent burning velocity was calculated using equation 2.43.

The exit velocity from the burner of the gas-air mixture was derived from the volume flow rate of combustion air and fuel flows. Density, viscosity, diffusion coefficients and other gas properties of the combustible mixture were calculated using polynomial fit coefficients available within the Chemkin database or taken from reference tables.

The Chemkin-Pro software and GRI-Mech v3.0 reaction mechanism were used to calculate laminar burning velocities and flame thicknesses for the various gas mixtures at different equivalence ratios. The laminar flame thickness calculation method was based on a classical approach of defining temperature gradient.

The LDA results were utilised to ensure that turbulence intensity and burner exit velocity profiles are uniform and to find integral time scales of turbulence. A description of LDA, PLIF and flame image processing methods is presented in chapter 4.

7.1 Isothermal LDA Results

Figure 7.1 shows the variation of mean axial velocity and velocity fluctuations respectively with radial position for a range of exit velocities. The burner edges are at the positions $r = 0\ mm$ and $r = 25\ mm$. The results show that the axial velocity profiles are uniform for low gas exit velocities. For higher exit velocities the velocity profile becomes convex towards the burner. In the experiments the gas flow did not exceed 2 m/s exit velocity, therefore for it can be assumed that the velocity profile was flat during all experiments. This confirms the suitability of the burner for the study.

It is seen from the graph (Fig. 7.1, b) that u' velocity is almost constant at the centre of the burner at low exit velocity. At larger exit velocities (4.9 m/s) larger inconsistency of u' are observed at the centre of the burner.

Using LDA, 3000 samples were collected at each position across the centre of the burner (radial position $r = 4 \div 21$ mm) at each condition. Due to the flow stream

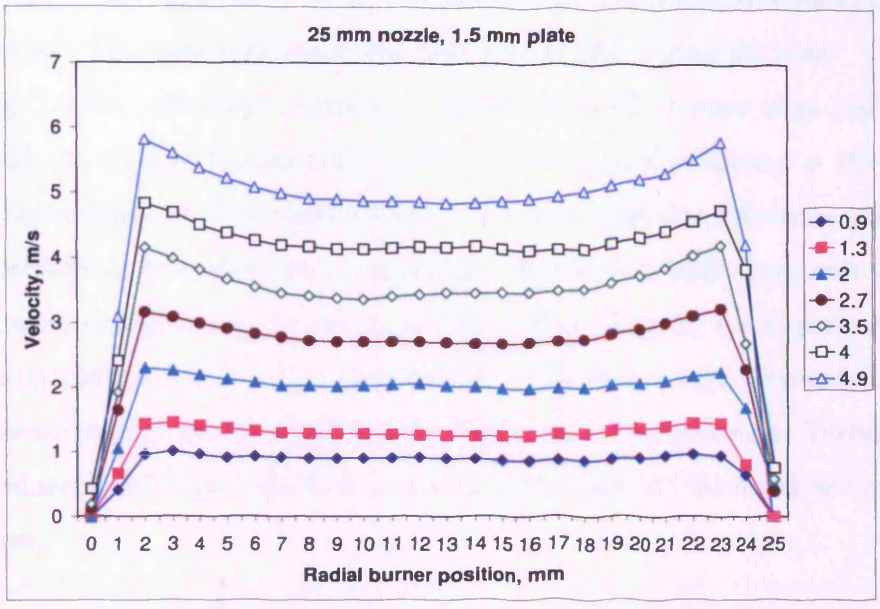

(a) axial mean velocity $\bar{u}$

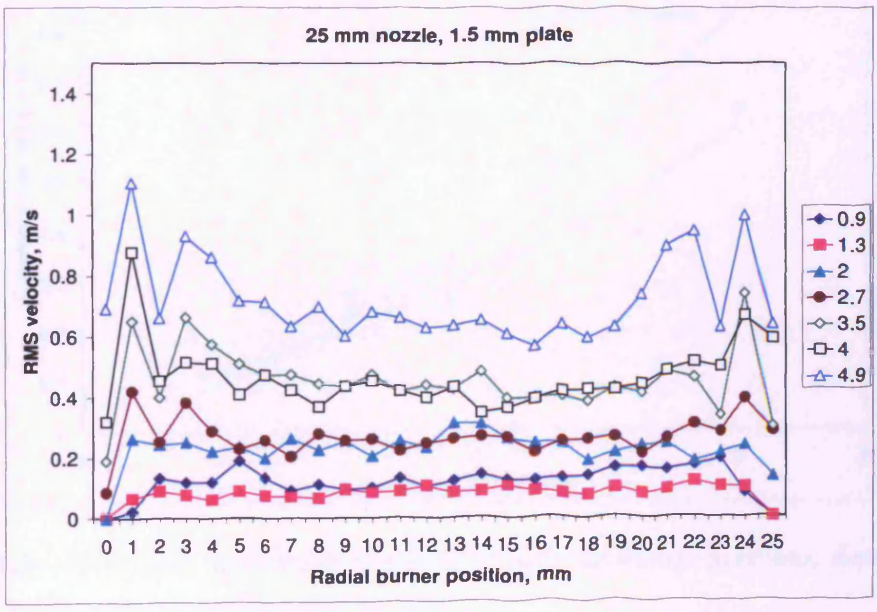

(b) axial RMS velocity u'

Figure 7.1: *Axial mean velocity $\bar{u}$ and axial RMS velocity u' measured 5 mm downstream burner exit at different bulk gas flow velocities at atmospheric conditions.*

shape the seeding rate was somewhat lower at the edges of the burner ($r = 0 \div 4$ mm and $r = 21 \div 25$ mm). The relative error did not reach 0.5% for the measurements in the centre of the burner and did not exceed 3% for the measurements at the edges of the burner. The data validation rate was above 95% during all tests.

In Fig. 7.2 the turbulence intensity q' measured at the burner edge (radial position $r = 21-25\,mm$) and at the centre of the burner (radial position $r = 10-15\,mm$) shows a dependence on bulk flow velocity. It is seen that the difference of q' at different positions at low velocities is negligible. However at higher gas exit velocities the difference is higher due to the shear layer effect. During the experiments bulk exit velocity did not reach 2 m/s, therefore for consistency with elevated conditions data q' measured at the edge of the burner was used for calculations. Turbulence intensity values at different bulk flow velocities were obtained from polynomial fitting correlation.

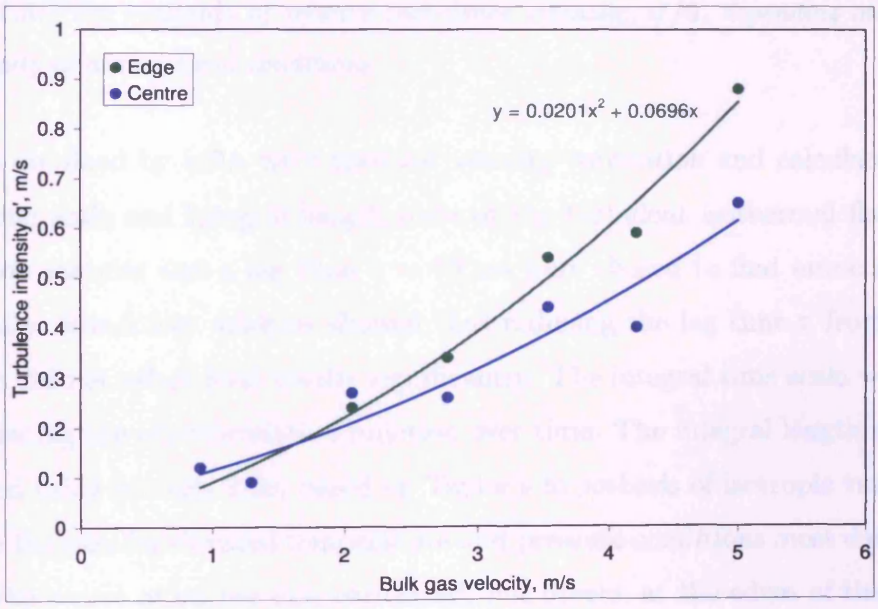

Figure 7.2: *Turbulence intensity q' measured at different burner positions, depending on bulk gas flow velocity at atmospheric conditions.*

The evolution of relative turbulence intensity ($q'/\bar{u}$) as a function of bulk flow velocity is represented in Fig. 7.3. The measurements taken at the burner edge and at the centre show slightly different results. Relative turbulence intensity is increasing when gas exit velocity increases at the edge of the burner. At the centre of the burner $q'/\bar{u}$ remains almost constant. In both cases $q'/\bar{u}$ did not exceed 15%

during the experiments for exit velocity up to 2 m/s.

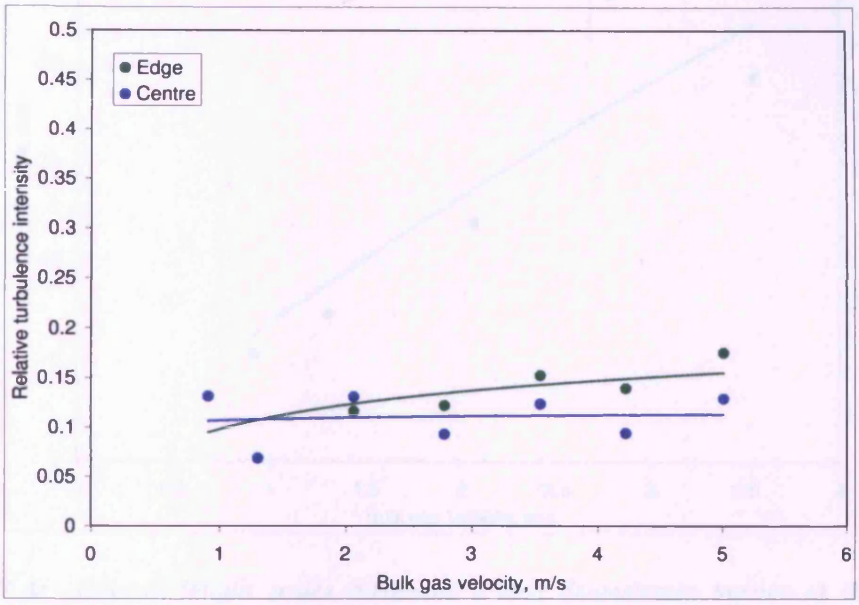

Figure 7.3: *The evolution of relative turbulence intensity, $q'/\bar{u}$, depending on bulk gas flow velocity at atmospheric conditions.*

Data obtained by LDA were used for velocity correlation and calculate the integral time scale and integral length scale of the turbulent isothermal flow. 1024 correlation samples and a lag time $\tau = 50$ ms were chosen to find autocorrelation coefficients. Sensitivity analysis showed that reducing the lag time τ from 100 ms to 50 ms did not affect final results significantly. The integral time scale was found by integrating the autocorrelation function over time. The integral length scale was calculated using formula 2.20, based on Taylor's hypothesis of isotropic turbulence.

As in the case for elevated temperature and pressure conditions most data points around the centre of burner exit correlated, but others, at the edges of the burner, oscillated and did not cross zero. The same behaviour was observed for the data obtained at elevated temperature and pressure conditions.

Averaged integral length scale data obtained from autocorrelation coefficients measured at the centre of the burner (radial position $10 < r < 15$ mm are presented in Fig. 7.4. Only correlated values have been used to process integral time scale and length scale.

It is seen from the graph (Fig. 7.4) that integral length scale tends to increase with increasing exit gas velocity. At tested conditions, where exit velocity did not

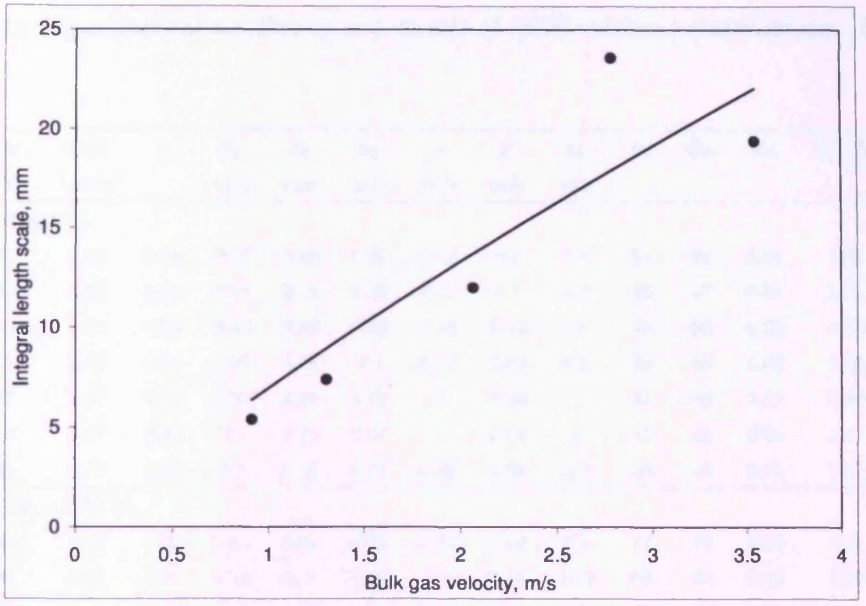

Figure 7.4: *Integral length scales measured 5 mm downstream burner at the burner centerline exit.*

exceed 2 m/s, l_0 was in the range of 5 - 12 mm.

7.2 Turbulent burning velocity

This study has investigated methane and methane-hydrogen flames at atmospheric conditions using PLIF. Only lean flames and flames close to the stoichiometric mixture were investigated. Laminar burning velocities and flame thicknesses were calculated using Chemkin. The tested flames and test results are presented in Table 7.1.

To identify the combustion regime, turbulence and combustion characteristics were calculated and measured. Turbulence intensity q', turbulent length scale l_0, were obtained from the experiments (Figs. 7.1, 7.2 and 7.4). Laminar flame thickness δ_L and laminar burning velocity S_L were computed using Chemkin-Pro. Re presented in the table was calculated using equation 2.53. Da number was computed suing equation 2.57. Karlovitz number was approximated using the equation 2.58 as was proposed by Driscoll [77].

It was found that Ka number was very low in all cases, implying that all tests were conducted in the wrinkled flamlets regime of Borghi - Peters diagram (Fig. 2.13).

A pilot flame was not used as only a narrow range of flames close to stoichio-

Table 7.1: *Experimental conditions and results of 100% methane and methane - hydrogen mixtures*

Test	Air	Gas	ϕ	S_L	δ_L	S_T	u	q'	l_0	Re	Da	Ka	S_T/S_L	q'/S_L
	l/min	l/min		m/s	mm	m/s	m/s	m/s	mm					
	100% CH_4													
1	30	2.96	0.94	0.37	0.46	0.45	1.12	0.1	7.8	51	63	0.02	1.22	0.27
2	30	2.66	0.84	0.31	0.51	0.45	1.11	0.1	7.7	50	47	0.03	1.45	0.32
3	35	3.65	0.99	0.39	0.45	0.45	1.31	0.13	9	76	60	0.03	1.15	0.33
4	25	2.47	0.94	0.37	0.46	0.4	0.93	0.08	6.5	34	65	0.02	1.08	0.22
5	27	2.47	0.87	0.33	0.49	0.46	1	0.09	7	41	52	0.02	1.39	0.27
6	27	2.37	0.83	0.3	0.52	0.47	1	0.09	7	41	45	0.03	1.57	0.3
7	25	2.17	0.83	0.3	0.52	0.47	0.92	0.08	6.4	33	46	0.03	1.57	0.27
	85% CH_4 - 15% H_2													
1	35	4.23	1.02	0.43	0.42	0.56	1.33	0.13	9.1	77	72	0.02	1.3	0.3
3	40	4.23	0.89	0.38	0.46	0.59	1.5	0.15	10.2	99	56	0.03	1.55	0.39
5	30	3.6	1.01	0.43	0.42	0.51	1.14	0.1	7.8	51	80	0.02	1.19	0.23
6	30	2.65	0.75	0.26	0.56	0.56	1.11	0.1	7.6	49	35	0.04	2.15	0.38
7	35	3.91	0.95	0.41	0.43	0.59	1.32	0.13	9	76	66	0.02	1.44	0.32
8	34	3.39	0.84	0.34	0.48	0.57	1.27	0.12	8.7	68	51	0.03	1.68	0.35
10	40	5.08	1.07	0.44	0.41	0.52	1.53	0.15	10.4	101	74	0.02	1.18	0.34
	70% CH_4 - 30% H_2													
11	40	5.74	1.06	0.5	0.38	0.62	1.55	0.16	10.5	107	86	0.02	1.24	0.32
2	45	6.32	1.04	0.49	0.39	0.64	1.74	0.18	11.7	135	82	0.02	1.31	0.37
3	50	6.89	1.02	0.49	0.39	0.69	1.93	0.21	12.9	173	77	0.03	1.41	0.43
4	55	6.89	0.93	0.45	0.41	0.71	2.1	0.23	14	207	67	0.04	1.58	0.51
5	40	5.17	0.96	0.47	0.4	0.7	1.53	0.15	10.4	100	81	0.02	1.49	0.32
6	37	4.59	0.92	0.44	0.42	0.64	1.41	0.14	9.6	86	72	0.02	1.45	0.32

metric conditions were tested. The flame stabilised at the burner without using any additional measures.

One of the limitation was the laser optics, which only allowed to create approximately a 30 mm deep laser sheet. Therefore the flame was adjusted in order to obtain full height flame images.

7.2.1 Turbulent burning velocity measurements

Turbulent burning velocity measurements were conducted using the same method as for elevated temperature and pressure conditions. The methods had been tested for laminar flames and compared with the flame cone angle method (chapter 4).

Equivalence ratio ϕ was calculated based on volumetric flow rates using equation:

$$\phi = \left(\frac{\dot{V}_a}{\dot{V}_g}\right)_{st} \cdot \frac{\dot{V}_g}{\dot{V}_a} \tag{7.1}$$

where ratio $\left(\dot{V}_a/\dot{V}_g\right)_{st}$ was volumetric air fuel ratio, which was constant for a particular gas mixture.

Rotameter accuracy according to the manufacture's data sheet is 3%. Therefore uncertainty analysis for error propagation was conducted in order to estimate the error of ϕ due to the measuring error. This error can be calculated using the equation:

$$\Delta f \approx \left|\frac{\partial f}{\partial X_1}\Delta X_1\right| + \left|\frac{\partial f}{\partial X_2}\Delta X_2\right| \tag{7.2}$$

Differentiating the equation 7.1 and applying equation 7.2 the error can be calculated:

$$\Delta\phi \approx \left|\frac{\partial\phi}{\partial\dot{V}_g}\Delta\dot{V}_g\right| + \left|\frac{\partial\phi}{\partial\dot{V}_a}\Delta\dot{V}_a\right| = \left|\left(\frac{\dot{V}_a}{\dot{V}_g}\right)_{st}\frac{\Delta\dot{V}_g}{\dot{V}_a}\right| + \left|-\left(\frac{\dot{V}_a}{\dot{V}_g}\right)_{st}\frac{\dot{V}_g\Delta\dot{V}_a}{\dot{V}_a^2}\right| \tag{7.3}$$

where $\Delta\dot{V}_a$ and $\Delta\dot{V}_g$ are air and gas rotameter errors respectively.

Due to large error the exact determination of ϕ was difficult. Even larger error was calculated for laminar flame (magenta triangles), which was obtained using 15 mm burner nozzle, because very low flow rate was required to obtain stable flame. At this flow rate the rotameters were close to the shut position, and the accuracy of the measurement was low. The results are presented in table 7.2.

Table 7.2: *Flow measurement experiment errors*

CH_4			$15\%H_2$			$30\%H_2$		
ϕ	ϕ error, %	S_T, m/s	ϕ	ϕ error, %	S_T, m/s	ϕ	ϕ error, %	S_T, m/s
0.94	±6.4	0.45	1.02	±5.9	0.55	1.06	±5.7	0.62
0.84	±6	0.45	0.89	±5.6	0.59	1.04	±5.8	0.64
0.99	±6.1	0.45	1.01	±5.9	0.51	1.02	±5.9	0.69
0.94	±5.3	0.4	0.75	±5.3	0.56	0.93	±6.5	0.71
0.87	±5.7	0.46	0.95	±6.3	0.59	0.96	±6.3	0.7
0.83	±6	0.47	0.84	±6	0.57	0.92	±6.5	0.64

Average turbulent burning velocity values of methane and methane-hydrogen mixtures are presented in Fig. 7.5.

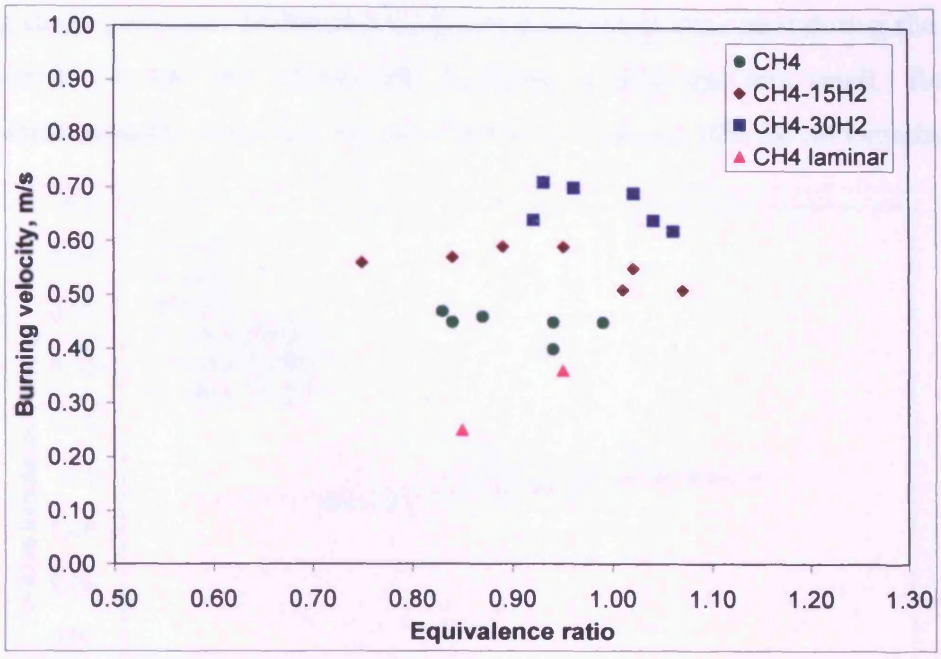

Figure 7.5: *Average turbulent burning velocity values measured at atmospheric conditions using PLIF-OH technique.*

In general the expected trends were observed in the experiments. S_T of methane-hydrogen mixtures was higher than that of pure methane. The burning velocity of $85\%CH_4 - 15\%H_2$ ws approximately 25-30% higher than methane in the range of tested equivalence ratios. S_T of $70\%CH_4 - 30\%H_2$ was approximately 20-25% higher than of $85\%CH_4 - 15\%H_2$ and approximately 50-55% higher than of pure methane. Very similiar results were observed during elevated temperature and pressure experiments. It was reported that increasing hydrogen content in the mixture up to 30% increased S_T about 45-50% at 3 bar 473 K $\phi \approx 1$ in comparison with pure methane. The same was observed comparing two methane-hydrogen mixtures, i.e. the augmentation of S_T was about 15-20% at 3 bar 473 K when the hydrogen content was increased from 15% to 30%. These observations show consistency of measurements.

7.2.2 Relative turbulence intensity

Methane and methane - hydrogen mixtures relative turbulence intensities for different test conditions are plotted in Fig. 7.6. Relative turbulence intensity is represented as turbulence intensity normalised by mean velocity, $q'/\bar{u}$.

The graph is presented to indicate the variation in turbulence characteristics

during the experiment. Different bulk gas exit velocities were used during the tests, however due to low exit velocity the variation in $q'/\bar{u}$ was very small. Relative turbulence intensity remained almost constant, at around 10% for all experiments.

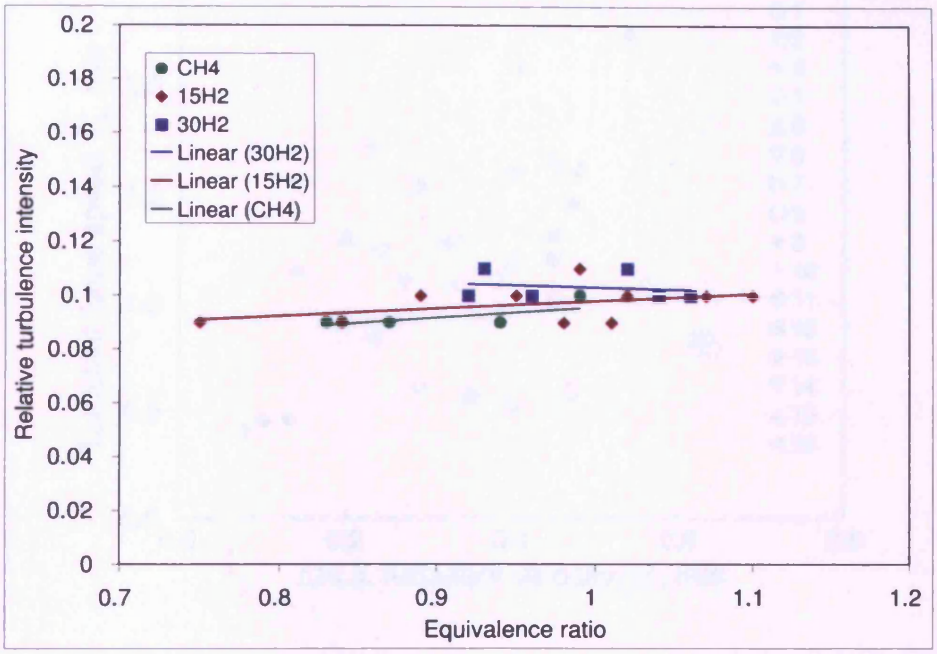

Figure 7.6: *Relative turbulence intensity of methane and methane - hydrogen mixtures in Bunsen burner tests.*

Although relative turbulence intensity is used as a measure of turbulence it does not really reveal the turbulence magnitude. During the tests at elevated temperature and pressure $q'/\bar{u}$ was found to be in the range of 14-18%, however the absolute values of q' were much higher than during the tests at atmospheric conditions, and therefore the combustion took place in the corrugated flamelet regime, which implies that absolute turbulence intensity value q' is more important in order to define turbulence characteristics.

7.2.3 Data comparison and correlation

The comparison of experimental results with the findings of other researchers are discussed in this section.

Lipatnikov and Chomiak in their review paper presented burning velocities of methane $\phi = 1$, collected from the experiments of other researchers at atmospheric

conditions [31]. For comparison purposes the data of the Bunsen burner experiment results were plotted into this graph (Fig. 7.7).

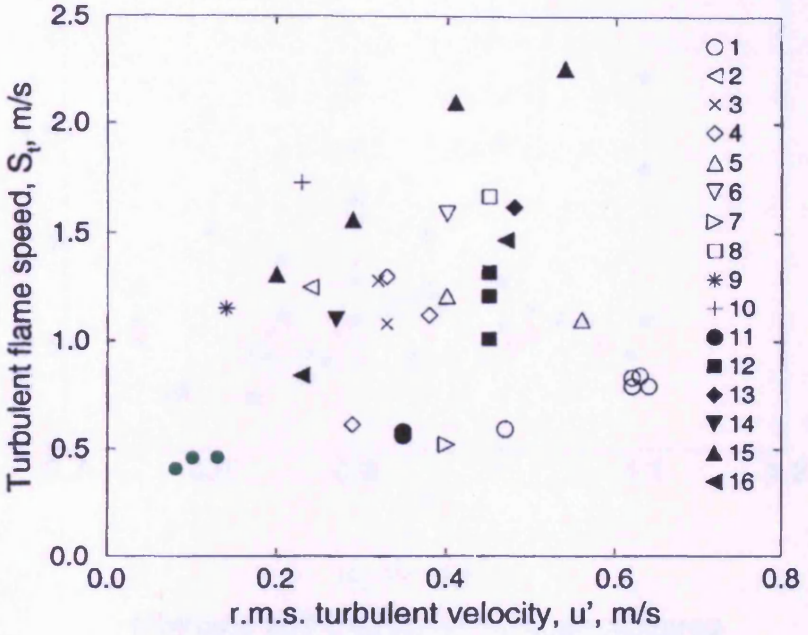

Figure 7.7: *Turbulent burning velocities of methane-air mixture measured by the different research groups at $\phi = 1$, replotted from Lipatnikov and Chomiak [31]. (1) Bourguignon et al. [169]; (2) Chan et al. [170]; (3) Cheng et al. [171], V-flame; (4) Cheng et al. [171], stagnation flame; (5) Cheng and Shepherd [168], V-flame; (6) Cheng and Shepherd [168], Bunsen flame; (7) Cheng and Shepherd [168], stagnation flame; (8) Gouldin and Dandekar [172]; (9) Gulati and Driscoll [173]; (10) Ho et al. [174]; (11) Shepherd [79]; (12) Smith and Gouldin [175]; (13) Cheng [176]; (14) Cho et al.; (15) Aldredge et al. [177]; (16) Shy et al. [178]; green circles are this experiment data of methane at $\phi = 0.94$ and $\phi = 0.99$.*

It is seen from the graph that experimental results data are widely scattered. The reasons of this phenomena were discussed by the authors of this graph [31]. Some of these reasons are related to the flame structures (propagating or stationary flames) or to different interpretation of the flame front position. The burning velocity data of this work fall into the lower left part of the graph, where turbulence intensity was the lowest. S_T of these tests was close to S_L due to the very low turbulence level, and seems sensible in comparison with the findings of other researchers.

The comparison of premixed methane-air mixtures of Bourguignon et al. [169],

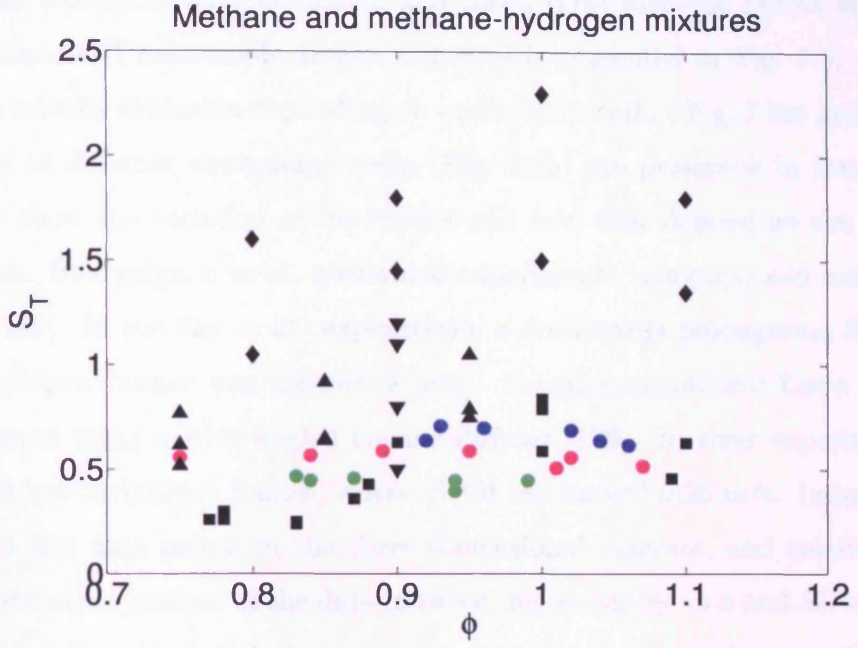

(a) S_T vs ϕ

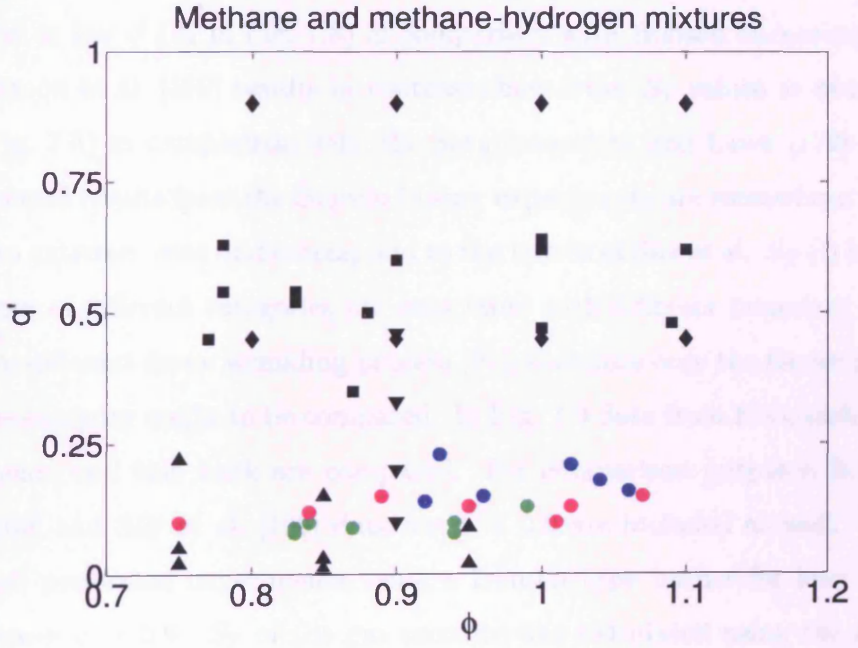

(b) q' vs ϕ

Figure 7.8: *Comparison of methane and methane-hydrogen turbulent burning velocities of this work with the results of Bourguignon et al. [169], Shy et al. [109], and Savarianandam and Lawn [179]. Black symbols:* □ *Bourguignon et al.;* △ *Savarianandam and Lawn;* ◊ *Shy et al. Colour* ◯ *represent the results from this work: green - CH_4, magenta - $85\%CH_4 - 15\%H_2$, blue - $70\%CH_4 - 30\%H_2$.*

Shy et al. [109], and Savarianandam and Lawn [179] with the results of this work for methane and methane-hydrogen mixtures is presented in Fig. 7.8. Turbulent burning velocity evolution depending on equivalence ratio (Fig. 7.8a) and turbulent intensity at different equivalence ratio (Fig. 7.8b) are presented in two graphs in order to show the variation of the results and how they depend on the measuring technique. Bourguignon et al. performed experiments using opposed axisymmetric flames [169]. In the Shy et al. experiments a downwards propagating flame speed in a cruciform burner was measured [109]. Savarianandam and Lawn conducted experiments using a wide-angled conical diffuser [179]. In their experiments they obtained low turbulence flames, where q' did not exceed 0.25 m/s. Larger symbols represent the data points in the three dimensional diagram, and smaller symbols represent the projections of the data in two-dimensional S_T vs ϕ and S_T vs q' planes.

It is seen from the graph that large inconsistency is observed comparing different experimental methods of obtaining data. S_T data from Savarianandam and Lawn are larger at low q' ($\triangle$ in Fig. 7.8) in comparison with Bunsen burner experiments. Bourguignon et al. [169] results in contrast show lower S_T values at even higher q' ($\square$ in Fig. 7.8) in comparison with the Savarianandam and Lawn [179] data. The experimental results from the Bunsen burner experiments are somewhere in between these two extreme cases and correspond to the trends of Shy et al. S_T ($\Diamond$ in Fig. 7.8).

Flames of different categories are associated with different boundary conditions and have different flame wrinkling process [91], therefore only the flames falling into the same category ought to be compared. In Fig. 7.9 data from Kobayashi et al. [34] experiments and this work are compared. For comparison purposes Bourguignon et al. [169] and Shy et al. [109] data for $\phi = 0.9$ are included as well. Kobayashi et al. [34] performed experiments using a Bunsen type burner for lean methane - air mixtures $\phi = 0.9$. S_T of the gas mixture was calculated using the flame cone angle method of averaged turbulent flame images, which corresponded to the flame at $< c >= 0.5$. In this work the flame position was assumed to be at the progress variable value $< c >= 0.5$ as well, therefore both these data sets can be directly compared.

It is seen from the graph that this work matches to that of Kobayashi et al. very well, while the Bourguignon et al. [169] and Shy et al. [109] data fall outside the

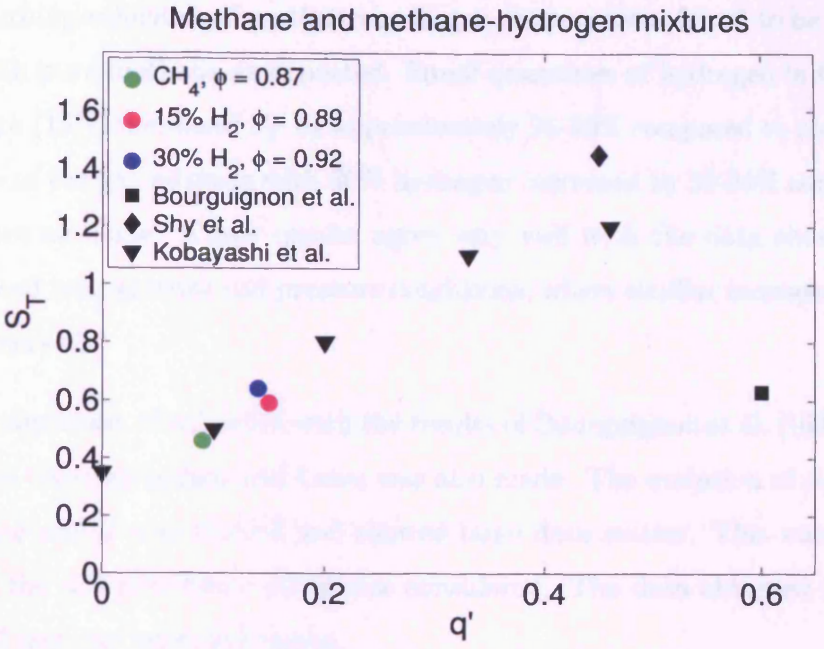

Figure 7.9: *Comparison of methane and methane-hydrogen turbulent burning velocities of this work with the results of Kobayashi et al. [34]. Bourguignon et al. [169] and Shy et al. [109] data for $\phi = 0.9$ are presented for comparison.*

these trends. Methane - hydrogen mixture data are expected to be slightly higher compared with Kobayashi et al. [34] data, therefore more detailed investigation of these mixtures at different turbulence intensities for lean mixtures is required. Although it was difficult to define the exact ϕ in this work, the results are promising and show that the PLIF technique combined with a novel flame front finding method are sufficiently accurate and can be used for S_T calculation.

7.3 Conclusion

1. Investigation of turbulent burning velocity of gaseous alternative fuels at atmospheric conditions was conducted using a PLIF-OH methods. Stoichiometric and lean methane and methane - hydrogen mixtures were tested. All flames considered fell into the wrinkled flamelet regime.

2. Low turbulence intensity level was maintained during the experiments. S_T of gas mixtures was approximately 10% to 60% higher than corresponding S_L.

3. Burning velocities of methane-hydrogen mixtures was found to be higher than with pure methane as expected. Small quantities of hydrogen in the gas mixture (15%) increased S_T by approximately 25-30% compared to pure methane. S_T of the gas mixture with 30% hydrogen increased by 50-55% compared with pure methane. These results agree very well with the data obtained at elevated temperature and pressure conditions, where similiar increases in S_T were observed.

4. Comparison of this work with the results of Bourguignon et al. [169], Shy et al., and Savarianandam and Lawn was also made. The evolution of S_T depending on ϕ and q' was plotted and showed large data scatter. This was mainly due to the different flame categories considered. The data obtained in this work fell into the expected region.

5. Methane - hydrogen mixture results show good agreement with data from Kobayashi et al. [34], who used the Bunsen burner method for quantifying turbulent burning velocity. This finding reveals that the PLIF method combined with the novel flame front area location method is promising and could be used for the creation of a database of S_T for alternative fuels at atmospheric as well as at elevated temperature and pressure conditions.

Chapter 8

Turbulent burning velocity analysis and extension to a generic swirl burner

Increasing demand for more sustainable fuels is stimulating research into hydrogen or hydrogen containing mixtures. However due to many limitations the practical application of such fuels at large scale causes problems, when existing combustors are used. Natural gas remains the most important gaseous fuel for industry and in the power generation sector. However in the future as natural gas becomes more expensive and scarce, it could be augmented by gasified coal or biomass or by the byproducts of industrial processes such as steel industry. Here in this chapter the investigation of such alternative fuels: methane-hydrogen and methane-carbon dioxide mixtures, which could represent the mixture of natural gas and gases produced form other sources (gasification, industrial waste gas, etc.) is presented. A novel turbulent burning velocity method is applied and results are compared with Bunsen burner data.

8.1 Experimental methodology

Five series of experiments were carried out to investigate the effect of CO_2 and H_2 on methane burning velocity and flame stability. Five different gaseous fuels: 100% methane, 85% methane - 15% carbon dioxide, 70% methane - 30% carbon dioxide, 85% methane - 15% hydrogen and 70% methane - 30% hydrogen were tested for lean and rich mixtures. The generic swirl burner was used to investigate flame stability

Table 8.1: *Gas composition, conditions and methods used to investigate CO_2 and H_2 addition effect on CH_4 turbulent combustion.*

Gas mixture	Bunsen burner tests	Swirl burner tests	Chemkin	Fluent
100%CH_4	3 bar, 473 K	1 bar, 293 K	1, 3 bar and 300, 473, 673 K	1 bar, 293 K
85%CH_4-15%CO_2	3 bar, 473 K	1 bar, 293 K	1, 3 bar and 300, 473, 673 K	1 bar, 293 K
70%CH_4-30%CO_2	3 bar, 473 K	1 bar, 293 K	1, 3 bar and 300, 473, 673 K	1 bar, 293 K
85%CH_4-15%H_2	3 bar, 473 K	1 bar, 293 K	1, 3 bar and 300, 473, 673 K	1 bar, 293 K
70%CH_4-30%H_2	3 bar, 473 K	1 bar, 293 K	1, 3 bar and 300, 473, 673 K	1 bar, 293 K
50%CH_4-50%H_2	-	-	1, 3 bar and 300, 473, 673 K	-
30%CH_4-70%H_2	-	-	1, 3 bar and 300, 473, 673 K	-
15%CH_4-85%H_2	-	-	1, 3 bar and 300, 473, 673 K	-
100%H_2	-	-	1, 3 bar and 300, 473, 673 K	-

at atmospheric conditions (1 bar, 293 K). Chemkin and Fluent have been used to model laminar and turbulent flames. The list of investigated mixtures and conditions is presented in Table 8.1, together with the high temperature and pressure results from chapter 6.

Flame stability and flashback experiments were conducted using the generic swirl burner designed in Cardiff University. The burner was designed to produce premixed, non premixed and partially premixed flames. Only premixed combustion was considered in this programme. Detail description of experimental rigs and methods is presented in chapters 3 and 4.

8.2 Turbulent premixed combustion modelling

In premixed combustion, fuel and oxidizer are mixed at the molecular level prior to ignition. It is assumed that combustion takes place in a thin flame sheet. The combustion reactions take place and the flame front moves from premixed reactants to products. For subsonic flows, the overall rate of propagation of the flame is determined by both the laminar flame speed and the turbulent eddies. The laminar flame speed is determined by the rate that species and heat diffuse upstream into the reactants and burn.

The flame front propagation is modelled by solving a transport equation for the density-weighted mean reaction progress variable c:

$$\frac{\partial}{\partial t}(\rho c) + \nabla \cdot (\rho \vec{v} c) = \nabla \cdot \left(\frac{\mu_t}{Sc_t} \nabla c \right) + \rho S_c \tag{8.1}$$

The progress variable is defined as a normalized sum of the product species, therefore $c = 0$ for unburnt mixture, and $c = 1$ for products. The value of c is defined as a boundary condition at all flow inlets. The mean reaction rate is modelled as [32]:

$$\rho S_c = \rho_u S_T \left| \nabla c \right| \tag{8.2}$$

S_T is computed using a model for wrinkled flames [32]:

$$S_T = A_z \cdot (u')^{3/4} S_L^{1/2} \alpha^{-1/4} l_0^{1/4} = A_z u' Da^{1/4} \tag{8.3}$$

The integral length scale l_0 is modeled using the equation:

$$l_0 = C_D \frac{(u')^3}{\epsilon} \tag{8.4}$$

The recommended value $A_z = 0.52$ and coefficient $C_D = 0.37$ have been used [32].

A non-adiabatic premixed combustion model is considered. The energy transport equation is solved in order to account for any heat losses or gains within the system. These losses/gains may include heat sources due to chemical reaction or radiation heat losses.

The shear-stress transport (SST) $k - \omega$ model has been used for modelling turbulence. It has feature that gives the SST $k - \omega$ model an advantage in terms of performance over both the standard $k - \omega$ model and the standard $k - \epsilon$ model. Other modifications include the addition of a cross-diffusion term in the ω equation and a blending function to ensure that the model equations behave appropriately in both the near-wall and far-field zones [180].

8.3 Turbulent burning velocity correlations

Empirical approximations of turbulent burning rate comprises an important part of turbulent combustion research. There are a number of correlations of turbulent

burning rate with Da and Ka numbers available in the literature [31]. A number of researchers correlate S_T with Karlovitz stretch factor K and Le number using the equation [28, 55]:

$$S_T = Bq'(KLe)^D \tag{8.5}$$

where q' is the turbulence intensity, and B and D model coefficients.

Another equation used in numerical calculations, proposed by Zimont et al. [32] correlates Da number with S_T:

$$S_T = 0.52q'Da^{0.25} \tag{8.6}$$

where 0.52 and 0.25 are model coefficients.

It should be mentioned that there are some debates in the combustion community concerning the optimal way to correlate turbulent burning rate, the most appropriate combination of non dimensional numbers and their calculation method.

Karlovitz and Reynolds numbers are two non-dimensional numbers, which may be calculated in different ways. Reynolds number based on integral length scale is calculated using equation:

$$Re_l = \frac{q'l_0}{\nu} \tag{8.7}$$

Re_l is highly dependent on temperature. Peters claims [97] that properties such as specific heat capacity, c_p and thermal conductivity λ should be calculated at the inner layer temperature T_0. This also holds for Reynolds number. Peters suggested to calculate Reynolds number using the equation [97]:

$$Re_l = \frac{q'l_0}{S_L\delta_L} \tag{8.8}$$

where ν is replaced by $S_L\delta_L$. Re_l calculated using actual gas mixture viscosity at inner layer temperature (found to be 1400 K - 1600 K in this work) is very close to Re_l calculated with assumption $\nu = S_L\delta_L$.

Veynante and Vervich [124] reported that the relation between thermal flame thickness δ_L, the laminar unstretched flame speed S_L and the kinematic viscosity of reactants ν is $\delta_L S_L/\nu \approx 4$, which means that the Reynolds number differs by a

factor of 4. The stretch factor, which is defined as the "ratio of chemical to turbulent lifetimes" [29] is calculated from the equation [127]:

$$K = \frac{q'}{l_\lambda}\frac{\delta_L}{S_L} \tag{8.9}$$

Obviously, if Taylor's length scale is calculated using $l_\lambda = l_0(15/Re_l)^{1/2}$ [29], due to the decrease of Re_l, l_λ will increase. Therefore the stretch factor will also change.

Another ambiguity lies in the use of the Karlovitz number Ka and Karlovitz stretch factor K. Although these variables are closely related, the main difference concerns the length scale used to calculate these quantities. The Kolmogorov length scale, accounting for the change of thermal diffusivity due to temperature effect, is used to define Ka number [77], whilst Taylor's length scale is used for the determination of Karlovitz stretch factor (equation 8.9). It has been proposed to use the following equation to calculate Ka number [77]:

$$Ka = \left(\frac{q'}{S_L}\right)^{1.5}\left(\frac{S_L l_0}{\alpha}\right)^{-0.5}\left(\frac{(T_P + T_R)/2}{300}\right)^{0.5} \tag{8.10}$$

Here α is thermal diffusivity of nitrogen at 300 K, which is 0.15 cm^2/s. The magnitude of the stretch factor, K, is lower than Karlovitz number, Ka, calculated for our conditions.

In order to be consistent Re_l was calculated using equation 8.8 and K stretch factor defined in equation 8.9 were used.

8.3.1 Methane and methane-carbon dioxide mixture flames

Turbulent burning velocities of methane and methane carbon dioxide mixtures have been calculated at 3 bar and 7 bar pressures, and 473 K, 573 K and 673 K inlet air temperatures. The comparison of the experimental data with the Zimont's model [32] is presented in Fig. 8.1.

The solid line in the graph represents Zimont's model $S_T = 0.52q'Da^{0.25}$. Circles represent methane data, triangles represent 85% methane - 15% carbon dioxide data and squares represent 70% methane - 30% carbon dioxide data. It may be observed from this graph that Zimont's model fits experimental data well. Non-parametric hypothesis testing has shown that the hypothesis, that model and experimental

data sets are identical, can not be rejected. Therefore it is tentatively assumed that Zimont's model fits the experimental burning velocity data adequately.

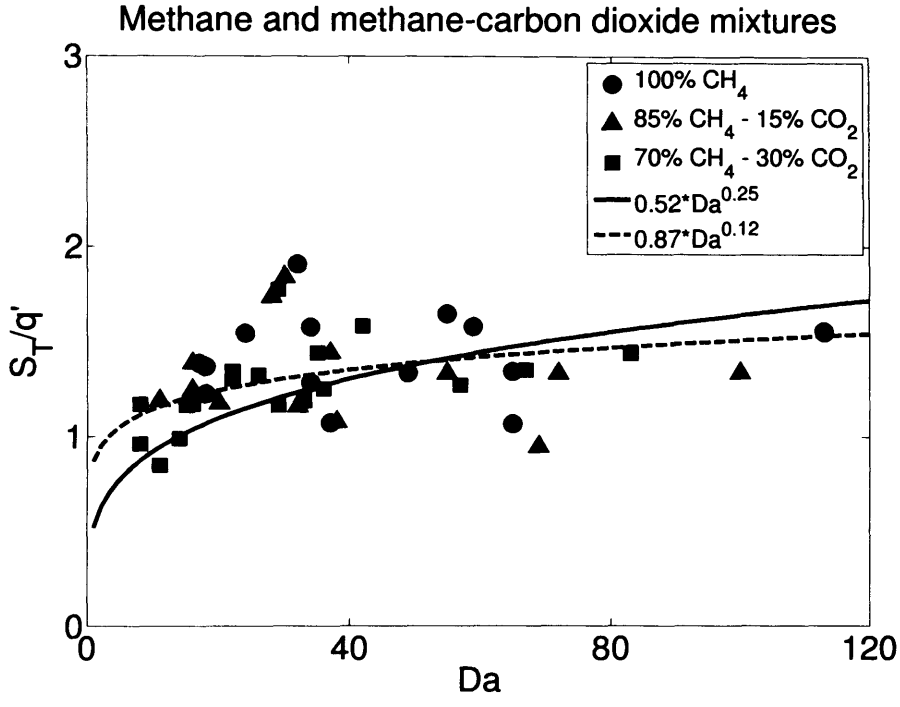

Figure 8.1: *Comparison of experimental results with Zimont's model.*

In order to estimate the relation of experimental data with Damköhler number a regression analysis has been carried out. A new correlation equation $S_T = 0.87q'Da^{0.12}$ (broken line in Fig. 8.1). has been found for methane and methane - carbon dioxide mixtures for all tested pressure and temperature conditions.

The Zimont's model is widely used for turbulent premixed flame modelling in commercial codes and the correlation of S_T/q' versus KLe or $KaLe$ is used to represent turbulent burning velocity evolution, which accounts for the effect of flame stretch. Bradley et al. [28] have proposed an approximate correlation for the turbulent burning velocity, $S_T = 0.88q'(KLe)^{-0.3}$. The correlation is considered valid for $0.02 \leq KLe \leq 1$. Later, a modified correlation of 1650 measurements of S_T was presented, $S_T = 1.01q'(KLe)^{-0.3}$ [29]. Regression analysis has been performed to find the optimal correlation for our experimental data. Gas mixtures of 100% methane and 70% methane - 30% carbon dioxide turbulent burning velocity values from different experiment condition have been used and a general correlation has

been found, $S_T = 0.91q'(KLe)^{-0.15}$. In Fig. 8.2 the correlations from Bradley et al. [28, 29] and the correlation obtained from the current data are presented.

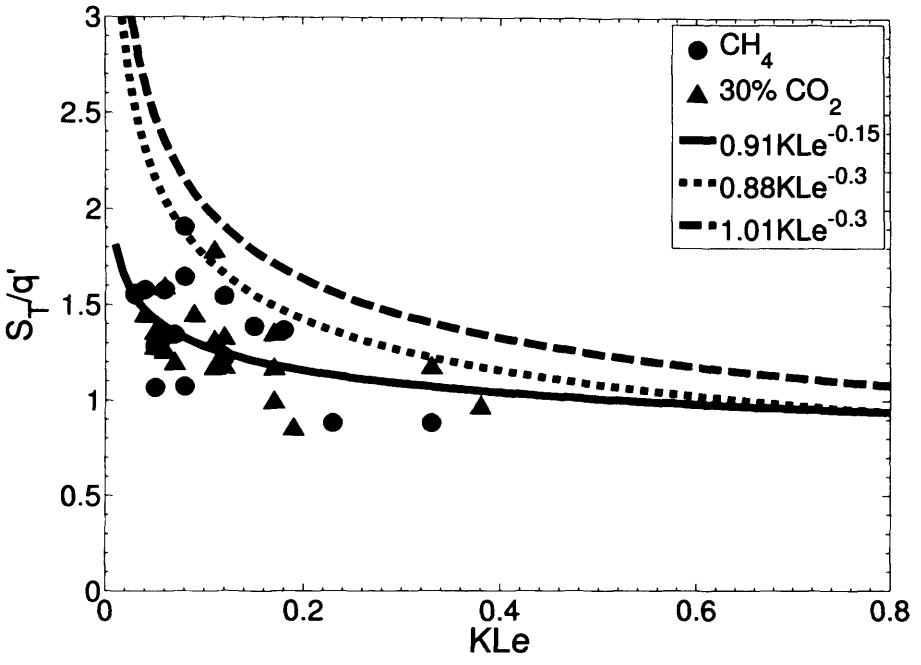

Figure 8.2: *S_T vs KLe for our experiments and correlation curves from Bradley et al. [28, 29]*

It should be noted that this attempt to correlate the current data assumes - in the spirit of Zimont - that variation in pressure, temperature and fuel mixtures, can be sufficiently represented by such a universal correlation. Hence, some data scatter is observed in the graph, which may be expected considering the broad range of experimental conditions studied. The new power factor -0.15, obtained from regression analysis indicates that at elevated pressure and temperature conditions the non dimensional number KLe has less effect on S_T. In our tests the Lewis number of the gases is close to unity, therefore it implies that K can replace KLe in the correlation. Lipatnikov and Chomiak in their review paper [31] presented S_T and Ka correlations. Different power factors, processed from various experimental data for Ka, have been reported. Although they have used Ka instead of K the trends are the same. The power factor varied from -0.23 to -0.41. From these observations it can be concluded that it is difficult to obtain one equation for all purposes as Ka

or K does not estimate pressure effects [31]. Therefore substantially more data and analysis are needed to investigate turbulent combustion at elevated pressure and temperature.

8.3.2 Methane-hydrogen mixture flames

Methane-hydrogen experimental dataset and the Zimont's model correlation $S_T = 0.52q'Da^{0.25}$ [32] are presented in Fig. 8.3.

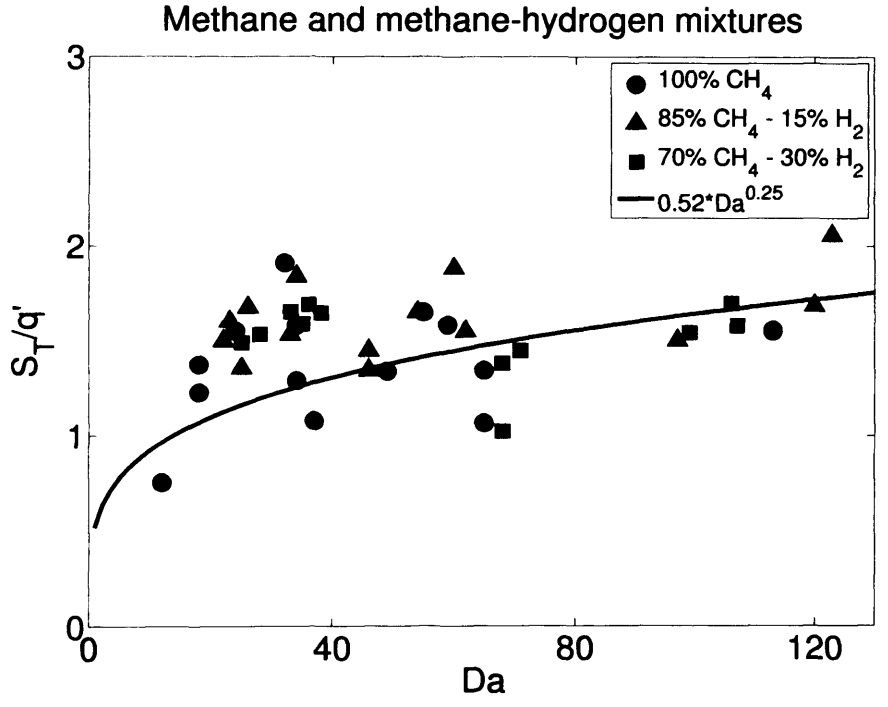

Figure 8.3: *Experimental data and* $S_T = 0.52q'(Da)^{0.25}$ *model plot.* ○ *- 100% methane;* △ *- 85% methane - 15% hydrogen;* □ *- 70% methane - 30% hydrogen.*

The experimental data fits the model surface reasonably well. These experiment results have been obtained under different conditions for different equivalence ratio ϕ, therefore model coefficients have not been calculated. Non-parametric hypothesis testing has shown that the hypothesis, that model and experimental data sets are identical, can not be rejected. This statistically justifies the agreement between data and prediction.

8.4 Swirl burner experiments with CH_4-CO_2 mixtures

8.4.1 Methane flame stability limits at atmospheric conditions

Flame stability depends on the operating pressure, initial temperature, equivalence ratio and total mass flow rate of the premixed mixture [181]. The experiments and modelling were performed for premixed methane flames at atmospheric conditions with the purpose of measuring the stability limits of the flame for a particular generic burner. The behaviour of swirl burner is complex, with a rich literature in this area [63, 64, 66, 67, 70–72, 74]. In the context of flashback for this generic swirl burner (geometric swirl number 1.47) the size and shape of the Central Reverse Flow Zone (CRZ) is crucial as in high velocity flows the flame initially stabilizes on the CRZ boundary. Under isothermal conditions for this swirl number a bulbous CRZ forms just past the exhaust and the fuel injector. This CRZ then typically forms an extension to its base which consists of a long columnar structure which passes into the burner, often over the fuel injector (unless it is very large) to the backplate. Premixed combustion especially can virtually eliminate this CRZ as the increased axial flux of angular momentum reduces the effective swirl number to below the critical value for vortex breakdown and CRZ formation of 0.5 (axial flux of angular momentum scarcely alters). Maximum effects occur around equivalence ratios $\phi \approx 1$ at maximum heat release. As the equivalence ratio is weakened vortex breakdown can occur, a CRZ forms, which gradually increases in strength so that at very weak mixtures the structure tends to that of the isothermal state. The problem this brings is that for lean combustion the flame burns not only in the exhaust but on the CRZ boundary surrounding the fuel injector; this is illustrated later. Here we consider the flashback of these flames radially to the tangential inlets and beyond. This condition represents the system behaviour both with and without the fuel injector. Other work has described techniques to eliminate this CRZ extension over the fuel injector [70]. In this system, flashback was more pronounced for lean combustion than for rich.

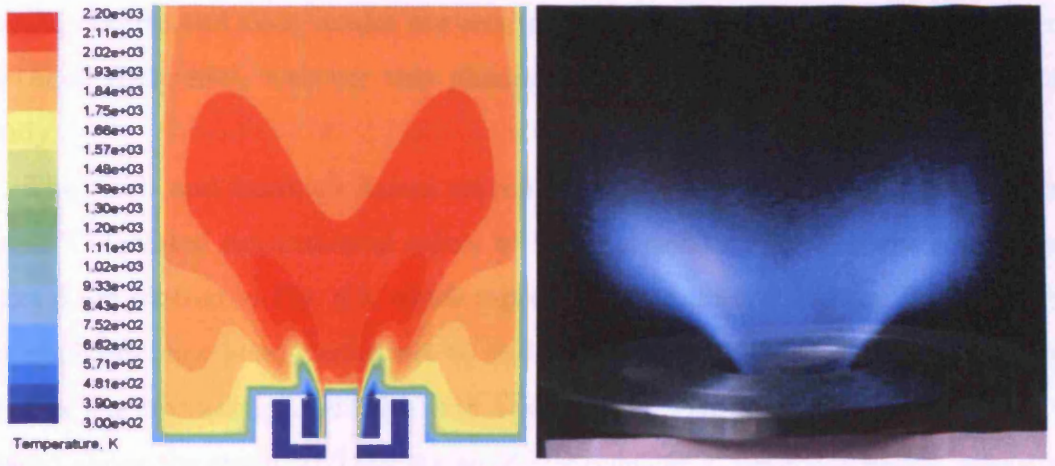

Figure 8.4: *Partial flashback of methane flame in model and experiments,* $\dot{m} = 2.74$ *g/s,* $\phi = 0.92$

As seen in Fig. 8.4 and discussed above, the CRZ and flame front can extend completely over the fuel injector to the baseplate due to the extension of the CRZ over the fuel injector at weak equivalence ratios. This is undesirable and is a precursor to full flashback . The phenomena is often referred to as Combustion Induced Vortex Breakdown (CIVB). Techniques for elimination are discussed elsewhere [72].

Full flashback is shown in Fig. 8.5. Here the flame has flashback to beyond the tangential inlets, and is operating as a cyclone combustor [64, 65], undesirably overheating the main components. It is seen in Fig. 8.5 that the temperature of the injector increases significantly due to the thermal radiation and convection.

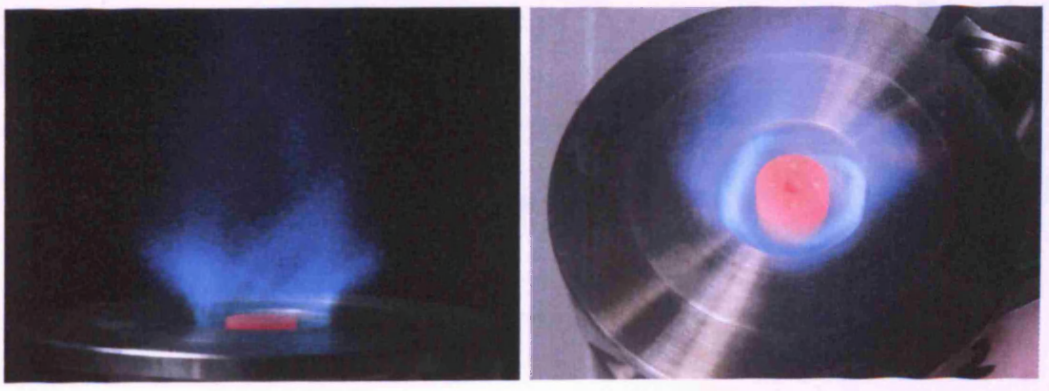

Figure 8.5: *Methane flame flashback,* $\dot{m} = 1.485$ *g/s,* $\phi = 0.79$

Swirl burner is manufactured using high grade stainless steel, which contains nickel, chromium and molybdenum. It has been reported that metals such as: nickel,

cobalt, copper and their oxides are very active in the total catalytical oxidation of methane [182, 183], however this phenomenon has not been investigated in this study.

The stable and flashback flames are reported under various air and fuels mass flow rates. Calculated experimental values of total mass flow rate $\dot{m}$ vs the equivalence ratio ϕ are plotted in Fig. 8.6, which represents the burner flame stability map. An interpolation has been performed to define the flame stability limits. The curve divides the operating conditions into two regions. The region of stable flames is placed above the curve, and the region of unstable flame, flashback region, is located under the curve. The mass flow rate of fuel mixture was increased and reached its peak at $\phi = 0.7$. For rich mixtures the fuel mass flow rate was reduced again, though here flashback was not observed.

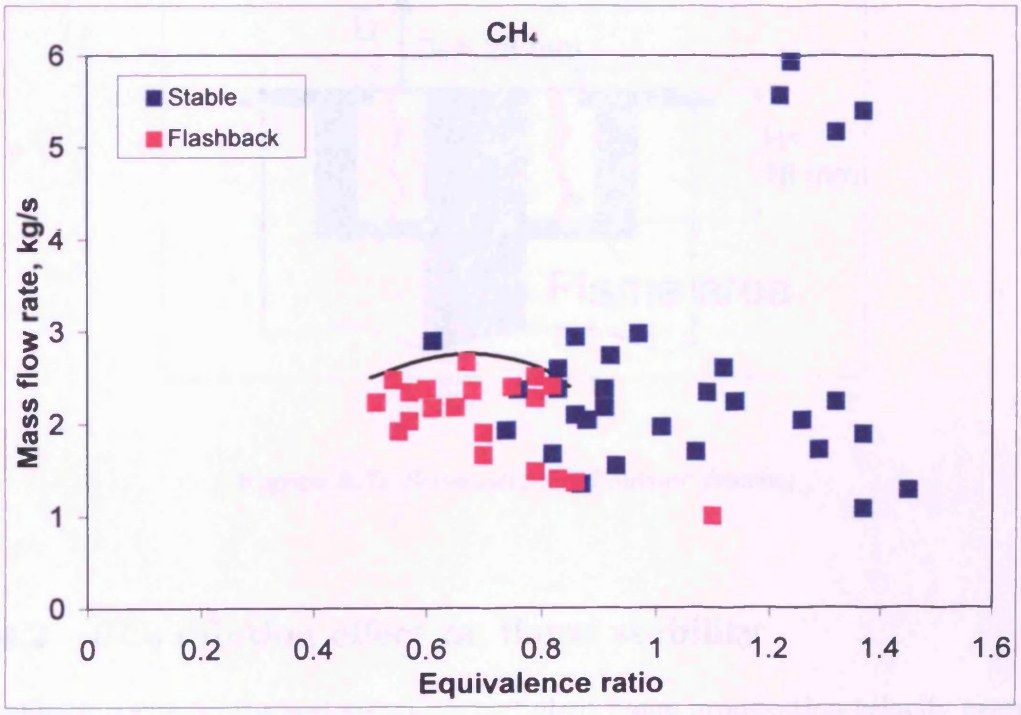

Figure 8.6: *Flashback velocities of methane flame*

Another problem that was observed during the experiments was flame blow off. It was difficult to hold the flame with higher mass flow rates. One possible solutions, in order to keep the flame within blow off limits, is to inject small quantities of diffusive fuel directly into the central recirculation zone, thus stabilizing the system,

as implemented in practical gas turbine combustors [67]. Another technique, which improves the CH_4 stability is to add H_2 [19, 73], however this does then worsen flame flashback susceptibility due to increase of S_T.

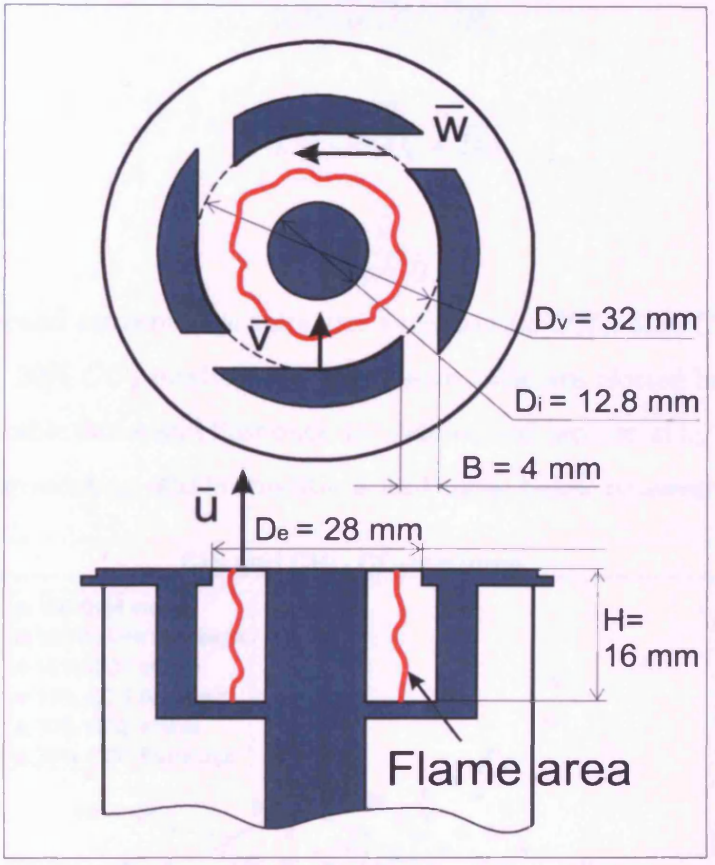

Figure 8.7: *Schematic swirl burner drawing*

8.4.2 CO_2 dilution effect on flame stability

Flashback occurs in the regions where turbulent flame propagation velocity exceeds the gas mixture supply streamlines. Therefore the flashback could be avoided if the flame speed and gas velocity could be kept in balance just above the burner exit. In the swirl burner the gas mixture flow velocity could be expressed as the components of axial u, radial v and tangential w velocities. These velocity vectors are presented in the schematic burner drawing Fig. 8.7. Based on the experimental data u, v and w were calculated from the known mass flow rate and gas mixture density. Axial, radial and tangential velocity in the inlets are represented by the following three

equations, which represent the average axial velocity u, the average radial velocity v at the flame front location and the average tangential velocity w:

$$u = \frac{\dot{m}}{0.25\pi\rho(D_e^2 - D_i^2)} \tag{8.11}$$

$$v = \frac{\dot{m}}{0.5\pi\rho H(D_v + D_i)} \tag{8.12}$$

$$w = \frac{\dot{m}}{4\rho HB} \tag{8.13}$$

The radial v and tangential w velocities variation for CH_4, 85% CH_4 - 15% CO_2 and 70% CH_4 - 30% CO_2 mixtures vs equivalence ratio are plotted in Fig. 8.8. The two regions of stable flame and flashback are defined and separated by the lines, with values above representing stable conditions and those below representing flashback.

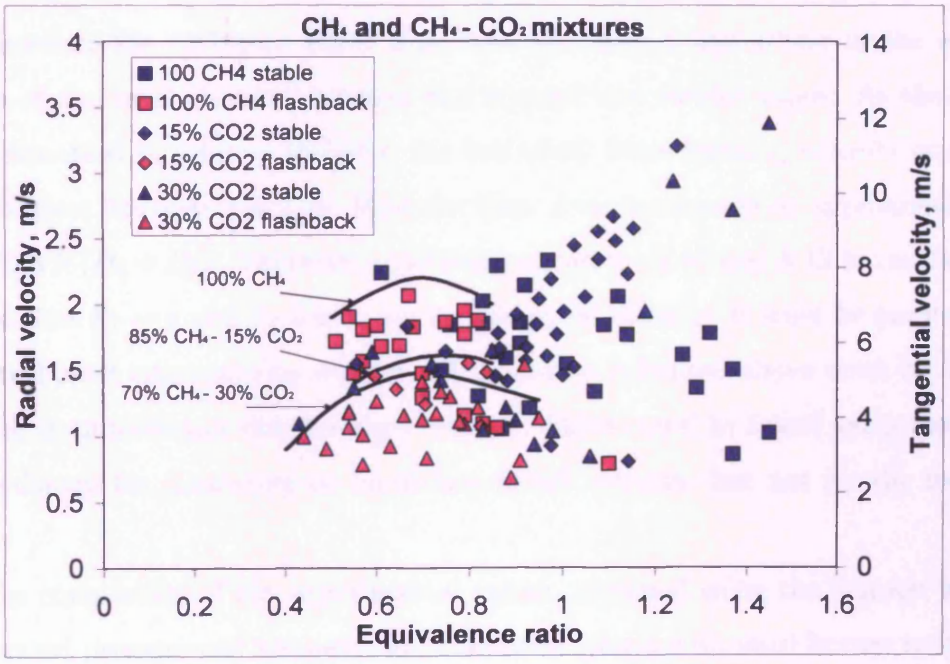

Figure 8.8: *Flashback velocities of methane and methane - carbon dioxide flames.*

Testing all mixtures, both stable and flashback flames were observed. For both mixtures 85%CH_4 - 15% CO_2 and 70% CH_4 - 30% CO_2 under certain conditions the CRZ and flame extended over the fuel injector as in the case of methane flames. The highest velocity levels for flashback were observed at $\phi = 0.7 - 0.8$ for all

mixtures. In general it was observed that the velocities, at which flashback occurs, decreased with increasing CO_2 amount in methane. CO_2 addition decreases the burning velocity [37, 41, 42], therefore lower velocities are required to stabilise the flame and stability limits are improved.

8.4.3 Comparison of test results from generic swirl burner and Bunsen burner with $CH_4 - CO_2$ mixtures

After the first flashback, the flame stabilised in the region around the injector as seen in Fig. 8.5 and in the schematical drawing Fig. 8.7. In a few tests with pure methane at very low mass flow rates secondary flashback was observed, where the flame propagated through the swirler slots upstream. However when testing methane - carbon dioxide mixtures, this phenomena did not occur. When the flame stabilised around the injector, the turbulent flame speed was balanced by the gas flow velocity, therefore the turbulent flame front was established somewhere in the middle region of the swirl chamber between the injector and swirler vanes. As the flame front remained in relative stability, the turbulent flame burning velocity could be derived from the equation 2.43. Here the flame front area could be approximated as $A = 0.5\pi H(D_v + D_i)$. Therefore combining equations 2.43 and 8.12 it can be concluded that $S_T = v$ and S_T and v can be compared directly. It must be pointed out that turbulent consumption velocity calculated as indicated above must be distinguished from turbulent displacement velocity, which could be found using the same methodology for measuring or modelling radial velocity, but not by the method above.

The comparison of our experimental values, obtained using the Bunsen burner at elevated pressure and temperature conditions (chapter 6), swirl burner radial velocity approximations and numerical S_T computations are represented in Fig. 8.9. The S_T and v have been normalised by a normalisation factor as explained elsewhere [41]. The coding "3-473" represents 3 bar and 473 K preheated unburned gas temperature conditions, and "15CO2" represents 85%CH_4 - 15% CO_2 gas mixture in the legend key. We have not been able to stabilise very lean methane and methane - carbon dioxide mixtures in the Bunsen burner, therefore only values close to the stoichiometric conditions are presented. For numerical calculations S_T computations

via Fluent at the burner exit position have been taken, where the progress variable $c = 0.5$.

Considerable difference of S_T and v is observed in Fig. 8.9 at $\phi = 0.7 - 0.8$. One obvious contributory explanation is that very different flame structures are compared, therefore some incompatibility is expected. Bunsen burner flames belong to "envelope" category flames and swirl burner flames considered here would fall into the "unattached" or "flat" flame category, which have different flame wrinkling processes [77, 91]. Another important consideration is the uncertainty in deriving the flame front area for swirl burner. It was observed that the flame front is corrugated, but thin, and the exact position could not be easily identified. The assumption was to take the flame front position as being located half way between the fuel injector radius and the burner exit radius (Fig. 8.7), this being based purely from visual interpretation. As an example, increasing the flame front diameter by 20% the S_T would decrease by 17%. Hence, more accurate flame front identification methods should be sought for future work.

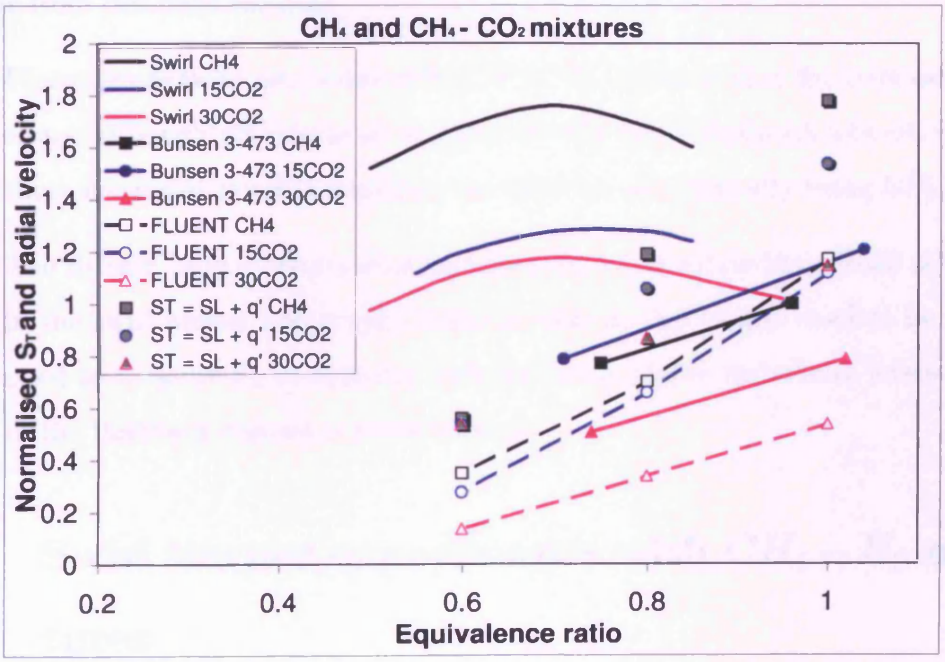

Figure 8.9: *Comparison of experimental values from Bunsen burner tests at elevated temperature and pressure and swirl burner tests at atmospheric conditions.*

It has already been noted that the definition for the turbulence characteristics for

the Bunsen burner experiments have some uncertainties in themselves. The relative turbulence intensity for Bunsen burner isothermal flows at elevated temperature and pressure has been found to be around 15-20% [41]. For the swirl burner, as no measurements have been possible to date, the turbulence kinetic energy has been computed using CFD at isothermal conditions in the middle of the burner, where the assumed flame front is located. The q' calculated from the turbulence kinetic energy has been found to be in the region of 0.6 - 1.83 m/s for CH_4 and CH_4-CO_2 mixtures. Therefore applying simple approximation $S_T = S_L + q'$, developed from Damköhler theory, the values of S_T can be readily calculated. The grey marks in Fig. 8.9 represent these normalised S_T values. Simplified theory underpredicts turbulent burning velocity for lean mixtures, but the results are much closer to experimental values at equivalence ratio between 0.8 and 0.9.

Numerical S_T computation via CFD, evaluated at the burner exit under the same conditions as the swirl burner experiments, where the progress variable $c = 0.5$, show lower values than the radial velocity results, Fig. 8.9. Several interesting conclusions emerge from this data analysis:

- Fluent predictions are better with CH_4-CO_2 mixtures than for pure methane alone, although all results show substantially lower flashback velocities than those measured experimentally in the swirl burner, typically being 50% lower.
- The Bunsen burner results show significantly lower values than those obtained in the swirl burner and maybe indicate that methodologies need to be developed to measure S_T in systems with the much higher turbulence levels found in the flashback regions of swirl burners.

8.5 Swirl burner experiments with $CH_4 - H_2$ mixtures

8.5.1 H_2 dilution effect on flame stability and flashback

Figure 8.10 shows results with 85% methane and 15% hydrogen. Clearly the CRZ and flame front extends over the fuel injector to the baseplate due to the extension of the CRZ over the fuel injector at weak equivalence ratios. This is undesirable and

is a precursor to full flashback. Hydrogen addition is well known increase the flame stability by reducing flame blow off [19, 73], however this does then worsen flame flashback susceptibility due to increase of S_L and S_T.

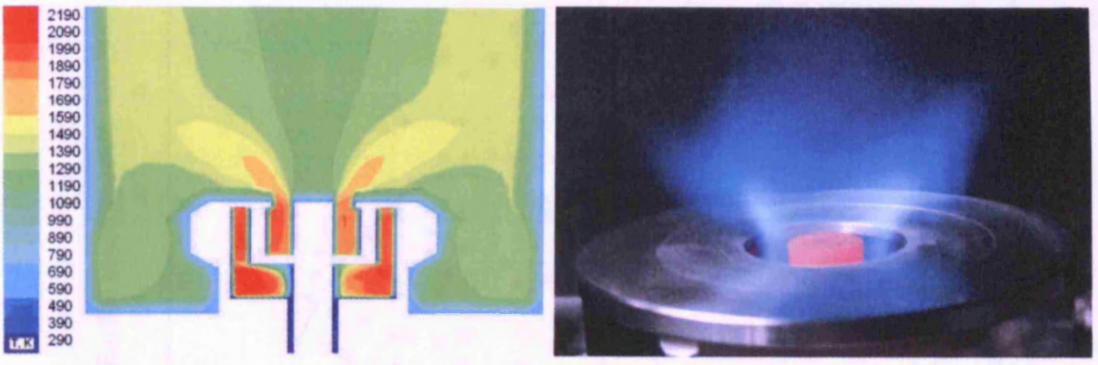

(a) (b)

Figure 8.10: *Flashback of 85% methane - 15% hydrogen mixture in model (a) and experiments (b),* $\dot{m} = 2.46\ g/s$, $\phi = 0.82$.

A similiar methodology for S_T analysis in the swirl burner is used for methane-hydrogen mixtures as for methane-carbon dioxide mixtures, presented in previous sections. Derivation of axial u, radial v and tangential w velocities is performed using the equations 8.11, 8.12, 8.13. Thus radial velocities of 85% CH_4 - 15% H_2 and 70% CH_4 - 30% H_2 vs ϕ are plotted in Fig. 8.11. The two regions of stable flame and flashback are defined and separated, with values above representing stable conditions and those below representing flashback.

A wide range of flows and equivalence ratios were investigated with mixtures, both stable and flashback flames being observed. For both mixtures 85%CH_4 - 15% H_2 and 70% CH_4 - 30% H_2 under certain conditions the CRZ and flame extended over the fuel injector. The highest velocity levels for flashback were observed at $\phi = 0.8 - 0.9$ for all mixtures. In general it was observed that the velocities, at which flashback occurs, increased with increasing H_2 concentration in methane. H_2 addition increases the laminar and turbulent burning burning velocity [22, 41], therefore higher velocities are required to stabilise the flame and avoid flashback.

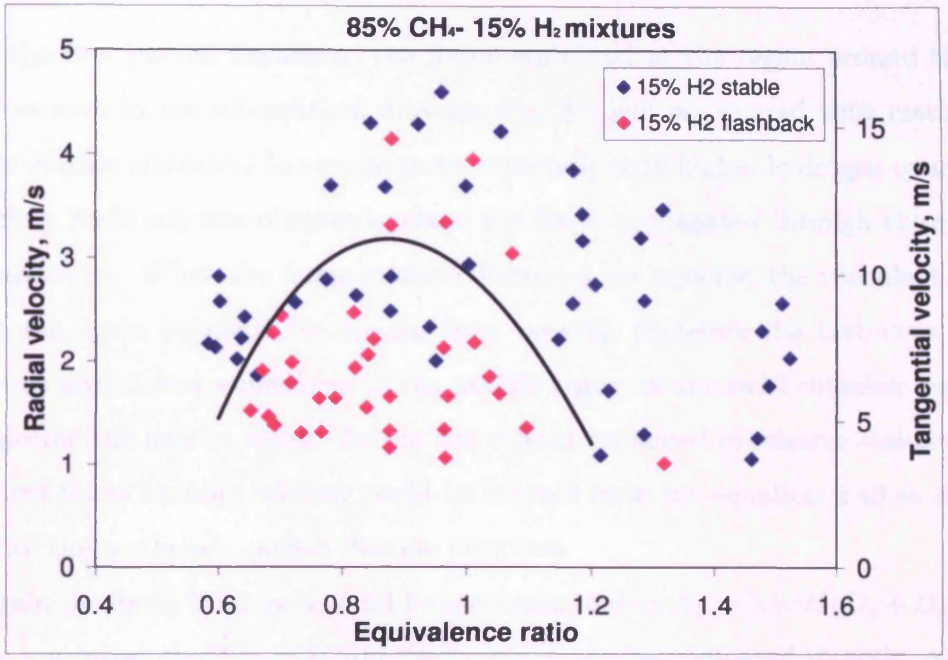

(a) 85% methane - 15% hydrogen mixture

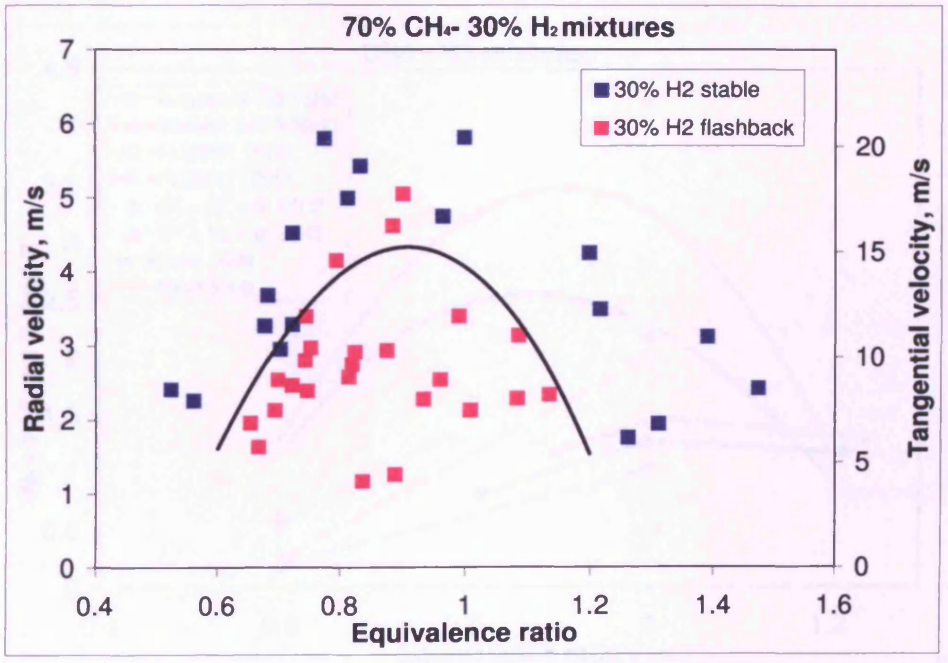

(b) 70% methane - 30% hydrogen mixture

Figure 8.11: *Flashback radial velocities in generic swirl burner.*

8.5.2 Comparison of test results from generic swirl burner and Bunsen burner with $CH_4 - H_2$ mixtures

After the first partial flashback, the flame stabilised in the region around the injector as seen in the schematical drawing Fig. 8.7 and as occured with methane - carbon dioxide mixtures. In several tests, especially with higher hydrogen quantities secondary flashback was observed, where the flame propagated through the swirler slots upstream. When the flame stabilised around the injector, the turbulent flame speed was again balanced by the gas flow velocity, therefore the turbulent flame front was established somewhere in the middle region of the swirl chamber between the injector and swirler vanes. As the flame front remained in relative stability, the turbulent flame burning velocity could be derived from the equation 2.43 as carried out with the methane - carbon dioxide mixtures.

Again the flame front area could be approximated as $A_f = 0.5\pi H(D_v + D_i)$, and it was concluded that $S_T \approx v$ and these values can be compared directly, as with methane - carbon dioxide mixtures.

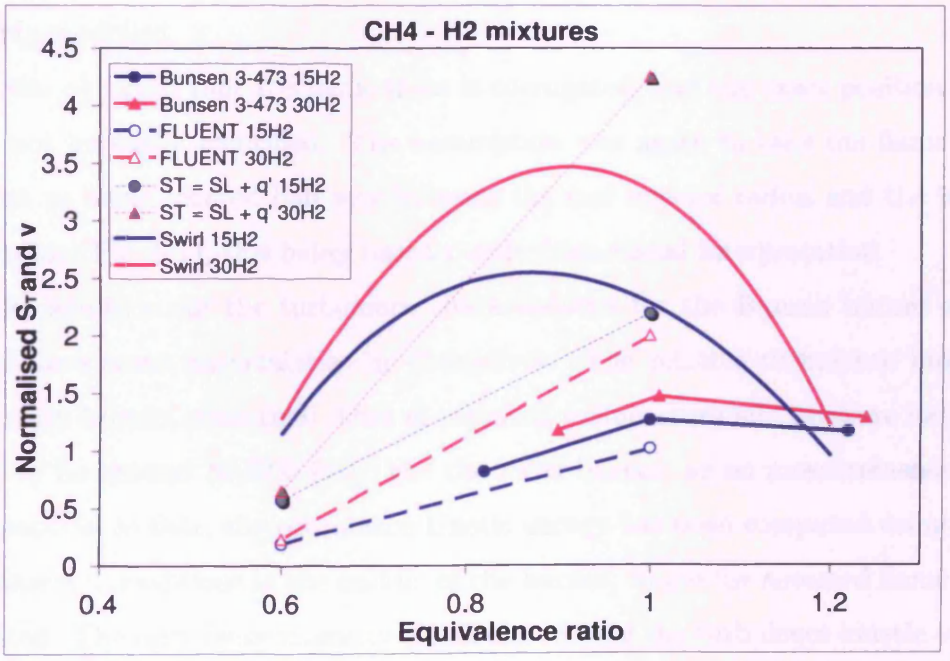

Figure 8.12: *Comparison of experimental values from experiments of generic swirl burner tests at atmospheric conditions, Bunsen burner experiments at elevated temperature and pressure, Fluent computations, and turbulent combustion model* $S_T = S_L + u'$.

The comparison of experimental values, obtained using the Bunsen burner at elevated pressure and temperature conditions [41], generic swirl burner radial velocity approximations and numerical S_T computations from Fluent are represented in Fig. 8.12. The S_T and v have been normalised by a factor as explained in chapter 6. The coding is as before "3-473" represents 3 bar and 473 K preheated unburned gas temperature conditions, and "15H2" represents $85\%CH_4 - 15\%H_2$ gas mixture, and "30H2" represents $70\%CH_4 - 30\%H_2$ gas mixture in the legend key. For numerical S_T computations the position at the burner exit have been taken, where the progress variable $c = 0.5$.

Considerable difference between S_T obtained from Bunsen burner and v from swirl burner is observed in Fig. 8.12 at $\phi = 0.8 - 1.1$. One obvious contributory explanation is that very different flame structures are compared, therefore some incompatibility is expected. Bunsen burner flames belong to "envelope" category flames and have different flame wrinkling process than swirl flames [77, 91]. Another important considerations are the uncertainty in deriving the flame front area for the swirl burner and the derivation of turbulence intensity, which has not been measured, but only modelled.

It was observed that the flame front is corrugated, and the exact position could again not be easily identified. The assumption was again to take the flame front position as being located half way between the fuel injector radius and the burner exit radius (Fig. 8.7), this being based purely from visual interpretation.

The definition for the turbulence characteristics for the Bunsen burner experiments have some uncertainties in themselves. The relative turbulence intensity for Bunsen burner isothermal flows at elevated temperature and pressure has been found to be around 15-20% [41]. For the swirl burner, as no measurements have been possible to date, the turbulence kinetic energy has been computed using CFD at isothermal conditions in the middle of the burner, where the assumed flame front is located. The turbulence intensity q' calculated from the turbulence kinetic energy has been found to be in the region of 0.6 - 4.83 m/s for CH_4-H_2 mixtures. Therefore applying simple approximation $S_T = S_L + q'$, developed from Damköhler theory, the values of S_T can be readily calculated. The grey marks and dotted lines in Fig. 8.12 represent these normalised S_T values. It is seen that this simplified theory underpre-

dicts turbulent burning velocity for lean mixtures, but the results are much closer to the experimental values at equivalence ratio between 0.9 and 1.0, although for $70\%CH_4 - 30\%H_2$ the predicted S_T is higher than radial velocity v. Presumably this is due to the very high turbulence kinetic energy level modelled by Fluent. Similar results have been found for methane - carbon dioxide mixtures [161].

Numerical S_T computation via CFD, evaluated at the burner exit under the same conditions as the experiments, where the progress variable $c = 0.5$, show much lower values than the radial velocity results, Fig. 8.12. It appears that Fluent model does not predict burning velocities particularly well for this swirl burner and fuel mixtures, although for Bunsen burner the model predictions are reasonably accurate [41, 161].

3. An attempt has been made to correlate the flashback and turbulent burning velocity data. Uncertainties have been emphasised and discussed. The differences in results found are likely to arise due to the following primary causes: the method used to derive flame front position, turbulent flow characteristics, flame regime, unburnt gas temperature. Modifications are needed to the Bunsen type burner to produce flame conditions at flashback closer to those pertaining in swirl burners.

8.6 Conclusion

The investigation of methane, methane-carbon dioxide and methane-hydrogen mixtures at atmospheric conditions using the generic swirl burner have been performed. Different research methods, using Bunsen and swirl burners, have been used to investigate the influence of CO_2 and H_2 addition to methane on fundamental combustion characteristics in turbulent swirling flames.

1. The correlations with Damköhler number of methane - carbon dioxide mixtures at 473 K, 573 K, 673 K temperature and 3 bar and 7 bar pressure, $S_T = 0.87q'Da^{0.12}$, has been found and compared with Zimont's model. Lower power factors (0.12) in our correlation has been observed in comparison with 0.25 for Zimont's model. A possible explanation of that is the difference in experimental conditions, i.e. different pressure, temperature and fuel composition.

2. The correlation with Karlovitz stretch factor of methane - carbon dioxide mixtures at 473 K, 573 K, 673 K temperature and 3 bar and 7 bar pressure, $S_T = 0.91q'(KLe)^{-0.15}$, has been found. Again through regression analysis, a slightly higher power factor of -0.15 has been found in comparison with the findings of other researchers [31], which is likely to be related to the difference in operating conditions.

3. Turbulent burning velocity model $S_T = 0.52q'Da^{0.25}$ [32] has been used to compare with methane - hydrogen experimental data at 473 K, 573 K, 673 K temperature and 3 bar and 7 bar pressure. Statistical analysis has shown the the model fits the experimental data reasonably well.

4. A generic swirl burner has been developed and used to test flame stability and flashback limits. The experiment results have shown that CO_2 addition reduces the flame flashback possibility primarily because of the lower burning velocities of methane - carbon dioxide mixtures. H_2 addition increases the flame flashback possibility primarily because of the increase in burning velocities of methane - hydrogen mixtures.

5. A first attempt has been made to correlate the flashback and turbulent burning rate data, as fundamentally the two processes must be related. Uncertainties have been emphasised and discussed. The differences in results are likely to arise due to the following primary causes: the method used to derive flame front position, turbulent flow characteristics, flame regime, unburnt gas temperature. Modifications are needed to the Bunsen type burner to produce flame conditions at flashback closer to those pertaining in swirl burners.

CO_2 and H_2 have clearly significant effect on methane flames, however due to the lack of experimental data at non-atmospheric conditions for premixed turbulent flames it is not easy to predict the behaviour of these flames using commercial models.

Chapter 9

Analysis of turbulent flame structure at elevated temperature and pressure

Experimental premixed turbulent combustion research data are of considerable practical importance, as it provides useful information, which could be used for validation of turbulent combustion models or as input parameters. The closures of chemical source term in different models are of great importance and these models rely ultimately on experimental research [76]. Flame surface density Σ, turbulent flame thickness δ_T and other flame structure quantities are important parameters in numerical investigation and modeling. Hence, it is desirable to create and record the database of these values for each flame category [77]. However, quality experimental data for model development and validation is not easily attainable, particularly under elevated ambient conditions.

In this chapter the investigation of the these parameters for 100% methane, 85% methane - 15% hydrogen and 70% methane - 30% hydrogen flames, tested over a range of pressures, temperatures and equivalence ratios, is reported. The Bray-Moss-Libby coefficient has been found and presented. The stretch factor I_0, using equation 1.5 is calculated, and the correlations with S_T/S_L are plotted.

The experiments were conducted in the HPOC rig. Detailed description of experiment rig and methods used is presented in chapter 3 and 4. Averaged flame image processing method was used to process and analyse the turbulent flame structures. Laminar flame speed S_L has been calculated using Chemkin-Pro software and the laminar flame thickness δ_L, has been calculated as described in chapter 5. Density,

viscosity, mass diffusion coefficients and thermal conductivity of the combustible mixture at the required temperature and pressure were calculated using polynomial fit coefficients available within Chemkin database or taken from the reference tables.

All experiment conditions for each fuel have been coded using 6 (for methane) and 7 (for methane - hydrogen mixtures) alpha-numerical code. For instance in the code "C43096" the first symbol "C" represents 100% methane-air mixture, second "4" stands for 473 K temperature, third symbol "3" means 3 bar pressure and the last three digits "096" mean equivalence ratio $\phi = 0.96$. For 85% methane - 15% hydrogen mixture the first two symbols "1H" have been used. For example "1H67103" represents 85% methane - 15% hydrogen mixture at 673 K, 7 bar conditions, $\phi = 1.03$. For 70% methane - 30% hydrogen mixture the first two symbols "3H" have been used. The list of tested gases, experimental conditions and calculated nondimensional numbers are presented in Table 9.1

9.1 Progress variable and flame brush thickness

Turbulent flame brush thickness is a flame characteristic used in premixed turbulent combustion modelling and facilitates the derivation of spatial profiles of progress variable. It is as important as turbulent flame velocity [31]. There are several methods available to calculate flame brush thickness δ_T from experimental data. Flame brush thickness can be estimated from the density variation using the maximum gradient method: $\delta_T = (\rho_U - \rho_B)/\left|d\rho/dx\right|_{max}$. Gouldin and Miles [116] have used the simpler definition of δ_T, which is equal to the distance along the axis between $\langle c \rangle = 0.1$ and $\langle c \rangle = 0.9$. Lee et al. [82] and Deschamps et al. [78] have defined δ_T as the distance between $\langle c \rangle = 0.05$ and $\langle c \rangle = 0.95$. Shepherd and Cheng [76] defined flame brush thickness by the maximum gradient of $\langle c \rangle$, $\delta_T = 1/(d\langle c \rangle/dz)_{max}$. Although different δ_T definitions have been used, Lipatnikov and Chomiak in their review paper [31] emphasized that spatial profile of the progress variable presented in the dimensionless form, approaches a universal curve corresponding to the error function under a wide range of conditions.

Shepherd [76] and Kostiuk [184] define the flame brush thickness δ_T relationship to the mean progress variable $\langle c \rangle$ using the equation:

Table 9.1: *Experimental conditions and results of 100% methane, 85% methane - 15% hydrogen and 70% methane - 30% hydrogen mixtures.*

Test	T	P	ϕ	S_L	δ_L	u	q'	l_0	Re	Da	K	Le	S_T/S_L
C43118	473	3	1.18	0.52	0.17	4.57	0.796	8	72	32	0.07	1.10	2.90
C43096	473	3	0.96	0.56	0.16	4.52	0.791	8	71	34	0.06	0.94	2.24
C43075	473	3	0.75	0.37	0.21	4.42	0.783	8	81	18	0.12	0.94	2.60
C63114	673	3	1.14	1.16	0.13	10.33	1.477	18	176	113	0.03	1.10	1.99
C63104	673	3	1.04	1.2	0.13	10.25	1.465	18	169	113	0.03	1.10	1.9
C63073	673	3	0.73	0.82	0.16	9.84	1.406	18	193	65	0.05	0.94	1.83
C47120	473	7	1.2	0.32	0.11	4.94	0.83	5	118	18	0.15	1.10	3.57
C47101	473	7	1.01	0.39	0.1	4.95	0.831	5	107	24	0.11	1.10	3.32
C47078	473	7	0.78	0.24	0.13	4.85	0.821	5	132	12	0.26	0.94	2.56
C57116	573	7	1.16	0.55	0.08	7.68	1.122	9	230	55	0.07	1.10	3.34
C57101	573	7	1.01	0.59	0.08	7.38	1.087	9	207	65	0.06	1.10	2.47
C57078	573	7	0.78	0.42	0.1	4.38	0.779	7	130	37	0.08	0.94	1.99
C53118	573	3	1.18	0.79	0.14	7.97	1.158	10	105	49	0.05	1.10	1.96
C53109	573	3	1.09	0.85	0.14	7.22	1.068	10	90	59	0.04	1.10	1.98
C53084	573	3	0.84	0.71	0.16	5.67	0.9	7	55	34	0.05	0.94	1.63
Test	T	P	ϕ	S_L	δ_L	u	q'	l_0	Re	Da	K	Le	S_T/S_L
1H63119	673	3	1.19	1.23	0.12	10.41	1.488	18	181	120	0.03	1.13	2.05
1H63102	673	3	1.02	1.31	0.12	10.82	1.55	18	177	123	0.03	1.13	2.43
1H63082	673	3	0.82	1.08	0.14	10.16	1.452	18	173	97	0.03	0.72	2.03
1H53119	573	3	1.19	0.85	0.13	7.89	1.148	11	114	62	0.04	1.13	2.1
1H53098	573	3	0.98	0.9	0.14	8.48	1.222	11	107	60	0.04	0.72	2.56
1H53081	573	3	0.81	0.71	0.16	7.32	1.079	11	104	46	0.06	0.72	2.04
1H43122	473	3	1.22	0.54	0.17	5.37	0.871	7	66	26	0.08	1.13	2.72
1H43100	473	3	1	0.62	0.15	5.25	0.859	7	65	34	0.06	0.72	2.54
1H43082	473	3	0.82	0.48	0.17	4.16	0.76	7	65	25	0.08	0.72	2.14
1H67122	673	7	1.22	0.81	0.07	11.02	1.58	-	-	-	-	1.13	3.29
1H67103	673	7	1.03	0.94	0.07	13.92	2.069	-	-	-	-	1.13	2.96
1H67079	673	7	0.79	0.69	0.08	10.12	1.446	-	-	-	-	0.72	2.32
1H57121	573	7	1.21	0.55	0.08	8.31	1.2	10	273	54	0.07	1.13	3.63
1H57099	573	7	0.99	0.62	0.07	9.96	1.423	-	-	-	-	0.72	3.29
1H57080	573	7	0.8	0.47	0.09	7.42	1.091	10	258	46	0.08	0.72	3.37
1H47123	473	7	1.23	0.32	0.11	6.92	1.034	8	235	22	0.17	1.13	4.86
1H47106	473	7	1.06	0.42	0.09	7.9	1.149	8	243	33	0.12	1.13	4.19
1H47086	473	7	0.86	0.34	0.1	5.47	0.88	6	155	23	0.13	0.72	4.16
Test	T	P	ϕ	S_L	δ_L	u	q'	l_0	Re	Da	K	Le	S_T/S_L
3H63125	673	3	1.25	1.3	0.12	13.89	2.063	18	238	99	0.04	1.18	2.44
3H63099	673	3	0.99	1.46	0.11	14.64	2.203	18	247	107	0.04	0.59	2.38
3H63082	673	3	0.82	1.21	0.13	11.16	1.602	18	183	106	0.03	0.59	2.25
3H53120	573	3	1.2	1	0.12	12.08	1.749	15	219	71	0.05	1.18	2.53
3H53103	573	3	1.03	1.08	0.12	13.72	2.032	15	235	68	0.06	1.16	1.94
3H53083	573	3	0.83	0.86	0.14	9.48	1.355	15	169	68	0.05	0.59	2.16
3H43124	473	3	1.24	0.61	0.16	7.33	1.081	7	78	25	0.09	1.18	2.65
3H43101	473	3	1.01	0.71	0.12	7.98	1.159	7	95	35	0.07	1.16	2.57
3H43090	473	3	0.9	0.63	0.14	5.36	0.87	7	69	36	0.06	0.59	2.33
3H67122	673	7	1.22	0.93	0.06	14.16	2.113	-	-	-	-	1.18	3.49
3H67101	673	7	1.01	1.03	0.06	16.97	2.673	-	-	-	-	1.16	3.67
3H57123	573	7	1.23	0.62	0.08	11.21	1.61	-	-	-	-	1.18	3.81
3H57103	573	7	1.03	0.73	0.07	13.4	1.975	-	-	-	-	1.16	3.5
3H47123	473	7	1.23	0.4	0.1	8.27	1.195	8	239	28	0.14	1.18	4.6
3H47099	473	7	0.99	0.48	0.08	8.53	1.228	8	256	38	0.1	0.59	4.17
3H47085	473	7	0.85	0.39	0.09	6.72	1.011	8	230	33	0.11	0.59	4.3

$$\langle c \rangle = \left[1 + exp\left(\frac{-A\,(x - x*)}{\delta_T}\right)\right]^{-1} \tag{9.1}$$

where the coefficient $A = 4$, x is the coordinate along the burner axis, $x*$ is the value of x where mean progress variable $\langle c \rangle = 0.5$. Some researchers have reported that the coefficient A should be 5.5 or even 6 [78].

Profiles of the mean progress variable for near stoichiometric flames along the burner axis at different pressures and temperatures are presented in Fig. 9.1. Here the simple flame brush thickness definition $\delta_T = x_{(c=0.95)} - x_{(c=0.05)}$ is utilised. Markers represent experimental data and the lines have been calculated using the equation 9.1.

In general the experimental data fit the predictions using equation 9.1 well. In our experiments the value of A has been found to vary mostly between 5 and 6, with the average being $A = 5.8$ for all mixtures and conditions. Therefore, a single value of $A = 5.8$ has been chosen to represent the relation of $\langle c \rangle$ and δ_T. For some mixtures, for instance "C63114" and "C63104" the coefficient has derived values above 7, however no consistent correlation of any increase due to pressure, temperature, equivalence ratio or hydrogen content in the mixture has been observed within this dataset.

Another representation of the mean progress variable profile normalised by the dimenensionless distance, $\psi = (x - x*)/\delta_T$, is shown in Fig. 9.2. Lipatnikov and Chomiak [31] suggested representing the relationship between mean progress variable and flame brush thickness using the error function. Here curve fitting was undertaken using the equation:

$$\langle c \rangle = \frac{1}{2}\,(erf(C\psi) + 1) \tag{9.2}$$

where C is the coefficient.

A similar approach has been adopted by other researchers [85]. The best fit of the data utilising equation 9.2 has been derived, utilising regression analysis to calculate the value of coefficient C. For the flames considered the average magnitude of coefficient has been found to be $C = 2.43$, and the value of the coefficient varied between $2.0 < C < 3.6$ (Fig. 9.2). Again the highest values C have been observed for "C63114" and "C63104" mixtures. As discussed above no consistent correlation

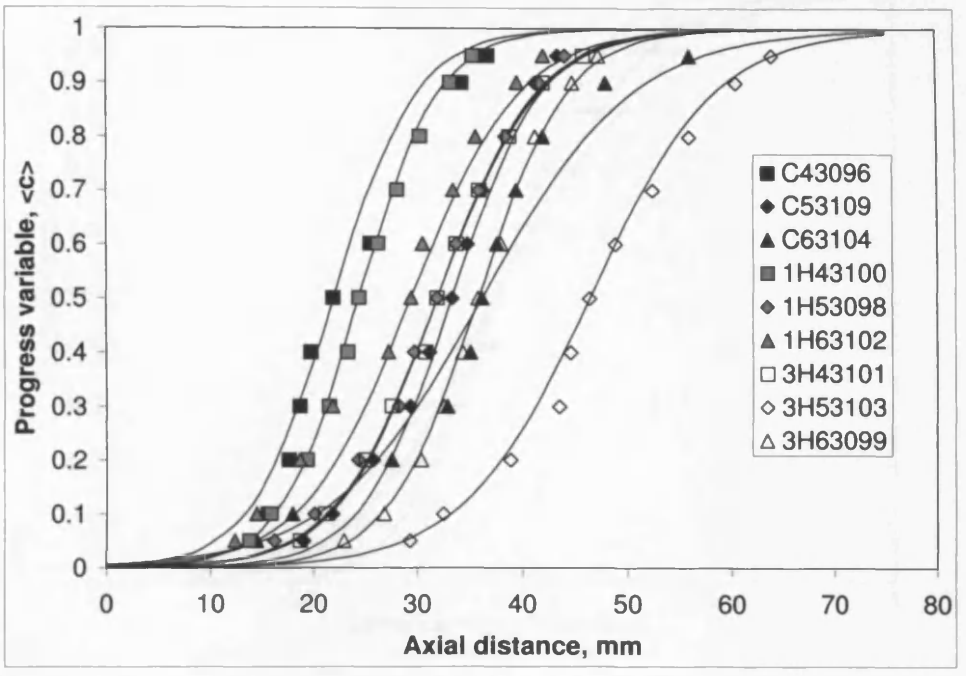

(a) at 3 bar pressure

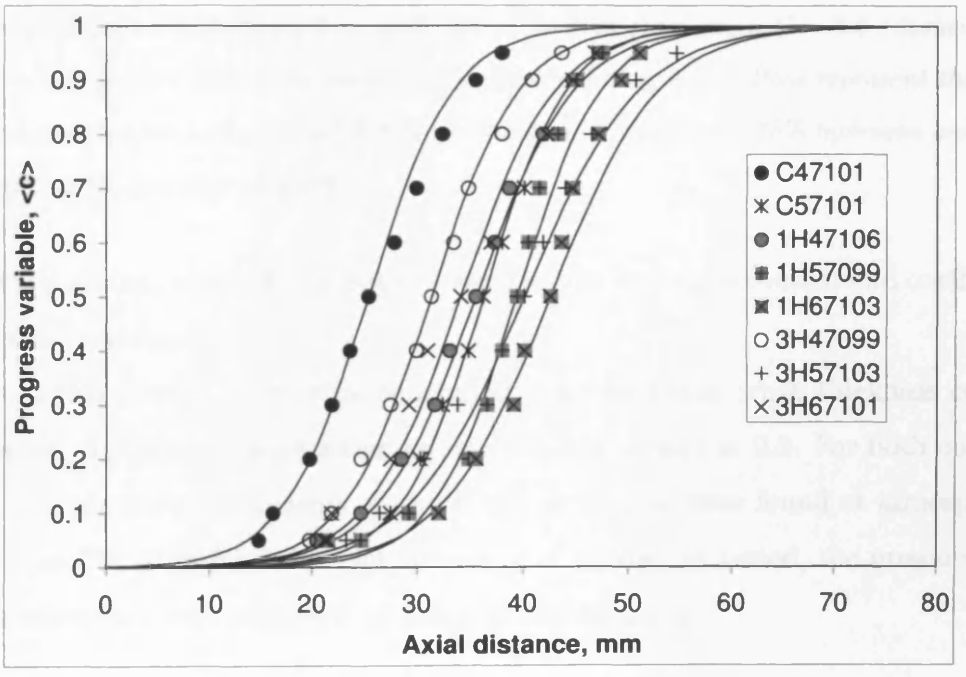

(b) at 7 bar pressure

Figure 9.1: *Evolution of the mean progress variable $\langle c \rangle$ along the burner axis. Markers represent the values obtained from the experiments, solid lines represent the data calculated by formula 9.1, using coefficient $A = 5.8$.*

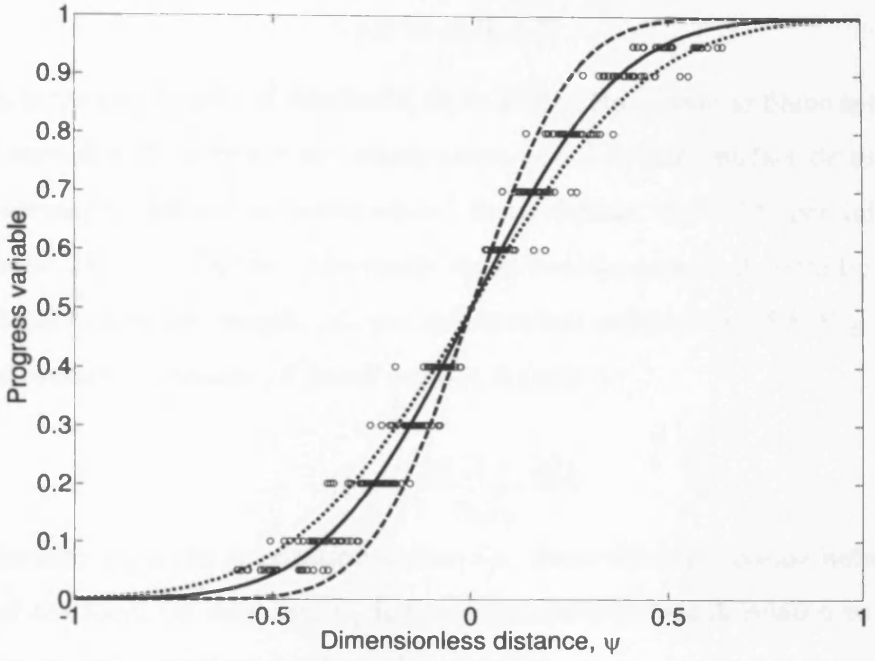

Figure 9.2: *Progress variable profiles vs dimensionless distance, ψ. The fitting curve has been calculated by formula 9.2, coefficient $C = 2.43$ (bold line), $C = 3.6$ (dashed line) and $C = 2.0$ (dotted line) have been used to draw a fitting lines. Dots represent the data points calculated for lean and rich 100% methane, 85% methane - 15% hydrogen and 70% methane - 30% hydrogen mixtures.*

between pressure, temperature, equivalence ratio or hydrogen content and coefficient magnitude was found.

From this dataset, it may be concluded that the flame brush thickness can be reasonably represented using either equation 9.1 or equation 9.2. For both correlations, the calculated coefficients A and C are similar to those found at atmospheric conditions [78]. It implies that, for the range of conditions tested, the pressure and temperature had little influence on flame brush thickness.

9.2 Flame surface density

It has been reported previously that the flames studied in this research programme fall into the 'corrugated flamelets' regime [41]. For flames in the flamelet regime, the mean chemical reaction rate can be defined thus:

$$\langle w \rangle = \rho_R S_L I_0 \Sigma \tag{9.3}$$

where ρ_R is the gas density of reactants, S_L is unstretched laminar flame speed, I_0 is a flamelet stretch and curvature correction term, and Σ is flame surface density. Flame surface density is defined as infinitesimal flame surface area, δA, per infinitesimal unit volume, δV; $\Sigma = \delta A / \delta V$. Alternatively, in two dimensions it could be defined as infinitesimal flame front length, δL, per infinitesimal surface area, δA; $\Sigma_{2D} = \delta L / \delta A$.

An algebraic expression of flame surface density is:

$$\Sigma = \frac{g \langle c \rangle (1 - \langle c \rangle)}{\sigma_y L_y} \tag{9.4}$$

where the term σ_y is the orientation factor, i.e. mean direction cosine between flame front and the local $\langle c \rangle$ contour, L_y is the characteristic length related to the flame wrinkling, g is the constant in the order of unity.

The balance equation of the flame surface density, as defined by Pope [117], can be expressed as:

$$\Sigma = \langle |\nabla c| \cdot \delta (c - c*) \rangle \tag{9.5}$$

where ∇c is the spatial flame front gradient, and $\delta (c - c*)$ is the Dirac delta function which represents the instantaneous flame position with $c* = 0.5$

We have defined the flame surface density from the tomographic images using the method described by Shepherd [79] and later by Lachaux et al. [84]. First, a progress variable contour map is obtained, with $\langle c \rangle$ ranging from 0.05 to 0.95 with the interval of 0.1. The areas, $A(\langle c \rangle)$, between adjacent isolines of progress variable are calculated. Then the instantaneous flame front contours are superimposed on the $\langle c \rangle$ contour map, and the length of the flame front contour line, $L(\langle c \rangle)$, falling within the area of interest, is calculated. The procedure is repeated for all areas. This method allows calculation of two dimensional flame surface density:

$$\Sigma_{2D} = \frac{A(\langle c \rangle)}{n_f L(\langle c \rangle)} \tag{9.6}$$

where Σ_{2D} is the two dimensional flame surface density, and n_f is the number of flame images.

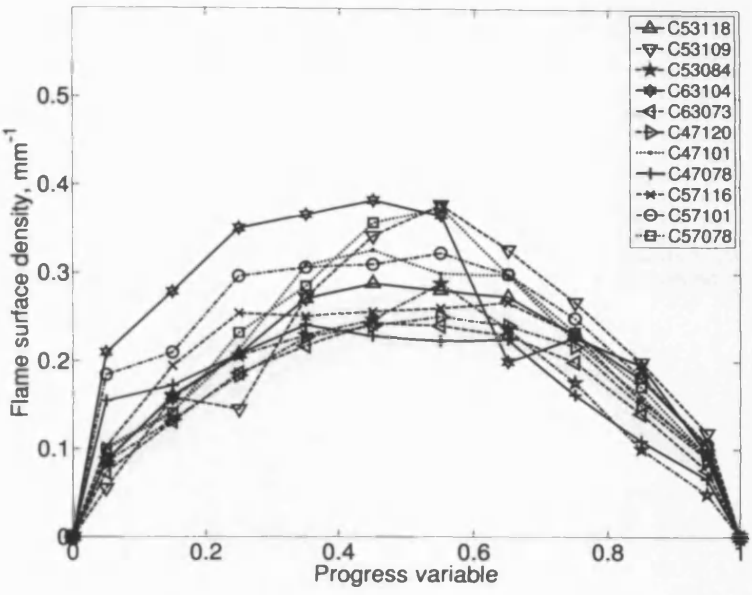

(a) flame surface density Σ

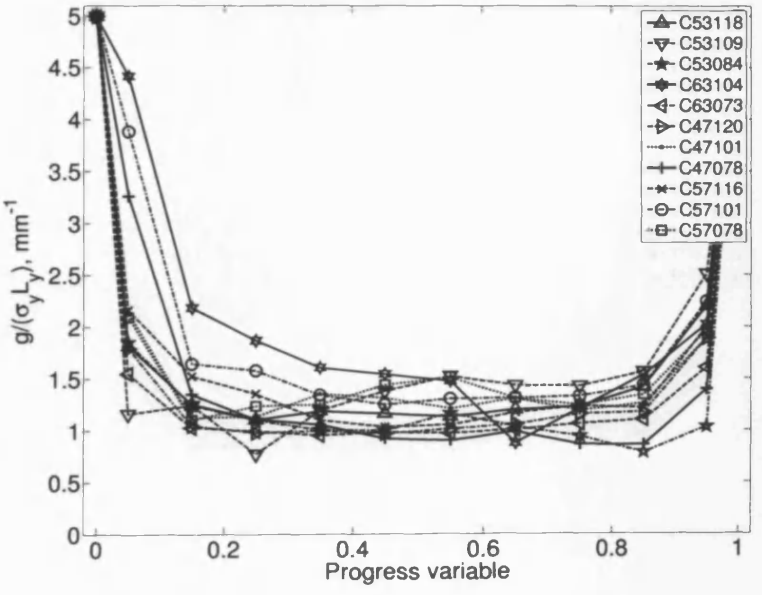

(b) BML coefficient $g/(\sigma_y L_y)$

Figure 9.3: *Flame surface density Σ and BML coefficient $g/(\sigma_y L_y)$ of methane at different conditions and equivalence ratios.*

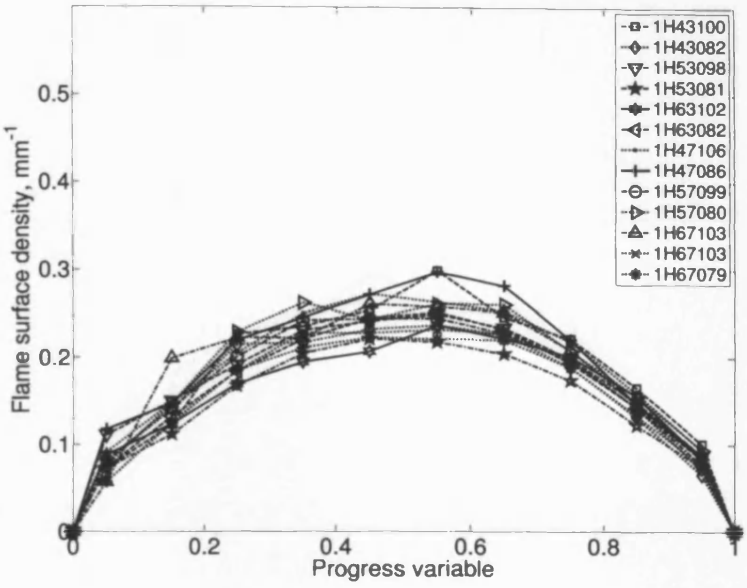

(a) flame surface density Σ

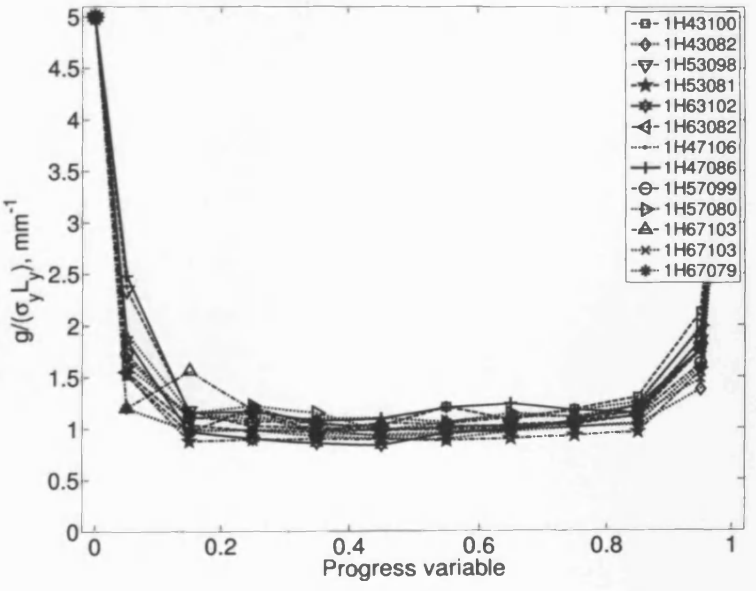

(b) BML coefficient $g/(\sigma_y L_y)$

Figure 9.4: *Flame surface density Σ and BML coefficient $g/(\sigma_y L_y)$ of 85%methane - 15% hydrogen mixture at different conditions and equivalence ratios.*

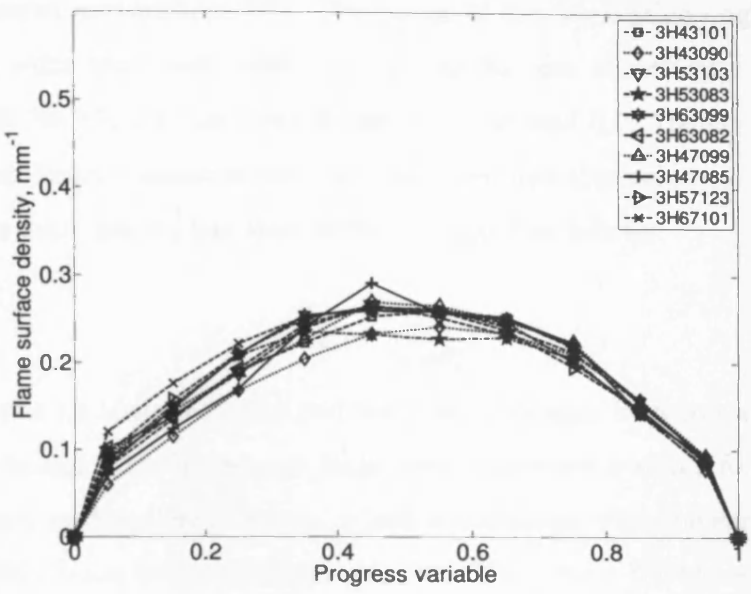

(a) flame surface density Σ

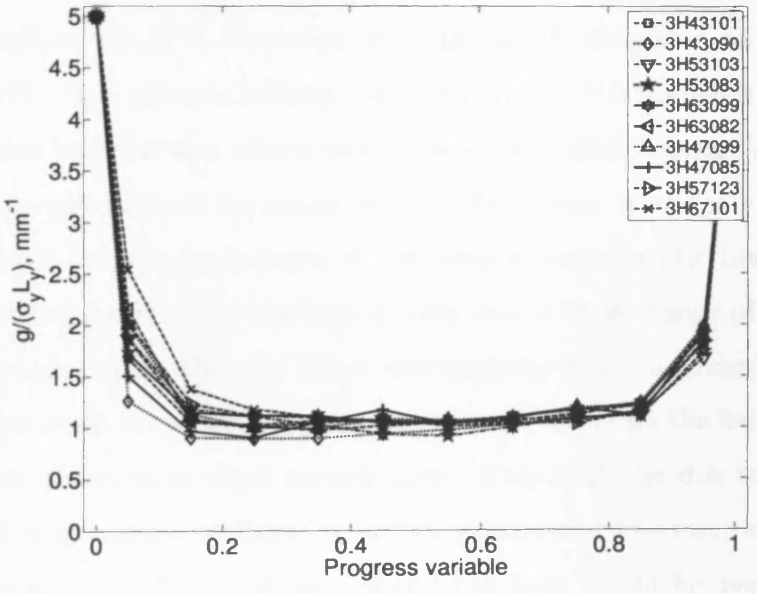

(b) BML coefficient $g/(\sigma_y L_y)$

Figure 9.5: *Flame surface density Σ and BML coefficient $g/(\sigma_y L_y)$ of 70%methane - 30% hydrogen mixture at different conditions and equivalence ratios.*

To obtain the three-dimensional flame surface density, the orientation angle θ must be found. This angle cannot be calculated without either three dimensional measurements or assumptions [87]. The cosine of the orientation angle for the Bunsen burner, calculated from experimental results and numerically by several researchers [78, 86, 87, 90], has been found to be around 0.7. Hence, in the absence of three-dimenionsal measurements, we have assumed this value in our calculation. The flame surface density has thus been calculated as follows:

$$\Sigma = \frac{\Sigma_{2D}}{\langle cos\theta \rangle} \tag{9.7}$$

FSD graphs for some methane and methane hydrogen mixtures are presented in Fig. 9.3a, 9.4a and 9.5a. In general, large data scattering is noted for pure methane data compared to the other mixtures, which is consistent with the earlier discussions concerning the flame brush thickness results. The reason for these differences for the pure methane data needs further investigation. Flame surface density variations for different experiment conditions are quite considerable. It has been noticed that pressure augmentation increases the flame surface density for methane - hydrogen mixtures slightly, which is consistent with the albeit limited data from other researchers [87]. This effect is believed to occur due to the influence of pressure on the turbulence length scales, which become smaller at high pressure [17, 35]. Therefore the flame wrinkledness increases, and the flame area in the same space volume increases, which leads to the increase of the flame surface density. Length scale measurements at the centreline of the burner have shown little change of integral length scale [41], which implies that the flame wrinkledness has not changed significantly. No noticeable effect of the initial gas mixture temperature on the flame surface density has been observed in these experiments. This could be due to the negligible influence of temperature on flame structure at elevated pressure, noted elsewhere [185]. However larger flame surface density has been found for methane at 3 bar 473 K than at 7 bar, in contrast to the observed trends for methane - hydrogen mixtures. The dataset is too sparse to draw generalised conclusions concerning this behaviour. In general, hydrogen addition reduces the flame surface density fluctuations at different pressure and temperature. This implies that hydrogen addition has a stabilising effect on flame surface density, which varies with pressure, and that

the flame surface density become less susceptible to pressure and temperature effect the higher the hydrogen content.

There is some evidence that hydrogen addition to methane increases the FSD [20]. However this has not been observed in these experiments. The flame surface density for 15% and 30% hydrogen-methane mixtures have not varied much. Therefore it is difficult to conclude from our data, that hydrogen content changes the flame surface density. However significant differences can be seen between pure methane and methane - hydrogen mixtures. Flame surface density peaks at around $\langle c \rangle = 0.5 - 0.6$ for hydrogen-methane mixtures and the majority of pure methane experiments. This behaviour has been reported by other reseachers [20, 78, 82]. However peaks at $\langle c \rangle = 0.4 - 0.5$ are observed for "C63104".

From flame surface density the the Bray-Moss-Libby (BML) model coefficient, $g/(\sigma_y L_y) = \Sigma / (\langle c \rangle (1 - \langle c \rangle))$, can be calculated. This coefficient is presented in Fig. 9.3b, 9.4b and 9.5b. Again, consistent with the other flame characteristics, larger data distribution is seen for pure methane data. The coefficient is almost constant for all investigated mixtures from $\langle c \rangle = 0.2$ to $\langle c \rangle = 0.8$, which agrees with the findings of other researchers [78]. The Bray-Moss-Libby (BML) coefficient is slightly higher for pure methane gas and falls in the range of 1.0-1.8 mm^{-1}. For methane - hydrogen mixtures, the coefficient is in the range of around 1.0-1.4 mm^{-1}. It is difficult to quantify the temperature, pressure and equivalence ratio effect on the BML coefficient as their influences are very small.

From the BML coefficient L_y can be estimated. If g is in the order of unity and $\sigma_y = 0.7$, then the characteristic length $L_y \approx 1.0 - 1.4$. Comparing this value with l_0 (Fig. 6.6) it is seen that the difference in the magnitude is tenfold. The explanation of this discrepancy might be that l_0 have been measured under isothermal conditions, which does not fully represent the real combustion conditions. The measurement postion may have influenced the accuracy of measurements as well. Notwithstanding these potential sources of error, these trends are believed to be valid.

9.3 Flame stretch factor

It has been deduced that all flames in the current experimental dataset fall into the flamelets regime [41]. Therefore for the flames in the flamelet regime the mean chemical reaction rate can be defined from the equation 9.3. From this equation the chemical description, $\rho_U S_L I_0$, and flame and turbulence interaction, Σ, can be decoupled [124]. Therefore, assuming that global and local consumption speeds are the same [77], the turbulent consumption speed, S_T, can be related through the equation 1.5 to the unstretched laminar burning rate, S_L, and the flamelet structure quantities flame surface density, Σ, and the stretch factor, I_0.

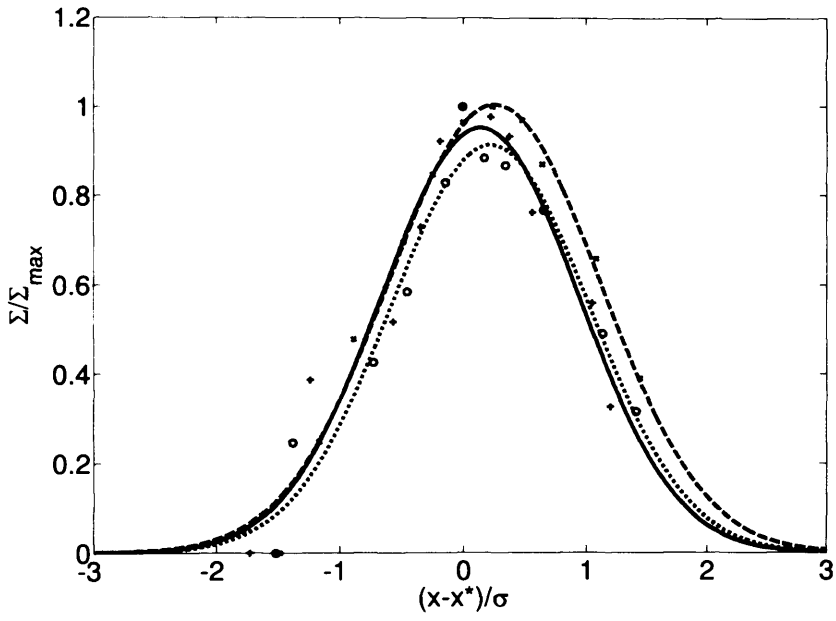

Figure 9.6: *Gaussian fitting curve. Normalised distance in axis line X, and normalised flame surface density, Σ/Σ_{max}, in axis line Y.*

To calculate the integral of the flame surface density, at first Gaussian fitting has been applied, as proposed by Shepherd and Cheng [76]. Σ has been normalised by its maximum value, Σ/Σ_{max}, and the distance has been normalised by the standard deviation, σ, of the Gaussian function. The correlation derived for some experimental conditions is plotted and presented in Fig. 9.6. The integral of the Gaussian fitting curve to find $\int \Sigma$ may now be evaluated.

S_T/S_L ratio has been calculated from the experiments and numerical computa-

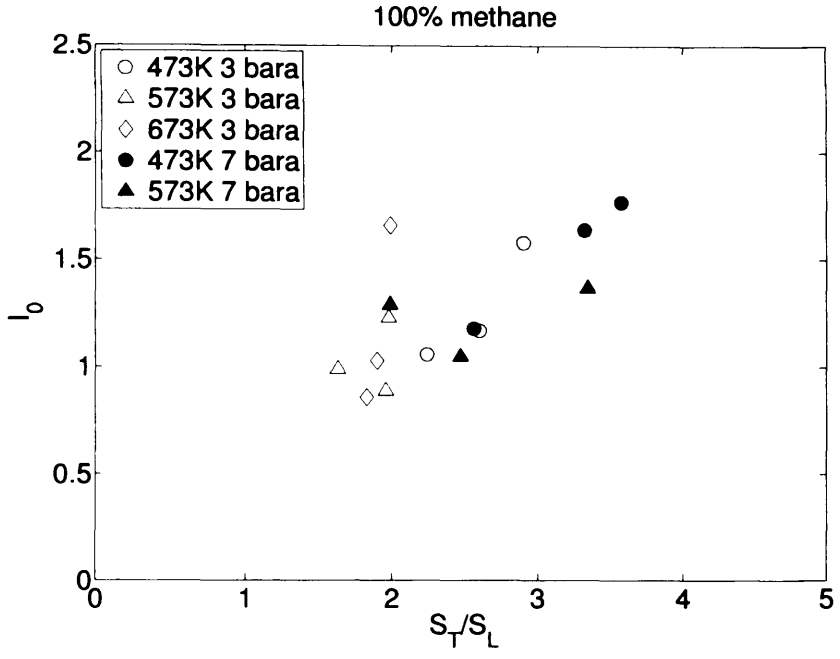

Figure 9.7: *Stretch factor, I_0, correlation with S_T/S_L of methane flames.*

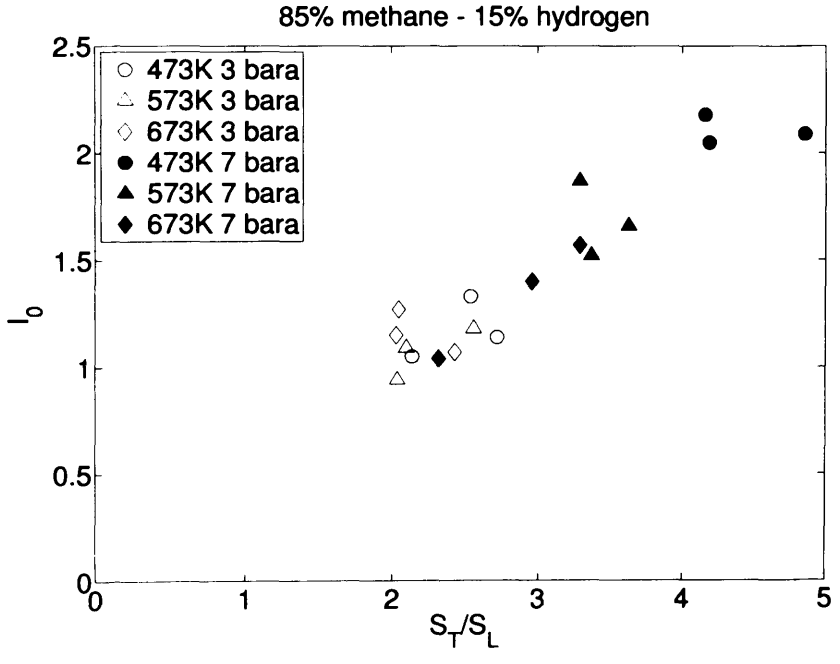

Figure 9.8: *Stretch factor, I_0, correlation with S_T/S_L of 85% methane - 15% hydrogen mixture flames.*

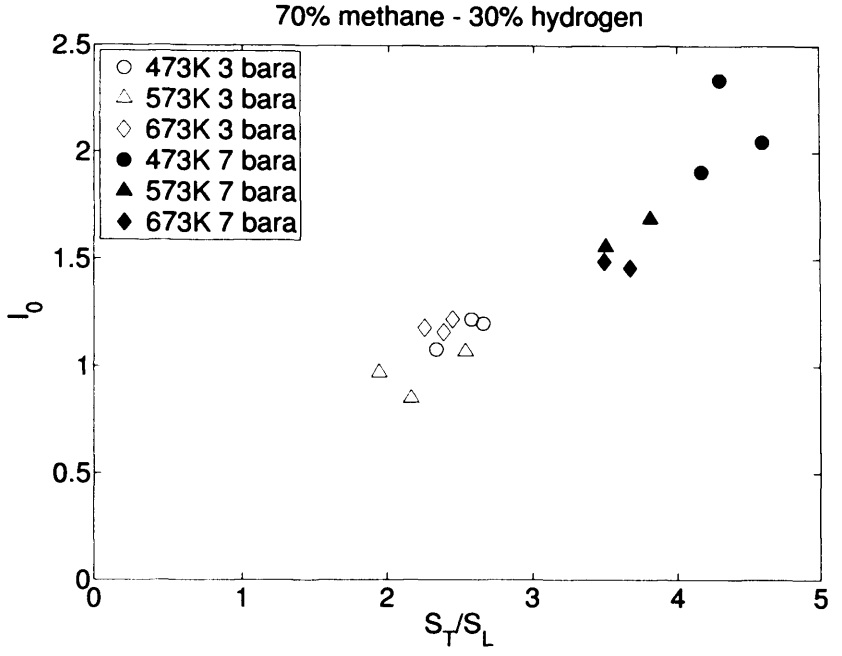

Figure 9.9: *Stretch factor, I_0, correlation with S_T/S_L of 70% methane - 30% hydrogen mixture flames.*

tion of S_L. As the $\int \Sigma$ is also known, the stretch factor I_0 can be estimated using equation 1.5. The computed values of I_0 as a function of S_T/S_L are presented in Figs. 9.7, 9.8 and 9.9.

More data scattering is noted for methane air mixtures than for mixtures containing hydrogen. Consistent augmentation of stretch factor is seen with increasing S_T/S_L ratio. For all mixtures at 3 bar pressure, I_0 is approximately unity. The temperature is observed to have little effect on I_0. However for increased pressure, I_0 increases from unity to approximately 2 for CH_4 and up to 2.5 for $70\%CH_4 - 30\%H_2$ as S_T/S_L increases. It implies that hydrogen enrichment increases I_0. The more significant increase in I_0 is seen at 7 bar 473 K. At 7 bar pressure the temperature effect is more pronounced, that is the higher temperature weakens the stretch factor. Almost linear increase of I_0 independent of gas mixture is observed.

It has been proposed that I_0 may be correlated to Markstein and Karlovitz numbers using [76]:

$$I_0 = 1 - 0.28MaKa \tag{9.8}$$

From Figs. 9.7, 9.8 and 9.9 it is seen that I_0 is higher than 1 in most cases. As

Ka numbers are positive, Ma numbers must be negative. Higher hydrogen quantity in methane increases I_0 so reducing Ma number and increasing the burning velocity. Markstein numbers decrease as the pressure increases and negative Markstein numbers increase the burning velocity [29]. The increase of S_T of lean methane - hydrogen mixtures with increasing pressure has been reported elsewhere [41].

9.4 Conclusion

Turbulent flame brush thickness and flame surface density of methane and methane - hydrogen mixtures at 473 K, 573 K and 673 K temperatures, and 3 bar and 7 bar pressures for a Bunsen burner turbulent flame has been derived.

- Flame brush thickness measurement have shown that pressure, temperature and hydrogen addition has little effect on methane and methane - hydrogen flame structure for the tested Bunsen burner. The coefficients used in the generalised equations for the determination of flame brush thickness have been found and compared with the findings of other researchers.

- Flame surface density and BML coefficients have been found for tested methane and methane - hydrogen mixtures. No significant temperature, pressure and equivalence ratio effect has been observed. Larger FSD and BML coefficient data scattering has been found for pure methane, which requires further investigation.

- Flame stretch factor I_0 has been derived. The analysis of I_0 revealed that it is directly proportional to the normalised turbulent burning velocity, S_T/S_L, which increases with increasing pressure, but is not affected by temperature very much under the conditions studied in this experimental programme.

Chapter 10

Conclusions and future work

10.1 Conclusion

This work has been undertaken to investigate the laminar and turbulent combustion characteristics of alternative fuels. Five fuel mixtures have been tested: 100% methane, 85% methane - 15% carbon dioxide, 70% methane - 30% carbon dioxide, 85% methane - 15% hydrogen and 70% methane - 30% hydrogen for a range of equivalence ratio.

Numerical computation of laminar flames characteristics: laminar burning velocity and laminar flame thickness, at atmospheric and elevated temperature and pressure conditions (298 K, 473 K, 573 K, 673 K temperature and 1 bar, 3 bar, 7 bar pressure) have been performed using Chemkin-Pro numerical tool.

Three series of tests have been performed. Bunsen burner experiments at two pressures 3 bar and 7 bar and three temperatures 473 K, 573 K and 673 K were conducted using High Pressure Optical Combustor at the Gas Turbine Research Centre. Two different measurement techniques were applied. First, a non-intrusive 2-D laser diagnostic technique, Laser Doppler Anemometry, was utilised to determine both the velocity profile and turbulence characteristics at the exit of the burner at elevated pressures and temperatures. Secondly, planar laser tomography was applied in order to measure the turbulent burning velocity for the different gas mixtures at a range of temperatures and pressures.

Bunsen burner experiments at atmospheric conditions were performed in the Cardiff University laboratory. Two different measurement techniques were applied.

Laser Doppler Anemometry was used to investigate three burner nozzles 10 mm, 15 mm and 25 mm diamter and two turbulence plates. Laser Induced Fluorescence tuned for OH radicals was used to obtain turbulent and laminar flame images.

A generic swirl burner was used to test flashback and blowoff limits of alternative fuels. Flame imaging was used in order to record these conditions. A new method to estimate the burning velocity was tested.

Novel image processing technique was utilised to calculate the flame front area of the flame. The technique was based on calculating the side area of the pixels, which compose the binary flame image. Two different approaches were tested. Statistical method was compared with the averaged method. Statistical method is based on calculation of the flame front area of every single image. The set of flame areas consisting of variables is treated using statistical methods, i.e. mean, median and other statistical quantities could be found. Averaging method is based on the average image, which is obtained by superimposing all available images and calculating the mean image from them.

From the numerical calculation and experimental data results it is concluded:

- Chemical kinetic mechanisms used in numerical calculations comprise an important part in combustion research, therefore it is very important to correctly select suitable mechanism for every conditions and fuel composition. The research has shown that GRI-Mech v3.0 kinetic mechanism is suitable for the investigation of methane and methane diluted with carbon dioxide (up to 30%) or enriched with hydrogen (up to 30%) flames at atmopsheric and elevated temperature and pressure conditions.

- A new image processing technique consisting of statistical and averaging methods has been developed and tested at atmospheric and elevated temperature and pressure conditions. The test has shown that both methods are comparable and suitable for turbulent flame burning velocity calculation in wrinkled and corrugated flamelets regime. Averaging method can be used to calculate flame brush thickness and the flame surface density, and statistical method provides the information about the flame area fluctuations in time.

- Experiments conducted under elevated temperature and pressure have shown

the reduction in turbulent burning rate induced by carbon dioxide addition to methane for a variety of equivalence ratios. Increase in initial ambient gas temperature significantly increases turbulent burning velocity, while increase in ambient pressure induces a reduction. Methane and methane - carbon dioxide mixtures demonstrate similar trends with respect to the influence of ambient conditions. Hydrogen addition to methane has been found to considerably increase turbulent burning velocity even for small volumes of hydrogen addition. For lean hydrogen-methane mixtures, an increase in temperature or pressure augments turbulent burning velocity, whereas the influence of ambient pressure is minimal for rich mixtures.

- Burning velocities of methane-hydrogen mixtures conducted at atmosperic conditions was found to be higher than with pure methane as expected. Small quantities of hydrogen in the gas mixture (15%) increased S_T by approximately 25-30% comparing with the pure methane. S_T of gas mixture with 30% hydrogen increased by 50-55% compared with pure methane. These results agree very well with the data obtained at elevated temperature and pressure conditions, where similiar increases in S_T were observed. Methane - hydrogen mixture results show good agreement with data from Kobayashi et al. [34], who used the Bunsen burner method for quantifying turbulent burning velocity. This finding reveals that the PLIF method combined with the novel flame front area location method is promising and could be used for the creation of a database of S_T for alternative fuels at atmospheric as well as at elevated temperature and pressure conditions.

- A generic swirl burner has been developed and used to test flame stability and flashback limits. The experiment results have shown that CO_2 addition reduces the flame flashback possibility primarily because of the lower burning velocities of methane - carbon dioxide mixtures. H_2 addition increases the flame flashback possibility primarily because of the increase in burning velocities of methane - hydrogen mixtures. An attempt has been made to correlate the flashback and turbulent burning rate data, as fundamentally the two processes must be related. Uncertainties have been emphasised and discussed. The differences in results are likely to arise due to the following primary

causes: the method used to derive flame front position, turbulent flow characteristics, flame regime, unburnt gas temperature. Modifications are needed to the Bunsen type burner to produce flame conditions at flashback closer to those pertaining in swirl burners.

- Flame brush thickness, flame surface density and BML coefficients have been found for tested methane and methane - hydrogen mixtures at elevated conditions. Measurement have shown that pressure, temperature and hydrogen addition has little effect on methane and methane - hydrogen flame structure for the tested Bunsen burner and no significant temperature, pressure and equivalence ratio effect has been observed for FSD and BML coefficient. Larger FSD and BML coefficient data scattering has been found for pure methane, which requires further investigation. Flame stretch factor I_0 has been derived. The analysis of I_0 revealed that it is directly proportional to the normalised turbulent burning velocity, S_T/S_L, which increases with increasing pressure, but is not affected by temperature very much under the conditions studied in this experimental programme.

10.2 Future work

This work has contributed to the understanding of pressure and temperature effect on premixed laminar and turbulents flames, however it also revealed some uncertainties and limits, which need to be addressed in the future.

1. The first question is how does the exit velocity profile affect the turbulent burning velocity measurements for Bunsen type burner flames. Obviously in Bunsen burner turbulent flows characteristics must be maintained constant for all exit velocities, therefore turbulence generation system must be carefully designed. It is especially important for low exit velocity flows as in these cases nearly laminar or transition flows prevail, when using conventional design turbulence plates.

2. Another related problem is the integral length scale measurements for the Bunsen burner. Some uncertainties have been shown in this work. It is im-

portant to measure integral length scales in the regions where the flame front actually exists. A conventional LDA system has not been able to provide accurate results of integral length scale in the regions where the shear layer forms. Therefore more advanced double LDA system capable of measuring longitudinal or transverse integral length scales or PIV system could be used in order to clearly define the turbulence processes at the shear layer or at flame front.

3. Seeding of the flow is necessary in order to measure velocity or get tomographic flame images. However seeding effect on turbulent burning velocity was not dicussed thoroughly. Simultaneous PLT and PLIF experiments would help to better understand this effect and to evaluate its influence on premixed combustion.

4. When performing PLIF experiments a narrow laser sheet has been obtained, which has limited the measurement area. The wider laser sheet is necessary to study turbulent flames. It however may affect the laser sheet power required to excite OH radicals and image intensity could drop. Therefore more powerful pumping laser might be needed in order to increase laser sheet power and to obtain suitable images. When considering simultaneous PLIF and PIV experiments, which could be helpful in understanding turbulent flames, much faster or double cavity laser should be used.

5. One of the limitations of PLT and PLIF methods nowadays is the two dimensionality. The estimation of burning velocities or investigation of flame structures, especially for turbulent flames, depends on many assumptions. Therefore more advanced three dimensional methods are needed in order to overcome these limitations. Stereo PLIF system could be one of the options.

6. Lean combustion is of primary importance, therefore deeper investigation of lean gaseous alternative fuels (most probably hydrogen and carbon monoxide enriched or carbon dioxide diluted methane or natural gas) at different ambient conditions for different turbulence levels is needed. Turbulence intensity is one of the most important characteristics for turbulent flames. The results of the burning velocities depend on the ambient conditions and turbulence intensities.

These must be collected in an alternative fuel database, which could be a useful tool for the validation of models and numerical calculations.

Bibliography

[1] *International Energy Outlook. www.eia.doe.gov/oiaf/ieo/index.html*: Energy Information Administration Office of Integrated Analysis and Forecasting U.S. Department of Energy, 2009.

[2] *Key world energy statistics. http : //www.iea.org/publications/*: International Energy Agency, 2009.

[3] I. Gökalp and E. Lebas, "Alternative fuels for industrial gas turbines (AFTUR)," *Applied Thermal Engineering*, vol. 24, pp. 1655–1663, 2004.

[4] *Gas Turbine Fuel Flexibility for Zero Emission Power Plants. http : //www.eu − gasturbine.org/pp.aspx*: European Turbine Network, 2007.

[5] V. di Sarli and A. di Benedetto, "Laminar burning velocity of hydrogen-methane/air premixed flames," *International Journal of Hydrogen Energy*, vol. 32, pp. 637–646, 2007.

[6] P. Chiesa, G. Lozza, and L. Mazzocchi, "Using hydrogen as gas turbine fuel," *Journal of Engineering for Gas Turbines and Power*, vol. 127, no. 1, pp. 73–80, 2005.

[7] *IEA Energy Technology Essentials: Biomass for Power Generation and CHP. http : //www.iea.org/publications/free_new_Desc.asp?PUBS_ID = 1917*: International Energy Agency, 2007.

[8] F. Miccio, B. Piriou, G. Ruoppolo, and R. Chirone, "Biomass gasification in a catalytic fluidized reactor with beds of different materials," *Chemical Engineering Journal*, vol. 154, pp. 369–374, 2009.

[9] P. Ammendola, L. Lisi, B. Piriou, and G. Ruoppolo, "Rh-perovskite catalysts for conversion of tar from biomass pyrolysis," *Chemical Engineering Journal*, vol. doi:10.1016/j.cej.2009.04.010, p. 8, 2009.

[10] P. S. Calabro, "Greenhouse gases emission from municipal waste management: the role of separate collection," *Waste Management*, vol. 29, pp. 2178–2187, 2009.

[11] P. Shanmugam and N. Horan, "Optimising the biogas production from leather fleshing waste by co-digestion with MSW," *Bioresource Technology*, vol. 100, pp. 4117–4120, 2009.

[12] S. Rasi, A. Veijanen, and J. Rintala, "Trace compounds of biogas from different biogas production plants," *Energy*, vol. 32, pp. 1375–1380, 2007.

[13] *CO_2 emissions from fuel combustion. Highlights. http://www.iea.org/publications/free_new_Desc.asp?PUBS_ID = 2143*: International Energy Agency, 2009.

[14] *Cambridge Dictionaries Online.*

[15] G. E. Andrews and D. Bradley, "Determination of burning velocities: A critical review," *Combustion and Flame*, vol. 18, pp. 133–153, 1972.

[16] F. N. Egolfopoulos, P. Cho, and C. K. Law, "Laminar flame speeds of methane-air mixtures under reduced and elevated pressures," *Combustion and Flame*, vol. 76, pp. 375–391, 1989.

[17] H. Kobayashi, "Experimental study of high-pressure turbulent premixed flames," *Experimental Thermal and Fluid Science*, vol. 26, pp. 375–387, 2002.

[18] H. Kobayashi, H. Hagiwara, H. Kaneko, and Y. Ogami, "Effects of CO_2 dilution on turbulent premixed flames at high pressure and high temperature," *Proceedings of the Combustion Institute*, vol. 31, pp. 1451–1458, 2007.

[19] P. Griebel, E. Boschek, and P. Jansohn, "Lean blowout limits and NO_x emissions of turbulent, lean, premixed, hydrogen-enriched methane/air flames at

high pressure," *Journal of Engineering for Gas Turbines and Power*, vol. 129, pp. 404–410, 2007.

[20] F. Halter, C. Chauveau, and I. Gökalp, "Characterization of the effects of hydrogen addition in premixed methane/air flames," *International Journal of Hydrogen Energy*, vol. 32, pp. 2585–2592, 2007.

[21] S. S. Shy, Y. C. Cheng, C. H. Yang, C. C. Liu, and C. M. Huang, "Effects of H_2 or CO_2, equivalence ratio, and turbulent straining on turbulent burning velocities for lean premixed methane combustion," *Combustion and Flame*, vol. 153, pp. 510–524, 2008.

[22] C. Mandilas, M. P. Ormsby, C. G. W. Sheppard, and R. Wooley, "Effects of hydrogen addition on laminar and turbulent premixed methane and iso-octane - air flames," *Proceedings of the Combustion Institute*, vol. 31, pp. 1443–1450, 2007.

[23] H. Kido, M. Nakahara, J. Hashimoto, and D. Barat, "Turbulent burning velocity of two-component fuel mixtures of methane, propane and hydrogen," *JSME International Journal*, vol. 45, no. 2, pp. 355–362, 2002.

[24] J. Natarajan, T. Lieuwen, and J. Seitzman, "Laminar flame speeds of H_2/CO mixtures: Effect of CO_2 dilution, preheat temperature, and pressure," *Combustion and Flame*, vol. 151, pp. 104–119, 2007.

[25] G. E. Andrews and D. Bradley, "The burning velocity of methane - air mixtures," *Combustion and Flame*, vol. 19, pp. 275–288, 1972.

[26] C. J. Rallis and A. M. Garforth, "The determination of laminar burning velocity," *Progress in Energy and Combustion Science*, vol. 6, pp. –, 1980.

[27] R. G. Abdel-Gayed, D. Bradley, and M. Lawes, "Turbulent burning velocities: a general correlation in terms of straining rates," *Proceedings of the the Royal Society of London*, vol. 414, pp. 389–413, 1987.

[28] D. Bradley, A. K. C. Lau, and M. Lawes, "Flame stretch rate as a determinant of turbulent burning velocity," *Philosophical Transactions of the Royal Society A*, no. 338, pp. 359–387, 1992.

[29] D. Bradley, P. H. Gaskell, X. J. Gu, and A. Sedaghat, "Premixed flamelet modelling: Factors influencing the turbulent heat release rate source term and the turbulent burning velocity," *Combustion and Flame*, vol. 143, pp. 227–245, 2005.

[30] D. Dunn-Rankin, *Lean combustion.* Elsevier, 2008.

[31] A. Lipatnikov and J. Chomiak, "Turbulent flame speed and thickness: Phenomenology, evaluation and application in multi-dimensional simulations," *Progress in Energy and Combustion Science*, vol. 28, pp. 1–74, 2002.

[32] V. Zimont, W. Polifke, M. Bettelini, and W. Weisenstein, "An efficient computational model for premixed turbulent combustion at high Reynolds numbers based on a turbulent flame speed closure," *Journal of Engineering for Gas Turbines and Power*, vol. 120, pp. 526–532, 1998.

[33] N. Peters, "The turbulent burning velocity for large-scale and small-scale turbulence," *Journal of Fluid Mechanics*, vol. 384, pp. 107–132, 1999.

[34] H. Kobayashi, T. Tamura, K. Maruta, T. Niioka, and F. A. Williams, "Burning velocity of turbulent premixed flames in a high pressure environment," *Proceedings of the Combustion Institute*, vol. 26, pp. 389–396, 1996.

[35] H. Kobayashi, T. Nakashima, T. Tamura, K. Maruta, and T. Niioka, "Turbulence measurements and observations of turbulent prmixed flames at elevated pressures up to 3.0 MPa," *Combustion and Flame*, vol. 108, pp. 104–117, 1997.

[36] H. Kobayashi, K. Seyama, H. Hagiwara, and Y. Ogami, "Burning velocity correlation of methane/air turbulent premixed flames at high pressure and high temperature," *Proceedings of the Combustion Institute*, vol. 30, pp. 827–834, 2005.

[37] R. Stone, A. Clarke, and P. Beckwith, "Correlations for the laminar-burning velocity of methane/diluent/air mixtures obtained in free-fall experiments," *Combustion and Flame*, vol. 114, pp. 546–555, 1998.

[38] W. Qin, F. N. Egolfopoulos, and T. T. Tsotsis, "Fundamental and environmental aspects of landfill gas utilization for power generation," *Chemical Engineering Journal*, vol. 82, pp. 157–172, 2001.

[39] S. S. Shy, S. I. Yang, W. J. Lin, and R. C. Su, "Turbulent burning velocities of premixed CH_4/diluent/air flames in intense isotropic turbulence with consideration of radiation losses," *Combustion and Flame*, vol. 143, pp. 106–118, 2005.

[40] Z. Chen, X. Qin, B. Xua, Y. Jua, and F. Liub, "Studies of radiation absorption on flame speed and flammability limit of CO_2 diluted methane flames at elevated pressures," *Proceedings of the Combustion Institute*, vol. 31, pp. 2693–2700, 2007.

[41] A. Bagdanavicius, P. J. Bowen, N. Syred, P. Kay, A. Crayford, G. Sims, and J. Wood, "Burning velocities of alternative gaseous fuels at elevated temperature and pressure," *AIAA Journal*, vol. 48, no. 2, pp. 317–329, 2010.

[42] C. Cohe, C. Chauveau, I. Gökalp, and D. F. Kurtulus, "CO_2 addition and pressure effects on laminar and turbulent lean premixed CH_4 air flames," *Proceedings of the Combustion Institute*, vol. 32, pp. 1803–1810, 2009.

[43] K. T. Aung, M. I. Hassan, and G. M. Faeth, "Effects of pressure and nitrogen dilution on flame/stretch interactions of laminar premixed $H_2/O_2/N_2$ flames," *Combustion and Flame*, vol. 112, pp. 1–15, 1998.

[44] Y. C. Chen and R. W. Bilger, "Experimental investigation of three-dimensional flame-front structure in premixed turbulent combustion - II: Lean hydrogen/air Bunsen flames," *Combustion and Flame*, vol. 138, pp. 155–174, 2004.

[45] C. K. Law and O. C. Kwon, "Effects of hydrocarbon substitution on atmospheric hydrogen-air flame propagation," *International Journal of Hydrogen Energy*, vol. 29, pp. 867–879, 2004.

[46] C. K. Law, G. Jomaas, and J. K. Bechtold, "Cellular instabilities of expanding

hydrogen/propane spherical flames at elevated pressures: Theory and experiment," *Proceedings of the Combustion Institute*, vol. 30, pp. 159–167, 2005.

[47] F. Liu and O. L. Gülder, "Effects of H_2 and H preferential diffusion and unity lewis number on superadiabatic flame temperatures in rich premixed methane flames," *Combustion and Flame*, vol. 143, pp. 264–281, 2005.

[48] M. Ilbas, A. P. Crayford, I. Ylmaz, P. J. Bowen, and N. Syred, "Laminar burning velocities of hydrogen-air and hydrogen-methane-air mixtures: An experimental study," *International Journal of Hydrogen Energy*, vol. 31, pp. 1768–1779, 2006.

[49] P. Griebel, E. Boschek, and P. Jansohn, "Flame stability and NO_x emission improvements due to h_2 enrichment of turbulent, lean premixed, high-pressure, methane/air flames.," *The Future of Gas Turbine Technology, 3rd International Conference, Brussels, Belgium, 11-12 October 2006*, 2006.

[50] D. Bradley, M. Lawes, K. Liu, and R. Wooley, "The quenching of premixed turbulent flames of iso-octane, methane and hydrogen at high pressures," *Proceedings of the Combustion Institute*, vol. 31, pp. 1393–1400, 2007.

[51] R. T. E. Hermanns, *Laminar Burning Velocities of Methane-Hydrogen-Air Mixtures*. PhD thesis, Technische Universiteit Eindhoven, 2007.

[52] Y. Lafay, B. Renou, G. Cabot, and M. Boukhalfa, "Experimental and numerical investigation of the effect of H_2 enrichment on laminar methane-air flame thickness," *Combustion and Flame*, vol. 153, pp. 540–561, 2008.

[53] T. Kitagawa, T. Nakahara, K. Maruyama, K. Kado, A. Hayakawa, and S. Kobayashi, "Turbulent burning velocity of hydrogen-air premixed propagating flames at elevated pressures," *International Journal of Hydrogen Energy*, pp. 1–8, 2008.

[54] C. Serrano, J. J. Hernandez, C. Mandilas, C. G. W. Sheppard, and R. Woolley, "Laminar burning behaviour of biomass gasification-derived producer gas," *International Journal of Hydrogen Energy*, vol. 33, no. 2, pp. 851–862, 2008.

[55] M. Fairweather, M. P. Ormsby, C. G. W. Sheppard, and R. Wooley, "Turbulent burning rates of methane and methane-hydrogen mixtures," *Combustion and Flame*, vol. doi:/j.combustflame.2009.02.001, 2009.

[56] Y. Zhang, J. Wu, and S. Ishizuka, "Hydrogen addition effect on laminar burning velocity, flame temperature and flame stability of a planar and a curved CH_4-H_2-air premixed flame," *International Journal of Hydrogen Energy*, vol. 34, pp. 519–527, 2009.

[57] A. Bagdanavicius, P. J. Bowen, N. Syred, P. Kay, A. Crayford, G. Sims, and J. Wood, "Burning velocities of alternative gaseous fuels at elevated temperature and pressure," in *47th AIAA Aerospace Sciences Meeting including The New Horizons Forum and Aerospace Exposition*, (Orlando, Florida, USA), 2009.

[58] J. Ströhle and T. Myhrvold, "An evaluation of detailed reaction mechanisms for hydrogen combustion under gas turbine conditions," *International Journal of Hydrogen Energy*, vol. 32, no. 1, pp. 125–135, 2007.

[59] G. P. Smith, D. M. Golden, M. Frenklach, N. W. Moriarty, B. Eiteneer, M. Goldenberg, C. T. Bowman, R. K. Hanson, S. Song, W. C. Gardiner, V. V. Lissianski, and Z. Qin, "GRI-Mech 3.0."

[60] "http://maeweb.ucsd.edu/ combustion/cermech/."

[61] P. Dagaut and A. Nicolle, "Experimental and detailed kinetic modeling study of hydrogen-enriched natural gas blend oxidation over extended temperature and equivalence ratio ranges," *Proceedings of the Combustion Institute*, vol. 30, pp. 2631–2638, 2005.

[62] N. Syred, "Generation and allevation of combustion instabilities in swirling flow," in *Advanced Combustion and Aerothermal Technologies* (N. Syred and A. Khalatov, eds.), pp. 3–20, Springer Netherlands, 2007.

[63] N. Syred, "A review of oscillation mechanisms and the role of the Precessing Vortex Core (PVC) in swirl combustion systems," *Progress in Energy and Combustion Science*, vol. 32, no. 2, pp. 93–161, 2006.

[64] N. Syred and J. M. Beer, "Combustion in swirling flows: A review," *Combustion and Flame*, vol. 23, no. 2, pp. 143–201, 1974.

[65] A. K. Gupta, D. G. Lilley, and N. Syred, *Swirl Flows*. Tunbridge Wells: Abacus Press, 1984.

[66] Y. Huang and V. Yang, "Bifurcation of flame structure in a lean-premixed swirl-stabilised combustor: transition from stable to unstable flame," *Combustion and Flame*, vol. 136, no. 3, pp. 383–389, 2004.

[67] Y. Huang and V. Yang, "Dynamics and stability of lean-premixed swirl-stabilized combustion," *Progress in Energy and Combustion Science*, vol. 35, pp. 293–364, 2009.

[68] K. Vanoverberghe, *Flow, Turbulence and Combustion of Premixed Switling Jet Flames*. PhD thesis, Katholieke Universiteit Leuven, 2004.

[69] A. Coghe, G. Solero, and G. Scribano, "Recirculation phenomena in a natural gas swirl combustor," *Experimental Thermal and Fluid Science*, vol. 28, no. 7, pp. 709–714, 2004.

[70] A. Valera-Medina, *Coherent structure and their effects on processes occurring in swirl combustors*. Phd, Cardiff University, 2009.

[71] A. Valera-Medina, N. Syred, and A. J. Griffiths, "Visualisation of isothermal large coherent structures in a swirl burner," *Combustion and Flame*, vol. 156, no. 9, pp. 1723–1734, 2009.

[72] M. Kröner, J. Fritz, and T. Sattelmayer, "Flashback limits for combustion induced vortex breakdown in a swirl burner," *Journal of Engineering for Gas Turbines and Power*, vol. 125, pp. 693–700, 2003.

[73] T. Lieuwen, V. McDonell, E. Petersen, and D. Santavicca, "Fuel flexibility influences on premixed combustor blowout, flashback, autoignition, and stability," *Journal of Engineering for Gas Turbines and Power*, vol. 130, pp. 1–10, 2008.

[74] S. K. Dhanuka, J. E. Temme, J. F. Driscoll, and H. C. Mongia, "Vortex-shedding and mixing layer effects on periodic flashback in a lean premixed prevaporized gas turbine combustor," *Proceedings of the Combustion Institute*, vol. 32, pp. 2901–2908, 2009.

[75] R. K. Cheng, D. Littlejohn, P. A. Strakey, and T. Sidwell, "Laboratory investigations of a low-swirl injector with H_2 and CH_4 at gas turbine conditions," *Proceedings of the Combustion Institute*, vol. 32, pp. 3001–3009, 2009.

[76] I. G. Shepherd and R. K. Cheng, "The burning rate of premixed flames in moderate and intense turbulence," *Combustion and Flame*, vol. 127, pp. 2066–2075, 2001.

[77] J. F. Driscoll, "Turbulent premixed combustion: Flamelet structure and its effect on turbulent burning velocities," *Progress in Energy and Combustion Science*, vol. 34, pp. 91–134, 2008.

[78] B. M. Deschamps, G. J. Smallwood, J. Prieur, D. R. Snelling, and O. L. Gülder, "Surface density measurements of turbulent premixed flames in a spark-ignition engine and a bunsen-type burner using planar laser-induced fluorescence," in *Twenty-Sixth Symposium on Combustion*, pp. 427–435, 1996.

[79] I. G. Shepherd, "Flame surface density and burning rate in premixed turbulent flames," *Proceedings of the Combustion Institute*, vol. 26, pp. 373–379, 1996.

[80] I. G. Shepherd, E. Bourguignon, T. Michou, and I. Gokalp, "The burning rate in turbulent bunsen flames," *Proceedings of the Combustion Institute*, vol. 27, pp. 909–916, 1998.

[81] J. M. Donbar, J. F. Driscoll, and C. D. Carter, "Reaction zone structure in turbulent nonpremixed jet flames - from $CH-OH$ PLIF images," *Combustion and Flame*, vol. 122, pp. 1–19, 2000.

[82] G. G. Lee, K. Y. Huh, and H. Kobayashi, "Measurement and analysis of the flame surface density for turbulent premixed combustion on a nozzle-type burner," *Combustion and Flame*, vol. 122, pp. 43–57, 2000.

[83] B. Renou, A. Mura, E. Samson, and A. Boukhalfa, "Characterization of the local flame structure and the flame surface density for freely propagating premixed flames at various Lewis numbers," *Combustion Science and Technology*, vol. 174, pp. 143–179, 2002.

[84] T. Lachaux, F. Halter, C. Chauveu, I. Gökalp, and I. G. Shepherd, "Flame front analysis of high-pressure turbulent lean premixed methane-air flames," *Proceedings of the Combustion Institute*, vol. 30, pp. 819 – 826, 2005.

[85] S. A. Filatyev, J. F. Driscoll, C. D. Carter, and J. M. Donbar, "Measured properties of turbulent premixed flames for model assessment, including burning velocities, stretch rates, and surface densities," *Combustion and Flame*, vol. 141, pp. 1–21, 2005.

[86] O. L. Gülder and G. J. Smallwood, "Flame surface densities in premixed combustion at medium to high turbulence intensities," *Combustion Science and Technology*, vol. 179, pp. 191–206, 2007.

[87] F. Halter, C. Chauveau, I. Gökalp, and D. Veynante, "Analysis of flame surface density measurements in turbulent premixed combustion," *Combustion and Flame*, vol. 156, pp. 657–664, 2009.

[88] Y. C. Chen and R. W. Bilger, "Simultaneous 2-D imaging measurements of reaction progress variable and OH radical concentration in turbulent premixed flames: Experimental methods and flame brush structure," *Combustion Science and Technology*, vol. 167, pp. 131–167, 2001.

[89] Y. C. Chen and R. W. Bilger, "Simultaneous 2-D imaging measurements of reaction progress variable and OH radical concentration in turbulent premixed flames: Instantaneous flame front structure," *Combustion Science and Technology*, vol. 167, pp. 187–222, 2001.

[90] Y. C. Chen and R. W. Bilger, "Experimental investigation of three-dimensional flame-front structure in premixed turbulent combustion - I: Hydrocarbon/air bunsen flames," *Combustion and Flame*, vol. 131, pp. 400–435, 2002.

[91] R. W. Bilger, S. B. Pope, K. N. C. Bray, and J. F. Driscoll, "Paradigms in turbulent combustion research," in *Proceedings of the Combustion Institute*, vol. 30, pp. 21–42, Elsevier Inc., 2005.

[92] C. K. Law, "Combustion at a crossroads: Status and prospects," *Proceedings of the Combustion Institute*, vol. 31, pp. 1–29, 2007.

[93] K. K. Kuo, *Principles of combustion.* New York, Chichester: John Wiley and Sons, 1986.

[94] C. Tanford and R. N. Pease, "Theory of burning velocity. ii. the square root law for burning velocity," *The Journal of Chemical Physics*, vol. 15, pp. 861–866, 1947.

[95] T. Poinsot and D. Veynante, *Theoretical and Numerical Combustion.* Philadelphia: R.T. Edwards, Inc., 2005.

[96] F. A. Williams, *Combustion theory.* Menlo Park, California: The Benjamin/Cummings Publishing Company, 1985.

[97] N. Peters, *Turbulent combustion.* Cambridge: Cambridge University Press, 2000.

[98] C. K. Law, *Combustion Physics.* Cambridge: Cambridge University Press, 2006.

[99] L. K. Tseng, M. A. Ismail, and G. M. Faeth, "Laminar burning velocities and markstein numbers of hydrocarbon/air flames," *Combustion and Flame*, vol. 95, pp. 410–426, 1993.

[100] N. Peters, "Fifteen lectures on laminar and turbulent combustion," *Ercoftac summer school, September 14-28, http://www.itv.rwth-aachen.de/fileadmin/LehreSeminar/Combustion/SummerSchool.pdf*, p. 245, 1992.

[101] L. P. H. G. Goey, A. Maaren, and R. M. Quax, "Stabilisation of adiabatic premixed laminar flames on a flat flame burner," *Combustion Science and Technology*, vol. 92, pp. 201–207, 1993.

[102] K. J. Bosschaart and L. P. H. de Goey, "The laminar burning velocity of flames propagating in mixtures of hydrocarbons and air measured with the heat flux method," *Combustion and Flame*, vol. 136, pp. 261–269, 2004.

[103] D. Bradley and A. Mitcheson, "Mathematical solutions for explosions in spherical vessels," *Combustion and Flame*, vol. 26, pp. 201–217, 1976.

[104] M. Nakahara, H. Kido, and K. Nakashima, "A study on the local flame displacement velocity of premixed turbulent flames," *JSME International Journal*, vol. 48, pp. 164–171, 2005.

[105] M. Weis, N. Zarzalis, and R. Suntz, "Experimental study of Markstein number effects on laminar flamelet velocity in turbulent premixed flames," *Combustion and Flame*, vol. 154, pp. 671–691, 2008.

[106] I. Glassman, *Combustion*. San Diego, London: Academic Press, third edition ed., 1996.

[107] T. W. Lee and S. J. Lee, "Direct comparison of turbulent burning velocity and flame surface properties in turbulent premixed flames," *Combustion and Flame*, vol. 132, pp. 492–502, 2003.

[108] S. S. Shy, W. J. Lin, and K. Z. Peng, "High-intensity turbulent premixed combustion: general correlations of turbulent burning velocities in a new cruciform burner," *Proceedings of the Combustion Institute*, vol. 28, pp. 561–568, 2000.

[109] S. S. Shy, W. J. Lin, and J. C. Wei, "An experimental correlation of turbulent burning velocities for premixed turbulent methane-air combustion," *Proceedings of the Royal Society*, vol. 456, pp. 1997–2019, 2000.

[110] R. Kee, J. Grcar, M. Smooke, and J. Miller, "PREMIX: A Fortran program for modeling steady, laminar, one-dimensional premixed flames," tech. rep., Sandia National Laboratories, 1983.

[111] "Chemkin-pro. http://www.reactiondesign.com," 2008.

[112] A. N. Lipatnikov and J. Chomiak, "Molecular transport effects on turbulent flame propagation and structure," *Progress in Energy and Combustion Science*, vol. 31, pp. 1–73, 2005.

[113] S. B. Pope, *Turbulent flows.* Cambridge: Cambridge University Press, 2008.

[114] R. S. Cant and E. Mastorakos, *An introduction to turbulent reacting flows.* London: Imperial College Press, 2008.

[115] H. Belmabrouk, "Acuracy of taylor length scale measurements by two-point laser doppler velocimetry: a theoretical study," *Flow Measurement and Instrumentation*, vol. 12, pp. 9–16, 2001.

[116] F. C. Gouldin and P. C. Miles, "Chemical closure and burning rates in premixed turbulent flames," *Combustion and Flame*, vol. 100, pp. 202–210, 1995.

[117] S. B. Pope, "The evolution of surfaces in turbulence," *International Journal of Engineering Science*, vol. 26, no. 5, pp. 445–469, 1988.

[118] H. Kobayashi, Y. Kawabata, and K. Maruta, "Experimental study on general correlation of turbulent burning velocity at high pressure," *Twenty-Seventh Symposium on Combustion, The Combustion Institute*, vol. 27, pp. 941–948, 1998.

[119] D. Bradley, M. Z. Haq, R. A. Hicks, T. Kitagawa, M. Lawes, C. G. W. Sheppard, and R. Wooley, "Turbulent burning velocity, burned gas distribution, and associated flame surface definition," *Combustion and Flame*, vol. 133, pp. 415–430, 2003.

[120] T. Plessing, C. Kortschik, N. Peters, M. S. Mansour, and R. K. Cheng, "Measurements of the turbulent burning velocity and the structure of premixed flames on a low-swirl burner," *Proceedings of the Combustion Institute*, vol. 28, pp. 359–366, 2000.

[121] S. P. R. Muppala, M. Nakahara, N. K. Aluri, H. Kido, J. X. Wen, and M. V. Papalexandris, "Experimental and analytical investigation of the turbulent burning velocity of two-component fuel mixtures of hydrogen, methane and propane," *International Journal of Hydrogen Energy*, vol. 34, no. 22, pp. 9258–9265, 2009.

[122] A. A. Burluka, "Raison d'etre and general formulation of two-point statistical description of turbulent premixed combustion," *C. R. Mecanique*, vol. 334, pp. 474–482, 2006.

[123] J. Warnatz, U. Maas, and R. W. Dibble, *Combustion. Physical and Chemical Fundamentals, Modeling and Simulation, Experiments, Pollutant Formation.* Berlin: Springer, 3rd ed., 2001.

[124] D. Veynante and L. Vervisch, "Turbulent combustion modeling," *Progress in Energy and Combustion Science*, vol. 28, pp. 193–266, 2002.

[125] U. C. Müller, M. Bollig, and N. Peters, "Approximation for burning velocities and Markstein numbers for lean hydrocarbon and methanol flames," *Combustion and Flame*, vol. 108, pp. 349–356, 1997.

[126] L. P. H. de Goey, R. T. E. Hermanns, and R. J. M. Bastiaans, "Analysis of the asymptotic structure of stoichiometric premixed ch4h2air flames," *Proceedings of the Combustion Institute*, vol. 31, pp. 1031–1038, 2007.

[127] D. Bradley, "How fast can we burn?," *Proceedings of the Combustion Institute*, vol. 24, pp. 247–262, 1992.

[128] J. K. Bechtold and M. Matalon, "The dependance of the Markstein length on stoiciometry," *Combustion and Flame*, vol. 127, pp. 1906–1913, 2001.

[129] M. Matalon, "Flame dynamics," *Proceedings of the Combustion Institute*, vol. 32, pp. 57–82, 2009.

[130] F. Dinkelacker, "Why the Lewis number seems to have an unexpected importance even in highly turbulent flames!," in *http://eetd.lbl.gov/aet/combustion/workshop/Montreal/dinkelacker.pdf*, 2008.

[131] A. Lipatnikov and J. Chomiak, "Global stretch effects in premixed turbulent combustion," *Proceedings of the Combustion Institute*, vol. 31, pp. 1361–1368, 2007.

[132] X. J. Gu, M. Z. Haq, M. Lawes, and R. Woolley, "Laminar burning velocity and Markstein lengths of methane-air mixtures," *Combustion and Flame*, vol. 121, pp. 41–58, 2000.

[133] D. Bradley, P. H. Gaskell, and X. J. Gu, "Burning velocities, Markstein lengths, and flame quenching for spherical methane-air flames: a computational study," *Combustion and Flame*, vol. 104, pp. 176–198, 1996.

[134] D. Bradley, P. H. Gaskell, A. Sedaghat, and X. J. Gu, "Generation of pdfs for flame curvature and for flame stretch rate in premixed turbulent combustion," *Combustion and Flame*, no. 135, pp. 503–523, 2003.

[135] A. N. Lipatnikov and J. Chomiak, "Application of the Markstein number concept to curved turbulent flames," *Combustion Science and Technology*, vol. 176, no. 3, pp. 331–358, 2004.

[136] P. Clavin and F. A. Williams, "Effects of molecular diffusion and of thermal expansion on the structure and dynamics of premixed flames in turbulent flows of large scale and low intensity," *Journal of Fluid Mechanics*, vol. 116, pp. 251–282, 1982.

[137] C. P. Syred, *Fundamental Scaling of Free Jet Burners.* PhD thesis, Cardiff University, 2002.

[138] J. Luque and D. R. Crosley, "Lifbase: Database and spectral simulation program (version 1.5)," *SRI International Report MP 99-009*, vol. http://www.sri.com/psd/lifbase/, 1999.

[139] F. Durst, A. Melling, and J. H. Whitelaw, *Principles and practice of Laser-Doppler Anemometry.* New York: Academic Press, 1976.

[140] "BSA Flow Software version 3, Installation and Users Guide," 2004.

[141] H. Belmabrouk and M. Michard, "Taylor length scale measurement by laser Doppler velocimetry," *Experiments in Fluids*, vol. 25, no. 1, pp. 69–76, 1998.

[142] D. D. Holm, "Taylor's hypothesis, Hamilton's principle, and the LANS-a model for computing turbulence," *Los Alamos Science*, vol. 29, 2005.

[143] J. O. Hinze, *Turbulence*. New York: McGraw-Hill, second ed., 1975.

[144] B. Renou and A. Boukhalfa, "An experimental study of freely propagating premixed flames at various Lewis numbers," *Combustion Science and Technology*, vol. 162, pp. 347–370, 2001.

[145] G. Coppola and A. Gomez, "Experimental investigation on a turbulence generation system with high-blockage plates," *Experimental Thermal and Fluid Science*, vol. 33, pp. 1037–1048, 2009.

[146] K. Kohse-Höinghaus, R. S. Barlow, M. Alden, and J. Wolfrum, "Combustion at the focus: laser diagnostics and control," *Proceedings of the Combustion Institute*, vol. 30, pp. 89–123, 2005.

[147] P. Griebel, R. Bombach, A. Inauen, R. Schären, S. Schenker, and P. Siewert, "Flame characteristics and turbulent flame speeds of turbulent, high-pressure, lean premixed methane/air flames," *ASME Turbo Expo 2005: Power for Land, Sea, and Air, Reno-Tahoe, Nevada, USA, 6-9 June 2005*, 2005.

[148] P. Griebel, P. Siewert, and P. Jansohn, "Flame characteristics of turbulent lean premixed methane/air flames at high pressure: Turbulent flame speed and flame brush thickness," *Proceedings of the Combustion Institute*, vol. 31, pp. 3083–3090, 2007.

[149] S. Pfadler, A. Leipertz, and F. Dinkelacker, "Systematic experiments on turbulent premixed bunsen flames including turbulent flux measurements," *Combustion and Flame*, vol. 152, pp. 616–631, 2008.

[150] J. Kiefer, Z. S. Li, J. Zetterberg, X. S. Bai, and M. Alden, "Investigation of local flame structures and statistics in partially premixed turbulent jet flames using simultaneous single-shot CH and OH planar laser-induced fluorescence imaging," *Combustion and Flame*, vol. 154, pp. 802–818, 2008.

[151] R. C. Gonzalez, R. E. Woods, and S. L. Eddins, *Digital image processing using MATLAB*. Upper Saddle River: Person Prentice Hall, 2004.

[152] W. Hubschmid and R. Bombach, "Lecture notes: Laser spectroscopy in combustion research," *Ercoftac summerschool, 15-21 March, 2002.*

[153] N. J. Dam, "Laser diagnostics in flames," *Lecture notes of the J. M. Burgerscentrum Course of Combustion*, pp. 235–280, 2008.

[154] T. H. v. d. Meer, "Application of laser diagnostics in turbulent flame analysis," *Lecture notes of the J. M. Burgerscentrum Course of Combustion*, pp. 315–329, 2008.

[155] C. J. Lawn and R. W. Schefer, "Scaling of premixed turbulent flames in the corrugated regime," *Combustion and Flame*, vol. 146, pp. 180–199, 2006.

[156] Y. C. Chen, N. Peters, G. A. Schneemann, N. Wruck, U. Renz, and M. S. Mansour, "The detailed flame structure of highly stretched turbulent premixed methane-air flames," *Combustion and Flame*, vol. 107, pp. 223–244, 1996.

[157] J. Hult, S. Gashi, N. Chakraborty, M. Klein, K. W. Jenkins, S. Cant, and C. F. Kaminski, "Measurement of flame surface density for turbulent premixed flames using PLIF and DNS," *Proceedings of the Combustion Institute*, vol. 31, pp. 1319–1326, 2007.

[158] B. Böhm, D. Geyer, A. Dreizler, K. K. Venkatesan, N. M. Laurendeau, and M. W. Renfro, "Simultaneous PIV/PTV/OH PLIF imaging: Conditional flow field statistics in partially premixed turbulent opposed jet flames," *Proceedings of the Combustion Institute*, vol. 31, pp. 709–717, 2007.

[159] M. Mansour, N. Peters, and L. U. Schrader, "Experimental study of turbulent flame kernel propagation," *Experimental Thermal and Fluid Science*, vol. 32, pp. 1396–1404, 2008.

[160] C. Kortschik, T. Plessing, and N. Peters, "Laser optical investigation of turbulent transport of temperature ahead of the preheat zone in a premixed flame," *Combustion and Flame*, vol. 136, pp. 43–50, 2004.

[161] A. Bagdanavicius, N. Shelil, P. J. Bowen, N. Syred, and A. P. Crayford, "Investigations of gaseous alternative fuels at atmospheric and elevated temperature and pressure conditions," *ASME Turbo Expo 2010: Power for Land, Sea, and Air, Glasgow, UK, 14-18 June 2010*, no. GT2010-23270, 2010.

[162] J. Göttgens, F. Mauss, and N. Peters, "Analytic approximation of burning velocities and flame thickness of lean hydrogen, methane, ethylene, ethane, acetylene, and propane flames." in *Twenty-Fourth Symposium on Combustion/The Combustion Institute*, pp. 129–135, 1992.

[163] M. O'Conaire, H. J. Curran, J. M. Simmie, W. J. Pitz, and C. K. Westbrook, "A comprehensive modeling study of hydrogen oxidation," *International Journal of Chemical Kinetics*, vol. 36, no. 11, pp. 603–622, 2004.

[164] A. A. Konnov, "Remaining uncertainties in the kinetic mechanism of hydrogen combustion," *Combustion and Flame*, vol. 152, pp. 507–528, 2008.

[165] J. Li, Z. Zhao, A. Kazakov, and F. L. Dryer, "An updated comprehensive kinetic model of hydrogen combustion," *International Journal of Chemical Kinetic*, vol. 36, no. 10, pp. 566–575, 2004.

[166] N. Shelil, A. Bagdanavicius, A. J. Griffiths, P. J. Roberts, and N. Syred, "Flashback analysis of hydrogen/methane mixtures for premixed swirl combustion," *16th International IFRF members conference*, 2009.

[167] N. Shelil, *Flashback studies with premixed swirl combustion.* PhD thesis, Cardiff University, 2009.

[168] R. K. Cheng and I. G. Shepherd, "The influence of burner geometry on premixed turbulent flame propagation," *Combustion and Flame*, vol. 85, pp. 7–26, 1991.

[169] E. Bourguignon, L. W. Kostiuk, Y. Michou, and I. Gökalp, "Experimentally measured burning rates of premixed turbulent flames," *Proceedings of the Combustion Institute*, vol. 26, pp. 447–453, 1996.

[170] C. K. Chan, K. S. Lau, W. K. Chin, and R. K. Cheng, "Freely propagating open premixed turbulent flames stabilized by swirl," *Proceedings of the Combustion Institute*, vol. 24, no. 1, pp. 511–518, 1992.

[171] R. K. Cheng, I. G. Shepherd, and L. Talbot, "Reaction rates in premixed turbulent flames and their relevance to the turbulent burning speed," *Proceedings of the Combustion Institute*, vol. 22, no. 1, pp. 771–780, 1989.

[172] F. C. Gouldin and K. V. Dandekar, "Time-resolved density measurements in premixed turbulent flames," *AIAA Journal*, vol. 22, no. 5, pp. 655–663, 1984.

[173] A. Gulati and J. F. Driscoll, "Velocity-density correlations and favre averages measured in a premixed turbulent flame," *Combustion Science and Technology*, vol. 48, pp. 285–307, 1986.

[174] C. M. Ho, K. Jakus, and K. H. Parker, "Temperature fluctuations in a turbulent flame," *Combustion and Flame*, vol. 27, pp. 113–123, 1976.

[175] K. O. Smith and F. C. Gouldin, "Turbulence effects on flame speed and flame structure," *AIAA Journal*, vol. 17, no. 11, pp. 1243–1250, 1979.

[176] R. K. Cheng, "Velocity and scalar characteristics of premixed turbulent flames stabilized by weak swirl," *Combustion and Flame*, vol. 101, no. 1-2, pp. 1–14, 1995.

[177] R. C. Aldredge, V. Vaezi, and P. D. Ronney, "Premixed-flame propagation in turbulent taylorcouette flow," *Combustion and Flame*, vol. 115, no. 3, pp. 395–405, 1998.

[178] S. S. Shy, W. J. Lin, and J. C. Wei in *17th International Colloquium on the Dynamics of Explosion and Reactive Systems*, (Heidelberg, Germany), CD ISBN 3-932217-01-2, 1999.

[179] V. R. Savarianandam and C. J. Lawn, "Burning velocity of premixed turbulent flames in the weakly wrinkled regime," *Combustion and Flame*, vol. 146, pp. 1–18, 2006.

[180] "Fluent 6.3 user's guide," 2006.

[181] N. Shelil, A. J. Griffiths, and N. Syred, "Numerical study of stability limits of premixed-swirl flame," *45th AIAA/ASME/SAE/ASEE Joint Propulsion Conference*, 2009.

[182] Y. Li, Y. Guo, and B. Xue, "Catalytic combustion of methane over M (Ni, Co, Cu) supported on ceria magnesia," *Fuel Processing Technology*, vol. 90, pp. 652–656, 2009.

[183] T. Xiao, S. Ji, H. Wang, K. S. Coleman, and M. L. H. Green, "Methane combustion over supported cobalt catalysts," *Journal of Molecular Catalysis A: Chemical*, vol. 175, pp. 111–123, 2001.

[184] L. W. Kostiuk and I. G. Shepherd, "Measuring the burning rate of premixed flames in stagnation flows," *Combustion Science and Technology*, vol. 112, pp. 359–368, 1996.

[185] H. Kobayashi, T. Kawahata, K. Seyama, T. Fujimari, and J. S. Kim, "Relationship between the smallest scale of flame wrinkles and turbulence characteristics of high-pressure, high-temperature turbulent premixed flames," *Proceedings of the Combustion Institute*, vol. 29, pp. 1793–1800, 2002.

Appendix. Selected journal and conference papers

1. Bagdanavicius A., Bowen P., Syred N., Kay P., Crayford A., Wood J., Sims G. 2010, "Burning Velocities of Alternative Gaseous Fuels at Elevated Temperature and Pressure", AIAA Journal 48(2), pp 317-329

2. Bagdanavicius A., Shelil N., Syred N., Griffiths A. J., Bowen P. J., 2010, "Premixed Swirl Combustion and Flashback Analysis with Hydrogen/Methane mixtures", 48th AIAA Aerospace Sciences Meeting, Orlando, USA, ref. AIAA-2009-1169 (submitted to Journal of Propulsion and Power)

3. Bagdanavicius A., Shelil N., Bowen P. J., Syred N., Crayford A., 2010, "Investigations Of Gaseous Alternative Fuels At Atmospheric And Elevated Temperature And Pressure Conditions", GT2010-23270, ASME Turbo Expo 2010, Glasgow, UK

Burning Velocities of Alternative Gaseous Fuels at Elevated Temperature and Pressure

A. Bagdanavicius* P. J. Bowen† N. Syred‡ P. Kay§ A. Crayford¶

Cardiff University, The Parade, Cardiff CF24 3AA, Wales, UK

G. Sims‖ J. Wood**

QinetiQ, Cody Technology Park, Ively Road, Farnborough GU14 0LX, England, UK

This study has been undertaken to investigate turbulent burning velocities of alternative gaseous fuels at elevated temperature and pressure using the established Bunsen burner method. The experiments were conducted in the industrial scale High Pressure Optical Chamber (HPOC) at the Gas Turbine Research Centre (GTRC) of Cardiff University. Five different gaseous fuels: methane, two methane - carbon dioxide mixtures and two methane - hydrogen mixtures were studied. Experiments were conducted at two different temperatures (473 K and 673 K), and two different pressures (3 bara and 7 bara). Analysis of measurements made using 100% methane showed anticipated burning velocity trends with variation in temperature and pressure. The results reported here showed reasonable agreement with the correlations proposed by Peters and Zimont et al., although the burning velocities recorded by Kobayashi et al. were somewhat higher. The stoichiometric flames considered were all purposely contained within one flame regime on the Borghi-Peters diagram namely the corrugated flamelet regime, through appropriate choice of operating conditions. Hydrogen enrichment and carbon dioxide dilution of methane show some expected trends, but others which require further consolidation and study.

*Marie Curie Researcher, Cardiff School of Engineering, The Parade, Cardiff CF24 3AA, Wales, UK.
†Professor, Cardiff School of Engineering, The Parade, Cardiff CF24 3AA, Wales, UK.
‡Professor, Cardiff School of Engineering, The Parade, Cardiff CF24 3AA, Wales, UK.
§Research Associate, Cardiff School of Engineering, The Parade, Cardiff CF24 3AA, Wales, UK.
¶Research Associate, Cardiff School of Engineering, The Parade, Cardiff CF24 3AA, Wales, UK.
‖QinetiQ, Cody Technology Park, Ively Road, Farnborough GU14 0LX, UK.
**QinetiQ, Cody Technology Park, Ively Road, Farnborough GU14 0LX, UK.

As expected, dilution of methane with carbon dioxide reduces the measured burning velocity. However, increasing pressure and temperature in this case have competing effects with temperature raising the burning velocity and pressure reducing it. Comparison of the results presented here are consistent with the qualitative trends recently reported by Kobayashi et al., but exhibit quantitative differences thought to be due to experimental and data analysis differences. Hydrogen enrichment of the methane leads to a significant increase in the measured burning velocity compared to methane, as anticipated. Comparison with the results of Shy et al. and Kido et al. show reasonable agreement with the measurements reported here, also with those of other researchers. Our measurements show that increases in temperature and pressure independently lead to increased turbulent burning velocity, with a more pronounced effect of pressure for lean flames.

Nomenclature

A	Flame area, m^2
a, b	Fraction ratio
D_{10}	Arithmetic mean diameter
h	Pixel height, mm
l_0	Integral length scale, m
Le	Lewis number
k	Number of pixel rows in the image
M	Molar mass, g/mol
$\dot{m}$	Mass flow rate, kg/s
n	Number of pixels
q'	Averaged turbulence intensity, m/s
$R(\tau)$	Autocorrelation function
r	Burner radial position, mm
S_L	Laminar burning velocity, m/s
S_T	Turbulent burning velocity, m/s
u, v	Instantaneous axial and radial velocity, m/s
$\bar{u}, \bar{v}$	Mean axial and radial velocity, m/s
u', v'	Fluctuating axial and radial velocity component, m/s
u_{rms}, v_{rms}	Axial and radial turbulence intensity, m/s
$\dot{V}$	Volume flow rate, m^3/s
w	Pixel width, mm
X	Molar fraction

Y	Mass fraction
δ_L	Laminar flame thickness, mm
φ	Equivalence ratio
τ_0	Integral time scale, s
τ	Lag time, s
ρ	Density, kg/m^3
$\rho(\tau)$	Autocorrelation coefficient

Subscript

rms	root mean square
st	stoichiometric
R	reactants

I. Introduction

INDUSTRIAL gas turbines have been increasingly used for a wide range of power generation and mechanical drive applications. However, with growing concerns regarding global warming and energy security, a new range of alternative fuels are being considered for use in such devices. Such fuels can be divided broadly into two groups; those containing methane diluted with an inert gas, often carbon dioxide in bio-derived fuels, and those containing methane enriched with hydrogen. Environmental constraints for gas turbines mean that NO_x production must also be considered implying that such fuels should be burnt using current lean premixed technology. A key parameter in the design of such systems, influencing flame stability and position, is the turbulent burning velocity.

The current study has been undertaken to investigate turbulent burning velocities of gaseous fuel mixtures with significant carbon dioxide dilution or hydrogen enrichment at elevated temperature and pressure using the established Bunsen burner method. The test programme has been carried out on behalf of a 23-partner EU progamme.[1] The aim of this work is to add to the understanding of the turbulent burning velocities of alternative fuels over a range of equivalence ratios, temperatures and pressures.

There have been many attempts to investigate laminar and turbulent methane flames,[2,3] methane and carbon dioxide mixtures,[4] methane and hydrogen mixtures[5-9] and even synthetic gas fuel mixtures[10] at atmospheric and non atmospheric conditions.

Laminar methane flames were investigated by Egolfopoulus et al.[2] under both reduced and elevated pressures using counterflow flame methodologies. Their study illustrated the influence of pressure on the laminar burning velocity, which decreases with increasing pressure. Kobayashi[3] investigated turbulent flames using a Bunsen burner technique and showed

that turbulent and laminar flame ratio S_T/S_L is pressure dependant and rises with increasing pressure. The study also showed that flame shape becomes more wrinkled at higher pressures.

The effect of carbon dioxide dilution on turbulent premixed flames was studied by Kobayashi et al.[4] using the Bunsen burner technique at elevated pressure and temperature. They reported that S_T/S_L decreased when air was diluted with CO_2 at 5 bara 573 K. This counter-intuitive result is explained principally through the effect of local flame stretch that reduces local burning velocity.

Burning rates of methane and hydrogen mixtures have been investigated previously, though few at elevated ambient conditions. Mandilas et al.[8] performed turbulent premixed flame experiments in a combustion chamber at 5 bara pressure with 5% of hydrogen by mass added to methane. The peak burning velocity occurred at $\phi = 0.85$. They concluded that hydrogen addition has a larger effect on burning velocity for lean flames and little effect for rich flames. A Bunsen burner type flame was used in the experiments of Halter et al.[6] to investigate turbulent premixed methane - hydrogen flames. An increase in S_T/S_L with hydrogen addition for elevated pressures of 3 and 5 bar was observed.

Several different methods have been utilised previously to identify the flame front of Bunsen type burner premixed turbulent flames. A popular approach to identify the average flame front is to superimpose raw flame images[3,11] and calculate the threshold based on the ensemble average of the mean and maximum signal intensities.[12]

Another common technique is to binarize raw images using bimodal intensity histograms[13] or to define the image conversion threshold value using manual or automatic methods. These binary images are subsequently averaged. The burning velocity can then be calculated using the flame cone angle method[14] or by rotating the averaged image around its central axis.[11] Most of the methods found in the literature rely on flame averaging. This flame averaging technique, the so called "Averaged Flame Shape" method, was initially applied to calculate the average flame front area for the current data-set. However, another method, a so-called "Average Flame Area" technique, was developed to process images and is considered more reliable in this study, hence utilised throughout.

II. Experimental methodology

In this experimental programme, five different gaseous fuels were tested over a range of pressures and temperatures. Approximately 20 data sets were generated for each gas mixture[a]: 100% methane, 85% methane - 15 % carbon dioxide, 70% methane - 30 % carbon dioxide, 85% methane - 15% hydrogen and 70% methane - 30% hydrogen were carried out

[a]all by volume

for lean and rich mixtures from 0.65 to 1.45 equivalence ratio at different pressures and temperatures (Table 1).

Table 1 Investigated gas mixtures

Gas mixture	CH_4, %	CO_2, %	H_2, %	Pressure, bara	Temperature, K
$100\%CH_4$	100	0	0	3, 7	473, 673
$85\%CH_4$-$15\%CO_2$	85	15	0	3, 7	473, 673
$70\%CH_4$-$30\%CO_2$	70	30	0	3, 7	473, 673
$85\%CH_4$-$15\%H_2$	85	0	15	3, 7	473, 673
$70\%CH_4$-$30\%H_2$	70	0	30	3, 7	473, 673

A. Test facility

The tests were performed in the High Pressure Optical Chamber (HPOC), integrated within the HPCR (High Pressure Combustion Rig) which is located at the Gas Turbine Research Centre (GTRC) of Cardiff University in Port Talbot, Wales, UK.

The HPOC consists of a horizontally mounted burner firing into an inner combustion chamber, enclosed within an optical pressure casing. The HPOC can operate with working pressures of up to 16 bara and inlet temperatures of up to 900 K. The pressure casing is a cylindrical geometry with four opposed quartz windows, affording excellent optical access (Fig. 1).

The optical combustion section is connected to a compressor and heat exchanger, allowing combustion air to be preheated to required operating temperatures. The inner combustion chamber is of rectangular form and has four internal quartz windows which align with the outer casing, giving full optical access to the combustion chamber. The width and the height of the combustion chamber is 150 mm. The inner combustion chamber is constructed from aero-grade stainless steel sheet allowing (if required) external cooling air to pass into the combustion chamber, mimicking the behaviour of practical gas turbine combustors. The flame is thus confined to the combustion chamber. The internal windows are continuously purged with air during the tests to ensure they are kept clear of any deposits of seed. Extensive experience with the rig shows that the windows purge has little effect on measured values. A simple Bunsen type burner is fired into the combustion chamber (diameter 25 mm). The burner is fitted with an annular pilot which supplies a methane diffusion flame to aid stability while adjusting the operating conditions. This pilot is switched off prior to making measurements.

The main burner is fed a premix of fuel and air via a turbulence mixing plate, 50 mm diameter, with 53 holes each of 1.5 mm diamter and blockage ratio 95%. This creates

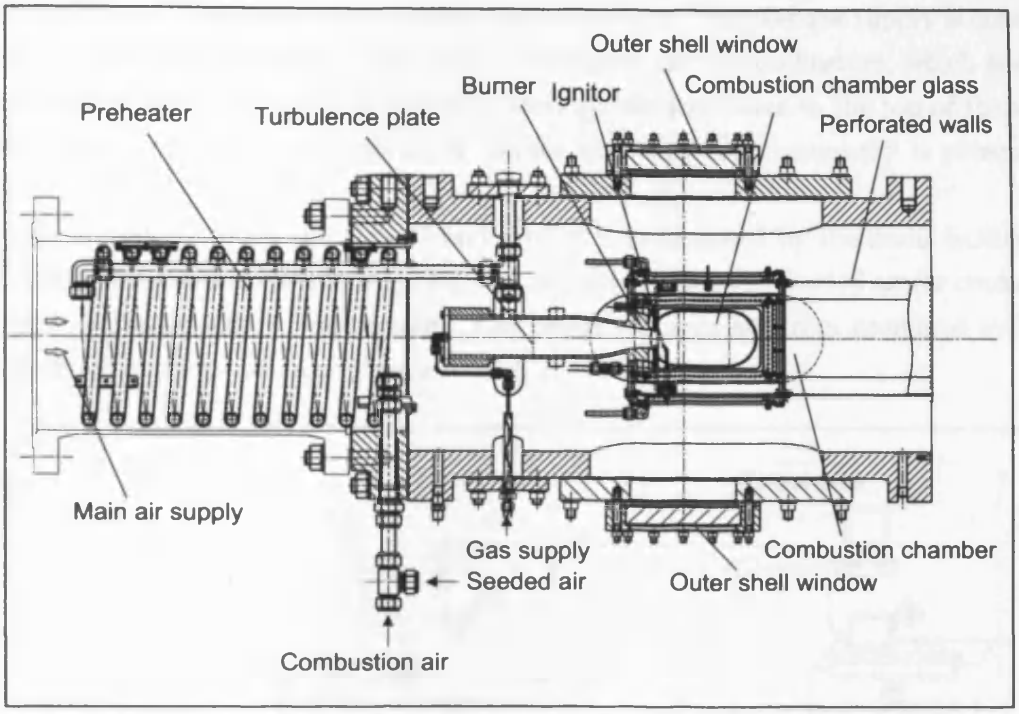

Fig. 1 Cross section of the High Pressure Optical Chamber

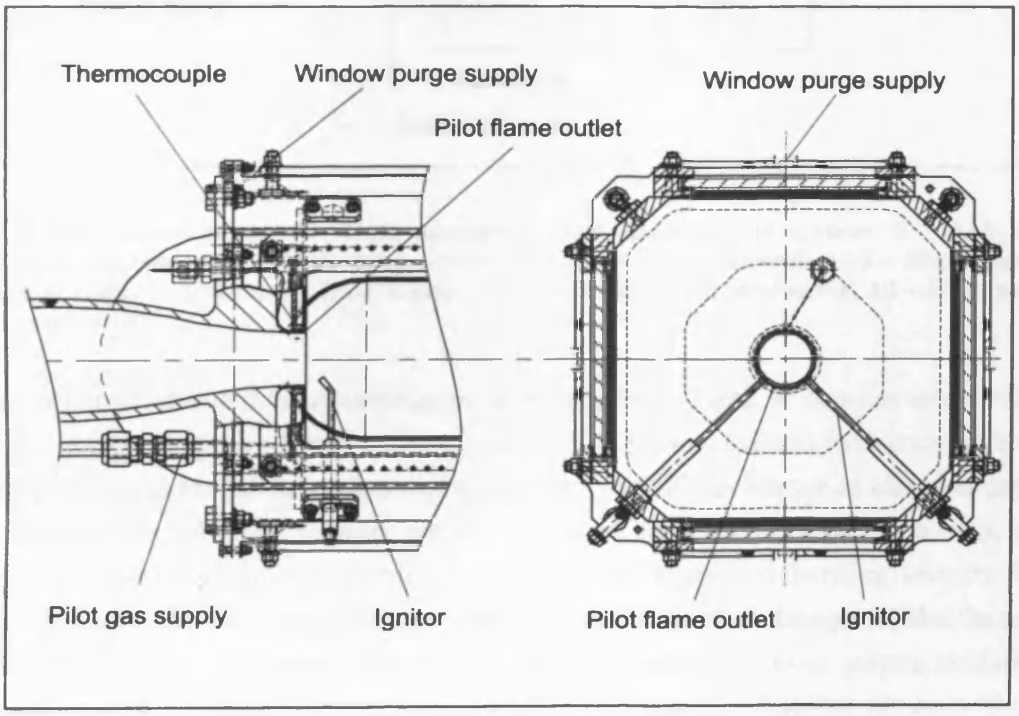

Fig. 2 Detailed combustor geometry

uniform turbulence and aids in the mixing of the reactants. The fuel gas supply is connected to a mixing chamber upstream of this plate. Preheated air for combustion, which is seeded with aluminium oxide particles[b], is delivered through the preheater to the top of the mixing chamber of the burner. A more detailed burner and combustor geometry is presented in Fig. 2.

The air supply for both the HPOC and burner is pressurised by the main facility compressor which is capable of delivering 5 kg/s at 16 bar(a) pressure. Seeded air for combustion is delivered by an auxiliary compressor. Fuel gases are supplied from premixed cylinders. The overall scheme for the rig is shown in Fig. 3.

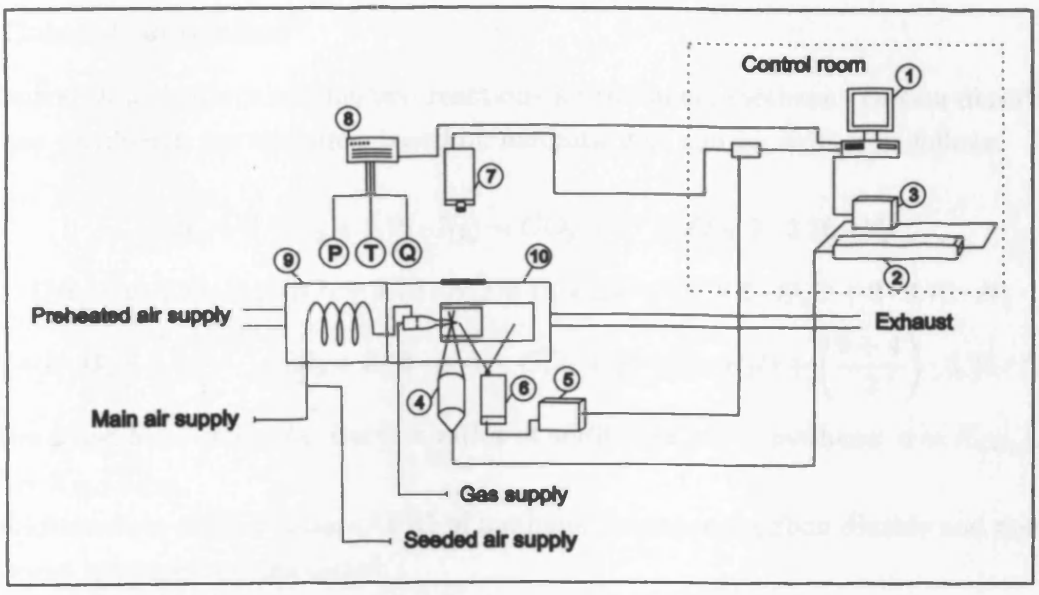

Fig. 3 Experimental setup. 1 - Data acquisition and laser control system, 2 - LDA laser, 3 - LDA laser processor, 4 - LDA laser probe, 5 - Sheet laser controller, 6 - Sheet laser, 7 - High-speed digital camera, 8 - Data logger, 9 - Combustion air preheater, 10 - High pressure optical combustor.

Two different measurement techniques were applied. First, a non-intrusive 2-D laser diagnostic technique, Laser Doppler Anemometry (LDA), was utilised to determine both the velocity profile and turbulence characteristics at the exit of the burner at elevated pressures and temperatures. A Dantec laser system was used for this purpose. Secondly, planar laser tomography was applied in order to measure the turbulent burning velocity for the different gas mixtures at a range of temperatures and pressures. Images of the flame front were recorded using a Photron APX-rs high speed camera mounted perpendicularly and synchronised with a pulsed (Nd:YAG) sheet laser. To ensure reliability for each test 1000

[b]Size $D_{10} < 1\ \mu m$

images were recorded at 10 Hz.

The experiments were run and monitored from a remote control room. LDA and laser planar tomography systems were controlled from their own dedicated computers, and the facility was controlled from its own PLC system. Fuel, combustion air and seed air were measured simultaneously using suitably ranged Coriolis flow meters. All experimental conditions, such as: pressure, temperature, air flow and gas flow were recorded by a facility data acquisition system. Measured temperatures and pressures were reasonably steady with fluctuations not exceeding 5% and 3% of the nominal values for pressure and temperature respectively.

B. Calculation method

General stoichiometric combustion reactions for methane, methane - carbon dioxide and methane - hydrogen gas mixtures, based on methane gas, can be written as follows:

$$CH_4 + 2 \cdot (O_2 + 3.76 \cdot N_2) = CO_2 + 2 \cdot H_2O + 2 \cdot 3.76 \cdot N_2 \quad (1)$$

$$CH_4 + a \cdot CO_2 + 2 \cdot (O_2 + 3.76 \cdot N_2) = (a+1) \cdot CO_2 + 2 \cdot H_2O + 2 \cdot 3.76 \cdot N_2 \quad (2)$$

$$CH_4 + b \cdot H_2 + \left(\frac{b+4}{2}\right) \cdot (O_2 + 3.76 \cdot N_2) = CO_2 + (b+2) \cdot H_2O + \left(\frac{b+4}{2}\right) \cdot 3.76 \cdot N_2 \quad (3)$$

Here a and b are the molar fraction ratios of additional gas in methane: $a = X_{CO_2}/X_{CH_4}$ and $b = X_{H_2}/X_{CH_4}$.

Stoichiometric air fuel ratios (AFR) of methane, methane - carbon dioxide and methane - hydrogen mixtures are calculated:

$$AFR_{st}^{CH_4} = \frac{2 \cdot (M_{0_2} + 3.76 \cdot M_{N_2})}{M_{CH_4}} \quad (4)$$

$$AFR_{st}^{CH_4-CO_2} = \frac{2 \cdot (M_{0_2} + 3.76 \cdot M_{N_2})}{M_{CH_4} + a \cdot M_{CO_2}} \quad (5)$$

$$AFR_{st}^{CH_4-H_2} = \frac{\left(\frac{b+4}{2}\right) \cdot (M_{0_2} + 3.76 \cdot M_{N_2})}{M_{CH_4} + b \cdot M_{H_2}} \quad (6)$$

The mass flow rate of gas mixture and air is measured and the equivalence ratio is calculated thus:

$$\phi = \frac{AFR_{st}}{\dot{m}_{air}/\dot{m}_{fuel}} \quad (7)$$

The tests were performed using a Bunsen type burner, thus, the tested flames were "Envelope" category flames. This means that the flame forms an envelope around the reactants and all reactants must pass through the flame.[15] Thus the burning velocity is

related to global consumption speed[16] and is calculated by the formula:

$$S_T = \frac{\dot{m}_R}{\rho_R \cdot A} = \frac{\dot{V}}{A} \tag{8}$$

It has been proposed that the consumption speed should be used to define the turbulent burning velocity[17] and that only flames within a particular category should be compared because the flame wrinkling process can be different for different flame types.[18] However in our study we compared "envelope" category flames as well as "spherical" type flames, due to the lack of research performed at elevated pressures and temperatures for the studied gas mixtures.

The exit velocity from the burner of the gas-air mixture is derived from the mass flow of combustion air, seed air and fuel flows, and displayed and logged simultaneously by the data acquisition system. Density, viscosity, diffusion coefficients and other gas properties of the combustible mixture at the required temperature and pressure were calculated using polynomial fit coefficients available within the CHEMKIN database or taken from reference tables. Lewis number, defined as the ratio of thermal diffusivity of the mixture and mass diffusivity of deficient species, was calculated for all mixtures considered.

The CHEMKIN-PRO software and GRI-Mech 3.0 reaction mechanism were used to calculate laminar burning velocities and flame thicknesses for the various gas mixtures at different pressures, temperatures and equivalence ratios. The laminar flame thickness calculation method was based on a classical approach of defining temperature gradient and agreed well with findings of Lafay et al.,[19] whom made hydrogen enriched methane-air flame thickness measurements. These results support the computational results obtained using the GRI-Mech 3.0 reaction mechanism for equivalence ratios above 0.55.

C. Measurement Technique

The LDA results were utilised to ensure that turbulence intensity and burner exit velocity profiles are uniform and to find integral time scales of turbulence. The velocity and turbulence profiles of isothermal air flow, seeded with aluminium oxide particles, were measured 10 mm downstream of the burner exit across the burner axis on the centreline plane. The axial and radial velocities were recorded for a range of exit velocities at ambient pressures of 3 and 7 bara and temperatures of 473 K to 673 K. LDA data processing was carried out using DANTEC Flow manager software. The autocorrelation coefficient $\rho(\tau)$ was calculated thus:

$$\rho(\tau) = \frac{R(\tau)}{R(0)} = \frac{\overline{u'(t)\,u'(t+\tau)}}{u_{rms}^2} \tag{9}$$

where τ is the time lag, $R(0)$ is the correlation estimated at lag time zero, $R(\tau)$ is the estimated correlation. From the autocorrelation coefficient the integral time scale τ_0 was found:

$$\tau_0 = \int_0^\infty \rho(\tau)\, d\tau \tag{10}$$

Then assuming that the field has uniform mean velocity and accepting Taylor's hypothesis the integral length scale can be computed from the formula:

$$l_0 = \bar{u} \cdot \tau_0 \tag{11}$$

It was assumed that the flow is statistically axis-symetric, therefore radial and circumferential root mean square velocities are equal, thus the total turbulence intensity can be calculated:

$$q' = \sqrt{\frac{u_{rms}^2 + 2 \cdot v_{rms}^2}{3}} \tag{12}$$

Measured velocities and turbulence characteristics data of isothermal air flow at different conditions later have been used to define velocities and turbulence parameters for every particular gas mixture.

D. Flame Imaging

The planar laser tomography technique used in this study is based on the observation that the density of the products is lower than that of the reactants. Consequently when the uniformly seeded reactants are converted to products the seed density reduces and the scattered light intensity falls. As the flame thickness is small, a clear demarcation is generated between products and reactants which can be identified as the flame front.

First, all raw flame images are averaged (Fig. 4, a) using a bespoke MATLAB script. Then a set of the background images (taken at the end of the test when the flame is no longer present) are averaged using the same image processing technique (Fig. 4, b). The average background image is then subtracted from the average flame front image (Fig. 4, c). The average flame front image is converted to the binary image using a defined threshold value (Fig. 4, d).

However, the "Averaged Flame Shape" method based on raw images is reliant on user interpretation of the results before defining the threshold value, which could introduce systematic errors. Also, it was observed that the flame front was very irregular in shape for all experiments independent of pressure and temperature. Hence this technique is considered unrepresentative for calculating the average flame front area from the average flame shape

based on raw flame images.

As is seen from the image (Fig. 4, c), due to the different levels of light, the conversion from a grey scale image to the binary image could be misinterpreted. Although the threshold value can be selected manually or automatically, using an image processing technique, subjectivity cannot be eliminated. Hence a more robust method for calculating the area of the flame front was developed, the so called "Averaged Flame Area" method.

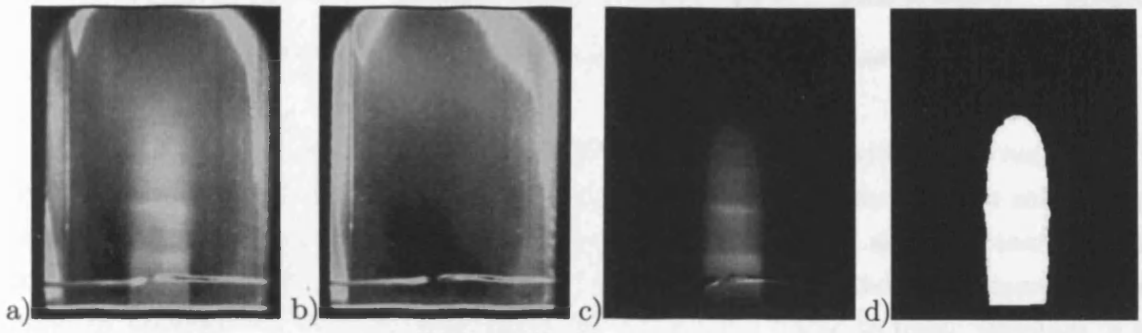

Fig. 4 "Averaged Flame Shape" method based on raw images. a) - averaged flame image, b) - averaged background image, c) - averaged flame image background subtracted, d) - converted binary image.

In this method, the area of each single flame image was calculated using MATLAB. First, each individual image was filtered, using morphological image processing techniques and median filters, and the background subtracted. Subsequently the greyscale image is converted into a binary image using manually selected threshold values. Different threshold values are required for each test case, due to the variance of background noise and seed rates. After conversion of the grey scale images (Fig. 5) to the binary images (Fig. 6) the pixels of the flame area of every single image are counted and flame area calculated.

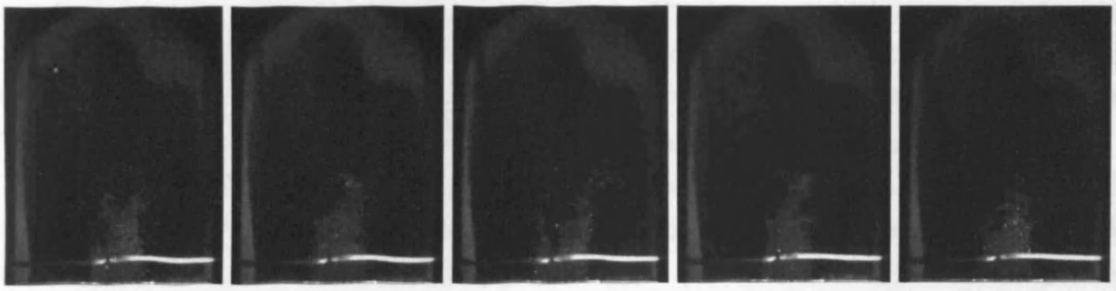

Fig. 5 Raw methane-hydrogen mixture flame images.

Flame area of each individual flame image is calculated using:

$$A = \sum_{1}^{k} (\pi \cdot n_k \cdot h \cdot w) \tag{13}$$

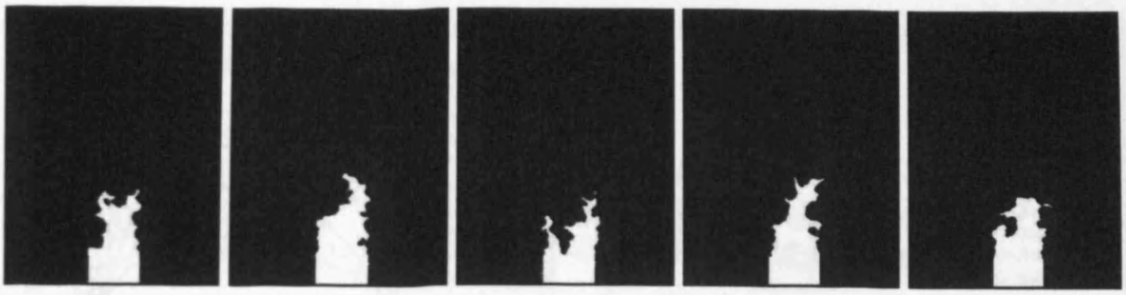

Fig. 6 Processed binary methane-hydrogen mixture flame images.

Here n - number of pixels; h - pixel height 0.353 mm; w - pixel width 0.353 mm, the pixel height and width were found by imaging a scale within the test section. To calculate the flame area each row of pixels within the image were then "rotated" around it own centreline axis. The side area of every cylinder made of pixels was calculated and summed. It was found by applying this method that there was substantial frame to frame variation in the surface area of the flames at a single operating point. In order to calculate the average turbulent burning velocity for each condition the statistical software MINITAB was applied. Using this approach it was possible to identify and reject all results which were outside the limit of two standard deviations. A new mean flame area could then be found and finally the turbulent burning velocity calculated.

III. Results and Discussion

A. Isothermal LDA Results

Figure 7 shows the variation of mean axial velocity and velocity fluctuations respectively with radial position for a range of exit velocities. The two vertical lines at radial position r = 12.5 mm and r = -12.5 mm represent the burner edges. Overall the results show that the axial velocity profiles are uniform, confirming the suitability of the burner for this study. Pressure has little effect on axial velocity and axial velocity fluctuations.

Using LDA, 5000 samples were collected at each position across the centre of the burner (radial position $r = -9 \div 9$ mm) at each condition. Due to the flow stream shape the seeding rate was somewhat lower at the edges of the burner ($r = 9 \div 13$ mm). The relative error did not reach 0.5% for the measurements in the centre of the burner and did not exceed 3% for the measurements at the edges of the burner. The data validation rate was above 90% during all tests.

LDA measurements of the isothermal flow showed that, in agreement with others,[20] turbulence intensity is almost insensitive to variation in pressure and temperature. Figure 8 shows that the turbulence intensity q' measured at the burner radial position r = 12 mm

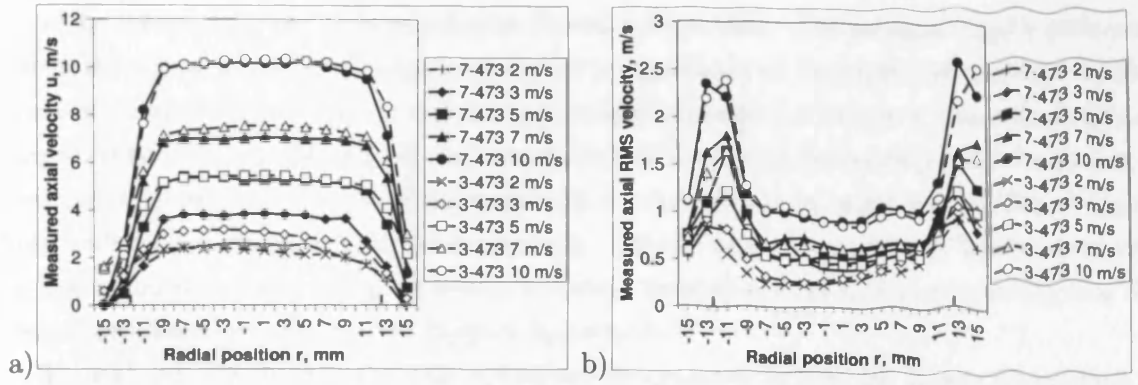

Fig. 7 Axial mean velocity $\bar{u}$ and axial RMS velocity u_{rms} measured 10 mm downstream burner exit at different bulk gas flow velocities. Velocities indicated in the legend represents bulk exit velocity at 3 bara 473 K (3-473) and 7 bara 473 K (7-473), a) axial mean velocity; b) axial RMS velocity.

shows a dependence on bulk flow velocity. During the experiments bulk exit velocity varied between 4 to 16 m/s and thus turbulence intensity values at different bulk flow velocities were interpolated from this correlation.

The evolution of relative turbulence intensity as a function of bulk flow velocity is represented in Fig. 9. The increase in relative turbulence intensity, $q'/\bar{u}$, at low bulk flow velocities is clearly seen from the graph.

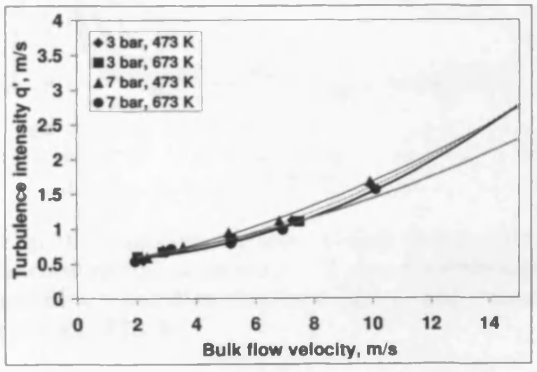

Fig. 8 Turbulence intensity, q', measured at radial position $r = 12$ mm, depending on bulk gas flow velocity at different at different temperatures and preasures: 3 bara (grey), 7 bara (black).

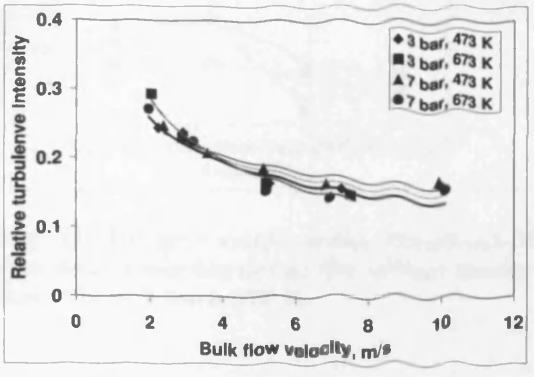

Fig. 9 The evolution of relative turbulence intensity, $q'/\bar{u}$, depending on bulk gas flow velocity at different temperatures and preasures: 3 bara (grey), 7 bara (black).

Data obtained by LDA were used to derive one point temporal velocity correlation and calculate the integral time scale and integral length scale of the turbulent isothermal flow at different pressures, temperatures and bulk flow velocities. 1024 correlation samples and a lag time $\tau = 100$ ms were chosen to find autocorrelation coefficients. The integral time scale was

found by integrating the autocorrelation function over time. The integral length scale was calculated using formula 11, based on Taylor's hypothesis of isotropic turbulence. As this frozen-turbulence hypothesis is a good approximation only if $q'/\bar{u} << 1$, the calculation of integral time scale should only be performed where the velocity fluctuation is relatively low.[21] Two point spatial velocity correlation should be carried out in order to calculate integral time scale where stronger turbulence prevails. Spatial and temporal correlation agree well for low turbulence flows, whilst strong streamline development of turbulence invalidates the frozen-turbulence assumption of Taylor's hypothesis.[22]

Typical autocorrelation function curves are represented in Fig. 10. It was found that at 10 m/s bulk exit velocity at 7 bara, 473 K and 673 K conditions, few data points around the centre of burner exit correlated, while others oscillated and did not cross zero or weakly correlated. The same behaviour was observed processing LDA data taken from the data points close to the burner rim ($r \approx 12$ mm). This could be due to increased normalized turbulence intensity (relative turbulence intensity) $q'/\bar{u}$ invalidating Taylor's frozen-turbulence theory. This data for this condition is not typical.

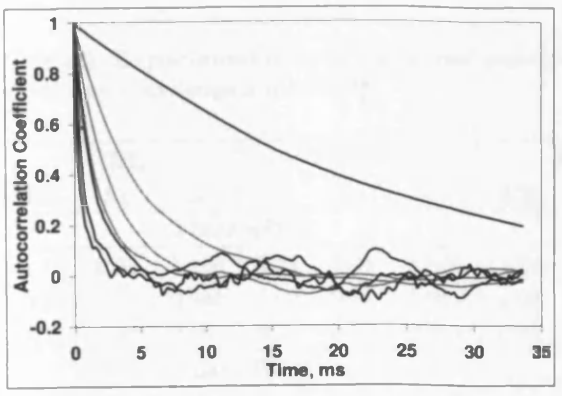

Fig. 10 Autocorrelation coefficient curves at burner radial position r = 3 mm for different gas flow velocities at 3 bara (grey) and 7 bara (black), 673 K.

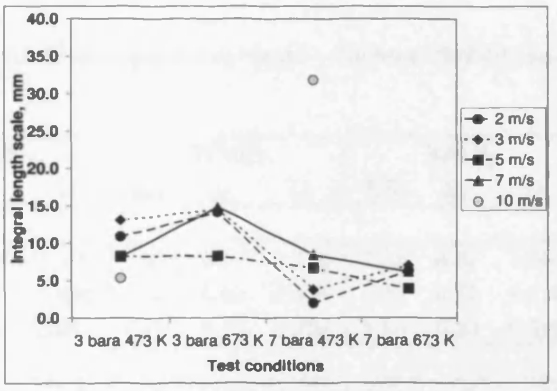

Fig. 11 Integral length scales measured 10 mm dowstream burner at the burner centerline exit at 7 bara 673 K.

Averaged integral length scale data obtained from autocorrelation coefficients measured at different burner radial position $r < 5$ mm are presented in Fig. 11. Only correlated values have been used to process integral time scale and length scale. The data are consistent at 3 bara, 473 K conditions for all exit velocities. In this case the integral length scale l_0 is between 5 to 13 mm. At 3 bara 673 K the integral length scale increases up to 15 mm. At 7 bara pressure the integral length scale reduces to a maximum of 10 mm for all exit velocities except for the aforementioned 10 m/s exit velocity case. For the other exit velocities the increase in pressure reduces integral length scale slightly to 2.5 mm - 10 mm.

The differences in the integral length scale results appears to arise from a number of

interacting factors. Although the mean axial velocity profiles follow well known similarity trends, this is not so with the turbulence (Fig. 9), which clearly shows much higher levels of relative turbulence intensity at low bulk flow velocities with a somewhat weaker effect due to pressure and temperature. These results translate into the shown variation of integral length scale and seem to arise from variations in the jet potential core and the generated shear flow on its boundary. Reynolds number effects are clearly important, the lowest value being around 2400 (2 m/s, 3 bar, 673 K), up to 58000 (10 m/s, 7 bar, 473 K), and do affect such jets in the lower Reynolds numbers ranges. Unfortunately for such measurements it is impossible to obtain higher Reynolds numbers without the use of very much larger throughput rigs allowing larger diameter jets to be used.

B. Turbulent burning velocity

This study has investigated a range of flames at elevated temperatures and pressures. Laminar burning velocities, calculated using CHEMKIN, and Lewis numbers for different gas mixtures at different temperatures and pressures are presented in Table 2.

Table 2 Experimental conditions and results of 100% methane, methane - carbon dioxide and methane - hydrogen mixtures

CH_4			$15\%CO_2$			$30\%CO_2$			$15\%H_2$			$30\%H_2$		
ER	S_L	Le	ER	S_L	Le	ER	S_L	Le	ER	S_L	Le	ER	S_L	Le
		3 bara 473 K												
1.18	0.52	1.106	1.21	0.41	1.096	1.20	0.33	1.083	1.22	0.54	1.145	1.24	0.61	1.194
0.96	0.56	0.948	1.04	0.50	1.096	1.02	0.41	1.084	1.00	0.62	0.725	1.01	0.71	1.178
0.75	0.37	0.954	0.71	0.29	0.951	0.74	0.27	0.944	0.82	0.48	0.724	0.90	0.63	0.593
		7 bara 473 K												
1.20	0.32	1.106	1.39	0.14	1.096	1.18	0.21	1.083	1.23	0.32	1.145	1.23	0.40	1.193
1.01	0.39	1.105	1.20	0.26	1.096	0.99	0.27	0.935	1.06	0.42	1.139	0.99	0.48	0.596
0.78	0.24	0.953	0.81	0.25	0.948	0.76	0.18	0.944	0.86	0.34	0.724	0.85	0.39	0.592
		3 bara 673 K												
1.14	1.16	1.104	1.25	0.86	1.094	1.17	0.82	1.081	1.19	1.23	1.139	1.25	1.30	1.187
1.04	1.20	1.103	1.03	1.07	1.094	1.03	0.91	1.082	1.02	1.31	1.134	0.99	1.46	0.595
0.73	0.82	0.948	0.79	0.86	0.942	0.74	0.68	0.937	0.82	1.08	0.722	0.82	1.21	0.591
		7 bara 673 K												
-	-	-	1.19	0.67	1.094	1.20	0.52	1.081	1.22	0.81	1.140	1.22	0.93	1.186
-	-	-	1.04	0.76	1.094	1.01	0.63	1.082	1.03	0.94	1.134	1.01	1.03	1.172
-	-	-	0.77	0.56	0.942	0.78	0.50	0.936	0.79	0.69	0.722	-	-	-

Only values close to the stoichiometric conditions are listed in order to show the variation trends of S_L and Lewis number.

For pure methane gas, the methane diffusion coefficient to the multi-component mixture

consisting of nitrogen and oxygen was calculated for lean mixtures. For rich mixtures oxygen diffusion to the mixture was calculated. For methane carbon dioxide mixtures methane was taken as the deficient component for lean mixtures and oxygen for the rich ones. However for methane carbon dioxide mixture the methane diffusion to the three component mixture (nitrogen, oxygen, carbon dioxide) was assumed. For methane and hydrogen gases methane and hydrogen were deficient species for lean mixtures and oxygen was the deficient gas for the rich mixtures.

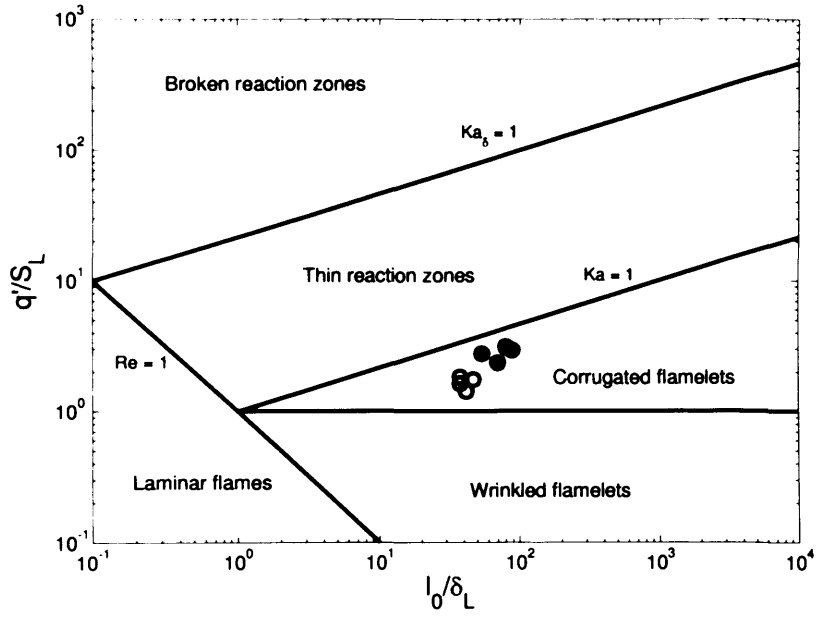

Fig. 12 Borghi - Peters diagram plotted on the logarithmic scale. Empty circles represent 3 bara 473 K, full circles - 7 bara 473 K conditions; CH_4 gas, and $CH_4 - CO_2$ and $CH_4 - H_2$ mixtures.

Lewis number of methane for all equivalence ratios was close to unity for the conditions considered. Lewis number decreased slightly with CO_2 addition compared with 100% methane. The most significant change in Lewis number are observed for methane hydrogen mixtures. Temperature and pressure had negligible effect on Lewis number.

To identify combustion regime, the flames studied under stoichiometric combustion are plotted on the Borghi diagram (Fig. 12). Turbulence intensity q', turbulent length scale l_0, obtained from our experiments (Figs. 8 and 11), and laminar flame thickness δ_L, laminar burning velocity S_L, obtained from CHEMKIN, have been used to calculate the data points. The graph shows that all the flames are within the 'corrugated flamelet regime'. This is consistent with the aims of the project as it was undesirable to produce flames located in different regions of the Borghi diagram, for instance higher temperatures may well have moved the operating regime to that of 'wrinkled flamelets'.

A pilot flame was required to stabilize the main flame for some cases of lean methane - carbon dioxide mixtures and with lean methane for all pressures and temperatures. This pilot was switched off before taking images. Methane - hydrogen mixtures stabilised easily for all conditions, and the pilot flame was not required. The methane - hydrogen flames were found to be much more stable. No significant change in flame shape was noticed when comparing methane, methane - carbon dioxide and methane - hydrogen mixtures, although increased wrinkledness of the methane - hydrogen flames was observed, as anticipated.[8]

1. Turbulent burning velocity measurements

Turbulent burning velocity dependance on the equivalence ratio of different gas mixtures are presented in Figs. 13, 14, 15 and 16. Methane data are presented in all graphs as a benchmark indicator. The turbulent burning velocity, S_T, has been normalised by the methane turbulent burning velocity at $\phi = 0.96$, 3 bara and 473 K, obtained in experiments. Trendlines are plotted through each data set. Only one test for each condition was conducted. The relative errors of the burning velocities, computed from the flame images, were below 1%, therefore the error bar were not determined. The graphs are grouped so that the dependence of S_T on pressure (Figs. 13 and 15) and temperature (Figs. 14 and 16) can be shown. Normalised S_T of methane and methane - carbon dioxide mixtures are presented in Figs. 13 and 14, and methane and methane - hydrogen mixtures in Figs. 15 and 16.

The peak of S_T of methane is observed at $\phi = 1$ - 1.1 at all conditions. When the methane air mixture at 3 bara is preheated to 673 K the burning velocity rises by approximately 55-60% in comparison with the methane burning velocity at 473 K at $\phi = 1$ (Fig. 13, a). For $\phi = 1.2$ the increase in S_T is around 50%. At $\phi = 0.8$, 70% increase in S_T is observed at 3 bara pressure. Tha data consistently show that temperature has a stronger effect on S_T for lean mixtures than for rich.

Increasing ambient pressure from 3 bara to 7 bara at 473 K reduces methane turbulent burning velocity by approximately 15-20% at $\phi = 1$ (Fig. 14, a). For the same temperature at $\phi = 1.2$ the increase in S_T is about 10%. Increased pressure has more influence for lean methane - air mixtures than is observed for rich ones.

The peaks of S_T of methane - carbon dioxide mixtures are observed at $\phi = 1$ - 1.1 at all conditions. For the higher temperatures, the peak of S_T is slightly shifted to richer mixtures. Small amounts of carbon dioxide added to methane did not change the mixture burning velocity significantly at 3 bara 473 K across all equivalence ratios (Fig. 13, a). The turbulent burning velocity of $85\%CH_4 - 15\%CO_2$ mixture remained virtually unchanged at this condition. However a decrease in S_T by approximately 20% is measured at 3 bara 673 K for $\phi = 0.8$ (Fig. 13, a) in comparision with pure methane. S_T of $85\%CH_4 - 15\%CO_2$ for rich mixtures ($\phi > 1.1$) at 3 bara 673 K are slightly higher than S_T of pure methane. This

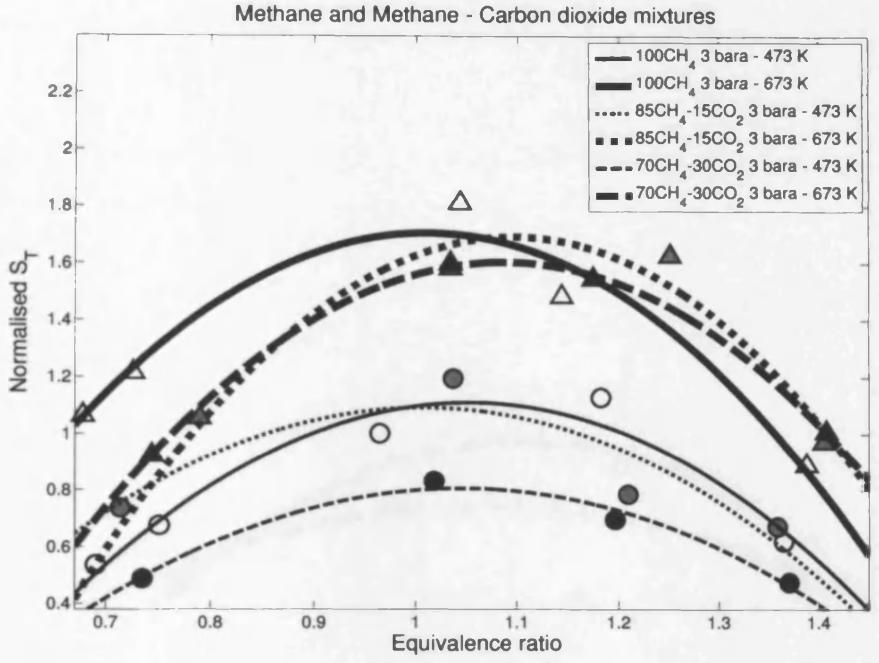

a)

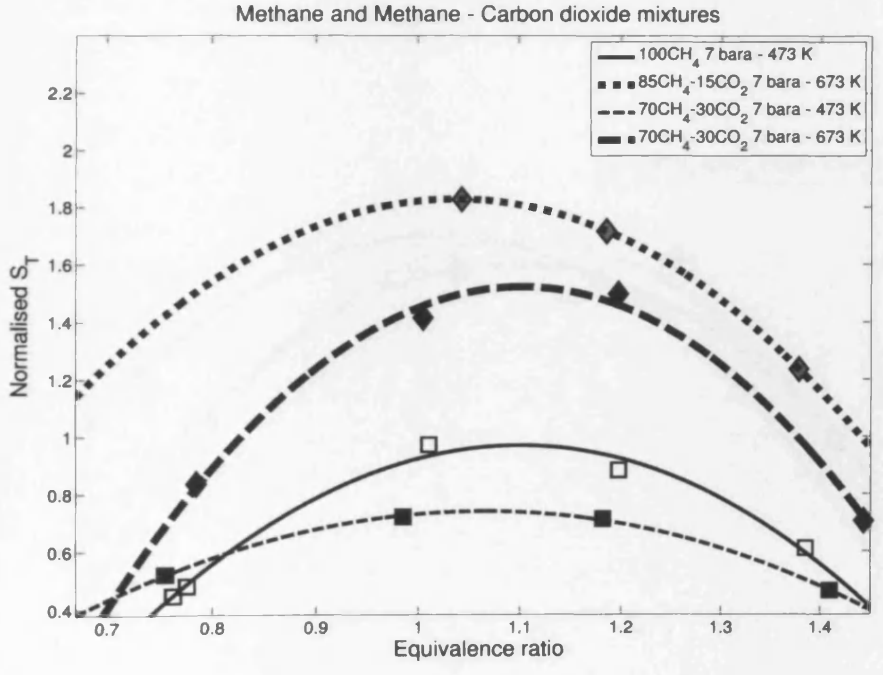

b)

Fig. 13 Normalised burning velocity of methane and methane - carbon dioxide mixtures at different pressures. a) 3 bara pressure; b) 7 bara pressure. Symbols: ○ - 3 bara 473 K, △ - 3 bara 673 K, □ - 7 bara 473 K, ◊ - 7 bara 673 K, blank - CH_4, grey - $85\%CH_4 - 15\%CO_2$, black - $70\%CH_4 - 30\%CO_2$.

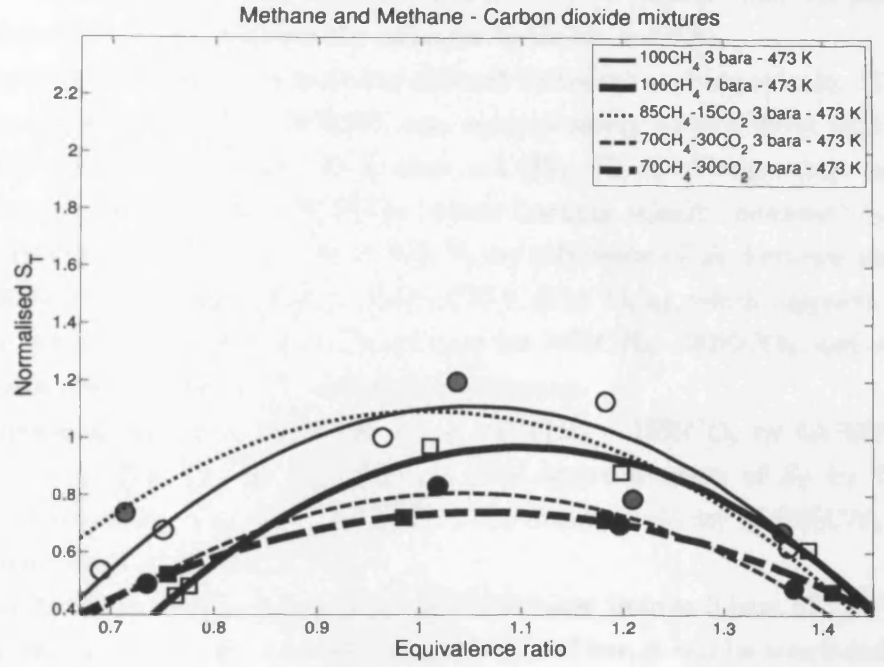

a)

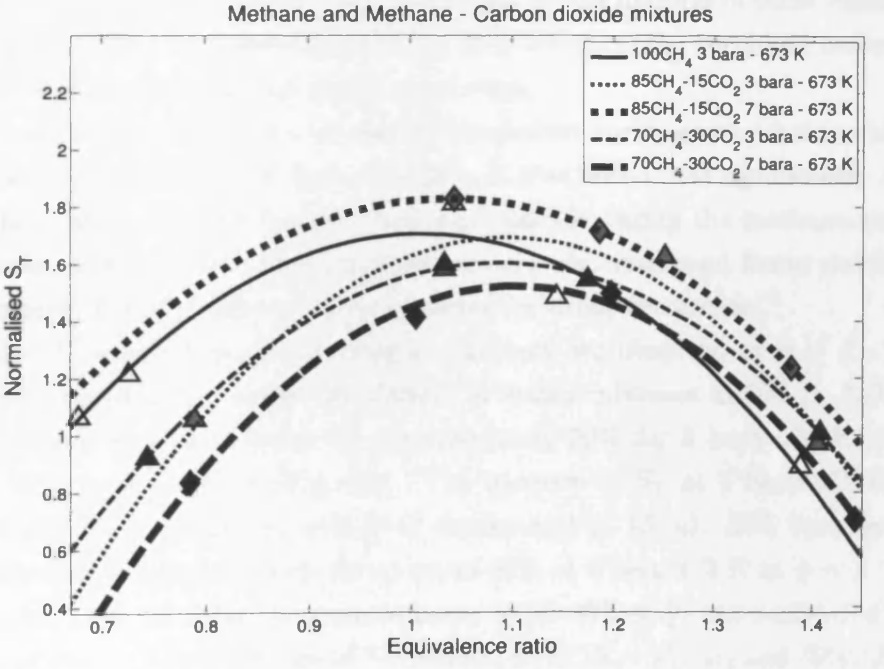

b)

Fig. 14 Normalised burning velocity of methane and methane - carbon dioxide mixtures at different temperatures. a) 473 K temperature; b) 673 K temperature. Symbols: ◯ - 3 bara 473 K, △ - 3 bara 673 K, □ - 7 bara 473 K, ◊ - 7 bara 673 K, blank - CH_4, grey - $85\%CH_4 - 15\%CO_2$, black - $70\%CH_4 - 30\%CO_2$.

implies that temperature effect on CO_2 enriched methane is stronger than for pure methane for rich mixtures ($\phi > 1.1$), whereas the converse holds for $\phi < 0.8$.

30% carbon dioxide content in methane reduced turbulent burning velocity. The burning velocity recorded for $70\%CH_4 - 30\%CO_2$ was approximately 20-25% lower than that measured for pure methane at 3 bara 473 K at $\phi = 1$ (Fig. 13, a). Temperature increase had a bigger influence for $70\%CH_4 - 30\%CO_2$, where burning velocity increased by 100-110% at 3 bara pressure at $\phi = 1$. At 3 bara 473 K the difference of S_T between methane and $70\%CH_4 - 30\%CO_2$ was higher than at 3 bara 673 K (Fig. 13, a), which supports the conclusion that the temperature effect on S_T is stronger for $70\%CH_4 - 30\%CO_2$, and temperature effect rises with the increase of CO_2 content in methane.

The temperature increase raised the S_T of $85\%CH_4 - 15\%CO_2$ by 60-70% at 3 bara pressure at $\phi = 1$ (Fig. 13, a). However an even larger increase of S_T by 70-80% was observed at 3 bara at $\phi = 1.2$. At 7 bara 673 K, the burning velocity of $85\%CH_4 - 15\%CO_2$ is slightly higher than at 3 bara 673 K.

The S_T of $70\%CH_4 - 30\%CO_2$ at 7 bara 673 K is lower than at 3 bara 673 K (Fig. 14, b). However the difference does not exceed 5% at $\phi = 1.1$. Thus, it can be concluded that there is a consistent trend for the effect of pressure on turbulent burning velocity of methane and methane carbon dioxide mixtures. This is supported by the findings of other researchers who have been reported that increased pressure has little effect on the turbulent burning velocity of methane,[11] and methane carbon dioxide mixtures.[7]

Hydrogen addition to methane increased the turbulent burning rate considerably (Fig. 15). Hydrogen addition also improved flame stability. It was noted that significantly leaner mixtures could be stabilised on the burner than was possible during the methane and methane - carbon dioxide experiments. Temperature increase also improved flame stability. These trends are expected, and similar to those reported by other researchers.[5]

The peaks of S_T of methane - hydrogen mixtures are observed at $\phi = 1$ - 1.1 at 473 K temperature, however the peaks are shifted to leaner mixtures at 673 K. 15% hydrogen addition increased burning velocity by approximately 20% for 3 bara 473 K at $\phi = 1$ in comparison with pure methane (Fig. 15). The increase of S_T at 3 bara 673 K at $\phi = 1$ was about 40-45% in comparison with pure methane (Fig. 15, a). 30% hydrogen addition increased turbulent burning velocity by up to 45-50% at 3 bara 473 K at $\phi = 1$ (Fig. 15) in comparison with pure methane. A larger increase by 80-90% of S_T was realised at 7 bara 473 K conditions at $\phi = 1$. The difference of S_T between $85\%CH_4 - 15\%H_2$ and $70\%CH_4 - 30\%H_2$ at 3 bara and 7 bara 473 K was about 15-20% (Fig. 16, a), and about 25-30% at 3 bara and 7 bara 673 K for stoichiometric mixtures (Fig. 16, b). Therefore it implies that the augmentation of S_T of methane - hydrogen mixtures are more susceptible to temperature increase, than for pure methane at stoichiometric conditions. The largest difference between

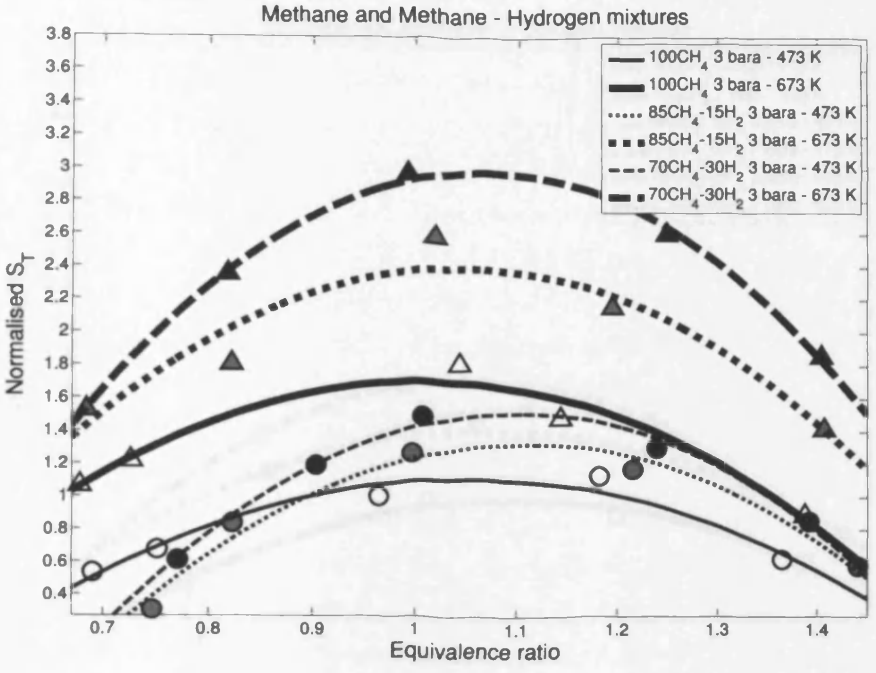

a)

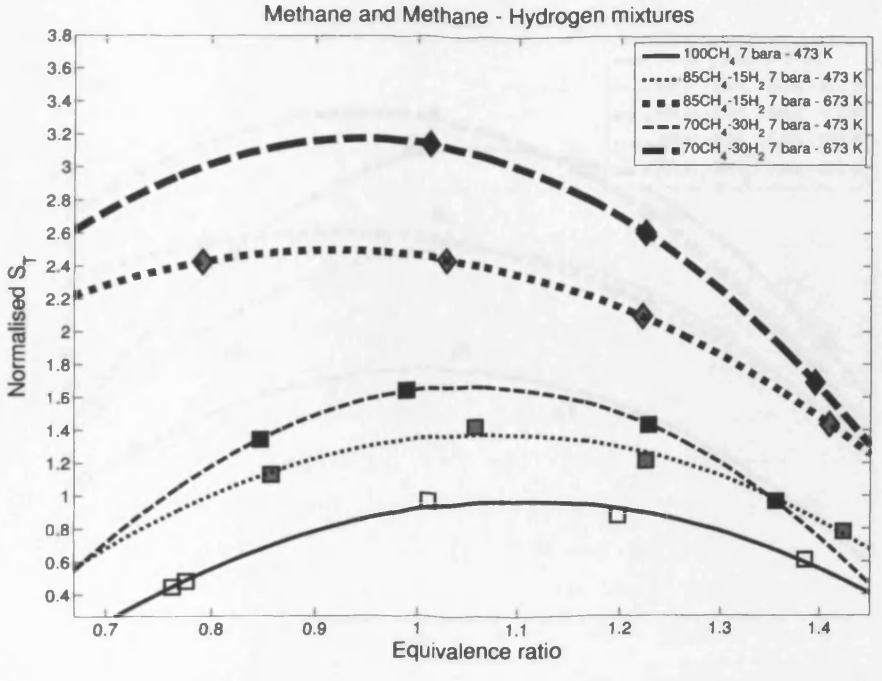

b)

Fig. 15 Normalised burning velocity of methane and methane - hydrogen mixtures at different pressures. a) 3 bara pressure; b) 7 bara pressure. Symbols: ○ - 3 bara 473 K, △ - 3 bara 673 K, □ - 7 bara 473 K, ◊ - 7 bara 673 K, blank - CH_4, grey - $85\%CH_4 - 15\%H_2$, black - $70\%CH_4 - 30\%H_2$.

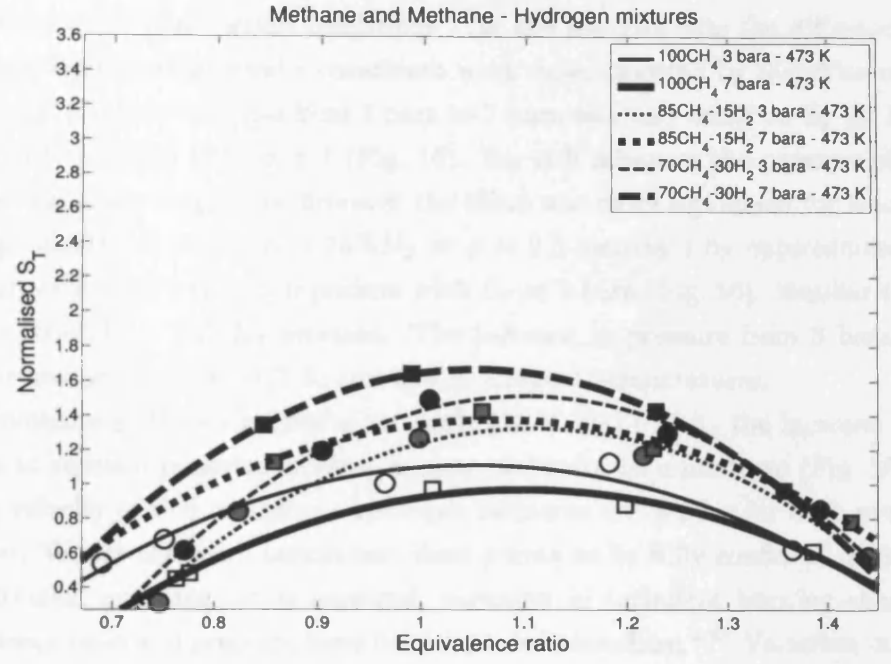

a)

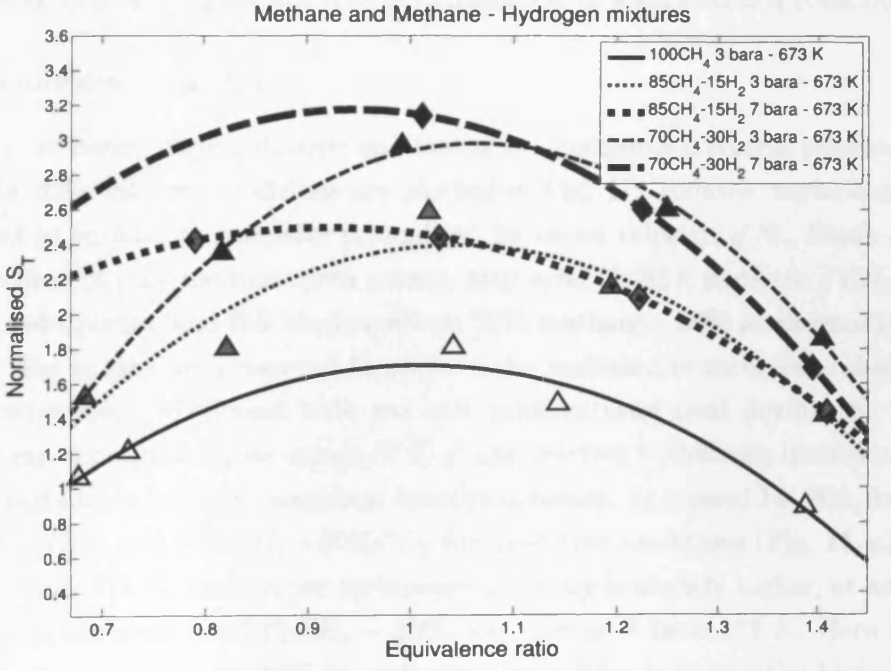

b)

Fig. 16 Normalised burning velocity of methane and methane - hydrogen mixtures at different temperatures. a) 473 K temperature; b) 673 K temperature. Symbols: ○ - 3 bara 473 K, △ - 3 bara 673 K, □ - 7 bara 473 K, ◊ - 7 bara 673 K, blank - CH_4, grey - $85\%CH_4 - 15\%H_2$, black - $70\%CH_4 - 30\%H_2$.

burning velocity rates of methane and different methane hydrogen mixtures was found to be around stoichiometric combustion conditions. On the fuel-rich side the difference becomes smaller. These trends are generally consistent with those reported by Mandilas et al.[8]

The effect of pressure increase from 3 bara to 7 bara was very small on S_T for $85\%CH_4 - 15\%H_2$ at 473 K and 673 K at $\phi = 1$ (Fig. 16). For rich mixtures the pressure effect at the same temperatures was negligible, however the effect was more significant for lean mixtures. The burning velocity of $85\%CH_4 - 15\%H_2$ at $\phi = 0.8$ increased by approximately 65% at 473 K, and by 40% at 673 K in comparison with S_T at 3 bara (Fig. 16). Similiar trends were observed for $70\%CH_4 - 30\%H_2$ mixture. The increase in pressure from 3 bara to 7 bara raised S_T for lean mixtures at 473 K and 673 K ambient temperatures.

For all methane-hydrogen mixtures, at both 473 K and 673 K, the increase in burning velocity due to ambient pressure increase is appreciable for lean mixtures (Fig. 16), whereas the burning velocity of rich methane - hydrogen mixtures are similar for both pressures and temperatures. Whilst there are insufficient data points to be fully confident of these trends and more detailed investigation is required, variation in turbulent burning characteristics with equivalence ratio and pressure have been reported elsewhere.[9,23] Variation in Markstein number and the influence of the preferential diffusion at different pressures and equivalence ratios are likely to play a significant role in explanation of such trends if consolidated.

2. Relative turbulence intensity

Methane, methane - carbon dioxide and methane - hydrogen mixtures relative tubulence intensities for different test conditions are plotted in Fig. 17. Relative turbulence intensity is represented as turbulence intensity normalised by mean velocity, $q'/\bar{u}$. Blank symbols in the graphs represent pure methane data points, grey symbols 85% methane - 15% additional gas mixture data points, and full black symbols 70% methane - 30% additional gas mixture data points. The graphs are presented to indicate the variation in turbulence characteristics during the experiment. Different bulk gas exit velocity were used during the tests, thus giving some variation in absolute values of $\bar{u}$, q' and relative turbulence intensity.

Relative turbulence intensity remained broadly constant, at around 14-18%, for methane, $85\%CH_4 - 15\%CO_2$ and $70\%CH_4 - 30\%CO_2$ for most test conditions (Fig. 17, a). For pure methane at 7 bara 473 K, the relative turbulence intensity is slightly higher, at around 19%. Variable $q'/\bar{u}$ is observed for $70\%CH_4 - 30\%CO_2$ also at 7 bara 473 K. Here $q'/\bar{u}$ drops from 20% for lean mixtures to 18% for rich mixtures. This is due to the higher bulk exit velocity of the gas mixture required to stabilise rich mixtures during the experiments. For $70\%CH_4 - 30\%CO_2$ at 7 bara 473 K at $\phi = 0.76$, very low bulk exit velocity at $\bar{u} = 3.5$ m/s has been maintained to keep the slow burning gas flame stable. Thus the $q'/\bar{u}$ increased to 20%. For methane $\phi = 0.78$ at the same condition the velocity $\bar{u} = 4.9$ m/s was maintained,

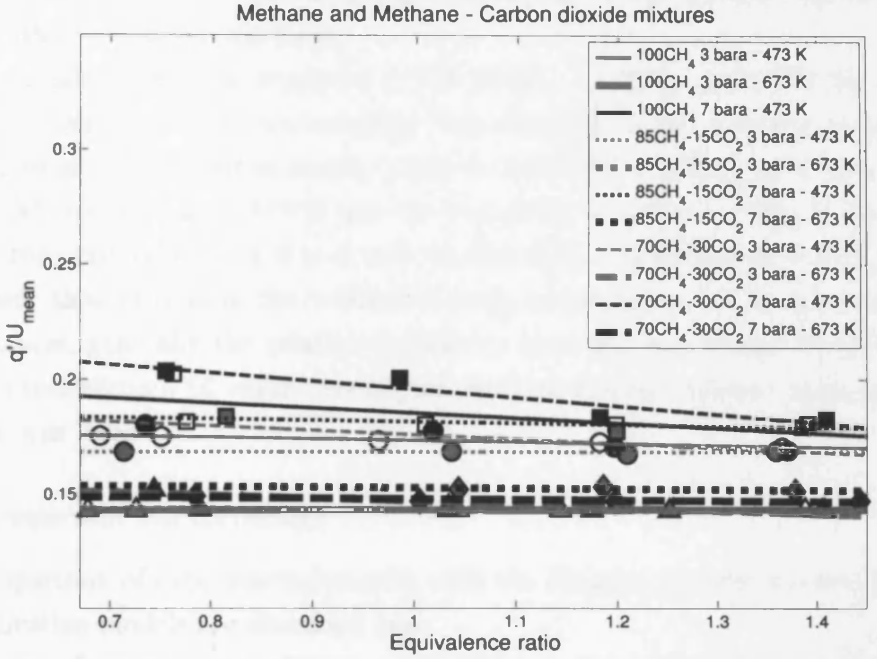

a)

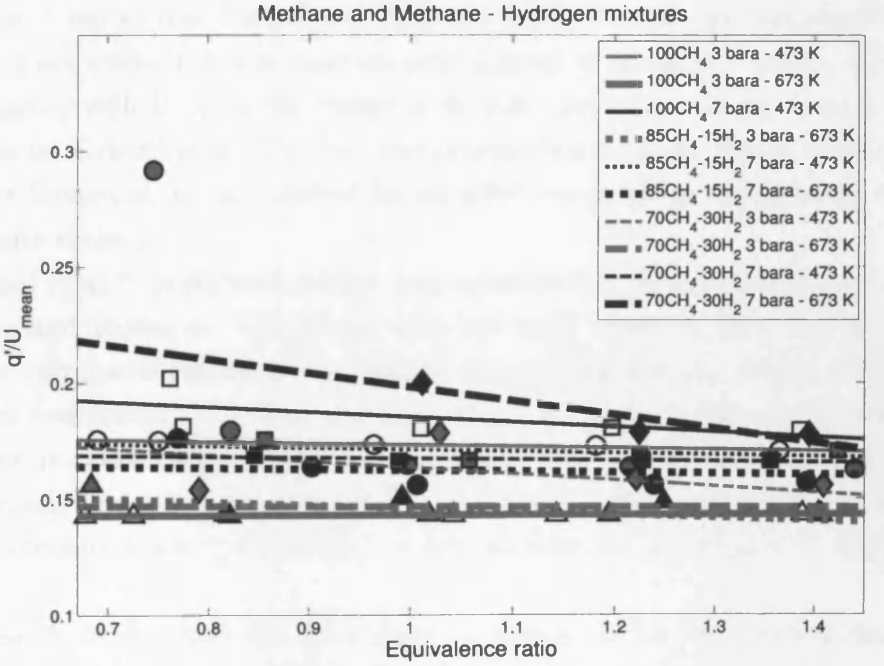

b)

Fig. 17 Relative turbulence intensity of methane, methane - carbon dioxide and methane - hydrogen mixtures. a) CH_4 and $CH_4 - CO_2$ mixtures; b) CH_4 and $CH_4 - H_2$ mixtures. Symbols: ○ - 3 bara 473 K, △ - 3 bara 673 K, □ - 7 bara 473 K, ◊ - 7 bara 673 K, blank - CH_4, grey - $85\%CH_4 - 15\%CO_2(H_2)$, black - $70\%CH_4 - 30\%CO_2(H_2)$.

therefore $q'/\bar{u}$ was lower. In general for all lean mixtures the velocity had to be slightly reduced in order to stabilise the flame.

Similiar trends have been observed for $85\%CH_4 - 15\%H_2$ and $70\%CH_4 - 30\%CO_2$ (Fig. 17, b). Relative turbulence intensity was constant in the majority of tests undertaken for methane - hydrogen mixtures. Only for $85\%CH_4 - 15\%H_2$ at 3 bara 473 K and $70\%CH_4 - 30\%H_2$ at 7 bara 673 K are the variations significant. This is due to a very low gas mixture exit velocity of $\bar{u} = 2$ m/s for $85\%CH_4 - 15\%H_2$ at $\phi = 0.75$, 3 bara 473 K being used, thus increasing the relative turbulence intensity. As for methane - carbon dioxide mixtures, generally the relative turbulence intensity was around 14-18%. At lower temperature conditions $q'/\bar{u}$ values are higher, because the exit velocity required for flame stabilisation was lower.

3. Data comparison and correlation

The comparision of experimental results with the findings of other researchers and turbulent combustion models are discussed here.

Comparison of methane experiment results with the Peters'[24] and Zimont's et al.[25] correlations, and the data from Kobayashi et al.[14] and Filatyev et al.[16] is presented in Fig. 18. Griebel et al.[11] report that Peters' and Zimont's at al. correlations overpredict their data, where flames are within the thin reaction zone regime. Our results - within the corrugated flamelet regime, with l_0/δ_L in the range of 60-100 - are closer to the Peters' correlation although, as for Griebel et al., they are also overpredicted by the Peters' predictions. Correlations for Zimont et al. are plotted for elevated temperature and pressure for different integral length scales l_0.

Kobayashi et al.[14] performed similar measurements for methane/air flames at elevated temperature and pressures. Consistent with the work reported here, the flames studied fell into the corrugated regime on the Borghi diagram making the results of Kobayashi et al. a useful comparison. As observed from Fig. 18, the turbulent and laminar burning velocity ratio recorded by Kobayashi et al. is higher than the current results. Their data is also significantly under predicted by Peters' correlation despite the fact it was seen to over predict the measurements reported here, as well as those by Griebel et al.[11] and Filatyev et al.[16]

One possible explanation for these discrepancies could be the different interpretation methods of processed flame images. Kobayashi et al. has calculated flame areas from contours obtained at progress variable value 0.1. This means that smaller flame areas have been derived and therefore higher burning velocities obtained, compared to those obtained from progress variable value 0.5, which the authors contend represents the averaged flame contour more accurately. The difference in image processing techniques employed may also account

for some of the difference - here the single image processing technique is utilised, whereas Kobayashi et al. used the average image processing technique.

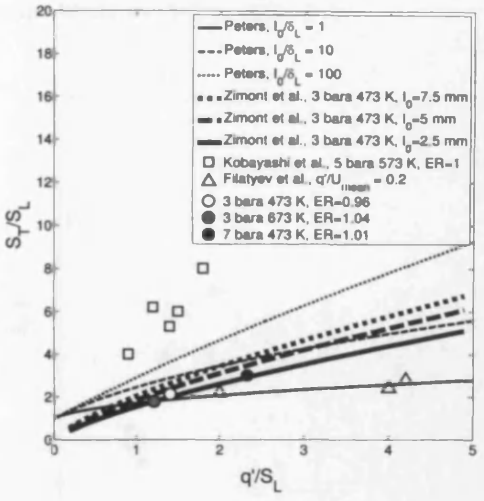

Fig. 18 Comparison of methane turbulent and laminar burning velocities ratio S_T/S_L of our experiments with Peters and Zimont et al. correlations at different lengthscale ratios l_0/δ_L and different integral length scales l_0, and Kobayashi et al. and Filatyev et al. experiments data.

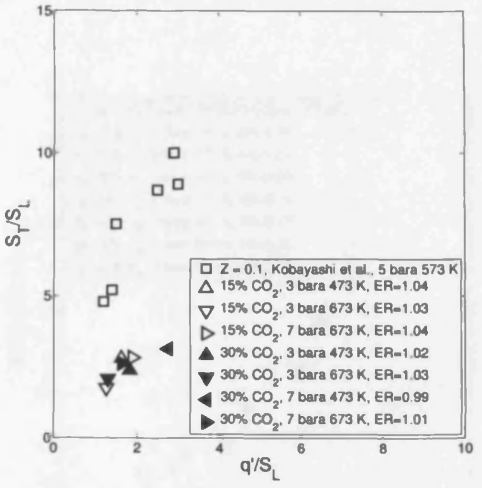

Fig. 19 Comparison of methane - carbon dioxide mixtures turbulent and laminar burning velocity ratio S_T/S_L of our experiments with Kobayashi et al. experiment data at elevated temperature and pressure. In Kobayashi et al. experiments CO_2 was diluted in air, $Z = X_{CO_2}/(X_{air} + X_{CO_2})$.

Another comparison with Filatyev et al. experiments[16] is presented in Fig. 18. Filatyev et al. have performed experiments in a slot type burner at 1 bara 296 K ambient conditions. The relative turbulence intensity in their experiment is 20%, which is very close to the conditions in this study. Filatyev et al. argue that turbulent burning velocity depends on mean velocity $\bar{u}$ and burner width, or in other words on burner geometry. They also propose that Bunsen burner flames should display a nonlinear dependance ("bending effect"). A slightly higher value of S_T/S_L at 7 bara 473 K is observed in the graph. This observation could imply that pressure affects turbulent and laminar burning velocity ratio as indeed has been reported by other researchers.[3,14]

In Fig. 19 a comparison of the turbulent and laminar burning velocity ratio from this test programme and the Kobayashi et al.[4] findings are presented. The data of Kobayashi et al. for methane and methane carbon dioxide mixtures are consistently higher that the current experiments, with contributory reasons for these findings discussed earlier. The effect of carbon dioxide addition have been reported by Kobayashi et al.[4] They found that the ratio of turbulent to laminar burning rate and mean fuel consumption rate decreased with increasing CO_2 dilution ratio. A possible explanation is offered by the effect of increased Markstein

length,[4] which means that local burning velocity in the turbulent flame region decreases with local stretch due to turbulence. Another possible influence considered concerns variation of the smallest wrinkling scale of a CH_4/air/CO_2 flame, which was smaller than that of the flame with no CO_2 dilution.

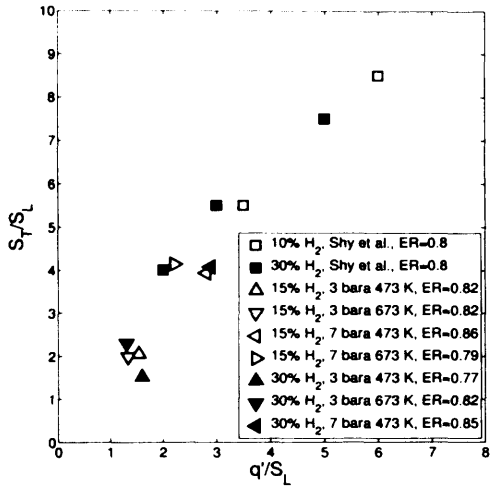

Fig. 20 Methane - hydrogen mixtures turbulent burning velocity comparison of our experiments with Shy et al. results. Turbulent burning velocity data normalised by laminar burning velocity.

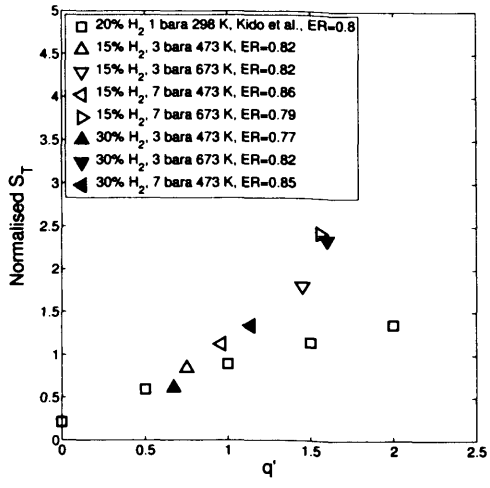

Fig. 21 Methane - hydrogen mixtures turbulent burning velocity comparison of our experiments with Kido et al. Kido et al. results of turbulent burning velocity are normalised by methane burning velocity at 3 bara 473 K at $\phi = 0.96$ obtained in our experiments.

The comparison of the methane - hydrogen results from this programme with those of Shy et al.[7] and Kido et al.[9] are presented in Figs. 20 and 21. Shy et al. performed their experiments at atmospheric conditions and show that the trends for S_T/S_L as a function of q'/S_L are in reasonable agreement with ours (Fig. 20). The same trends are reported for pure hydrogen in the paper of Kitagawa et al.[23] Figure 21 presents the turbulent burning velocity reported by Kido et al. (after normalizing the data by the methane burning velocity at 3 bara 473 K at $\phi = 0.96$). Kido's et al. experiments were undertaken utilising propagating flames. The current data correlates well with their findings for q' less than 1. For higher q' the differences are noticeable. This implies that both temperature and pressure have a strong effect on S_T, and this effect arises from differences both in the type of flames and especially the turbulence characteristics of a propagating as opposed to that of a conical shape flame.

IV. Conclusion

1. Investigations of turbulent burning velocity of gaseous alternative fuels at elevated pressure and temperature have been undertaken in a new large-scale High Pressure Optical Combustor facility. Methane, methane-carbon dioxide and methane - hydrogen mixtures have been tested across a broad range of equivalence ratio with pressures up to 7 bar and inlet temperature up to 673 K. All flames considered have been chosen in the corrugated flamelet regime, through appropriate choice of operating conditions.

2. An alternative analysis method for turbulent flame image processing and hence turbulent burning velocity calculation has been proposed and applied. The results have been assessed against other commonly used methodologies, and although the method proved to be reliable in this programme, further investigation and refinement is ongoing.

3. Methane and methane-carbon dioxide mixtures turbulent burning velocity results have been compared with Peters' and Zimont's et al. correlations and recent data of Kobayashi et al. and Filatyev at al. The results show reasonable agreement with Peters' predictions. However, the results show differences with the findings of Kobayashi et al., most likely due to data analysis differences, such as the selected value of progress variable.

4. Methane-hydrogen mixture results correlate well with recent data from Shy et al., who utilised the alternative propagating flame method for quantifying turbulent burning velocity, notwithstanding differences in pressure and temperature between datasets.

5. These data quantify the reduction in turbulent burning rate induced by carbon dioxide addition to methane for a variety of equivalence ratios. Increase in initial ambient gas temperature significantly increases turbulent burning velocity, while increase in ambient pressure induces a reduction. Methane and methane-carbon dioxide mixtures demonstrate similar trends with respect to the influence of ambient conditions.

6. Hydrogen addition to methane has been found to considerably increase turbulent burning velocity even for small volumes of hydrogen addition. For lean hydrogen-methane mixtures, an increase in temperature or pressure augments turbulent burning velocity, whereas the influence of ambient pressure is minimal for rich mixtures.

Acknowledgments

This research was financed by the European Comission under their Alternative Fuels for Industrial Gas Turbines (AFTUR) project (ENK5-CT-2002-00662). A.B. thanks EU for sponsoring his research under the Marie Curie programme Inegrated Energy Conversion for Sustainable Environment (INECSE) (MEST-CT-2005-021018). The authors thank GTRC Facility Manager Mr S. Morris for helping to perform experiments and Mr T. Treherne and

Mr P. Malpas for technical assistance.

References

[1]Gokalp, I. and Lebas, E., "Alternative Fuels for Industrial Gas Turbines (AFTUR)," *Applied Thermal Engineering*, Vol. 24, 2004, pp. 1655 1663.

[2]Egolfopoulus, F. N., Cho, P., and Law, C. K., "Laminar Flame Speeds of Methane-Air Mixtures Under Reduced and Elevated Pressures," *Combustion and Flame*, Vol. 76, 1989, pp. 375–391.

[3]Kobayashi, H., "Experimental Study of High-Pressure Turbulent Premixed Flames," *Experimental Thermal and Fluid Science*, Vol. 26, 2002, pp. 375 387.

[4]Kobayashi, H., Hagiwara, H., Kaneko, H., and Ogami, Y., "Effects of CO2 Dilution on Turbulent Premixed Flames at High Pressure and High Temperature," *Proceedings of the Combustion Institute*, Vol. 31, 2007, pp. 1451 1458.

[5]Griebel, P., Boschek, E., and Jansohn, P., "Lean Blowout Limits and NOx Emissions of Turbulent, Lean, Premixed, Hydrogen-Enriched Methane/Air Flames at High Pressure," *Journal of Engineering for Gas Turbines and Power*, Vol. 129, 2007, pp. 404 410.

[6]Halter, F., Chauveau, C., and Gokalp, I., "Characterization of the Effects of Hydrogen Addition in Premixed Methane/Air Flames," *International Journal of Hydrogen Energy*, Vol. 32, 2007, pp. 2585–2592.

[7]Shy, S., Chen, Y. C., Yang, C. H., Liu, C. C., and Huang, C. M., "Effects of H2 or CO2 Addition, Equivalence Ratio, and Turbulent Straining on Turbulent Burning Velocities for Lean Premixed Methane Combustion," *Combustion and Flame*, Vol. 153, 2008, pp. 510 524.

[8]Mandilas, C., Ormsby, M. P., Sheppard, C. G. W., and Wooley, R., "Effects of Hydrogen Addition on Laminar and Turbulent Premixed Methane and Iso-Octane-Air Flames," *Proceedings of the Combustion Institute*, Vol. 31, 2007, pp. 1443 1450.

[9]Kido, H., Nakahara, M., Hashimoto, J., and Barat, D., "Turbulent Burning Velocities of Two Component Fuel Mixtures of Methane, Propane and Hydrogen," *JSME nternational Journal*, Vol. 45, 2002.

[10]Natarajan, J., Lieuwen, T., and Seitzman, J., "Laminar Flame Speeds of H2/CO Mixtures: Effect of CO2 Dilution, Preheat Temperature, and Pressure," *Combustion and Flame*, Vol. 151, 2007, pp. 104–119.

[11]Griebel, P., Bombach, R., Inauen, A., Scharen, R., Schenker, S., and Siewert, P., "Flame Characteristics and Turbulent Flame Speeds of Turbulent, High-Pressure, Lean Premixed Methane/Air Flames," *Proceedings of GT2005, ASME Turbo Expo 2005: Power for Land, Sea and Air*, 2005.

[12]Griebel, P., Siewert, P., and Jansohn, P., "Flame Characteristics of Turbulent Lean Premixed Methane/Air Flames at High Pressure: Turbulent Flame Speed and Flame Brush Thickness," *Proceedings of the Combustion Institute*, Vol. 31, 2007, pp. 3083 3090.

[13]Pfadler, S., Leipertz, A., and Dinkelacker, F., "Systematic Experiments on Turbulent Premixed Bunsen Flames Including Turbulent Flux Measurements," *Combustion and Flame*, Vol. 152, 2008, pp. 616–631.

[14]Kobayashi, H., Seyama, K., Hagiwara, H., and Ogami, Y., "Burning Velocity Correlation of Methane/Air Turbulent Premixed Flames at High Pressure and High Temperature," *Proceedings of the Combustion Institute*, Vol. 30, 2005, pp. 827 834.

[15]Bilger, R. W., Pope, S. B., Bray, K. N. C., and Driscoll, J. F., "Paradigms in Turbulent Combustion Research," *Proceedings of the Combustion Institute*, Vol. 30, 2005, pp. 21 42.

[16]Filatyev, S. A., Driscoll, J. F., Carter, C. D., and Donbar, J. M., "Measured Properties of Turbulent

Premixed Flames for Model Assessment, Including Burning Velocities, Stretch Rates, and Surface Densities," *Combustion and Flame*, Vol. 141, 2005, pp. 1–21.

[17]Cheng, R. K. and Shepherd, I. G., "The Influence of Burner Geometry on Premixed Turbulent Flame Propagation," *Combustion and flame*, Vol. 85, 1991, pp. 7–26.

[18]Driscoll, J. F., "Turbulent Premixed Combustion: Flamelet Structure and its Effect on Turbulent Burning Rate," *Progress in Energy and Combustion Science*, Vol. 34, 2008, pp. 91–134.

[19]Lafay, Y., Renou, B., Cabot, G., and Boukhalfa, M., "Experimental and Numerical Investigation of the Effect of H2 Enrichment on Laminar Methane-Air Flame Thickness," *Combustion and Flame*, Vol. 153, 2008, pp. 540–561.

[20]Lachaux, T., Halter, F., Chauveu, C., Gokalp, I., and Shepherd, I. G., "Flame Front Analysis of High-Pressure Turbulent Lean Premixed Methane-Air Flames," *Proceedings of the Combustion Institute*, Vol. 30, 2005, pp. 819–826.

[21]Hinze, J. O., *Turbulence*, McGraw-Hill, New York, 1975.

[22]Chen, Y. C. and Bilger, R. W., "Simultaneous 2-D Imaging Measurements of Reaction Progress Variable and OH Radical Concentration in Turbulent Premixed Flames: Experimental Methods and Flame Brush Structure," *Combustion Science and Technology*, Vol. 167, 2001, pp. 131–167.

[23]Kitagawa, T., Nakahara, T., Maruyama, K., Kado, K., Hayakawa, A., and Kobayashi, S., "Turbulent Burning Velocity of Hydrogen-Air Premixed Propagating Flames at Elevated Pressures," *International Journal of Hydrogen Energy*, Vol. 33, 2008, pp. 5842–5849.

[24]Peters, N., "The Turbulent Burning Velocity for Large-Scale and Small-Scale Turbulence," *Journal of Fluid Mechanics*, Vol. 384, 1999, pp. 107–132.

[25]Zimont, V., Polifke, W., Bettelini, M., and Weisenstein, W., "An Efficient Computational Model for Premixed Turbulent Combustion at High Reynolds Numbers Based on a Turbulent Flame Speed Closure," *Journal of Engineering for Gas Turbines and Power*, Vol. 120, 1998, pp. 526–532.

Premixed Swirl Combustion and Flashback Analysis with Hydrogen/Methane Mixtures

A. Bagdanavicius* N. Shelil† N. Syred‡ A. Griffiths § P. J. Bowen¶

Cardiff University, The Parade, Cardiff CF24 3AA, Wales, UK

Increased interest in the combustion of hydrogen and hydrogen blends is the driving force in the research of the alternative fuels. The usage of the new hydrogen enriched fuels is unavoidably related to changes in the flame structure, burning velocity and as a consequence - flame stability. Flame flashback and blow off are the important characteristics in practical application.

Flame flashback problems arising due to the use of lean premixed combustion of methane-hydrogen mixtures is discussed in this paper. Firstly, one of the most important flame characteristics, laminar burning velocity S_L, has been calculated for CH_4-H_2 mixtures with different hydrogen content at various pressures, temperatures and equivalence ratios. Chemkin-Pro software package with Premix code has been used for that purpose. A new approximation equation, used to calculate S_L of CH_4-H_2 mixtures having different hydrogen content has been compared with the experimental results and validated. The equation predicts the values of low hydrogen content mixtures quite accurately.

Secondly, the flashback limits have been determined for CH_4-H_2 mixtures using generic swirl burner. New turbulent burning velocity determination method has been applied and tested. The experiment results have been compared with the Bunsen burner experiment results and Fluent computations. It has been found that hydrogen enriched methane flames are more prone to flashback, although the blow off limits are extended. This is clearly due to the increased burning velocity of the methane-hydrogen gas mixture.

*Marie Curie Researcher, Cardiff School of Engineering, The Parade, Cardiff CF24 3AA, Wales, UK, AIAA member

†Research Student, Cardiff School of Engineering, The Parade, Cardiff CF24 3AA, Wales, UK.

‡Professor, Cardiff School of Engineering, The Parade, Cardiff CF24 3AA, Wales, UK, AIAA member

§Professor, Cardiff School of Engineering, The Parade, Cardiff CF24 3AA, Wales, UK.

¶Professor, Cardiff School of Engineering, The Parade, Cardiff CF24 3AA, Wales, UK.

Nomenclature

A	=	Model constant
A_f	=	Flame front area
B	=	Swirl burner swirler slot width, m
c	=	Progress variable
C_D	=	Coefficient
Da	=	Damkohler number
D_e	=	Swirl burner exit diameter
D_{eq}	=	Equivalent nozzle diameter
D_i	=	Swirl burner injector diameter
D_v	=	Swirl burner internal swirler diameter
G_x	=	Axial flux of axial momentum
G_θ	=	Axial flux of angular momentum
H	=	Swirl burner swirler height, m
k	=	Turbulent kinetic energy
l_0	=	Integral length scale, m
$\dot{m}$	=	Mass flow rate, kg/s
q'	=	Averaged turbulence intensity, m/s
S	=	Swirl number
S_c	=	Reaction progress source term, s^{-1}
Sc_t	=	Turbulent Schmidt number
S_L	=	Laminar burning velocity, m/s
S_T	=	Turbulent burning velocity, m/s
T	=	Temperature, K
t	=	Time, s
u, v, w	=	Axial, radial and tangential velocity, m/s
u', v', w'	=	Fluctuating axial, radial and tangential velocity component, m/s
$\vec{v}$	=	Velocity vector
$\dot{V}$	=	Volume flow rate, m^3/s
X	=	Mole fraction
Y	=	Mass fraction
α	=	Thermal diffusivity, m^2/s
δ_L	=	Laminar flame thickness, mm
ϵ	=	Turbulence dissipation rate
ϕ	=	Equivalence ratio
ρ	=	Density, kg/m^3

ω = Specific turbulence dissipation rate

Subscript

rms = root mean square
st = stoichiometric
P = products
R = reactants

I. Introduction

HYDROGEN is considered as one of the most promising alternative to existing fuels. However the high cost of production of pure hydrogen, safety issues and different combustion characteristics restrict its commercial usage. Instead of using pure hydrogen, hydrogen-methane blends receive more attention as an alternative fuel for power generation applications. The main reason of using hydrogen is related to the reduction of CO_2 emissions so decreasing global warming effects. The second reason is to enhance the utilization of gasified biomass and other by-product gases derived from some industrial processes in the form of producer gases containing mainly H_2 and CO which can also be mixed with methane.[1,2] The third reason is to improve air quality by replacing petrol or diesel in transport.

While hydrogen enriched fuel combustion technologies are under development, Lean Premixed (LP) combustion allowing the reduction of pollution emissions, particularly NO_x, is widely used in practical applications. LP combustion is mainly achieved by using swirl-stabilised combustion. It reduces the flame temperature so reducing thermal NO_x emissions. However LP combustion is often accompanied by stability problems. Premixed flames are naturally more susceptible to static and dynamic instability due to a lack of inherent damping mechanisms.[3] Therefore the understanding of swirl-stabilised combustion is an important prerequisite for the development of novel technologies.

Combustion in swirl burners has been studied for decades and the reviews can be found in the works of Syred,[4,5] Gupta et al.,[6] Huang et al.[7,8] and others. Vanoverberghe[9] and Coghe et al.[10] have demonstrated the reduction of emissions by increasing swirl, producing flames stabilized by the surrounding structures, such as inner and outer recirculation zones, formed as a consequence of the dynamics of the swirling mechanism. Huang et al.,[7] and Huang and Yang[8] studied combustion dynamics and instability in lean premixed swirl-stabilized combustors. They concluded that in combustion systems the dominant mechanism responsible for driving unsteady flow oscillations arise from either heat release or gasdynamic fluctuations, or both.[8]

Valera-Medina[11,12] investigated coherent structures in swirl flows. He performed flashback analysis[11] for swirl burner using different exit geometries and concluded that there are two types of flashback. Type 1 flashback occurred due to the backwards propagation of Central Recirculation Zone (CRZ), and type 2 flashback occurred due to radial propagation into the outer swirl chamber from the exhaust sleeve. He argued that type 2 flashback occurred as a consequence of S_T, boundary layer flame propagation and Combustion Induced Vortex Breakdown (CIVB).

CIVB and its effect on flame flashback has been discussed by Kröner et al.[13] They stated that there are four causes initiating flame flashback in swirl burners:

- Flame propagation in the boundary layer;
- Turbulent flame propagation in the boundary core flow;
- Combustion instabilities;
- Combustion induced vortex breakdown.

They derived the flame quench factor as the ratio of flame chemical time and mixing time, and emphasised that using this factor, flashback behaviour of the burner can be characterised.

Blowout, flashback and stability issues have been discussed by Lieuwen et al.[14] They have used the Damköhler number, which can be expressed as inverse of quench factor, to relate the blowout limits, and have shown that blowout occurs at $Da = 0.6$ for a number of permutations of $CO/H_2/CH_4$ blends.

Most analysis conducted for turbulent and swirl flames relies on the laminar flame characteristics, such as: laminar burning velocity S_L and laminar flame thickness. During the last decades significant progress has been achieved in understanding of methane as well as hydrogen flames. While the combustion characteristics of pure mixtures of methane-air and hydrogen-air have been extensively studied over the years, the knowledge regarding the combustion of mixtures containing both methane and hydrogen is limited.[15] Experimental data at ambient conditions[15,16] and at elevated pressure and temperature conditions[17,18] can be found in literature. Numerical investigations[19–21] have been conducted to define hydrogen addition effect. All investigations of laminar and turbulent flames show an increase of the burning velocities as a result of hydrogen addition to methane.

In this paper the experimental results and modelling of a generic swirl burner are discussed. Firstly, the laminar flame speed of methane-hydrogen mixtures are calculated using Chemkin software. The results are compared with a new approximation equation[22] for calculating the laminar flame speed for methane-hydrogen mixtures. Then the experimental results obtained from generic swirl burner of methane-hydrogen mixtures at atmospheric conditions are discussed and compared with Fluent numerical calculations, and with Bunsen burner results, obtained at elevated temperature and pressure conditions.[23]

II. Experimental facilities and modelling

Two series of experiments were carried out to investigate H_2 effect on methane burning velocity and flame stability. Two methane - hydrogen mixtures: 85% methane - 15% hydrogen and 70% methane - 30% hydrogen, were tested over a wide range of conditions. The generic swirl burner was used to investigate flame stability at atmospheric conditions (1 bara, 293 K). A Bunsen burner was used to calculate the turbulent burning velocity of premixed gas mixtures at 473 K temperature and 3 bara pressure. Chemkin and Fluent have been used to model laminar and turbulent flames. The list of ivestigated mixtures and conditions is presented in Table 1.

Table 1. Investigated gas mixtures and conditions

Gas mixture	Bunsen burner tests	Swirl burner tests	Chemkin	Fluent
$100\%CH_4$	3 bar, 473 K	1 bar, 293 K	1, 3 bar and 300, 473, 673 K	1 bar, 293 K
$85\%CH_4$-$15\%H_2$	3 bar, 473 K	1 bar, 293 K	1, 3 bar and 300, 473, 673 K	1 bar, 293 K
$70\%CH_4$-$30\%H_2$	3 bar, 473 K	1 bar, 293 K	1, 3 bar and 300, 473, 673 K	1 bar, 293 K
$50\%CH_4$-$50\%H_2$	-	-	1, 3 bar and 300, 473, 673 K	-
$30\%CH_4$-$70\%H_2$	-	-	1, 3 bar and 300, 473, 673 K	-
$15\%CH_4$-$85\%H_2$	-	-	1, 3 bar and 300, 473, 673 K	-
$100\%H_2$	-	-	1, 3 bar and 300, 473, 673 K	-

A. Laminar flame speed modeling

Laminar flame burning velocity is an important characteristic in turbulent flame research. S_L of a premixed flame is defined as the propagation velocity of a plane, undisturbed flame without heat loss and buoyancy effect.[24] It is difficult to produce such flames experimentally, however this definition is suitable for numerical calculations using detailed kinetic reaction schemes. Laminar burning velocity is constant under specific pressure and temperature.

Unstretched laminar burning velocity of methane - hydrogen flames have been modelled using the Chemkin-Pro[25] software package. It consists of a set of different application models, which are used to solve various chemical kinetic problems. "Flame Speed Calculator" reactor model has been used to determine the laminar speed of one-dimensional freely propagating flame. The Premix[26] code, developed by Sandia National Laboratories, has been used to run this model.

"Flame Speed Calculator" model with "Parameter Study Facility" option has been utilised to perform the numerical burning velocity calculations. The model simulates a freely propagating flame in which the point of reference is a fixed position on the flame, thus the flame speed is defined as the velocity of unburned gas moving towards the flame1. This model uses mixture averaged transport properties with correction velocity formulation. Equivalence ratio has been chosen as variable parameter. A number of runs have been per-

formed for different temperature and pressure conditions. The domain length of 10 cm has been specified and the grid of 200 points has been selected, which has facilitated faster convergence. Adaptive grid control parameter based on gradient GRAD = 0.1 and adaptive grid control parameter based on curvature CURV = 0.1 have been selected. The initial grid based on temperature profile estimate has been specified. Mixture averaged transport correction velocity formalism, with automatic estimation of temperature profile options, has been used.

"Flame Speed Calculator" reactor model requires the set of gas phase kinetic data, species thermal properties data and species transport properties data to be chosen before calculation. There are many chemical kinetic mechanisms developed for combustion research. Different kinetic models should be used for different gas mixtures as no one mechanism can be considered as universal model for all possible gas mixtures.

GRI-Mech[27] mechanism is often used in the combustion research of hydrocarbons. It considers 53 species and 325 elementary reactions. This mechanism has been developed to investigate methane and natural gas flames and has been validated at various pressure and temperature conditions. The researchers have reported that this mechanism could also be suitable to some extent for biomass gasification-derived producer gas,[28] methane hydrogen mixtures[20,21] and for hydrogen air mixtures[29,30] at atmospheric conditions. However there have been larger discrepancies observed between experimental data and numerical calculations using GRI-Mech kinetic mechanism for pure and diluted hydrogen at higher pressures.[29,31]

Another well known kinetic mechanism, which has been developed by University of California in San Diego, is widely used. This kinetic mechanism considers 46 species and 235 elementary reactions. Lafay et al.[32] has utilised GRI-Mech and San Diego mechanisms to calculate flame thickness. They have proved that these mechanisms are in good agreement with the experimental data at the atmospheric conditions at equivalence ratio above 0.55.

Ströhle and Myhrvold reported[29] that Li et al.[33] and O'Conaire et al.[31] chemical kinetics mechanisms for hydrogen provide more accurate results in comparison with experimental data at elevated pressures, whilst GRI-Mech underpredicts laminar flame speed considerably. They also showed that the San Diego[34] mechanism yields reasonable results for helium diluted high pressure hydrogen flames. Sarli and Benedetto[1] found that GRI-Mech kinetic mechanism, used in their simulation, underpredicted laminar burning velocity at high hydrogen content in the methane-hydrogen mixture. They identified three different regimes in flame propagation depending on hydrogen mole fraction in fuel mixture.

The comparison of GRI-Mech and San Diego kinetic mechanisms is presented in Fig. 1. GRI-Mech and San Diego results are almost identical for the 70% methane and 30% hydrogen mixture. The largest discrepancies between these two models can be observed in the region of equivalence ratio below 1 and above 1.4, although in the region from 1 to 1.4 GRI-Mech

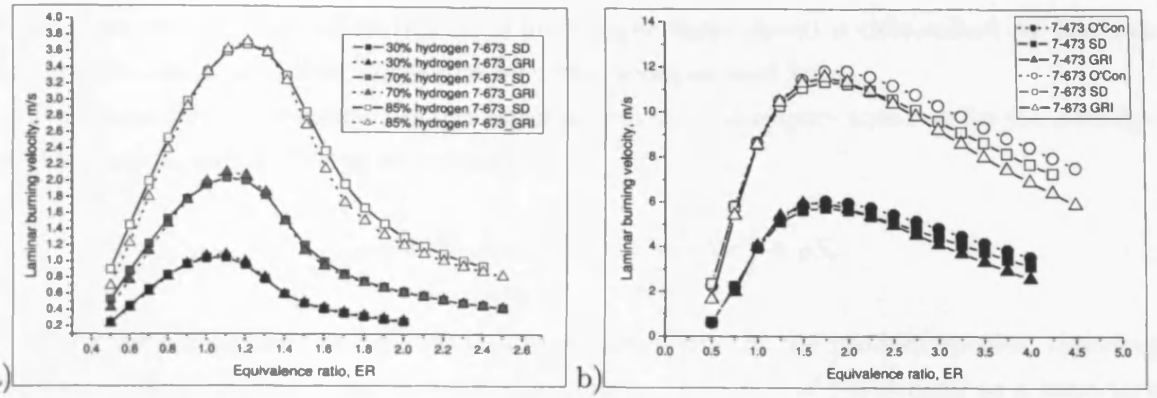

Figure 1. Chemkin calculated S_L: a) methane - hydrogen mixtures at 7 bara and 673 K, b) hydrogen at 7 bara and 473 K and 7 bara and 473 K. Numbers represent hydrogen amount in the mixture; O'Con - O'Conaire mechanism, SD - San Diego mechanism, GRI - GRI-Mech mechanism.

produces higher flame speed results. At higher hydrogen quantities in the mixture GRI-Mech underpredicts flame speed. This supports similar findings of other researchers.[29]

Similar comparison has been udertaken for pure hydrogen. The results of these calculation are presented in Fig. 1. Three mechanisms: O'Conaire et al. mechanism, San Diego mechanism and GRI-Mech, have been compared at 7 bara 473 K and 673 K. The O'Conaire et al. mechanism has been developed to simulate the combustion of hydrogen and oxygen in a variety of combustion environments and over a wide range of temperatures, pressures and equivalence ratios. The kinetic mechanism comprises of 8 species and 19 elementary reactions for a temperature range from 298 to 2700 K, the pressure from 0.05 to 87 atmospheres, and the equivalence ratios from 0.2 to 6. The GRI-Mech mechanism underpredicts hydrogen flame speed in the region of equivalence ratio up to 1 and above 1.5 in comparison with O'Conaire mechanism. The San Diego mechanism predictions are more accurate in comparison with GRI-Mech whilst O'Conaire mechanism predicts the highest flame speed.

As the hydrogen content in the mixture is not high (up to 30% by volume) it is believed that methane combustion kinetics prevail in the combustion process. Thus taking into account the findings of other researchers it has been decided to use GRI-Mech mechanism for all methane - hydrogen mixtures.

B. Turbulent premixed combustion modelling

In premixed combustion, fuel and oxidizer are mixed at the molecular level prior to ignition. It is assumed that combustion takes place in a thin flame sheet. The combustion reactions take place and the flame front moves from premixed reactants to products. For subsonic flows, the overall rate of propagation of the flame is determined by both the laminar

flame speed and the turbulent eddies. The laminar flame speed is determined by the rate that species and heat diffuse upstream into the reactants and burn.

The flame front propagation is modelled by solving a transport equation for the density-weighted mean reaction progress variable c:

$$\frac{\partial}{\partial t}(\rho c) + \nabla \cdot (\rho \vec{v} c) = \nabla \cdot \left(\frac{\mu_t}{Sc_t} \nabla c \right) + \rho S_c \tag{1}$$

The progress variable is defined as a normalized sum of the product species, therefore $c = 0$ for unburnt mixture, and $c = 1$ for products. The value of c is defined as a boundary condition at all flow inlets. The mean reaction rate is modelled as:[35]

$$\rho S_c = \rho_R S_T \left| \nabla c \right| \tag{2}$$

The S_T is computed using a model for wrinkled flames:[35]

$$S_T = A \cdot (u')^{3/4} S_L^{1/2} \alpha^{-1/4} l_0^{1/4} = A u' Da^{1/4} \tag{3}$$

The integral length scale l_0 is modeled using the equation:

$$l_0 = C_D \frac{(u')^3}{\epsilon} \tag{4}$$

The recommended value $A = 0.52$ and coefficient $C_D = 0.37$ have been used.[35]

Non-adiabatic premixed combustion model is considered. The energy transport equation is solved in order to account for any heat losses or gains within the system. These losses/gains may include heat sources due to chemical reaction or radiation heat losses.

The shear-stress transport (SST) $k - \omega$ model has been used for modelling turbulence. It has feature that gives the SST $k - \omega$ model an advantage in terms of performance over both the standard $k - \omega$ model and the standard $k - \epsilon$ model. Other modifications include the addition of a cross-diffusion term in the ω equation and a blending function to ensure that the model equations behave appropriately in both the near-wall and far-field zones.[36]

C. Generic swirl burner tests

Flame stability and flashback experiments were conducted using the generic swirl burner designed and commissioned at GTRC. The burner was designed to produce premixed, non premixed and partially premixed flames, although only premixed combustion was considered in this programme. Air and fuel flows were measured simultaneously using suitably ranged Coriolis flow meters. The tests were conducted at atmospheric conditions.

The burner construction is shown in Fig. 2. Air/fuel gas mixture is supplied through a tangential inlet pipe into a plenum chamber, then via 4 tangential inlets into the swirl chamber forming the main part of the burner. The fuel injector, which is normally used for the non premixed and partially premixed flames, is not used in our experiments, but is left in place as being representative of industrial practice, where it might for instance be used for liquid fuel injection. Such a burner design normally produces a Central Recirculation Zone (CRZ), which plays an important role in flame stabilisation. The effect of CRZ is reduced by fitting a constrain in the nozzle, which also helps to reduce flashback.

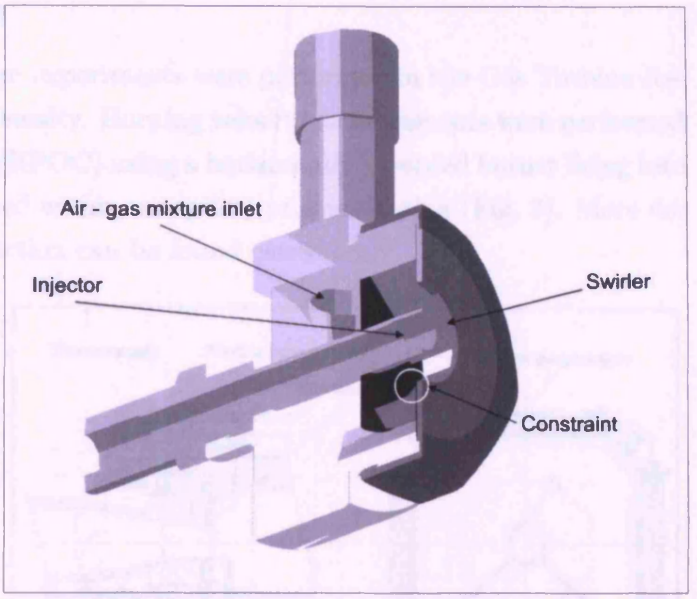

Figure 2. Generic swirl burner

Swirl burners and combustors are usually characterised by the swirl number. The swirl number, S, is the variable non-dimensional number representing axial flux of angular momentum, G_θ, divided by axial flux of axial momentum, G_x, and equivalent nozzle radius $D_{eq}/2$:[5]

$$S = \frac{G_\theta}{G_x D_{eq}/2} \tag{5}$$

However, as the flow patterns in swirl burners are complicated, it is difficult to calculate a specific swirl number without simplification. The swirl number varies with the burner, because the axial and tangential flow rates change at different levels within the burner. It is hence generally impractical to use local values of the swirl number, since this would require detailed velocity, and pressure measurements. To determine a more practical and comparable value, various simplifications have been used, resulting in the geometric swirl number S_g.[6] The S_g, calculated based on the geometrical configurations, was 1.47 for the burner studied in this programme.

D. Bunsen burner experiments

Elevated temperature and pressure experiments were performed in the Gas Turbine Research Centre (GTRC) of Cardiff University. Burning velocity measurements were performed in High Pressure Optical Combustor (HPOC) using a horizontally mounted burner firing into an inner combustion chamber, enclosed within an optical pressure casing (Fig. 3). More detail description of the burner construction can be found elsewhere.[23]

Two different measurement techniques were applied. A non-intrusive 2-D laser diagnostic technique, Laser Doppler Anemometry (LDA), was utilised to determine the velocity profile and turbulence characteristics at the exit of the burner at elevated pressures and temperatures. The velocity and turbulence profiles of isothermal air flow, seeded with aluminium oxide particles, were measured downstream of the burner exit across the burner axis on the centreline plane.

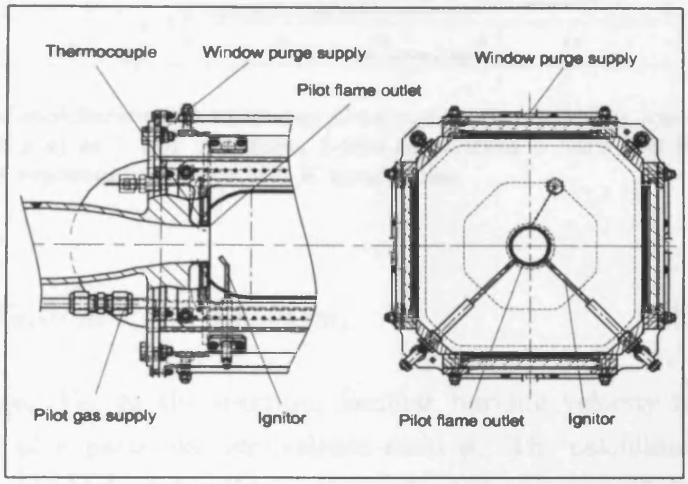

Figure 3. High Pressure Optical Combustor

Planar laser tomography was applied in order to measure the turbulent burning velocity at a range of temperatures and pressures. This technique is based on the observation that the density of the products is lower than that of the reactants. Images of the flame front were recorded using a high speed camera. More detail description of calculation methods and experimental techniques can be found elsewhere.[23]

III. Laminar burning velocity modelling results

Laminar burning velocities S_L of lean and rich methane-hydrogen mixtures have been calculated using Chemkin at different pressures and temperatures. A new approximation method, proposed by Shelil et al.,[22] has been used to compute S_L for different methane - hydrogen mixture ratios and compared with Chemkin calculations. This method can be used to calculate the laminar burning velocity of the mixture, when the S_L of pure gases and mass fractions Y are known. Having S_L values of pure gases at required ambient conditions and equivalence ratio known, the approximation equation could be used.

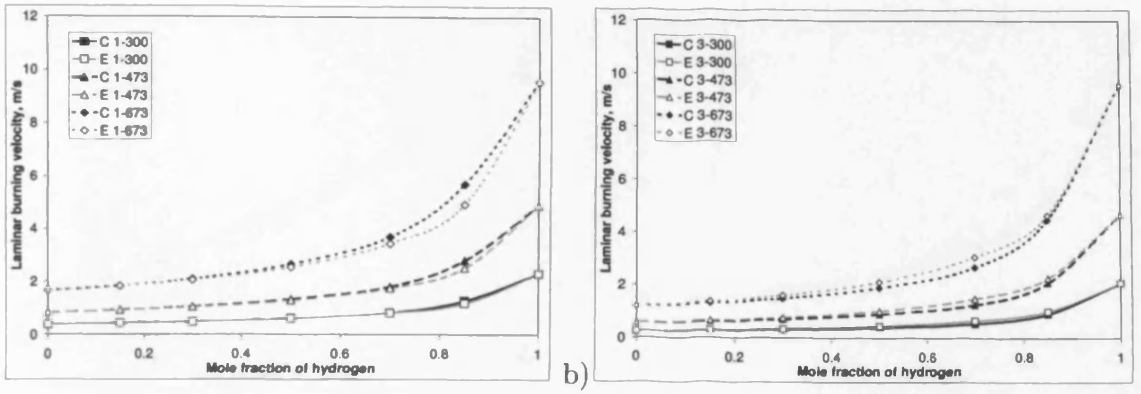

Figure 4. Laminar burning velocity of stoichiometric mixtures obtained from Chemkin computations (C) and using equation 6 (E): a) at 1 bar pressure, 1-300 represents 1 bara 300 K conditions; b) at 3 bar pressure, 3-300 represents 3 bara 300 K conditions.

$$S_{L,mix} = Y_{H_2} S_{L,H_2} + (1 - Y_{H_2}) S_{L,CH_4} \tag{6}$$

Here the mass fraction of hydrogen Y_{H_2} in the mixture, laminar burning velocity of hydrogen S_{L,H_2} and methane S_{L,CH_4} of a particular equivalence ratio ϕ. The calculated laminar burning velocity of the methane-hydrogen mixture $S_{L,mix}$ for the same ϕ will be found. For instance calculating the S_L of 70% CH_4 - 30% H_2 stoichiometric mixture ($\phi = 1$), the S_L of CH_4 and H_2 stoichiometric air - gas mixtures are used as an input in equation 6.

Similar approaches, which simplify the calculation of S_L for the gas mixture have been discussed elsewhere.[1,22] The comparison of Chemkin calculations and laminar burning velocity results for the mixtures obtained from the equation 6 for different gas mixtures at $\phi = 1$ at 1 bar and 3 bar pressures and different temperatures is presented in Fig. 4.

It is seen from the graphs that the equation 6 predicts the S_L values fairly well especially for the mixtures with lower hydrogen quantities in the mixture (mole fraction $X < 0.5$) and lower pressure. For higher hydrogen quantities the difference is larger. At higher pressure (Fig. 4, b) the calculated S_L values computed using equation 6 are higher than Chemkin predictions.

To compare the equation 6 predictions with experimental results the Hermanns[15] data have been used. Hermanns[15] used heat flux method to calculate the laminar burning velocities of methane - hydrogen mixtures with air. The comparison of Chemkin prediction, calculation results using the equation 6 and Hermanns experiments are presented in Fig. 5. It is seen from the graph that difference between experimental results and the results calculated from equation 6 is not significant.

To validate the equation for the higher hydrogen content mixtures the data of Ilbas et

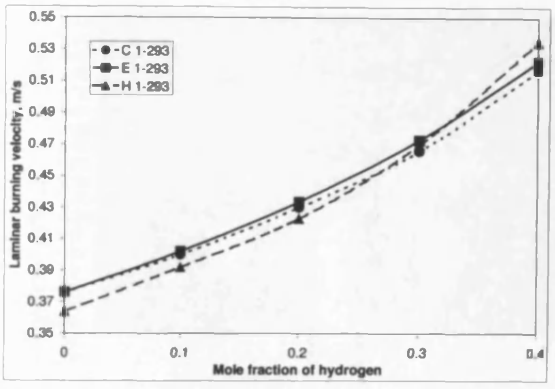

Figure 5. Comparison of S_L data obtained from Chemkin (C), equation 6 (E) and Hermanns[15] (H) experimental resuts at atmospheric conditions, $\phi = 1$.

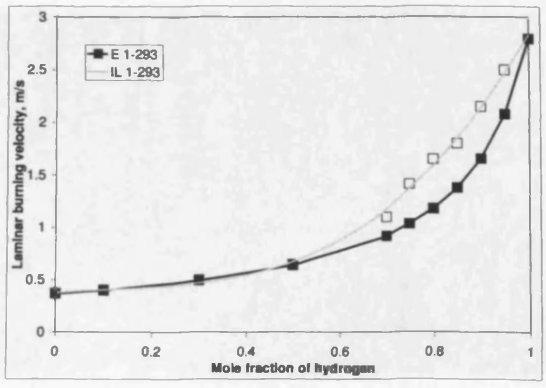

Figure 6. Comparison of S_L data obtained from the equation 6 (E) and Ilbas et al.[16] (IL) experimental resuts at atmospheric conditions, $\phi = 1$.

al.[16] has been used as a reference. The graph of experimental values[16] and calculations using the equation 6 is presented in Fig. 6. The experimental S_L values of 100% methane and 100% hydrogen has been taken as input values in equation 6. It is seen from the graph that equation predicts S_L fairly well for low hydrogen content mixtures ($X < 0.5$). For higher hydrogen content mixtures the difference between results is considerably larger. Therefore for transition ($0.5 < X < 0.9$) and methane-inhibited hydrogen combustion zones ($0.9 < X < 1$), as defined by di Sarli and di Benedetto,[1] more sophisticated formula is rquired.

However the equation 6 could be a useful tool for calculation of S_L for low hydrogen content methane - hydrogen mixtures at atmospheric and elevated temperature and pressure conditions.

Fluent was used for the simulation of premixed combustion. The boundary conditions were chosen to be 700 K for all walls. Simulations were not sensitive to this value apart from the exit tip of the burner. More detailed analysis of the results and discussions on numerical modeling can be found elsewhere.[37]

IV. Experiments in a generic swirl burner at atmospheric conditions

Flame stability depends on the operating pressure, initial temperature, equivalence ratio and total mass flow rate of the premixed mixture.[38] The experiments were performed for premixed methane-hydrogen flames at atmospheric conditions to measure the stability limits of the flame for a particular generic burner. In the context of flashback for this generic swirl

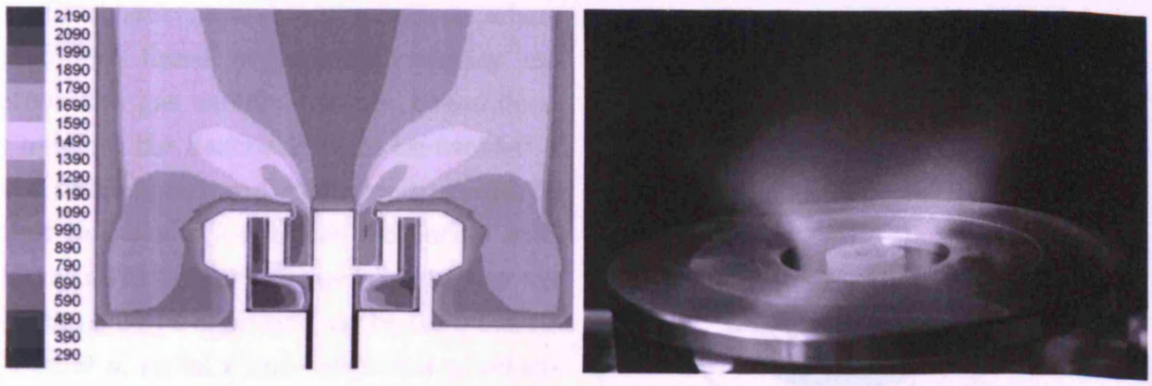

Figure 7. Flashback of 85% methane - 15% hydrogen mixture in model and experiments, $\dot{m} =$ 2.46 g/s, $\phi = 0.82$

burner (geometric swirl number 1.47) the size and shape of the Central Reverse Flow Zone (CRZ) is crucial as in high velocity flows the flame initially stabilizes on the CRZ boundary. Under isothermal conditions for this swirl number a bulbous CRZ forms just past the exhaust and the fuel injector. This CRZ then typically forms an extension to its base which consists of a long columnar structure which passes into the burner to the backplate.

Premixed combustion especially can virtually eliminate this CRZ as the increased axial flux of angular momentum reduces the effective swirl number to below the critical value for vortex breakdown and CRZ formation of ~ 0.5. Maximum effects occur around equivalence ratios $\phi \approx 1$ at maximum heat release. As the equivalence ratio is weakened vortex breakdown can occur, a CRZ forms, which gradually increases in strength so that at very weak mixtures the structure tends to that of the isothermal state. The problem this brings is that for lean combustion the flame can burn not only in the exhaust but on the CRZ boundary surrounding the fuel injector. Here we consider the flashback of these flames radially to the tangential inlets and beyond. This condition represents the system behaviour both with and without the fuel injector. In this system, flashback was more pronounced for lean combustion than for rich.

As seen in Fig. 7, the CRZ and flame front can extend over the fuel injector to the baseplate due to the extension of the CRZ over the fuel injector at weak equivalence ratios. This is undesirable and is a precursor to full flashback. The phenomena is often referred to as Combustion Induced Vortex Breakdown (CIVB). Techniques for elimination are discussed elsewhere.[13]

Hydrogen addition increased flame stability by reducing flame blow off. Similar findings were reported elsewhere,[14,39] however this does then worsened flame flashback susceptibility due to increase of S_L and S_T.

Flashback occurs in the regions where turbulent flame propagation velocity exceeds the gas mixture supply streamlines. Therefore the flashback could be avoided if the flame speed and gas velocity could be kept in balance just above the burner exit. In the swirl burner the gas mixture flow velocity could be expressed as the components of axial u, radial v and tangential w velocities. These velocity vectors are presented in the schematic burner drawing Fig. 8. Based on the experimental data u, v and w were calculated from the known mass flow rate and gas mixture density. Axial, radial and tangential velocity in the inlets are presented in the following three equations:

$$u = \frac{\dot{m}}{0.25\pi\rho(D_e^2 - D_i^2)} \tag{7}$$

$$v = \frac{\dot{m}}{0.5\pi\rho H(D_v + D_i)} \tag{8}$$

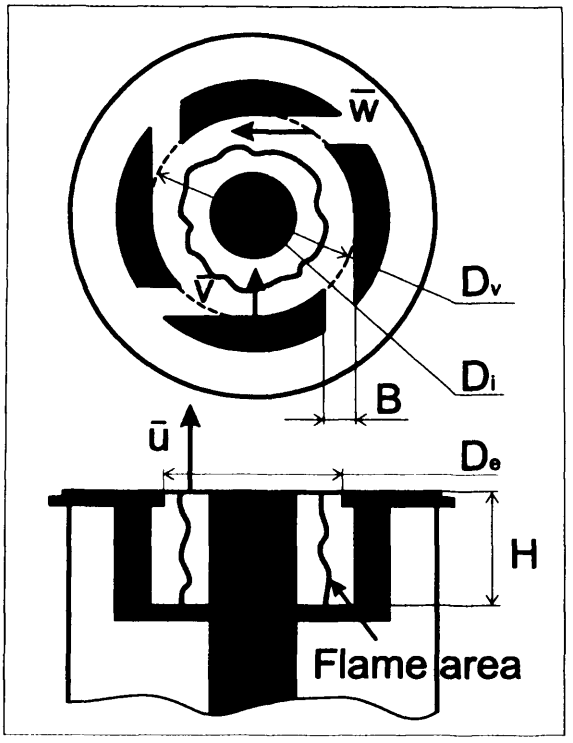

Figure 8. Generic swirl burner

$$w = \frac{\dot{m}}{4\rho HB} \tag{9}$$

The radial velocities of 85% CH_4 - 15% H_2 and 70% CH_4 - 30% H_2 vs ϕ are plotted in Fig. 9. The two regions of stable flame and flashback are defined and separated by the lines, with values above representing stable conditions and those below representing flashback.

Testing all mixtures, both stable and flashback flames were observed. For both mixtures 85%CH_4 - 15% H_2 and 70% CH_4 - 30% H_2 under certain conditions the CRZ and flame extended over the fuel injector. The highest velocity levels for flashback were observed at $\phi = 0.8-0.9$ for all mixtures. In general it was observed that the velocities, at which flashback occurs, increased with increasing H_2 concentration in methane. H_2 addition increases the laminar and turbulent burning burning velocity,[18,23] therefore higher velocities are required to stabilise the flame and avoid flashback.

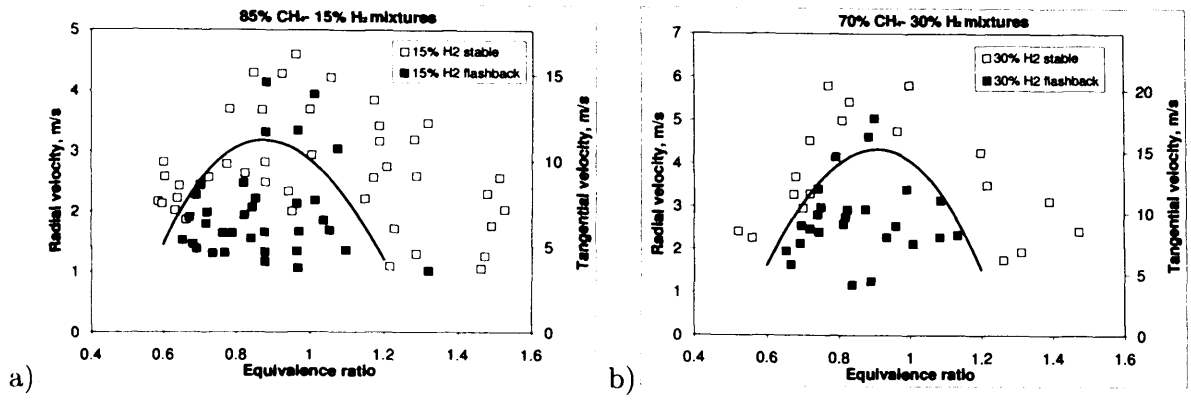

Figure 9. Flashback radial velocities in generic swirl burner: a) 85% methane - 15% hydrogen mixture; b) 70% methane - 30% hydrogen mixture.

V. Comparison of test results from generic swirl burner and Bunsen burner

After the first flashback, the flame stabilised in the region around the injector as seen in the schematical drawing Fig. 8. In several tests, especially with higher hydrogen quantities secondary flashback was observed, where the flame propagated through the swirler slots upstream. When the flame stabilised around the injector, the turbulent flame speed was balanced by the gas flow velocity, therefore the turbulent flame front was established somewhere in the middle region of the swirl chamber between the injector and swirler vanes. As the flame front remained in relative stability, the turbulent flame burning velocity could be derived from the equation:

$$S_T = \frac{\dot{m}_R}{\rho_R \cdot A_f} = \frac{\dot{V}}{A_f} \tag{10}$$

Here the flame front area could be approximated as $A_f = 0.5\pi H(D_v + D_i)$. Therefore it can be concluded that $S_T \approx v$ and these values can be compared directly. Similar analysis applied for methane - carbon dioxide mixtures have been reported elsewhere.[40]

The comparison of our experimental values, obtained using the Bunsen burner at elevated pressure and temperature conditions,[23] generic swirl burner radial velocity approximations and numerical S_T computations are represented in Fig. 10. The S_T and v have been normalised by a normalisation factor as explained elsewhere.[23] The coding "3-473" represents 3 bara and 473 K preheated unburned gas temperature conditions, and "15H2" represents $85\%CH_4 - 15\%H_2$ gas mixture, and "30H2" represents $70\%CH_4 - 30\%H_2$ gas mixture in the legend key. For numerical S_T computations the position at the burner exit have been taken, where the progress variable $c = 0.5$.

Considerable difference between S_T obtained from Bunsen burner and v from swirl burner is observed in Fig. 10 at $\phi = 0.8 - 1.1$. One obvious contributory explanation is that very different flame structures are compared, therefore some incompatibility is expected. Bunsen burner flames belong to "envelope" category flames and have different flame wrinkling process than swirl flames.[41,42] Another important considerations are the uncertainty in deriving the flame front area for swirl burner and the turbulence intensity, which has not been measured, but only modelled.

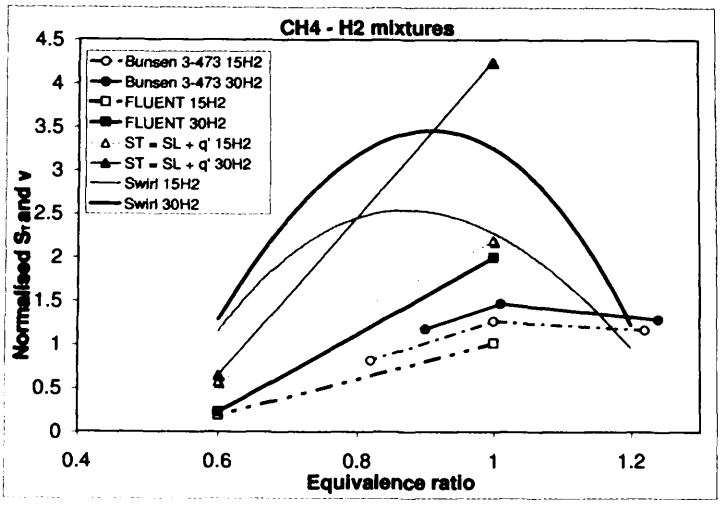

Figure 10. Comparison of experimental values from experiments of generic swirl burner tests at atmospheric conditions, Bunsen burner experiments at elevated temperature and pressure, Fluent computations, and turbulent combustion model $S_T = S_L + u'$.

It was observed that the flame front is corrugated, and the exact position could not be easily identified. Our assumption was to take the flame front position as being located half way between the fuel injector radius and the burner exit radius (Fig. 8), this being based purely from visual interpretation.

The definition for the turbulence characteristics for the Bunsen burner experiments have some uncertainties in themselves. The relative turbulence intensity for Bunsen burner isothermal flows at elevated temperature and pressure has been found to be around 15-20%.[23] For the swirl burner, as no measurements have been possible to date, the turbulence kinetic energy has been computed using CFD at isothermal conditions in the middle of the burner, where the assumed flame front is located. The turbulence intensity q' calculated from the turbulence kinetic energy has been found to be in the region of 0.6 - 4.83 m/s for CH_4-H_2 mixtures. Therefore applying simple approximation $S_T = S_L + q'$, developed from Damköhler theory, the values of S_T can be readily calculated. The grey marks and dotted lines in Fig. 10 represent these normalised S_T values. It is seen that this simplified theory underpredicts turbulent burning velocity for lean mixtures, but the results are much closer to the experimental values at equivalence ratio between 0.9 and 1.0, although for $70\%CH_4 - 30\%H_2$ the predicted S_T is higher than radial velocity v. It is due to a very high turbulence kinetic energy modelled by Fluent. Similar results have been found for methane - carbon dioxide mixtures.[40]

Numerical S_T computation via CFD, evaluated at the burner exit under the same conditions as the swirl burner experiments, where the progress variable $c = 0.5$, show much lower values than the radial velocity results, Fig. 10. It appears that Fluent model does not predict burning velocities particularly well for this swirl burner, although for Bunsen burner the model predictions are reasonably accurate.[23,40]

VI. Conclusions

The laminar burning velocity approximation method for methane - hydrogen mixtures has been discussed and comparison with Chemkin modelling tool has been performed. The investigation of methane - hydrogen flames in a generic swirl burner at atmospheric conditions has been conducted and the results from swirl burner experiments have been compared with Bunsen burner experiments.

1. The laminar burning velocity approximation equation, based on the mass fraction of the gas which compose the mixture, for methane - hydrogen mixtures, proposed by Shelil et al.[22] has been investigated and compared with the experimental results. The approximation produces quite accurate results for the low hydrogen content mixtures and could be used as a tool for practical calculations when the mixture composition and the S_L of pure mixtures are known. However for larger hydrogen content mixtures more accurate approximation equation should be developed.

2. A generic swirl burner has been developed and used to test flame stability and flashback limits. The experiment results have shown that H_2 addition increases the flame flashback possibility primarily because of the increase in burning velocities of methane - hydrogen mixtures.

3. An attempt has been made to correlate the flashback and turbulent burning velocity data. Uncertainties have been emphasised and discussed. The differences in results found are likely to arise due to the following primary causes: the method used to derive flame front position, turbulent flow characteristics, flame regime, unburnt gas temperature. Modifications are needed to the Bunsen type burner to produce flame conditions at flashback closer to those pertaining in swirl burners.

Acknowledgments

A. Bagdanavicius thanks EU for sponsoring his research under the Marie Curie programme INECSE (Integrated Energy Conversion for Sustainable Environment, MEST-CT-2005-021018). N. Shelil wishes to express his thanks to the Egyptian Government for sponsoring his research.

References

[1]di Sarli, V. and di Benedetto, A., "Laminar Burning Velocity of Hydrogen-Methane/Air Premixed Flames," *International Journal of Hydrogen Energy*, Vol. 32, 2007, pp. 637–646.

[2]Chiesa, P., Lozza, G., and Mazzocchi, L., "Using Hydrogen as Gas Turbine Fuel," *Journal of Engineering for Gas Turbines and Power*, Vol. 127, No. 1, 2005, pp. 73–80.

[3]Syred, N., "Generation and Allevation of Combustion Instabilities in Swirling Flow," *Advanced Combustion and Aerothermal Technologies*, edited by N. Syred and A. Khalatov, Springer Netherlands, 2007, pp. 3 20.

[4]Syred, N., "A review of oscillation mechanisms and the role of the Precessing Vortex Core (PVC) in swirl combustion systems," *Progress in Energy and Combustion Science*, Vol. 32, No. 2, 2006, pp. 93–161.

[5]Syred, N. and Beer, J. M., "Combustion in swirling flows: A review," *Combustion and Flame*, Vol. 23, No. 2, 1974.

[6]Gupta, A. K., Lilley, D. G., and Syred, N., *Swirl Flows*, Abacus Press, Tunbridge Wells, 1984.

[7]Huang, Y. and Yang, V., "Bifurcation of flame structure in a lean-premixed swirl-stabilised combustor: transition from stable to unstable flame," *Combustion and Flame*, Vol. 136, No. 3, 2004, pp. 383–389.

[8]Huang, Y. and Yang, V., "Dynamics and stability of lean-premixed swirl-stabilized combustion," *Progress in Energy and Combustion Science*, Vol. 35, 2009, pp. 293 364.

[9]Vanoverberghe, K., *Flow, Turbulence and Combustion of Premixed Switling Jet Flames*, Ph.D. thesis, Katholieke Universiteit Leuven, 2004.

[10]Coghe, A., Solero, G., and Scribano, G., "Recirculation phenomena in a natural gas swirl combustor," *Experimental Thermal and Fluid Science*, Vol. 28, No. 7, 2004, pp. 709–714.

[11]Valera-Medina, A., *Coherent structure and their effects on processes occurring in swirl combustors*, Phd, Cardiff University, 2009.

[12]Valera-Medina, A., Syred, N., and Griffiths, A. J., "Visualisation of isothermal large coherent structures in a swirl burner," *Combustion and Flame*, Vol. 156, No. 9, 2009, pp. 1723–1734.

[13]Kröner, M., Fritz, J., and Sattelmayer, T., "Flashback limits for combustion induced vortex breakdown in a swirl burner," *Journal of Engineering for Gas Turbines and Power*, Vol. 125, 2003, pp. 693–700.

[14]Lieuwen, T., McDonell, V., Petersen, E., and Sanatvicca, D., "Fuel flexibility influences on premixed combustor blowout, flashback, autoignition, and stability," *Journal of Engineering for Gas Turbines and Power*, Vol. 130, 2008.

[15]Hermanns, R. T. E., *Laminar Burning Velocities of Methane-Hydrogen-Air Mixtures*, Ph.D. thesis, Technische Universiteit Eindhoven, 2007.

[16]Ilbas, M., Crayford, A. P., Ylmaz, I., Bowen, P. J., and Syred, N., "Laminar burning velocities of hydrogen-air and hydrogen-methane-air mixtures: An experimental study," *International Journal of Hydrogen Energy*, Vol. 31, 2006, pp. 1768 1779.

[17]Halter, F., Chauveau, C., and Gökalp, I., "Characterization of the effects of hydrogen addition in premixed methane/air flames," *International Journal of Hydrogen Energy*, Vol. 32, 2007, pp. 2585–2592.

[18]Mandilas, C., Ormsby, M. P., Sheppard, C. G. W., and Wooley, R., "Effects of hydrogen addition on laminar and turbulent premixed methane and iso-octane - air flames," *Proceedings of the Combustion Institute*, Vol. 31, 2007, pp. 1443 1450.

[19]Law, C. K. and Kwon, O. C., "Effects of hydrocarbon substitution on atmospheric hydrogen-air flame propagation," *International Journal of Hydrogen Energy*, Vol. 29, 2004, pp. 867–879.

[20]Liu, F. and Gülder, O. L., "Effects of H_2 and H Preferential Diffusion and Unity Lewis Number on Superadiabatic Flame Temperatures in Rich Premixed Methane Flames," *Combustion and Flame*, Vol. 143, 2005, pp. 264 281.

[21]Zhang, Y., Wu, J., and Ishizuka, S., "Hydrogen Addition Effect on Laminar Burning Velocity, Flame Temperature and Flame Stability of a Planar and a Curved CH_4-H_2-air premixed flame," *International Journal of Hydrogen Energy*, Vol. 34, 2009, pp. 519 527.

[22]Shelil, N., Bagdanavicius, A., Griffiths, A. J., Roberts, P. J., and Syred, N., "Flashback analysis of Hydrogen/Methane mixtures for premixed swirl combustion," *16th International IFRF members conference*, 2009.

[23]Bagdanavicius, A., Bowen, P. J., Syred, N., Kay, P., Crayford, A., Sims, G., and Wood, J., "Burning Velocities of Alternative Gaseous Fuels at Elevated Temperature and Pressure," *AIAA Journal*, , No. Accepted 03.11.2009, 2009.

[24]Göttgens, J., Mauss, F., and Peters, N., "Analytic approximation of burning velocities and flame thickness of lean hydrogen, methane, ethylene, ethane, acetylene, and propane flames," *Twenty-Fourth Symposium on Combustion/The Combustion Institute*, 1992, pp. 129–135.

[25]"CHEMKIN-PRO," 2008.

[26]Kee, R., Grcar, J., Smooke, M., and Miller, J., "PREMIX: A Fortran Program for Modeling Steady, Laminar, One-Dimensional Premixed Flames," Tech. rep., Sandia National Laboratories, 1983.

[27]Smith, G. P., Golden, D. M., Frenklach, M., Moriarty, N. W., Eiteneer, B., Goldenberg, M., Bowman, C. T., Hanson, R. K., Song, S., Gardiner, W. C., Lissianski, V. V., and Qin, Z., "GRI-Mech 3.0," .

[28]Serrano, C., Hernandez, J. J., Mandilas, C., Sheppard, C. G. W., and Woolley, R., "Laminar burning behaviour of biomass gasification-derived producer gas," *International Journal of Hydrogen Energy*, Vol. 33, No. 2, 2008, pp. 851 862.

[29]Ströhle, J. and Myhrvold, T., "An evaluation of detailed reaction mechanisms for hydrogen combustion under gas turbine conditions," *International Journal of Hydrogen Energy*, Vol. 32, No. 1, 2007, pp. 125–135.

[30]Aung, K. T., Hassan, M. I., and Faeth, G. M., "Effects of Pressure and Nitrogen Dilution on Flame/Stretch Interactions of Laminar Premixed $H_2/O_2/N_2$ Flames," *Combustion and Flame*, Vol. 112, 1998, pp. 1 15.

[31]O'Conaire, M., Curran, H. J., Simmie, J. M., Pitz, W. J., and Westbrook, C. K., "A comprehensive modeling study of hydrogen oxidation," *International Journal of Chemical Kinetic*, Vol. 36, No. 11, 2004, pp. 603 622.

[32]Lafay, Y., Renou, B., Cabot, G., and Boukhalfa, M., "Experimental and Numerical Investigation of the Effect of H_2 Enrichment on Laminar Methane-Air Flame Thickness," *Combustion and Flame*, Vol. 153, 2008, pp. 540 561.

[33]Li, J., Zhao, Z., Kazakov, A., and Dryer, F. L., "An Updated Comprehensive Kinetic Model of Hydrogen Combustion," *International Journal of Chemical Kinetic*, Vol. 36, No. 10, 2004, pp. 566–575.

[34]"http://maeweb.ucsd.edu/ combustion/cermech/," .

[35]Zimont, V., Polifke, W., Bettelini, M., and Weisenstein, W., "An Efficient Computational Model for Premixed Turbulent Combustion at High Reynolds Numbers Based on a Turbulent Flame Speed Closure," *Journal of Engineering for Gas Turbines and Power*, Vol. 120, 1998, pp. 526–532.

[36] "FLUENT 6.3 User's Guide," 2006.

[37] Shelil, N., Griffiths, A., Bagdanavicius, A., and Syred, N., "Stability limits of premixed H_2/CH_4 flames," *ASME Turbo Expo 2010: Power for Land, Sea, and Air, Glasgow, UK, 14-18 June 2010*, , No. GT2010-23623 (submitted), 2010.

[38] Shelil, N., Griffiths, A. J., and Syred, N., "Numerical Study of Stability Limits of Premixed-Swirl Flame," *45th AIAA/ASME/SAE/ASEE Joint Propulsion Conference*, 2009.

[39] Griebel, P., Boschek, E., and Jansohn, P., "Lean blowout limits and NO_x emissions of turbulent, lean, premixed, hydrogen-enriched methane/air flames at high pressure," *Journal of Engineering for Gas Turbines and Power*, Vol. 129, 2007, pp. 404 410.

[40] Bagdanavicius, A., Shelil, N., Bowen, P. J., Syred, N., and Crayford, A. P., "Investigations of gaseous alternative fuels at atmospheric and elevated temperature and pressure conditions," *ASME Turbo Expo 2010: Power for Land, Sea, and Air, Glasgow, UK, 14-18 June 2010*, , No. GT2010-23270 (submitted), 2010.

[41] Bilger, R. W., Pope, S. B., Bray, K. N. C., and Driscoll, J. F., "Paradigms in turbulent combustion research," *Proceedings of the Combustion Institute*, Vol. 30, Elsevier Inc., 2005, pp. 21–42.

[42] Driscoll, J. F., "Turbulent premixed combustion: Flamelet structure and its effect on turbulent burning velocities," *Progress in Energy and Combustion Science*, Vol. 34, 2008, pp. 91–134.

Proceedings of ASME Turbo Expo 2010: Power for Land, Sea and Air
GT2010
June 14-18, 2010, Glasgow, UK

GT2010-23270

INVESTIGATIONS OF GASEOUS ALTERNATIVE FUELS AT ATMOSPHERIC AND ELEVATED TEMPERATURE AND PRESSURE CONDITIONS

Audrius Bagdanavicius*
Institute of Energy
Cardiff School of Engineering
Cardiff University
Queen's Buildings, The Parade
Cardiff CF24 3AA, Wales, UK
Email: bagdanaviciusa@cardiff.ac.uk

Nasser Shelil
Institute of Energy
Cardiff School of Engineering
Cardiff University
Queen's Buildings, The Parade
Cardiff CF24 3AA, Wales, UK
Email: shelilnm@cardiff.ac.uk

Philip J Bowen
Institute of Energy
Cardiff School of Engineering
Cardiff University
Queen's Buildings, The Parade
Cardiff CF24 3AA, Wales, UK
Email: bowenpj@cardiff.ac.uk

Nick Syred
Institute of Energy
Cardiff School of Engineering
Cardiff University
Queen's Buildings, The Parade
Cardiff CF24 3AA, Wales, UK
Email: syredn@cardiff.ac.uk

Andrew P Crayford
Institute of Energy
Cardiff School of Engineering
Cardiff University
Queen's Buildings, The Parade
Cardiff CF24 3AA, Wales, UK
Email: crayfordap1@cardiff.ac.uk

ABSTRACT

Increasing interest in alternative fuels for gas turbines stimulates research in gaseous fuels other than natural gas. Various gas mixtures, based on methane as the main component, are considered as possible fuels in the future. In particular, methane enrichment with hydrogen or dilution with carbon dioxide is of considerable interest. Some experiments and numerical calculations have been undertaken to investigate methane-hydrogen and methane-carbon dioxide gas flames, however most of these investigations are limited by particular pressure or temperature conditions.

This paper presents the investigation of the combustion of methane - carbon dioxide mixtures at atmospheric and elevated temperature and pressure conditions. Two experimental rigs were used, a Bunsen burner and swirl burner.

Bunsen burner experiments were performed in the High Pressure Optical Chamber, which is located within the Gas Turbine Research Centre of Cardiff University - at 3 bara and 7 bara pressure, and 473 K, 573 K and 673 K temperature conditions for lean and rich mixtures. Planar Laser Tomography (PLT) was applied to investigate turbulent burning velocity. Burning velocity of the gas mixture was calculated using two different image processing techniques and the difference in the results obtained using these two techniques is presented and discussed. Laser Doppler anemometry (LDA) was utilised to define turbulence characteristics such as turbulence intensity and integral length scale. Due to the variability of the velocity flow field and turbulence intensity across Bunsen burners, the importance of measuring position and conditions is discussed. The sensitivity of this variance on the flame regime as defined in the Borghi diagram is evaluated. In the second part of the study, a generic swirl burner was used to define the flame flashback limits for methane - carbon dioxide mixtures at atmospheric conditions. The gas mixture stability graphs are plotted, and the effect of CO_2 addition are discussed.

*Address all correspondence to this author.

NOMENCLATURE

A Flame front area
B Swirl burner swirler slot width
c Progress variable
D_e Swirl burner exit diameter
D_{eq} Equivalent nozzle diameter
D_i Swirl burner injector diamter
D_v Swirl burner internal swirler diameter
G_x Axial flux of axial momentum
G_θ Axial flux of angular momentum
H Swirl burner swirler height
h Image pixel height
l_0 Integral length scale
l_λ Taylor's length scale
$\dot{m}$ Mass flow rate, kg/s
n_k Number of pixels
S Swirl number
S_g Geometrical swirl number
S_L Laminar burning velocity
S_T Turbulent burning velocity
T_P Temperature of the products
T_R Temperature of the reactants
u Axial velocity, m/s
$\bar{u}$ Mean axial velocity, m/s
v Radial velocity, m/s
q' Root mean square (RMS) velocity, m/s
w Tangential velocity, m/s
w_p Image pixel width
α Thermal diffusivity of nitrogen
ρ Density
δ_L Laminar flame thickness
ϕ Equivalence ratio
Da Damköhler number
K Karlovitz stretch factor
Ka Karlovitz number
Le Lewis number

1 INTRODUCTION

Increasing demand for more sustainable fuels is stimulating research into hydrogen or hydrogen containing mixtures. However due to many limitations the practical application of such fuels at large scale is not feasible yet. Natural gas remains the most important gaseous fuel for industry and in the power generation sector. However in some areas the natural gas could be replaced by methane mixtures, which are produced unavoidably due to certain industrial and other processes. These methane and carbon dioxide mixtures become unwanted products, however their direct emission to the atmosphere is more harmful than the CO_2 emissions released through combustion. Therefore the utilisation of these gases for heat and/or power would be a useful fuel supplement, which could save natural gas resources and reduce the negative impact on climate change.

Sources of these gases include waste and sewage from industry, municipalities and farms. Due to complicated anaerobic digestion technology and the feedstock the gas composition is very variable. The main components in such mixtures are methane and carbon dioxide [1]. The gas mixture can consist of 30 to 70% of methane with the rest of carbon dioxide. Sometimes small amounts of other gases can be found [2, 3].

Combustion is the only realistic conversion technology allowing the generation of heat and power in gas turbines or large steam boilers, using such gases. Therefore greater understanding of the fuel behaviour at different conditions is required. Clearly carbon dioxide dilution reduces the burning velocity of the laminar flame, and this can be quantified through modelling tools such as CHEMKIN. However more detailed investigation is necessary for the turbulent flames, especially for conditions greater than atmospheric. Different aspects of methane and carbon dioxide mixtures were investigated at different conditions [4–11].

Lean and rich laminar flames of air and methane - carbon dioxide mixtures at 1 bara and 298 K were tested in a combustion vessel at near-zero gravity conditions [4]. The results indicated that the laminar burning velocity of pure methane is around 37 cm/s at equivalence ratio $\phi = 1$. The CO_2 addition reduced burning velocity considerably. For instance the burning velocities of 80% CH_4 - 20% CO_2 mixture and 50% CH_4 - 50% CO_2 mixture were around 32 cm/s and 18 cm/s respectively. Based on these experiments the authors derived the coefficients for a quartic fitting equation, adapting it for a wide range of temperatures (295 K - 454 K) and pressures (0.5 bara - 10.4 bara).

Consideration of landfill gas in the stagnation flow configuration revealed that laminar burning velocities and extinction strain rates reduce in comparison with pure methane, which could create stability problems in practical combustors [5].

Turbulent CH_4 - CO_2 gas mixture combustion has been investigated in a fan-stirred cruciform burner [6, 7]. The investigators pointed out the importance of an increased radiative heat loss due to CO_2 dilution in methane, which affects turbulent burning velocity. A general correlation with Damköhler number $(S_T - S_L)/q' = 0.06Da^{0.58}$ for N_2 and CO_2 diluted gas mixture flames was proposed [6].

A Bunsen burner was used to study the effect of CO_2 addition on methane flames in air at elevated temperature by Kobayshi et al. [8]. The findings showed that turbulent burning velocity normalised by laminar burning velocity S_T/S_L reduces with increasing CO_2 amounts in the mixture, and that this effect might be caused due to the influence of Markstein length. The researchers concluded that CO_2 has "significant effect in terms of decreasing the smallest scale of flame wrinkles", and that this could possibly restrain oscillations in combustion systems with exhaust gas recirculation.

Table 1. INVESTIGATED GAS MIXTURES AND CONDITIONS

Gas mixture	Bunsen burner tests	Swirl burner tests	Chemkin	Fluent
$100\%CH_4$	3 bar, 473 K	1 bar, 293 K	1, 3 bar and 300, 473, 673 K	1 bar, 293 K
$85\%CH_4$-$15\%CO_2$	3 bar, 473 K	1 bar, 293 K	1, 3 bar and 300, 473, 673 K	1 bar, 293 K
$70\%CH_4$-$30\%CO_2$	3 bar, 473 K	1 bar, 293 K	1, 3 bar and 300, 473, 673 K	1 bar, 293 K

More recent work on laminar and turbulent flames conducted at elevated temperature and pressure was reported by Cohe et al. [11]. The comparison of laminar experimental results with CHEMKIN numerical calculations using the PREMIX code with the GRI-Mech 3.0 kinetic mechanism, showed modest discrepancies in estimating S_L at increased pressures. Turbulent flame image analysis showed that flame wrinkling parameters and flame surface density did not depend on CO_2 addition and that the pressure had more pronounced effect on flame structure. It was concluded that S_T/S_L increases with pressure and CO_2 addition rate.

Several studies of the fuel dilution effect, oscillations, and combustion instability in swirl burners have been recently conducted [12–14]. The gas turbine combustor operability issues: blowout, flashback, combustion instability, and autoignition were discussed by Lieuwen et al. [12]. The researchers reviewed the fuels and their properties emphasising the differences in combustion properties of individual gases compared to combustions properties of mixtures of the same gases. Turbulent burning velocity behaves in a nonlinear manner as the fuel mixture changes, and a possible reason for that are the changes in chemical kinetic rates and radiative heat transfer [12]. The oscillation mechanism in the industrial swirl combustor were investigated by Dhanuka et al. [13]. PIV and PLIF techniques were used to obtain velocity profiles and images. The authors concluded that the lean premixed prevaporised combustor, used in the experiments, at off-design conditions exhibits unsteady behavior if the ratio of the main fuel flow rate to the pilot fuel flow rate exceed a critical value. Two major recirculation zones Primary Recirculation Zone (PRZ) and Lip Recirculation Zone (LRZ) were identified, both having a stabilising effect. The low frequency unsteadiness found during the experiments was driven by periodic flashback oscillations through the premixed reactants that fill the Corner or External Recirculation Zone (ERZ).

In this paper the investigation of the methane - carbon dioxide mixtures conducted using Bunsen and swirl burners at elevated temperature and pressure and at atmospheric conditions respectively is reported. The correlations of S_T/q' with Da and Ka numbers are derived, using Bunsen burner results, measured at elevated temperature and pressure. Flashback limits at atmospheric conditions for a generic swirl burner with a range of CH_4 - CO_2 fuel mixtures are interpreted in the light of the Bunsen burner results and other work from the literature.

2 EXPERIMENTAL FACILITIES

Two series of experiments were carried out to investigate CO_2 effect on methane burning velocity and flame stability. Three different gaseous fuels: 100% methane, 85% methane - 15% carbon dioxide and 70% methane - 30% carbon dioxide, were tested over a range of pressures and temperatures for lean and rich mixtures. A Bunsen type burner was used to test premixed flames at elevated temperatures of 473 K, 573 K and 673 K, and pressures of 3 bara and 7 bara conditions. The swirl burner was used to investigate flame stability at atmospheric conditions (293 K, 1 bara). The list of experimental conditions and research methods is presented in Table 1.

2.1 Bunsen burner experiments

Elevated temperature and pressure experiments were performed in the Gas Turbine Research Centre (GTRC) of Cardiff University. GTRC is equipped with an air compressor, which supplies pressurised air to the testing rigs, a large scale heat exchanger, which is used to preheat air, delivered to the test rig at the required temperature. The compressor capacity is up to 5 kg/s at 16 bar.

Burning velocity measurements were performed in the HPOC using a horizontally mounted burner firing into an inner combustion chamber, enclosed within an optical pressure casing (Figure 1). The pressure casing is a cylindrical geometry with four diametrically opposed quartz windows, affording excellent optical access. The optical combustion section is fitted with a heat exchanger, allowing combustion air to be preheated to required operating temperatures. The inner combustion chamber is of rectangular form and has four internal quartz windows which align with the outer casing, giving full optical access to the combustion chamber. The inner combustion chamber is constructed from aero-grade stainless steel sheet, allowing (if required) external cooling air to pass into the combustion chamber, mimicking the behaviour of practical gas turbine combustors. The flame is thus confined to the combustion chamber. The windows are continuously purged with air during the tests to ensure they are kept clear of any deposits of seed. A simple Bunsen type burner is

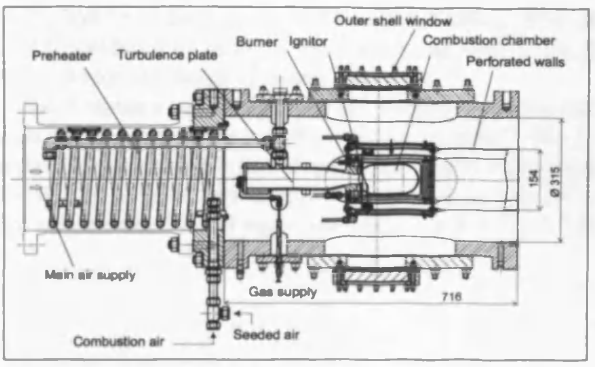

Figure 1. HIGH PRESSURE OPTICAL COMBUSTOR

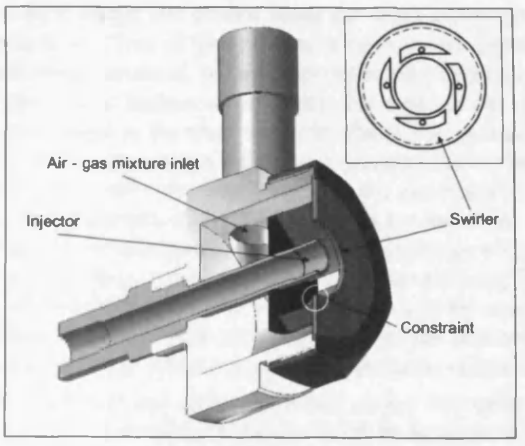

Figure 2. SWIRL BURNER

fired into the combustion chamber (diameter 25 mm). The burner is fitted with an annular pilot which supplies a methane diffusion flame to aid stability while adjusting the operating condition. This pilot was switched off prior to making measurements. The main burner is fed a premix of fuel and air via a turbulence mixing plate, 50 mm diameter, with 53 holes each of 1.5 mm, blockage ratio 95%. This creates uniform turbulence and aids in the mixing of the reactants. The fuel gas supply is connected to a mixing chamber upstream of this plate. Preheated air for combustion, which is seeded with aluminium oxide particles, is delivered through the preheater to the top of the mixing chamber of the burner. The air supply for the both HPOC and burner is pressurised by the main facility compressor. Seeded air for combustion is delivered by an auxiliary compressor. Fuel gases are supplied from premixed gas cylinders.

The experiments were controlled and monitored from a remote control room. Fuel, combustion air and seed air were measured simultaneously using suitably ranged Coriolis flow meters. All experimental conditions, such as: pressure, temperature, air flow and gas flow were recorded by a facility data acquisition system. Measured temperatures and pressures were reasonably steady with fluctuations not exceeding 5% and 3% of the nominal values for pressure and temperature respectively.

Two different measurement techniques were applied. A non-intrusive 2-D laser diagnostic technique, Laser Doppler Anemometry (LDA), was utilised to determine the velocity profile and turbulence characteristics at the exit of the burner at elevated pressures and temperatures. The velocity and turbulence profiles of isothermal air flow, seeded with aluminium oxide particles, were measured 10 mm downstream of the burner exit across the burner axis on the centreline plane. The axial and radial velocities were recorded for a range of exit velocities at ambient pressures of 3 and 7 bara and temperatures of 473 K, 573 K and 673 K. LDA data processing was carried out using DANTEC Flow manager software. More detail description of calculation method can be found elsewhere [10]. Planar laser tomography was applied in order to measure the turbulent burning velocity for the different gas mixtures at a range of temperatures and pressures. This technique is based on the observation that the density of the products is lower than that of the reactants. Consequently when the uniformly seeded reactants are converted to products the seed density reduces and the scattered light intensity reduces. As the flame thickness is small a clear demarcation is generated between products and reactants which can be identified as the flame front. Images of the flame front were recorded using a high speed camera mounted perpendicularly and synchronised with a pulsed sheet laser. To ensure reliability for each test 1000 images were recorded at 10 Hz.

2.2 Swirl burner tests

Flame stability and flashback experiments were conducted using the generic swirl burner designed and commissioned at GTRC. The burner was designed to produce premixed, non premixed and partially premixed flames, although only premixed combustion was considered in this programme. Air and fuel flows were measured simultaneously using suitably ranged Coriolis flow meters. The tests were conducted at atmospheric conditions.

The burner components are shown in Figure 2.

Air/fuel gas mixture is supplied through a tangential inlet pipe into a plenum chamber, then via 4 tangential inlets into the swirl chamber forming the main part of the burner. The fuel injector, which is normally used for the non premixed and partially premixed flames, is not used in our experiments, but is left in place as being representative of industrial practice, where it might for instance be used for liquid fuel injection. Such a burner design normally produces a Central Recirculation Zone (CRZ),

which plays an important role in flame stabilisation. The effect of CRZ is reduced by fitting a constrain in the nozzle (Figure 2 (inset)), which also helps to reduce flashback.

Swirl burners and combustors are usually characterised by the degree of swirl or the so-called "swirl number". The swirl number, S, is the variable non-dimensional number representing axial flux of angular momentum, G_θ, divided by axial flux of axial momentum, G_x, and equivalent nozzle radius $D_{eq}/2$ [15]:

$$S = \frac{G_\theta}{G_x D_{eq}/2} \tag{1}$$

However, as the flow patterns in swirl burners are complicated, it is difficult to calculate a specific swirl number without simplification. The swirl number varies with the burner, because the axial and tangential flow rates change at different levels within the burner. It is hence generally impractical to use local values of the swirl number, since this would require detailed velocity, and pressure measurements. To determine a more practical and comparable value, various simplifications have been used, resulting in the geometric swirl number S_g [16]. The S_g, calculated based on the geometrical configurations, was 1.47 for the burner studied in this programme.

3 IMAGE PROCESSING METHODS

The image processing of the images obtained using the Bunsen burner was carried out in order to calculate the turbulent burning velocity. Several different methods are utilised to identify the flame front of premixed turbulent flames [17–20]. Most of these techniques rely on the averaging of the flame images. One of the biggest issues in image processing is the conversion of gray scale images into the binary images as the image intensity is variable. Some researchers suggest converting images applying a dynamic threshold technique, which selects variable threshold values depending on image intensity at different image areas [21].

In our investigation we used two different methods. The first image processing method was based on statistical data treatment of the set of images. Using this method every single gray scale image was converted to the binary image. At first all images were reviewed and unreadable images were deleted. The background images were subtracted from every single image, in order to avoid background noise. Then, using morphological image processing functions, which are as standard included in MATLAB Image Processing Toolbox, the gray scale images were filtered. The threshold value was calculated and the gray scale images were converted to binary images. The binary images then were used to calculate the flame front area [10].

The second image processing method is a well established and widely used image averaging method. Using this method every single image was treated using the same image processing technique. Then all binary images were superimposed and the final image obtained. In such superimposed images the pixel count reached its highest value (which was equal to the number of binary image) in the areas where the flame was present in all images. In the areas where the flame is present in fewer images, obviously the pixel value was lower than the maximum possible value. In the patches where the flame was not presented at all, the pixel values remained 0. Thus the average image was calculated by converting superimposed binary image to binary image, using the threshold value which was equal to half the number of all processed images. This technique allowed the production of the averaged image which represents the progress variable 0.5.

It was noted that using the binary image averaging technique, image conversion problems could be recognised easier than using a "statistical" method. When the final average binary images were processed, it was found that in some cases pixel values outside the flame region were equal to 1, although in reality it should have been zero, as the region was not in the flame zone. This can occur because of the large background noise due to large amount of seeding passing into the combustion chamber (especially during methane tests). Aluminium oxide particles collected in the combustion chamber and created a background noise. Even after the subtraction of the background images the noise remained in the gray scale images and then created unwanted spots in the final average binary image. The averaging technique was more reliable in comparison with the "statistical" method, as it helped to identify the areas which were "polluted" with seed.

The flame front area of every single image was calculated using the "statistical" method. Therefore in order to calculate the average flame front area for each condition the statistical data processing was carried out. Using this approach it was possible to identify and reject all results which were outside the limit of two standard deviations. A new mean flame area then was found and accepted as the representative value.

Only one flame front area value was obtained using "averaging" method. For both methods the same equation was used to calculate the flame front area:

$$A = \sum_{1}^{k} (\pi \cdot n_k \cdot h \cdot w_p) \tag{2}$$

Each row of pixels within the image were "rotated" around it own centreline axis. The side area of every cylinder made of pixels was calculated and summed.

Finally having the flame front areas calculated, the burning velocity is computed by the formula:

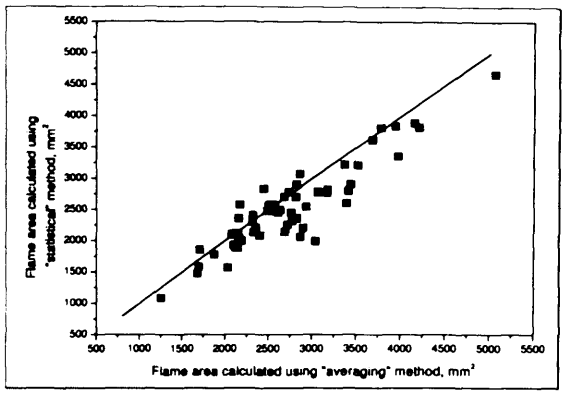

Figure 3. COMPARISON OF FLAME AREA CALCULATION RESULTS OBTAINED USING DIFFERENT IMAGE PROCESSING METHODS

$$S_T = \frac{\dot{m}}{\rho_R \cdot A} \tag{3}$$

The mass flow rate $\dot{m}$ is measured during experiments, and the density of the reactants ρ_R is calculated from the experiment conditions. Flame front area A is calculated using either "statistical" or "averaging" methods.

The comparison of the flame front area results, obtained using "statistical" and "averaging" methods is presented in Figure 3.

The results show reasonably good agreement, though some degree of data scatter can be observed. Higher flame front areas calculated using "averaging" methods correspond the lower flame front areas compared with the "statistical" method, which means that the burning velocity calculated from equation 3 gives the higher results. However the statistical non-parametric hypothesis test shows that there is no significant difference in these data sets. The turbulent burning velocity S_T values based on the "averaging" flame front area calculation method is used throughout this paper.

4 MEASUREMENTS OF TURBULENCE CHARACTERISTICS AND VELOCITY

Laser Doppler Anemometry (LDA) was utilised to measure turbulence intensity and burner exit velocity profiles. The time and length scales were obtained integrating temporal autocorrelation functions adopting Taylor's hypothesis. The velocity and turbulence profiles of isothermal air flow, seeded with aluminium oxide particles, were measured 10 mm downstream of the burner exit across the burner axis on the centreline plane. The axial and radial velocities were recorded for a range of exit velocities at

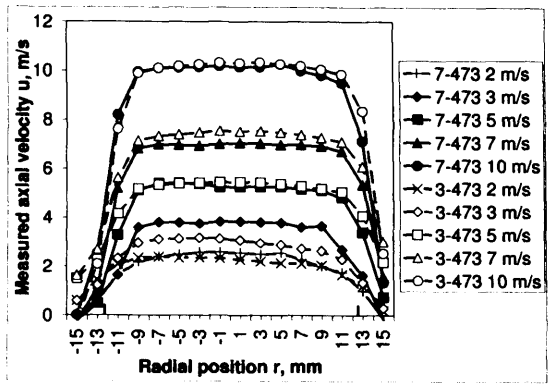

Figure 4. AXIAL MEAN VELOCITY [10]

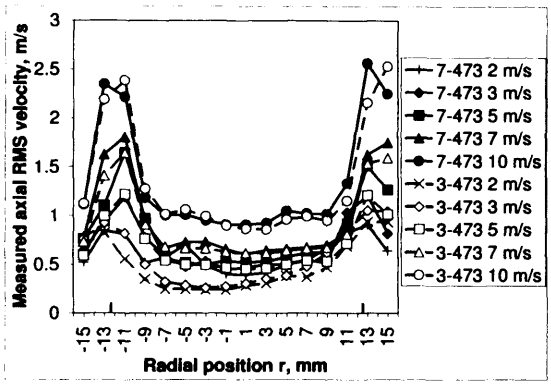

Figure 5. AXIAL ROOT MEAN SQUARE VELOCITY [10]

ambient pressures of 3 and 7 bara, and temperatures of 473 K to 673 K. LDA data processing was carried out using DANTEC Flow manager software. The results of axial velocity and turbulence intensity at 3 bara 473 K are presented in Figs. 4 and 5.

In Figure 4 axial velocity profiles are uniform across the burner. The magnitude of radial velocity (not shown) is very small in comparison with axial velocity, therefore the effect of radial velocity on total mean velocity, $\bar{u}$, is negligible. Axial root mean square velocity profile (Figure 5) shows large differences in the centre of the burner and at the edges. The highest turbulence is at the edges.

The turbulence intensity, q', has been calculated from the data measured at the edges of the burner $r = 9 - 12$ *mm*. The main reason to take measurements at the edge of the burner is that the flame front normally presents at the edges where the shear layer forms.

However high temperature affects the velocity field via its influence on turbulence characteristics [22]. Flame and turbu-

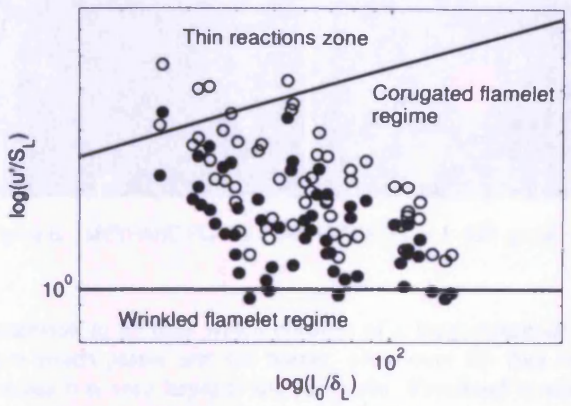

Figure 6. EXPERIMENT RESULTS PLOTTED IN BORGHI-PETERS DIAGRAM

lence interaction change the turbulence characteristics. In order to test the influence of the flame on velocity fields, several experiments were performed using the Bunsen burner with fully developed turbulence at atmospheric conditions. Measurements were taken 5 mm downstream of the burner exit at different exit velocities under rich methane-air mixture conditions. The exit velocity in this combustion test was the same as in the corresponding isothermal test facilitating a comparison of the respective velocity fields. It has been observed that axial mean velocity is almost identical at isothermal and combustion conditions in the centre of the burner. At the edges, where the flame front normally exists, the axial velocity at combustion conditions is higher. This is due to temperature effect on velocity field. The opposite effect has been observed for root mean square (RMS) velocity, which is less stable at the centre of the burner at combustion conditions. At the edges of the burner the RMS velocity tends to increase at isothermal flows, however at combustion conditions RMS velocity fluctuates around the average value or even decreases. Combustion dampens the turbulence intensity at the edges, which means that the flame becomes more laminar due to temperature effect. Similar findings has been reported by other researchers [23]. However, although the temperature effect exists, the measurements of the turbulence characteristics at isothermal conditions are generally conducted and used [23, 24].

As turbulence intensity fluctuates across the burner the question arises of where the turbulence characteristics should be measured. The turbulence intensity measured at the edge of the burner differs from the measurements at the centre of the burner (Figure 5). However, it is shown here that this difference has very little effect on turbulent flame regime. The magnified Borghi-Peters diagram is plotted in Figure 6. An empty mark represents data collected from the edge of the burner, and for each empty

Figure 7. PARTIAL FLASHBACK OF METHANE FLAME IN MODEL AND EXPERIMENTS, $\dot{m} = 2.74$ g/s, $\phi = 0.92$

mark there is a corresponding black mark representing the data from the centre of the burner. Hence, data presented in Figure 6 exist in pairs corresponding to the same experimental conditions. It can be seen that the vast majority of experiments have been conducted in the corrugated flamelet regime. The reduced turbulence intensity has not changed the position of the data points - represented by the separation distance between data pairs - in the diagram considerably. Therefore it can be concluded that the measurement position of the turbulence intensity is not a decisive factor in determining the turbulent combustion regime. This, however, is not a case for integral length scales. We have not obtained integral length scale measurements at the edge of the burner in our experiments [10]. Therefore it is not possible to estimate the changes of the integral length scale due to the measurement position, and its corresponding effect on the turbulent combustion regime.

5 FLAME STABILITY TESTS IN A GENERIC SWIRL BURNER AT ATMOSPHERIC CONDITIONS

For comparison purposes the test results of methane and methane carbon dioxide mixture at atmospheric conditions are presented.

5.1 Methane flames stability limits

Flame stability depends on the operating pressure, initial temperature, equivalence ratio and total mass flow rate of the premixed mixture [25]. The experiments and modelling were performed for premixed methane flames at atmospheric conditions with the purpose of measuring the stability limits of the flame for a particular generic burner. The behaviour of swirl burner is complex, with a rich literature in this area [13, 15, 26–31]. In the context of flashback for this generic swirl burner (geometric swirl number 1.47) the size and shape of the Central Reverse Flow Zone (CRZ) is crucial as in high velocity flows the flame initially stabilizes on the CRZ boundary. Under isothermal conditions for this swirl number a bulbous CRZ forms just past the exhaust and the fuel injector. This CRZ then typically forms an

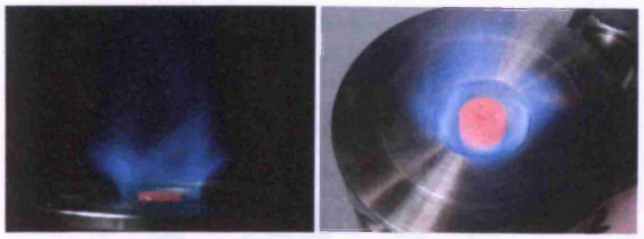

Figure 8. METHANE FLAME FLASHBACK, $\dot{m} = 1.485$ g/s, $\phi = 0.79$

extension to its base which consists of a long columnar structure which passes into the burner, often over the fuel injector (unless it is very large) to the backplate. Premixed combustion especially can virtually eliminate this CRZ as the increased axial flux of angular momentum reduces the effective swirl number to below the critical value for vortex breakdown and CRZ formation of $\tilde{0}.5$ (axial flux of angular momentum scarcely alters). Maximum effects occur around equivalence ratios $\phi \approx 1$ at maximum heat release. As the equivalence ratio is weakened vortex breakdown can occur, a CRZ forms, which gradually increases in strength so that at very weak mixtures the structure tends to that of the isothermal state. The problem this brings is that for lean combustion the flame burns not only in the exhaust but on the CRZ boundary surrounding the fuel injector; this is illustrated later. Here we consider the flashback of these flames radially to the tangential inlets and beyond. This condition represents the system behaviour both with and without the fuel injector. Other work has described techniques to eliminate this CRZ extension over the fuel injector. In this system, flashback was more pronounced for lean combustion than for rich.

As seen in Figure 7 and discussed above, the CRZ and flame front can extend completely over the fuel injector to the baseplate due to the extension of the CRZ over the fuel injector at weak equivalence ratios. This is undesirable and is a precursor to full flashback . The phenomena is often referred to as Combustion Induced Vortex Breakdown (CIVB). Techniques for elimination are discussed elsewhere [28].

Full flashback is shown in Figure 8. Here the flame has flashback to beyond the tangential inlets, and is operating as a cyclone combustor [15, 16], undesirably overheating the main swirl components.

The stable and flashback flames are reported under various air and fuels mass flow rates. Calculated experimental values of total mass flow rate $\dot{m}$ vs the equivalence ratio ϕ are plotted in Figure 9, which represents the burner flame stability map. An interpolation has been performed to define the flame stability limits. The curve divides the operating conditions into two regions. The region of stable flames is placed above the curve, and the region of unstable flame, flashback region, is located under the curve. The mass flow rate of fuel mixture was increased and

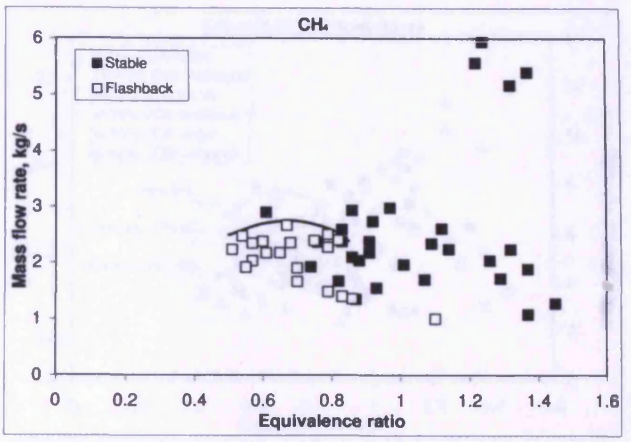

Figure 9. FLASHBACK VELOCITIES OF METHANE FLAME

reached its peak at $\phi = 0.7$. For rich mixtures the fuel mass flow rate was reduced again, though here flashback was not observed.

Another problem that was observed during the experiments was flame blow off. It was difficult to hold the flame with higher mass flow rates. One of possible solutions, in order to keep the flame within blow off limits, is to inject small quantities of diffusive fuel directly into the central recirculation zone, thus stabilizing the system, as implemented in practical gas turbine combustors [27]. Another technique, which improves the CH_4 stability is to add H_2 [12, 32], however this does then worsen flame flashback susceptibility due to increase of S_T.

5.2 CO_2 dilution effect on flame stability

Flashback occurs in the regions where turbulent flame propagation velocity exceeds the gas mixture supply streamlines. Therefore the flashback could be avoided if the flame speed and gas velocity could be kept in balance just above the burner exit. In the swirl burner the gas mixture flow velocity could be expressed as the components of axial u, radial v and tangential w velocities. These velocity vectors are presented in the schematic burner drawing Figure 10. Based on the experimental data u, v and w were calculated from the known mass flow rate and gas mixture density. Axial, radial and tangential velocity in the inlets are presented in the following three equations:

$$u = \frac{\dot{m}}{0.25\pi\rho(D_e^2 - D_i^2)} \tag{4}$$

$$v = \frac{\dot{m}}{0.5\pi\rho H(D_v + D_i)} \tag{5}$$

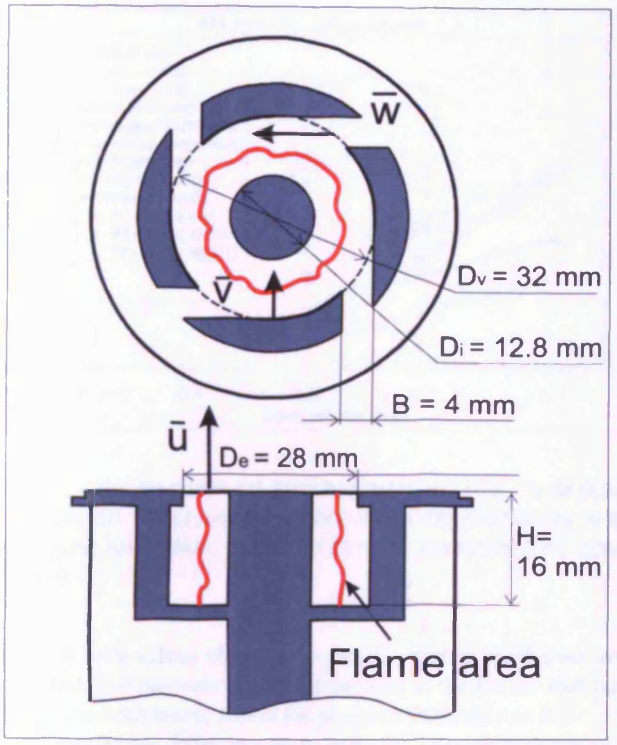

Figure 10. SCHEMATIC SWIRL BURNER DRAWING

$$w = \frac{\dot{m}}{4\rho HB} \tag{6}$$

The radial and tangential velocities of CH_4, 85% CH_4 - 15% CO_2 and 70% CH_4 - 30% CO_2 vs equivalence ratio are plotted in Figure 11. The two regions of stable flame and flashback are defined and separated by the lines, with values above representing stable conditions and those below representing flashback.

Testing all mixtures, both stable and flashback flames were observed. For both mixtures 85%CH_4 - 15% CO_2 and 70% CH_4 - 30% CO_2 under certain conditions the CRZ and flame extended over the fuel injector as in the case of methane flames. The highest velocity levels for flashback were observed at $\phi = 0.7 - 0.8$ for all mixtures. In general it was observed that the velocities, at which flashback occurs, decreased with increasing CO_2 amount in methane. CO_2 addition decreases the burning velocity [4, 10, 11], therefore lower velocities are required to stabilise the flame and stability limits are improved.

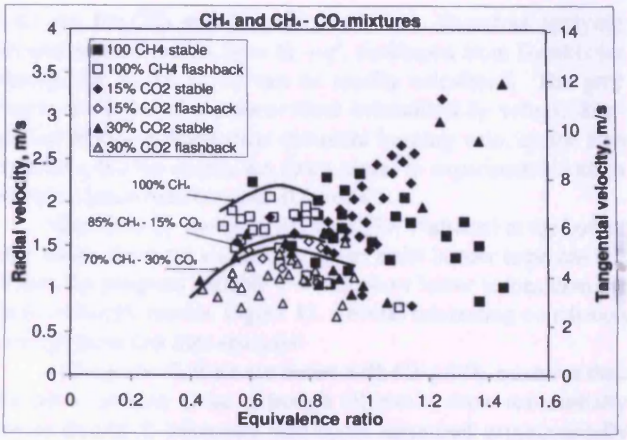

Figure 11. FLASHBACK VELOCITIES OF METHANE AND METHANE CARBON-DIOXIDE FLAMES

6 THE COMPARISON OF THE BUNSEN BURNER AND SWIRL BURNER TEST RESULTS

After the first flashback, the flame stabilised in the region around the injector as seen in Figure 8 and in the schematical drawing Figure 10. In a few tests with pure methane at very low mass flow rates secondary flashback was observed, where the flame propagated through the swirler slots upstream. However when testing methane - carbon dioxide mixtures, this phenomena did not occur. When the flame stabilised around the injector, the turbulent flame speed was balanced by the gas flow velocity, therefore the turbulent flame front was established somewhere in the middle region of the swirl chamber between the injector and swirler vanes. As the flame front remained in relative stability, the turbulent flame burning velocity could be derived from the equation 3. Here the flame front area could be approximated as $A = 0.5\pi H(D_v + D_i)$. Therefore combining equations 3 and 5 it can be concluded that $S_T = v$. It must be pointed out that turbulent consumption velocity calculated as indicated above must be distinguished from turbulent displacement velocity, which could be found using the same method measuring or modelling radial velocity, but not by the method above. Therefore these values S_T and v can be compared directly.

The comparison of our experimental values, obtained using the Bunsen burner at elevated pressure and temperature conditions [10], swirl burner radial velocity approximations and numerical S_T computations are represented in Figure 12. The S_T and v have been normalised by a normalisation factor as explained elsewhere [10]. The coding "3-473" represents 3 bara and 473 K preheated unburned gas temperature conditions, and "15CO2" represents 85%CH_4 - 15% CO_2 gas mixture in the legend key. We have not been able to stabilise very lean methane and methane - carbon dioxide mixtures in the Bunsen burner,

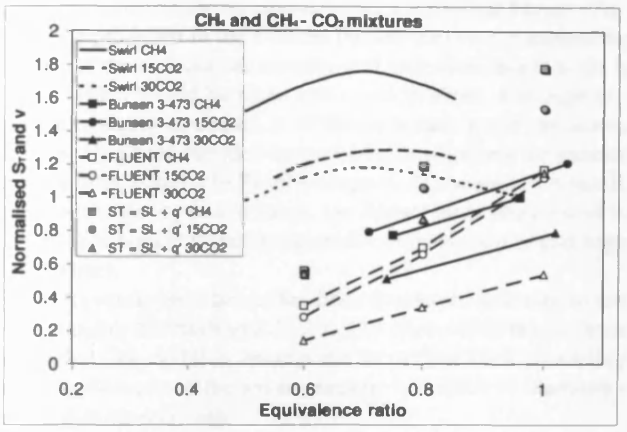

Figure 12. COMPARISON OF EXPERIMENTAL VALUES FROM BUNSEN BURNER EXPERIMENTS AT ELEVATED TEMPERATURE AND PRESSURE AND SWIRL BURNER TESTS AT ATMOSPHERIC CONDITIONS

therefore only values close to the stoichiometric conditions are presented. For numerical S_T computations at the burner exit position have been taken, where the progress variable $c = 0.5$.

Considerable difference of S_T and v is observed in Figure 12 at $\phi = 0.7 - 0.8$. One obvious contributory explanation is that very different flame structures are compared, therefore some incompatibility is expected. Bunsen burner flames belong to "envelope" category flames and swirl burner flames considered here would fall into the "unattached" or "flat" flame category, which have different flame wrinkling process [33, 34]. Another important consideration is the uncertainty in deriving the flame front area for swirl burner. It was observed that the flame front is corrugated, but thin, and the exact position could not be easily identified. Our assumption was to take the flame front position as being located half way between the fuel injector radius and the burner exit radius (Figure 10), this being based purely from visual interpretation 8. As an example, increasing the flame front diameter by 20% the S_T would decrease by 17%. Hence, more accurate flame front identification methods should be sought for future work.

It has already been noted that the definition for the turbulence characteristics for the Bunsen burner experiments have some uncertainties in themselves. The relative turbulence intensity for Bunsen burner isothermal flows at elevated temperature and pressure has been found to be around 15-20% [10]. For the swirl burner, as no measurements have been possible to date, the turbulence kinetic energy has been computed using CFD at isothermal conditions in the middle of the burner, where the assumed flame front is located. The q' calculated from the turbulence kinetic energy has been found to be in the region of 0.6 - 1.83 m/s for CH_4 and CH_4-CO_2 mixtures. Therefore applying simple approximation $S_T = S_L + q'$, developed from Damköhler theory, the values of S_T can be readily calculated. The grey marks in Figure 12 represent these normalised S_T values. Simplified theory underpredicts turbulent burning velocity for lean mixtures, but the results are much closer to experimental values at equivalence ratio between 0.8 and 0.9.

Numerical S_T computation via CFD, evaluated at the burner exit under the same conditions as the swirl burner experiments, where the progress variable $c = 0.5$, show lower values than the radial velocity results, Figure 12. Several interesting conclusion emerge from this data analysis:

- Fluent predictions are better with CH_4-CO_2 mixtures than for pure methane alone, although all results show substantially lower flashback velocities than those measured experimentally in the swirl burner, typically being 50% lower.
- The Bunsen burner results show significantly lower values than those obtained in the swirl burner. Due to different turbulence characteristics, and different presure and temperature conditions these experiments can not be directly compared, however S_T curve profile obtained from swirl burner experiments indicate that maybe new methodologies need to be developed to measure S_T in systems with the much higher turbulence levels found in the flashback regions of swirl burners.

7 CONCLUSIONS

The investigation of methane and methane - carbon dioxide flames at atmospheric and elevated temperature and pressure have been performed. Different research methods, using Bunsen and swirl burners, have been used to investigate the influence of CO_2 addition to methane on fundamental combustion characteristics in turbulent and swirling flames.

1. Turbulent burning velocities of methane and methane - carbon dioxide mixtures at elevated pressures and temperatures have been defined for Bunsen burner flames, applying different image processing techniques. The difference in results obtained from two different image processing techniques have been found to be statistically insignificant.

2. Turbulence isothermal flow characteristics for the Bunsen burner at elevated temperature and pressure have been determined using LDA. Comparison of experiments of isothermal and non-isothermal velocity and turbulence intensity measurements have been conducted in order to analyse the temperature effect on turbulence characteristics. Combustion influences the velocity field and turbulence intensity at the edges of the burner, where normally the flame front is located. The axial velocity increases and the turbulence intensity is reduced due to the flame effect. Therefore for the Bunsen burner, velocity measurements under combustion conditions would produce more reliable results at the edges of the burner than isothermal measurements, which should be considered in future studies.

3. Variable turbulence characteristics across the burner (Figure 5) are produced in the Bunsen burner, and so the measuring position of the turbulence intensity and turbulent length scale is a factor which should be taken into consideration. Although turbulence intensity measured at different burner positions across the burner has been found to be variable, its effect on the general flame regime, defined in Borghi diagram, is shown to be small. In the vast majority of test cases, the flames have been found to lie in the corrugated flamelet regime for both the centre and edge of the burner.

4. A generic swirl burner has been developed and used to test flame stability and flashback limits. The experiment results have shown that CO_2 addition reduces the flame flashback possibility primarily because of the lower burning velocities of methane - carbon dioxide mixtures.

5. A first attempt has been made to correlate the flashback and turbulent burning rate data, as fundamentally the two diagnostics must be related. Uncertainties have been emphasised and discussed. The differences in results found are likely to arise due to the following primary causes: the method used to derive flame front position, turbulent flow characteristics, flame regime, unburnt gas temperature. Modifications are needed to the Bunsen type burner to produce flame conditions at flashback closer to those pertaining in swirl burners.

CO_2 has clearly significant effect on methane flames, however due to the lack of experimental data at non-atmospheric conditions for premixed turbulent flames it is not easy to predict the behaviour of these flames using commercial models.

ACKNOWLEDGMENT

This research was part-financed by the European Commission project AFTUR (Alternative Fuels for Gas Turbines, ENK5-CT-2002-00662). A. Bagdanavicius thanks EU for sponsoring his research under the Marie Curie programme INECSE (Integrated Energy Conversion for Sustainable Environment, MEST-CT-2005-021018). N. Shelil wishes to express his thanks to the Egyptian Government for sponsoring his research.

REFERENCES

[1] Calabro, P. S., 2009. "Greenhouse gases emission from municipal waste management: the role of separate collection". *Waste Management,* ***29***, pp. 2178–2187.

[2] Shanmugam, P., and Horan, N., 2009. "Optimising the biogas production from leather fleshing waste by co-digestion with MSW". *Bioresource Technology,* ***100***, pp. 4117–4120.

[3] Rasi, S., Veijanen, A., and Rintala, J., 2007. "Trace compounds of biogas from different biogas production plants". *Energy,* ***32***, pp. 1375–1380.

[4] Stone, R., Clarke, A., and Beckwith, P., 1998. "Correlations for the laminar-burning velocity of methane/diluent/air mixtures obtained in free-fall experiments". *Combustion and Flame,* ***114***, pp. 546–555.

[5] Qin, W., Egolfopoulos, F. N., and Tsotsis, T. T., 2001. "Fundamental and environmental aspects of landfill gas utilization for power generation". *Chemical Engineering Journal,* ***82***, pp. 157–172.

[6] Shy, S. S., Yang, S. I., Lin, W. J., and Su, R. C., 2005. "Turbulent burning velocities of premixed CH_4/diluent/air flames in intense isotropic turbulence with consideration of radiation losses". *Combustion and Flame,* ***143***, pp. 106–118.

[7] Shy, S. S., Cheng, Y. C., Yang, C. H., Liu, C. C., and Huang, C. M., 2008. "Effects of H_2 or CO_2, equivalence ratio, and turbulent straining on turbulent burning velocities for lean premixed methane combustion". *Combustion and Flame,* ***2008***, pp. 510–524.

[8] Kobayashi, H., Hagiwara, H., Kaneko, H., and Ogami, Y., 2007. "Effects of CO_2 dilution on turbulent premixed flames at high pressure and high temperature". *Proceedings of the Combustion Institute,* ***31***, pp. 1451–1458.

[9] Chen, Z., Qin, X., Xua, B., Jua, Y., and Liub, F., 2007. "Studies of radiation absorption on flame speed and flammability limit of CO_2 diluted methane flames at elevated pressures". *Proceedings of the Combustion Institute,* ***31***, pp. 2693–2700.

[10] Bagdanavicius, A., Bowen, P. J., Syred, N., Kay, P., Crayford, A., Sims, G., and Wood, J., 2010. "Burning velocities of alternative gaseous fuels at elevated temperature and pressure". *AIAA Journal,* ***48***(2), pp. 317–329.

[11] Cohe, C., Chauveau, C., Gökalp, I., and Kurtulus, D. F., 2009. "CO_2 addition and pressure effects on laminar and turbulent lean premixed CH_4 air flames". *Proceedings of the Combustion Institute,* ***32***, pp. 1803–1810.

[12] Lieuwen, T., McDonell, V., Petersen, E., and Sanatvicca, D., 2008. "Fuel flexibility influences on premixed combustor blowout, flashback, autoignition, and stability". *Journal of Engineering for Gas Turbines and Power,* ***130***.

[13] Dhanuka, S. K., Temme, J. E., Driscoll, J. F., and Mongia, H. C., 2009. "Vortex-shedding and mixing layer effects on periodic flashback in a lean premixed prevaporized gas turbine combustor". *Proceedings of the Combustion Institute,* ***32***, pp. 2901–2908.

[14] Cheng, R. K., Littlejohn, D., Strakey, P. A., and Sidwell, T., 2009. "Laboratory investigations of a low-swirl injector with H_2 and CH_4 at gas turbine conditions". *Proceedings of the Combustion Institute,* ***32***, pp. 3001–3009.

[15] Syred, N., and Beer, J. M., 1974. "Combustion in swirling flows: A review". *Combustion and Flame,* ***23***(2).

[16] Gupta, A. K., Lilley, D. G., and Syred, N., 1984. *Swirl Flows*. Abacus Press, Tunbridge Wells.

[17] Griebel, P., Bombach, R., Inauen, A., Schären, R., Schenker, S., and Siewert, P., 2005. "Flame characteristics

and turbulent flame speeds of turbulent, high-pressure, lean premixed methane/air flames". *ASME Turbo Expo 2005: Power for Land, Sea, and Air, Reno-Tahoe, Nevada, USA, 6-9 June 2005*.

[18] Griebel, P., Siewert, P., and Jansohn, P., 2007. "Flame characteristics of turbulent lean premixed methane/air flames at high pressure: Turbulent flame speed and flame brush thickness". *Proceedings of the Combustion Institute, **31***, pp. 3083–3090.

[19] Kobayashi, H., 2002. "Experimental study of high-pressure turbulent premixed flames". *Experimental Thermal and Fluid Science, **26***, pp. 375–387.

[20] Pfadler, S., Leipertz, A., and Dinkelacker, F., 2008. "Systematic experiments on turbulent premixed bunsen flames including turbulent flux measurements". *Combustion and Flame, **152***, pp. 616–631.

[21] Kiefer, J., Li, Z. S., Zetterberg, J., Bai, X. S., and Alden, M., 2008. "Investigation of local flame structures and statistics in partially premixed turbulent jet flames using simultaneous single-shot *CH* and oh planar laser-induced fluorescence imaging". *Combustion and Flame, **154***, pp. 802–818.

[22] Poinsot, T., and Veynante, D., 2005. *Theoretical and Numerical Combustion*. R.T. Edwards, Inc., Philadelphia.

[23] Chen, Y. C., and Bilger, R. W., 2001. "Simultaneous 2-D imaging measurements of reaction progress variable and OH radical concentration in turbulent premixed flames: Experimental methods and flame brush structure". *Combustion Science and Technology, **167***, pp. 131–167.

[24] Chen, Y. C., and Bilger, R. W., 2004. "Experimental investigation of three-dimensional flame-front structure in premixed turbulent combustion - II: Lean hydrogen/air bunsen flames". *Combustion and Flame, **138***, pp. 155–174.

[25] Shelil, N., Griffiths, A. J., and Syred, N., 2009. "Numerical study of stability limits of premixed-swirl flame". *45th AIAA/ASME/SAE/ASEE Joint Propulsion Conference*.

[26] Huang, Y., and Yang, V., 2004. "Bifurcation of flame structure in a lean-premixed swirl-stabilised combustor: transition from stable to unstable flame". *Combustion and Flame, **136***(3), pp. 383–389.

[27] Huang, Y., and Yang, V., 2009. "Dynamics and stability of lean-premixed swirl-stabilized combustion". *Progress in Energy and Combustion Science, **35***, pp. 293–364.

[28] Kröner, M., Fritz, J., and Sattelmayer, T., 2003. "Flashback limits for combustion induced vortex breakdown in a swirl burner". *Journal of Engineering for Gas Turbines and Power, **125***, pp. 693–700.

[29] Syred, N., 2006. "A review of oscillation mechanisms and the role of the Precessing Vortex Core (PVC) in swirl combustion systems". *Progress in Energy and Combustion Science, **32***(2), pp. 93–161.

[30] Valera-Medina, A., Syred, N., and Griffiths, A. J., 2009. "Visualisation of isothermal large coherent structures in a swirl burner". *Combustion and Flame, **156***(9), pp. 1723–1734.

[31] Valera-Medina, A., 2009. "Coherent structure and their effects on processes occurring in swirl combustors". Phd, Cardiff University.

[32] Griebel, P., Boschek, E., and Jansohn, P., 2007. "Lean blowout limits and no_x emissions of turbulent, lean, premixed, hydrogen-enriched methane/air flames at high pressure". *Journal of Engineering for Gas Turbines and Power, **129***, pp. 404–410.

[33] Bilger, R. W., Pope, S. B., Bray, K. N. C., and Driscoll, J. F., 2005. "Paradigms in turbulent combustion research". In Proceedings of the Combustion Institute, Vol. 30, Elsevier Inc., pp. 21–42.

[34] Driscoll, J. F., 2008. "Turbulent premixed combustion: Flamelet structure and its effect on turbulent burning velocities". *Progress in Energy and Combustion Science, **34***, pp. 91–134.